SYNTHESIS AND EVALUATION OF PARTHENOLIDE ANALOGUES: CHEMICAL PROBES AND THERAPEUTIC AGENTS

A Thesis
SUBMITTED TO THE FACULTY OF
UNIVERSITY OF MINNESOTA
BY

Dan Wang

IN PARTIAL FULFILLMENT OF THE REQUIREMENTS
FOR THE DEGREE OF
MASTER OF SCIENCE

Advisor: Dr. Daniel A. Harki

MARCH 2013

Acknowledgements

I would like to begin by thanking my advisor, Dr. Dan Harki for his mentorship and support over these years. Your wisdom, knowledge and enthusiasm for science were a guiding light throughout my graduate school career. I wouldn't be where I am without your vision, encouragement and advise. Additional thanks goes to Professor Rick Wagner, Professor Chengguo Xing and Professor Mark Distefano for serving on my dissertation committee, and for the helpful critiques and suggestions provided throughout my graduate career.

Then, I would like to extend my sincere thanks to every past and present member of Harki group. Thank you all for the scientific help you have provided me all these years as well as being a constant source of support. In particular, Dr. Fred Meece for guiding me into the "parthenolide field" and Joe Hexum and Tim Andrew for providing some of the biological data in chapter 2.

I would also like to thank and recognize my collaborators for all their assistance with regards to my projects. In particular, I would like to thank Professor David Largaespada, Sue Rathe and Zohar Sachs for their help and valuable discussion in primary AML cells; Professor John Ohlfest and Chani Becker for performing the brain tumor animal studies; Dr. Victor G. Young, Jr. and the UMN X-Ray Crystallographic Laboratory for solving several structures for me.

Additionally, my sincerest thanks goes to Department of Medicinal Chemistry for giving me the chance to study in the US, and for providing the intense, but vivid research environment. I would also like to thank every individual person in the department,

especially my fellow classmates, who were amazing friends and an invaluable source of support and laughter all these years and beyond.

I would also like to acknowledge the American Heart Association (Midwest affiliates) for financial support of my research through a predoctoral fellowship (2011-2013, 11PRE7240035).

Finally, I'd like to dedicate the thesis to my friends and family for their never-ending support. Thanks for being the cheerleaders throughout my journey. I would have never made it this far without your unconditional love, support and encouragement.

Abstract

Cancer stem cells (CSCs), also known as tumor-propagating cells or tumor-initiating cells, are subpopulations of undifferentiated, highly tumorigenic cells found within bulk tumors. The rapid advances of cancer research and development of relative technologies have provided more and more evidence for the existence of CSCs, as well as the important roles they play in drug resistance and disease relapse of cancer. However, because of their quiescent nature and the similarities to normal stem cells, eradicating CSCs presents a challenging task. Chapter one provides an overview of cell surface markers of CSCs. Those markers are potential diagnostic macromolecules and targets for drug delivery.

Parthenolide (**PTL**) is a sesquiterpene lactone natural product isolated from Mexican Indian medicinal herb *Tanacetum parthenum* (feverfew plant), a known medical herb utilized for centuries. **PTL** has been extensively studied as an anticancer agent, showing significant efficacy towards a wide spectrum of human cancer cells. In 2005, the identification of **PTL** as the first stand-alone and selective cytotoxic agent against the acute myeloid leukemia CSCs further heightened its therapeutic potential. However, the mechanism of action of **PTL**'s CSC inhibitory activity is still an area of debate. Our efforts to elucidate the molecular targets of **PTL** is described in chapter two. The design and synthesis of two PTL affinity probes with diverse biological activity as well as their utilization in comparative and competitive protein pull-down experiments to enrich the cellular protein targets of **PTL** is presented.

Although exhibiting promising anticancer and anti-CSC activities, the modest biological potency and poor water solubility prevent further development of **PTL**. Chapter three describes our efforts to synthesize PTL analogues, as well as our strategy to prepare water-soluble PTL prodrugs.

Table of Contents

List of Tables

List of Schemes

List of Figures

List of Abbreviation

Alloc: allyloxycarbonyl, Boc_2O: Di-*tert*-butyl dicarbonate, DBU: 1,8-Diazabicyclo [5.4.0]undec-7-ene, DCM: dichloromethane, DIAD: Diisopropyl azodicarboxylate**,** DIPEA: *N*,*N*-diisopropylethylamine, DME: 1,2 – dimethoxyethane, DMSO: dimethyl sulfoxide, EDCI: *N*-(3-Dimethylaminopropyl)-*N*′-ethylcarbodiimide hydrochloride, ESI: electrospray ionization, Et_2O: Diethyl ether, HBTU: *O*-(Benzotriazol-1-yl)-*N,N,N′,N′*-tetra methyluronium hexafluorophosphate, HOBt: 1-Hydroxybenzotriazole hydrate**,** HPLC: high performance liquid chromatography, hr: hour, HRMS: high resolution mass spectrometry, mCPBA: *meta*-chloroperoxybenzoic acid**,** MS: molecular sieves, NMA: *N*-methyl aniline, NMP: *N*-Methyl-2-pyrrolidinone, PDB: protein database, RT: room temperature, TEA: triethylamine, TFA: trifluoroacetic acid, THF: tetrahydrofuran, TLC: thin layer chromatography.

NMR abbreviation

s: singlet, d: doublet, t: triplet, dt: doublet of triplets, dd: doublet of doublets, td: triplet of doublets, ddd: doublet of doublet of doublets, 5d: quintet of doublets, q: quartet, m: multiplet, br s: broad singlet, *J*: coupling constant.

Preface

Please Note the following:

Chapter 1. This chapter is a review article co-authored with Tim Andrews and Dr. Daniel A. Harki. ***Drug Delivery and Translational Research.*** 2013, *3*, 121-141 DOI: 10.1007/s13346-012-0075-1

Chapter 2: Biological testing of parthenolide analogues was assisted by the following Harki lab members: Joe Hexum, Tim Andrews, Fred Meece, Margaret Olson, Matt Bockman, Erick Carlson, and Ezra Menon.

Chapter I. Cell Surface Markers of Cancer Stem Cells: Diagnostic Macromolecules and Targets for Drug Delivery

1.1 Introduction

Cancer stem cells (CSCs), also known as tumor-propagating cells or tumor-initiating cells, are subpopulations of undifferentiated, highly tumorigenic cells found within bulk tumors. CSCs have the ability to self-renew, differentiate, and generate a phenotype-identical copy of the tumor from which they were isolated upon implantation in a recipient animal (**Fig. 1.1**). Accordingly, CSCs reside at the apex of the tumor cell hierarchy and can differentiate into all of the cell types that comprise the host tumor.[1-8] CSC theory directly challenges the traditional stochastic model of cancer cell growth

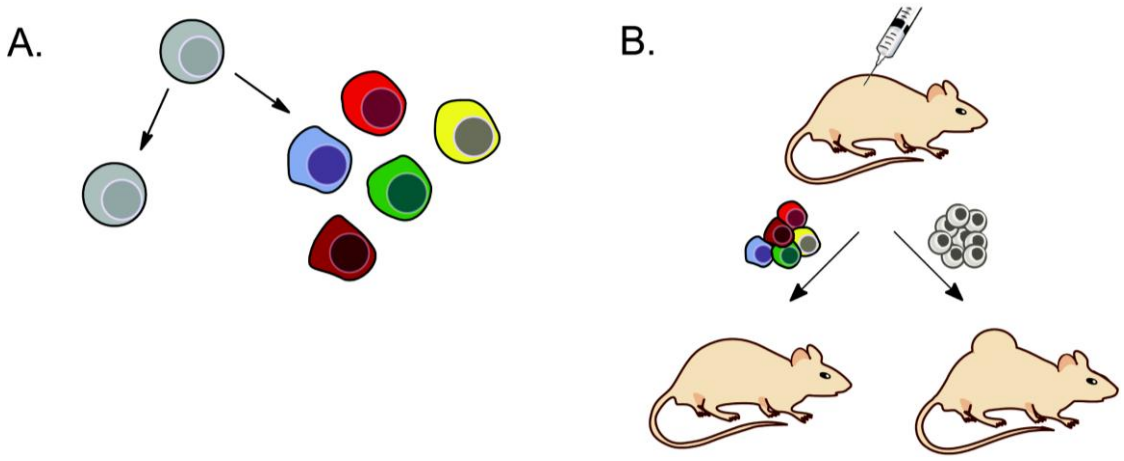

Figure1.1 Depiction of the properties that are characteristic of cancer stem cells (CSCs). A: CSCs (shown in gray) can self-renew and undergo multi-lineage differentiation (cells in color). B: Tumorigenicity. CSCs are more tumorigenic than differentiated bulk tumor cells.

that predicts that all cells from a tumor have tumorigenic potential.[9]

The development of suitable technologies to isolate CSCs from tumors (e.g., monoclonal antibodies of unique CSC surface macromolecules coupled with fluorescence-activated cell sorting (FACS) techniques) and appropriate animal models

for xenotransplantation assays of isolated cell populations (e.g., non-obese diabetic, severe combined immuno-deficient (NOD/SCID) mice) have facilitated the identification of CSC populations from a variety of blood and solid tumors.[4] These technological advancements were prerequisite to the discovery of CSCs in acute myelogenous leukemia (AML), which is arguably the prototypical human cancer bearing an established CSC hierarchy. Seminal work by John Dick and colleagues provided the first critical evidence for CSCs by isolating (with FACS) the $CD34^{+}/CD38^{-}$ fraction of human donor AML cells and engrafting those cells into severe combined immunodeficient (SCID) mice.[9,10] Engrafted cells were able to proliferate and differentiate, resulting in identical disease to that of the donor. Isolation of the AML CSC population ($CD34^{+}/CD38^{-}$) from the recipient mouse, followed by serial transplantation into a secondary recipient mouse yielded the same disease, thereby demonstrating the selfrenewal properties of the initially engrafted $CD34^{+}/CD38^{-}$ AML cell fraction. This pioneering study provided insight into the long-standing observation that AML cells have only limited proliferative capacity by supporting the hypothesis that a rare leukemic clone must maintain the AML population.[11-13] Additionally, this work provided crucial evidence for the hierarchy model of tumor heterogeneity by demonstrating that some populations of leukemic cells ($CD34^{+}/CD38^{-}$) exhibited CSC activity, whereas other leukemic cell populations (e.g., $CD34^{+}/CD38^{+}$ and $CD34^{-}$) did not.[10] The feature that only a sub-population of cells from a tumor can facilitate tumorigenesis is a tenant of the hierarchy model of tumor cell growth.[4] AML CSCs exclusively give rise to clinical AML.[9,10]

Cancer therapies that are resisted by the CSC population are predicted to fail by the CSC model.[6,7] Although outside the focus of this review, the drug resistance properties of CSCs may result due to increased cell quiescence,[14,15] expression of anti-apoptotic proteins,[16] and upregulation of ABC multidrug resistance transporter proteins.[16,17] The CSC hypothesis is also supported by clinical data. In the case of AML, approximately 44,000 new cases of AML are diagnosed annually in the United States, and 5-year survival rates are only 24%.[18] Front-line small molecule treatments for AML include nucleoside analogues (e.g., cytarabine) and anthracyclines (e.g., idarubicin, daunorubicin), which are designed to induce apoptosis in rapidly dividing cancer cells.[19,20] AML CSCs, which are largely quiescent, are typically resistant to standard chemotherapeutic agents. Furthermore, recent data have demonstrated that cytarabine actually facilitates AML CSC entry into G0/G1 phase, thereby promoting cell cycle quiescence and providing a mechanism that allows AML CSCs to survive chemotherapy.[21] Consequently, viable strategies to eradicate CSC populations are clearly needed if curative cancer therapies are to be developed. A realized example of this concern has been documented with patients receiving the targeted bcr-abl tyrosine kinase antagonist imatinib (Gleevec®) for chronic myelogenous leukemia (CML). Although imatinib effectively converts CML into a chronically managed disease,[22,23] patient withdrawing from imatinib treatment ultimately results in disease relapse because imatinib does not eliminate CML CSCs.[24,25]

Elucidation of the molecular differences between differentiated cancer cells with high proliferation rates and nondifferentiated CSCs that are mostly quiescent is an intense area of ongoing research.[4,26-28] Equally important is the need to characterize

those chemical features that confer cancerous versus non-cancerous stem cells (e.g., the differences in biochemistry between a leukemic stem cell and a normal hematopoietic stem cell).[4] A variety of cytosolic and cell surface macromolecules have been characterized as diagnostic markers for the identification of CSCs from differentiated cancer cells, normal stem cells, or other cells from tissue. Many of these markers are utilized in combination for characterization of the CSC population (e.g., $CD34^{+}$/ $CD38^{-}$ for AML CSCs described above).[10] However, for isolation and drug targeting of CSCs, surface markers have proven to be more useful.[29-32] Cell surface macromolecules are readily captured by magnetic micro-bead isolation techniques and are easily detected by flow cytometry, and the unique ligands presented on the cell surface offer receptors for targeted drug delivery.[33] In this review, we have consolidated the known CSC cell surface markers that have been described for various blood and solid tumors into one document. Since intracellular markers for CSCs have been described and reviewed elsewhere,[30,34] we have focused this review only on well-characterized cell surface markers due to their ability to serve as mediators for drug delivery into CSCs. In addition to compiling CSC surface markers, we review the unique chemical and structural features of the most well-known CSC surface markers and report recent efforts to deliver therapeutic agents into CSCs mediated by CSC specific cell surface macromolecules.

1.2 Compendium of cell surface markers for identification of cancer stem cells

Summarized herein is the current knowledge of CSC markers from the following human cancers: leukemias (**Table 1.1**), breast, colorectal, liver, pancreatic, prostate,

melanoma, brain, bladder, lung, and ovarian carcinomas (**Table 1.2**). Recent efforts to deliver therapeutic molecules to CSCs are described in **Table 1.3**. **Table 1.4** provides a compendium of the other commonly used names of the CSC markers discussed in the following sections.

1.2.1 Leukemia

Leukemia is a family of diseases, comprised of blood, bone marrow, or lymphoid system cancers that are characterized by abnormal increases in white blood cell count.[35] In 2011, more than 44,000 children and adults in the United States were expected to develop some form of leukemia, and approximately 22,000 deaths were projected.[18,36,37] In 1994, Dick and coworkers first characterized the acute myelogenous leukemia stem cell population utilizing the $CD34^{+}/CD38^{-}$ cell surface marker combination.[10] This landmark discovery catalyzed the search for CSC populations from related blood as well as solid tumors. The repertoire of CSC markers in leukemia is complicated and variable depending on leukemia subtype and stage of disease.[38] The current state of knowledge of leukemia CSC surface markers is described herein and shown in **Table 1.1**.

1.2.1.1 Acute myelogenous leukemia (AML)

As has been introduced above, $CD34^{+}/CD38^{-}$ (**Table 1.1**) is the earliest documented stem cell marker combination in cancer and is still widely used to identify leukemic CSCs. In a seminal study, Dick and coworkers demonstrated that a small subpopulation of AML cells with the $CD34^{+}/CD38^{-}$ cell surface phenotype was capable of producing a large number of colony-forming progenitors when engrafted to SCID

mice. On the other hand, $CD34^+/CD38^+$ and $CD34^-$ cell fractions did not exhibit these properties.[10] Later studies from the same group provided evidence that $CD34^+/CD38^-$ was a common immune phenotype for leukemic CSCs in multiple AML subtypes and also demonstrated their self-renewal potential.[9]

Additional studies have further refined and developed the cell surface phenotypes of AML. The Suthland group has shown that, in both in vitro and in vivo models, $CD34^+/CD90^-$ (Thy-1), $CD34^+/CD71^-$/HLA-DR^-, and $CD34^+/CD117^-$ (c-kit) are unique cell surface marker phenotypes of AML CSCs.[39-41] In 2000, the Jordan group indicated that $CD34^+/CD38^-/CD123^+$ (interleukin-3 receptor α chain) is a specific cell surface phenotype for human AML stem cells.[42] Additionally, CD123 expression has also been reported on CSCs in CML, myelodysplastic syndrome, and systemic mastocytosis,[43] suggesting that CD123 might be a broadly applicable cell surface marker for the development of targeted therapies against CSCs across multiple leukemias. CD33 is another important surface marker for characterizing AML CSCs. CD33 has long been known for its extensive expression on leukemic blasts,[44] but only recently has it been reported as a marker for AML CSCs. Hauswirth et al. have shown that addition of $CD33^+$ to phenotype $CD34^+/CD38^-/CD123^+$ yields a robust marker combination for AML CSCs that is unique to cancerous stem cells.[45] Additionally, Florian et al. demonstrated that $CD34^+/CD38^-/CD45^+/CD123^+$ was a general marker phenotype for AML CSCs and that additional markers, such as $CD13^+$, $CD71^-$, $CD33^+$, $CD117^+$, $CD133^+$, and $HLADR^-$, were observed in variable combinations with the CD34+/CD38−/CD45+/CD123+ phenotype.[43] $CD34^+/ CD38^-/CD123^+$ CSC populations have also been noted for their upregulation of drug efflux pumps. Compared with bulk

(differentiated) tumor cells, the upregulation of multidrug-resistance related protein 1, breast cancer resistance protein, and lung resistance protein have been observed in AML CSC populations.[46] C-type lectin-like molecule-1 (CLL-1), which is a transmembrane protein with a heavily N-glycosylated extracellular domain, has been found to be exclusively expressed on AML CSCs in 92% of all studied AML cases. Isolation and transplantation of $CD34^+/CD38^-/CLL\text{-}1^+$ cells generated AML blasts in NOD/SCID mice.[47] Another important marker of AML CSCs is CD96, which belongs to the immunoglobulin superfamily. Recent studies have demonstrated that CD96 protein might be selectively overexpressed as a $CD34^+/CD38^-/CD90^-/Lin^-/CD96^+$ phenotype on AML CSCs as compared with the basal expression level of CD96 on normal HSCs.[48] The elevated expression of several isoforms of adhesion molecule CD44 has been identified in the interaction between hematopoietic progenitor cells and the surrounding stromal cells (i.e., CSC niche) in primary human AML samples.[49] CD44 has been previously exploited in targeted drug delivery to AML CSCs[20] (see section 1.3, **Table 1.3**). The Ishikawa group has reported the identification of CD25 and CD32 in conjunction with $CD34^+/CD38^-$ as potential CSC markers for AML. In their study, they found that both $CD34^+/CD38^-/CD25^+$ and $CD34^+/CD38^-/CD32^+$ leukemia cells are enriched in quiescent, chemotherapeutic drug-resistant CSCs, are capable of initiating AMLs in vivo, and are expressed at a very limited level in normal HSCs.[50] Majeti et al. also reported CD47 as a new potential target for CSC therapy of AML. $CD34^+/CD38^-/CD90^-/ Lin^-/CD47^+$ expression was observed only in AML CSCs when compared with their HSC counterparts.[51] See **Table 1.1** for a listing of AML CSC surface markers.

1.2.1.2 Acute lymphoblastic leukemia

Acute lymphoblastic leukemia (ALL) is the most common childhood cancer and is characterized by clonal proliferation of lymphoblasts.[18] ALL CSCs present the same $CD34^+/CD38^-$ cell surface marker phenotype as AML CSCs; however, the $CD34^+/CD38^-/CD33^-/CD19^-$ phenotype has been characterized as a more robust marker to define ALL CSCs.[52] A population of ALL CSCs that are committed to lymphoid differentiation has been shown to express the Philadelphia chromosome ($CD34^+/CD38^-/Ph^+$).[53] The Philadelphia chromosome contains a chromosomal translocation between the break point cluster region (bcr) and the gene encoding c-Abl (abl), which encodes for the bcr-abl tyrosine kinase.[54] The presence of the Philadelphia chromosome in ALL indicates an overall poor prognosis.[55] Subsequent studies have shown that, in $CD34^+/CD38^-$ bone marrow cells, a predominant and aberrant $CD34^+/CD38^-/CD19^+$ cell population that is not present in healthy individuals carries the Philadelphia chromosome, while the $CD19^-$ cell population in this compartment does not.[56] These results indicate that the $CD34^+/CD38^-/CD19^+$ phenotype marrow compartment in childhood ALL is another potential marker of ALL CSCs,[56] which is contradictory to previous findings,[52] However, it has been suggested that $CD19^+$ might not be a broadly applicable AML CSC marker.[56] ALL can be classified as T lineage (T-ALL) or B lineage (B-ALL).[57] Cox et al. have demonstrated that ALL cells capable of long-term proliferation and differentiation into pre-B-ALL in vitro (suspension culture assay) and in vivo (NOD/SCID transplant model) were derived from only

CD34+/CD10− or $CD34^{+}/CD19^{-}$ sub-fractions, indicating that the target cells for transformation in pre-B-ALL have a more immature phenotype than the bulk ALL population.[58] The same group also discovered that $CD34^{+}/CD4^{-}$ or $CD34^{+}/CD7^{-}$ sub-fractions of childhood T-ALL cells were highly proliferative and capable of NOD/SCID engraftmen.[59] More recently, Cox et al. reported that in childhood ALLs, the small subpopulation of $CD133^{+}/CD19^{-}$ cells were capable of initiating and maintaining long-term in vitro cultures of B-ALLs and engrafting serially into NOD/SCID recipient mice.[60] In a recent study from the Morimoto group, the stem cell characteristics of $CD9^{+}$ cell populations in B-ALL were demonstrated both in vitro and in transplantation experiments, suggesting that CD9 is a useful positive-selection marker for the identification of CSCs in B-ALL. Their study also showed that, in some cases, $CD9^{+}$ in ALL CSCs was a more reliable CSC marker than $CD34^{+}$.[61] The same group also reported the importance of CD90 (Thy-1) and CD110 (c-Mpl) as positive-selection markers for T-ALL CSCs. In both in vitro and in vivo assays, their results suggested that small subpopulations of $CD90^{+}/CD110^{+}$ cells isolated from either childhood or adult ALL specimens retained the ability to self-renew, proliferate, and differentiate.[62] See **Table 1.1** for a listing of ALL CSC surface markers.

1.2.1.3 Chronic myelogenous leukemia (CML)

CML is often characterized by the overproduction of mature myeloid cells. As with ALL, CML is most closely associated with the bcr-abl chromosomal translocation, which is present in pluripotent stem cells.[38] CML CSCs are also characterized by the $CD34^{+}/Ph^{+}$ cell phenotype (**Table 1.1**) and are phenotypically similar to normal HSCs.[63]

In addition to its role as an AML CSC marker, CD123+ has also been characterized as a surface marker for CML CSCs (phenotype $CD34^{+}/CD38^{-}/CD123^{+}$). Queries for the presence of other markers in CML cells bearing the $CD34^{+}/ CD38^{-}/CD123^{+}$ phenotype revealed variable positivity for CD13, CD33, CD44, and CD117 molecules;[43] however, the presence of CD117 on the surface of CML CSCs conflicts with previous reports.[41]

Leukemia Type	Marker(s)	Reference
Acute Myelogenous Leukemia (AML)	$CD34^{+}/CD38^{-}$	[10]
	$CD34^{+}/CD90^{-}$	[39]
	$CD34^{+}/CD71^{-}$/HLA-DR^{-}	[40]
	$CD34^{+}/CD117^{-}$	[2, 41]
	$CD34^{+}/CD38^{-}/CD123^{+}$	[42, 46]
	$CD34^{+}/CD38^{-}/CD45^{+}/CD123^{+}$	[43]
	$CD34^{+}/CD38^{-}/CD123^{+}/CD33^{+}$	[4, 45]
	$CD34^{+}/CD38^{-}$/CLL-1^{+}	[47]
	$CD34^{+}/CD38^{-}/CD90^{-}/Lin^{-}/CD96^{+}$	[48]
	$CD44^{+}$	[49]
	$CD34^{+}/CD38^{-}/CD25^{+}$	[50]
	$CD34^{+}/CD38^{-}/CD32^{+}$	[50]
	$CD34^{+}/CD38^{-}/CD90^{-}/Lin^{-}/CD47^{+}$	[51]
Acute Lymphocytic Leukemia (ALL)	$CD34^{+}/CD38^{-}/CD33^{-}/CD19^{-}$	[10, 52]
	$CD34^{+}/CD38^{-}/Ph^{+}$	[53]
	$CD34^{+}/CD38^{-}/CD19^{+}$	[56]
	$CD34^{+}/CD10^{-}$	[58]
	$CD34^{+}/CD19^{-}$	[12, 58]
	$CD34^{+}/CD4^{-}$	[59]
	$CD34^{+}/CD7^{-}$	[59]
	$CD133^{+}/CD19^{-}$	[60]
	$CD9^{+}$	[61]
	$CD90^{+}/CD110^{+}$	[62]
Chronic Myelogenous Leukemia (CML)	$CD34^{+}/CD38^{-}/CD123^{+}$	[43]
	$CD34^{+}/Ph^{+}$	[63]

Table 1.1. Previously reported CSC markers for human leukemias.
See **Table 1.1** for a listing of CML CSC surface markers.

1.2.2 Breast cancer

Breast cancer accounts for the deaths of more than 40,000 women each year in the United States. Although the 5-year survival rate for breast cancer patients has

dramatically increased over the past few decades, tumor relapse and metastasis is still a significant problem in breast cancer therapy.[18,64] The evasion of breast CSCs during therapy is a significant contributor to disease relapse.[65]

Al-Hajj et al. were the first to identify breast CSCs from whole cell population of breast cancer specimens using the cell surface marker profile $CD44^{+}/CD24^{-/low}/Lin^{-}$ (see **Table 1.2** at the end of section 1.2), which was the seminal report of CSCs identified from a solid tumor.[66] The marker profiles $CD44^{+}/CD24^{-/low}/Lin^{-}$ has been correlated with high resistance to traditional cancer therapies,[67] poor prognosis,[68] and enhanced invasive properties.[69] Notably, lineage (Lin) markers are a standard combination of monoclonal antibodies including CD2, CD3, CD4, CD5, CD8, NK1.1, B220, TER-119, and Gr-1 in mice and CD3, CD14, CD16, CD19, CD20, and CD56 in humans.[70] Addition of epithelial cell adhesion molecule (EpCAM), yielding marker combination $CD44^{+}/CD24^{-/low}/ EpCAM^{high}$, was later found to be a more robust surface marker combination for the isolation of human breast CSCs.[66] The multiplexing of cytoplasmic enzyme ALDH1, membrane protein CD44, and cytokeratin has been employed to identify putative breast CSCs and indicate poor prognosis, which is independent of tumor size, nodal status, ER-, PR-, and HER2-status, and histological grade.[71]

Another important cell surface marker of human breast CSCs is Thy1 (CD90). In an MMTV-Wnt-1 breast cancer mouse model, cancer cells with the phenotype $THY1^{+}/CD24^{+}$ (1–4% of tumor cell population) were identified to be highly tumorigenic in comparison to non-THY1+/CD24+ populations and displayed properties of CSCs.[72] The observation of CD24+ phenotype in combination with Thy1 is contradictory to previous reports that found breast CSCs to have a $CD44^{+}/CD24^{-/low}/Lin^{-}$ phenotype.[66]

The expression of cell surface marker CD133 is also reported to be of significance and prognostic value for identifying CSCs in breast tumors, especially when combined with $CD44^+$.[73-75] CD173 (H2) and CD174 (Lewis Y) are cell surface carbohydrate antigens that are expressed to varying extents on different human carcinomas. Co-expression of CD173 and CD174 with CD44 is another cell surface marker combination proposed to identify breast CSCs.[76] Similar to CD173 and CD174, CD176 is also a cell surface carbohydrate antigen that has been reported to be co-expressed with CD44 and CD133 in breast carcinoma.[77] Another study has shown that in BRCA1 (breast cancer-associated gene 1)-mutant breast cancer cell lines, a small subpopulation of cancer cells expressing $CD24^+/CD29^+$ (β integrin) or $CD24^+/CD49f^+$ (α6 integrin) surface markers exhibited enhanced proliferation and colony forming ability in vitro and increased tumor generating ability in vivo. In addition, purified $CD24^+/CD29^+$ cells exhibit self-renewal capability, and as low as 500 cells could reconstitute the heterogeneity of the parent cancer cells in vivo, which is strongly indicative of a CSC population.[78] Shipistin et al. confirmed that CD201, which is also known as protein C receptor (PROCR), was expressed on 100% of $CD44^+$ breast cancer cells and was used as a cell surface marker to isolate CSCs from primary invasive breast cancer tumors.[79] In addition, high PROCR expression was also reported to associate with poor prognosis in clinical patients.[79] See **Table 1.2** for a listing of breast CSC surface markers.

1.2.3 Colorectal cancer

Dalerba et al. have isolated colorectal CSCs from specimens using cell surface markers CD44 and EpCAM.[80] When purified $CD44^+/EpCAM^{high}$ epithelial cells (**Table**

1.2) were injected into immunodeficient mice, the engrafted tumors yielded the differentiated phenotype profile as well as the morphologic heterogeneity of the parent lesions from which the $CD44^{+}/EpCAM^{high}$ epithelial cells were isolated. Furthermore, the authors also reported $CD166^{+}$ as a co-marker that could be used for validation of colorectal CSCs in both xenografts and primary tumors, and the $CD44^{+}/EpCAM^{high}/CD166^{+}$ phenotype was consistent with poor prognosis.[80] However, the CD44/EpCAM marker phenotypes were not the first reported colorectal CSCs. Prior studies had first indicated that CD133 was a potential cell surface CSC marker in primary human colorectal cancer,[81,82] but more recent findings by Shmelkov et al. have shown that both $CD133^{+}$ and $CD133^{-}$ populations are tumorigenic and contain tumor-initiating cells.[83] In order to explain this discrepancy, Du et al. have suggested that, unlike CD44, a surface protein that is of functional importance for the survival of CSCs, CD133 has not been found to have any essential functions associated with the growth and survival of colorectal CSCs.[84] Although $CD44^{+}/EpCAM^{high}/CD166^{+}$ is a relatively more reliable marker for colorectal CSCs than $CD133^{+}$, some exceptions have also been documented. Lugli et al. reported that the loss of this combined marker ($CD44^{+}/EpCAM^{high}/CD166^{+}$) was rather linked to an aggressive tumor phenotype.[85,86] Studies have also shown that CD49f, which has been reported as a CSC marker in breast cancer,[78] is expressed on colon cancer cells, and that even higher levels of CD49f expression are observed with $CD44^{+}$ cells, a known marker of colorectal CSCs.[80] Additionally, $CD133^{+}/CD24^{+}$ has been identified as a colorectal CSC marker.[87] See **Table 1.2** for a listing of colorectal CSC surface markers.

1.2.4 Liver cancer

The incidence of hepatocellular carcinoma (HCC) cases has risen by 3% every year since 1992, and the 5-year survival rate ranges from 14% to 26% depending on the stage of diagnosis.[18] In spite of the intensive research efforts devoted to the discovery of new HCC drugs, tumor relapse is still observed in the majority of cases.[88] The recent identification of liver CSCs has yielded new targets for HCC drug discovery efforts, which, if successful, may help to address the problem of disease relapse.

The $CD133^+$ phenotype was the first reported putative HCC CSC population.[89] In this report by Ma et al. $CD133^+$ HCC cells exhibited greater colony-forming capacities and higher proliferation rates than $CD133^-$ HCC cells, as well as the ability to generate new tumors in both in vitro and in vivo models. Additionally, in $CD133^+$ tumor cells, the expression level of stemness genes such as those involved in Wnt/β-catenin, Notch, and Hedgehog/SMO signaling were largely upregulated, indicating those $CD133^+$ tumor cells were putative HCC CSCs. The $CD133^+$ population was further characterized for other common CSC markers and CD34 and CD44 were found to be upregulated when compared with the $CD133^-$ population.[89] Another well-established cell surface marker of HCC stem cell is $CD44^+$. Within the HCC $CD133^+$ population, $CD44^+$ cells were found to be more tumorigenic than $CD44^-$ cells in NOD/SCID mouse model. Recent studies also revealed that the blocking of CD44 function by treatment with a CD44 specific monoclonal antibody might be a potential strategy to eradicate liver CSCs[90] (see section 1.3). Moreover, the cell surface carbohydrate antigen CD176 was found to co-express with CD44 at a high rate on the surface of HCC stem cells in both cancer cell lines and surgical specimens of malignant tumors.[77] Besides CD133 and

CD44, EpCAM was identified as an early biomarker of HCC CSCs.[91,92] The sorted $EpCAM^+$ subpopulation of HCC cells yielded more colonies in clonogenicity assays than the sorted $EpCAM^-$ cells from the same cell line. Further in vivo evaluation in mouse models indicated that as little as 100 $EpCAM^+$ HCC cells were needed to generate a new tumor, and $EpCAM^+$ cells retained the ability to differentiate into both $EpCAM^+$ and $EpCAM^-$ cells, while $EpCAM^-$ cells always sustained their phenotype during cell propagation.[91] Additionally, CD133 expression was observed in both $EpCAM^+$ and $EpCAM^-$ populations, indicating that EpCAM functions as a better indicator of the CSC population.[92] Recently, CD13 (alanine aminopeptidase), which is a membranebound enzyme, has been identified as a marker for semiquiescent CSCs and a potential therapeutic target for liver cancers. $CD13^+/CD133^+$ and $CD13^+/CD90^-$ populations were observed to be extremely tumorigenic, requiring only 100 cells for tumor formation upon transplantation.[93] In a xenograft mouse model, CD13 inhibition, which was achieved with either a CD13 neutralizing antibody or by the CD13 inhibitor Ubenimex, repressed tumor-initiating and self-renewing capability of the majority of CSCs[93] (see section 1.3). CD90 (Thy-1) has also been identified as a CSC marker in HCC cell lines.[94] In comparison to $CD90^-$ cells, $CD90^+$ cells sorted from HCC cells lines were found to exhibit strong tumorigenic capacity, and the subpopulation of cells with $CD90^+/CD45^-$ phenotype could generate tumor nodules in an immunodeficient mouse model.[94] OV6, which is a marker of hepatic progenitor (oval) cells, has been shown to be another CSC marker in HCC cells. $OV6^+$ HCC cells are capable of generating new tumors in vivo and show substantial resistance to standard chemotherapeutic drugs compared with $OV6^-$ HCC cells. Furthermore, the inhibition of

the Wnt/β-catenin signaling pathway, which is known to be important for the survival of CSCs,[95] decreases the population of $OV6^+$ cells. The $OV6^+$ cell population also gained higher proliferation potential after β-catenin activation.[96] See **Table 1.2** for a listing of liver CSC surface markers.

1.2.5 Pancreatic cancer

Pancreatic cancer is one of the deadliest forms of human cancers. Currently, there are no known methods of early detection, and the average 5-year survival rate is 6%.[18] The mortality rate of this disease approaches 100% because of its characteristically high resistance to radiation and chemotherapy, and the tendency of early systemic dissemination.[97] In spite of the significant advances in cancer biology over the past decade, the efficacy of drugs to treat pancreatic cancer has not substantially improved.[98] Targeting the pancreatic CSC population could allow development of more efficacious therapies to combat this lethal disease.

A pancreatic CSC population was identified only recently.[98] A small population (0.2–0.8%) of highly tumorigenic pancreatic cancer cells with the $CD44^+/CD24^+/EpCAM^{high}$ phenotype (**Table 1.2**) from primary human pancreatic adenocarcinomas was xenografted into immunocompromised mice. In comparison with non-tumorigenic cells, the $CD44^+/CD24^+/EpCAM^{high}$ pancreatic cancer cells exhibited a 100-fold increase in tumorigenic potential, and as few as 100 such cells could reconstitute tumors that were indistinguishable by histology from the original ones.[98] In related studies, Hermann et al. demonstrated that $CD133^+$ expression on the surface of pancreatic cancer cells was consistent with increased tumorigenicity and high resistance to standard

chemotherapy. In addition, they further revealed that a unique small population of CSCs bearing the $CD133^{+}$/ $CXCR4^{+}$ phenotype determined the metastatic potential of the tumor. Although $CD133^{+}/CXCR4^{+}$ cells and $CD133^{+}/CXCR4^{-}$ cells showed similar tumorigenicity when xenografted into nude mice, only the $CD133^{+}/CXCR4^{-}$ cells eliminated tumor metastasis.[99] See **Table 1.2** for a listing of pancreatic CSC surface markers.

1.2.6 Melanoma

Approximately 70,000 new cases of human melanoma and 9,000 melanoma-related deaths were expected in the United States in 2011[18]. Although melanoma is not a leading cause of cancer-related mortality, it is one of few cancer types associated with both annual increases in incidence and death rate[100]. Human malignant melanoma cells are highly aggressive and drug resistant and contain cell populations with enhanced tumorigenicity.[101] The discovery of putative CSCs in melanoma cell lines was first reported in 2005,[101] preceding their subsequent isolation and characterization from cell lines and surgical specimens.[102] Nestin (**Table 1.2**), which is an intermediate filament protein, was first described as a potential stem cell marker in melanoma cell lines.[103] Nestin expression was associated with aggressive behavior of the malignant tumors and was found to be upregulated during the development of invasive melanoma from banal nevi (a benign chronic lesion of the skin).[103] Co-expression of nestin with CD133 has been described in context with stem cell populations in circulating melanoma cells, which are closely related to their metastatic potentials.[104] Monzani et al. first utilized CD133 as a cell surface marker to separate melanoma stem cells. Their data showed that

in contrast to $CD133^-$ cells, $CD133^+$ melanoma cells were highly tumorigenic and able to generate a Mart-1 (a typical melocytic marker) positive tumor when implanted into NOD/SCID mice. In the same study, they also revealed that melanoma cells expressing both CD133 and ABCG2 (ATP-binding cassette sub-family G member 2) were able to self-renew and differentiate into astrocytes and mesenchymal lineages under specific conditions, demonstrating the utility of ABCG2 as a CSC marker.[102] Schatton et al. identified a small subpopulation of melanoma cells that were enriched for human malignant melanoma-initiating cells, which were defined by the expression of P-glycoprotein ABCB5, a well-known chemoresistance mediator. $ABCB5^+$ melanoma cells were found to be highly aggressive, possess greater tumorigenic capacity than $ABCB5^-$ cells, and could re-establish clinical tumor heterogeneity. ABCB5 has also been studied as a target of anticancer therapy[105,106] (see section 1.3). See **Table 1.2** for a listing of melanoma CSC surface markers.

1.2.7 Brain cancer

Malignant brain tumors are among the deadliest human cancers. Glioblastoma (GBM) multiforme is the most common primary brain tumor in adults with 12,000 deaths in the United States annually.[107] In children, glioblastoma multiforme occurs less frequently, accounting for 7–9% of all intracranial tumors, yet the median survival after diagnosis is 50 weeks.[108] Currently, there is a scarcity of effective treatments for brain cancers, which is attributable to the sensitive environment of the disease and the inability of many drugs to permeabilize the blood–brain barrier. Unfortunately, most drugs that can access brain malignancies are inefficient at eradicating the tumor cells and

frequently leave behind a side population of radio- and chemoresistant cells. The existence of this side population provides a mechanism for disease relapse,[33] and recent studies strongly suggest that brain tumors have an established CSC hierarchy.[109,110] Drug targeting of brain CSCs may yield better therapy outcomes.

In 2003, Singh et al. first identified CD133 as a CSC marker (**Table 1.2**) in glioblastomas and medulloblastomas.[111] Studies of human medulloblastoma specimens from children have also revealed a $CD133^+$ subpopulation of cells that is positive for nestin.[112] Sorted $CD133^+$ populations of childhood medulloblastoma specimens have demonstrated the stem cell characteristics of self-renewal and differentiation, and subjection of these cells to differentiation conditions resulted in the loss of the $CD133^+$ marker.[111] The tumorigenicity of $CD133^+$ human donor medulloblastoma and glioblastoma cancer cells were evaluated in NOD/SCID mice, and as few as 100 cells were required for the development of new tumors of the same phenotype.[112]

Another glioblastoma CSC marker that has been identified is integrin A2B5, a polysialo ganglioside. Tchoghandjian et al. used A2B5 to characterize CSC populations in glioblastoma samples using magnetic micro-beads and FACS. In addition, the authors sorted the cells for a secondary known CSC marker, CD133. $A2B5^+$ populations expressed characteristic features of CSCs regardless of CD133 expression, and both $A2B5^+/CD133^+$ and $A2B5^+/CD133^-$ populations were highly tumorigenic, requiring only 1,000 cells for development of a new tumor of the same phenotype. However, only the $A2B5^+/CD133^-$ population of cells was found to be invasive within the brain.[113] Studies by Ogden et al. have suggested that only the $A2B5^+$ phenotype is characteristic of glioblastoma CSCs, and CD133 positivity is not indicative of a CSC population.[114] In

support of the evidence that $CD133^+$ cells are putative CSCs, studies by Wang et al. found that $CD133^+$ glioblastomas were aggressive tumors and were typified by the onset of angiogenesis, shorter survival times, and metastatic potential. However, the $CD133^-$ populations were also shown to be capable of differentiating into $CD133^+$ cells, which suggests that $CD133^-$ are stem cell-like.[115] Although characterization of universal diagnostic markers for CSCs is the ultimate goal for the development of targeted therapies, these contradictory results with CD133 clearly illustrate that patients can express different surface markers for the same disease and/or that multiple CSC populations can be present in glioblastoma specimens.

L1CAM, a transmembrane adhesion protein found in $CD133^+$ glioma cell populations, was identified as a brain CSC marker in 2008.[116] D456MG pediatric glioblastoma xenografts and primary human samples were utilized to study the role of L1CAM.[117] Neurosphere formation, a cellular morphology consistent with a stem cell-like state, was quantified as a measure of the self-renewal properties of the CSC population. Targeting L1CAM with shRNA decreased the ability of the $CD133^+$ cells to form neurospheres, indicating that the $L1CAM^+/CD133^+$ population was the in vitro CSC population. In vivo studies conducted in nude mice also showed that knockdown of L1CAM with shRNA resulted in a reduction in tumor size and increased survival.[116]

Stage-specific embryonic antigen-1 (SSEA-1), or CD15, has also been identified as a potential marker of GBM CSCs.[118] Utilizing primary human samples, $SSEA\text{-}1^+$ cells were isolated and characterized for self-renewal, differentiation, and tumorigenicity. The presence of $CD133^+$ was also investigated in the $SSEA\text{-}1^+$ populations in early studies; however, $SSEA\text{-}1^+/CD133^+$ and $SSEA\text{-}1^+/CD133^-$ were

both shown to have CSC characteristics. Sorting of primary human GBM specimens for only SSEA-1 expression and xenograftment of isolated cells into NOD/SCID mice revealed that SSEA-1$^+$ cells exhibited at least 100-fold greater tumorigenic potential than SSEA-1$^-$ GBM cells. Therefore, SSEA-1$^+$ can be used to identify CSC populations in GBM.[118] SSEA-1 has also been identified as a medulloblastoma CSC marker.[119] See **Table 1.2** for a listing of brain CSC surface markers.

1.2.8 Lung cancer

Lung cancer is the most common, yet preventable, cancerrelated death worldwide, resulting in more mortalities than colon, breast, and prostate cancers combined. The 5-year survival rate for small cell lung carcinoma is 6% while nonsmall cell carcinoma is 17%.[18] Current lung cancer therapies are usually transient and fail to completely eradiate the tumor, causing resistance. One potential hypothesis for drug resistance to chemotherapy is the presence of drugrefractory lung CSC populations in the tumor masses.[120] Eramo et al. identified CD133$^+$ CSC subpopulations (**Table 1.2**) in small cell and non-small cell lung cancer from primary human donors. CD133 expression was observed on the surface of 0.32–22% of lung cancer cells by flow cytometry analyses, which varied depending on different disease stages of the sample. In vivo analysis showed that tumor formation required only 1,000 cells to be implanted into SCID mice, while differentiated cell populations injected at 50,000 cells per animal failed to produce tumors.[121] CD176 has also been identified as a potential marker for lung CSC populations and has been observed in combination with CD133 and CD44 cell surface markers. CD176$^+$/CD133$^+$ and CD176$^+$/CD44$^+$ phenotypes were observed after

sorting cells for CD176 expression, and $CD176^+$ cell populations were found to exhibit features of CSCs, such as tumorigenicity. These results imply that $CD176^+$ may be used as a potential lung CSC marker.[77] See **Table 1.2** for a listing of lung CSC surface markers.

1.2.9 Bladder cancer

Bladder transitional cell carcinoma (BTCC) is the second most prevalent cancer of the urinary tract.[122] Five-year survival rates for BTCC vary by stage of development, ranging from 6% to 97%.[18] Traditional therapy consists of surgery, radiation, and chemotherapy,[123] but if disease becomes invasive, then treatment outcomes are typically poor due to metastasis.[124] The development of diagnostic markers and new therapies for BTCC is currently needed.

Yang and Chang have identified a subpopulation of BTCC samples from primary human donors that display a $CD44^+/EMA^-$ (epithelial membrane antigen) phenotype (specifically the isoform CD44v6; **Table 1.2**). $CD44^+/EMA^-$ populations were shown to overexpress Bmi-1 and EZH2, which are proteins that play a role in self-renewal of normal bladder stem cells. $CD44^+/EMA^-$ cells also were able to form colonies and proliferate in vitro, which are characteristic features of CSCs.[125]

Chan et al. have also postulated that BTCC CSCs can be characterized by the cell surface phenotype $Lin^-/CD44^+$/cytokeratin $(CK)5^+/CK20^-$. Tumors from primary human donors were sorted for $CD44^+$ and $CD44^-$ cells and then transplanted into immunocompromised mice ($RAG2^-/\gamma c^-$). The $CD44^+$ cells were found to be more tumorigenic, requiring only 100–1,000 cells to form tumors, while the $CD44^-$ population

required 200,000–500,000 cells to elicit tumors in mice. Immunofluorescence analysis of $CD44^+$ xenografts showed co-expression of CK5 and lack of expression of CK20 (phenotype $Lin^-/CD44^+/CK5^+/ CK20^-$), and this marker phenotype was deemed to be the BTCC CSC population. The authors also queried for other common CSC cell surface markers and discovered that CD47 is highly expressed on $CD44^+$ cells. CD47 inhibits phagocytosis by macrophages, allowing for pathogenesis of the bladder cancer.[124]

Hoechst 33342 dye is a widely used indicator of side populations with potential CSC characteristics.[126] ATP binding cassette (ABC) and multidrug resistance efflux pumps are responsible for the elimination of Hoechst 33342 dye, as well as cytotoxic drugs, from cells. This process is detectable by FACS and allows for the identification and isolation of subpopulations of cells displaying these characteristics that are common of CSCs.[126,127] ABC-G2 transporters were detected in the BTCC cell line T24. ABC-$G2^+$ and ABC-$G2^-$ cells were cultured in vitro, and their growth characteristics were evaluated. ABC-$G2^+$ cells demonstrated consistent proliferation, whereas the ABC-$G2^-$ did not. Side populations of ABC-$G2^+$ also were able to differentiate into ABC-$G2^-$ cells, which further supports the hypothesis that ABC-$G2^+$ is a marker of BTCC CSCs.[126] See **Table 1.2** for a listing of bladder CSC surface markers.

1.2.10 Prostate cancer

Prostate cancer is the most commonly diagnosed malignancy and second leading cause of death in men in the United States.[18] More than 80% of men will develop prostate cancer in their lifetime, and most diseases will not be diagnosed.[128] Prostate cancer is routinely treated by hormone ablation therapy, but this therapy regimen fails

when the disease progresses to a hormone-refractory state.[129] Currently, cytotoxic small molecules are the only therapeutic regimen able to improve outcomes for patients with hormone-refractory prostate cancers.[130] Identification of CSC surface markers could provide a foundation for the development of next-generation drugs that target prostate CSCs.[129]

The first CSC surface marker identified for prostate cancer was CD44 (**Table 1.2**). In 1997, Liu et al. reported their observation that $CD44^+$ prostate cancer cells were negative for prostate-specific antigen (PSA) and prostate acid phosphatase secretion, which are proteins that are produced during cancer cell differentiation. On the other hand, when $CD44^+$ prostate cancer cells were co-cultured with stromal cells, the secretion of PSA was detected, indicating that the interaction between stromal cells and $CD44^+$ prostate cancer cells stimulated the differentiation ability of the latter, since PSA production was not detected when either stromal cells or $CD44^+$ prostate cancer cells when cultured alone.[131] Collins et al. demonstrated that prostate CSCs could be identified from human specimens with a $CD44^+/\alpha2\beta1^{high}/CD133^+$ phenotype, and this population comprised 0.1– 0.3% of the total amount of cells in the tumor. In a colony-forming assay, the $CD44^+/\alpha2\beta1^{high}/CD133^+$ population yielded 3.7-fold greater number of colonies compared with the total cell population and more than 30-fold greater number of colonies compared with $CD44^+/\alpha2\beta1^{high}/CD133^-$ or $CD44^+/\alpha2\beta1^{low}$ cells, which suggests the $CD44^+/\alpha2\beta1^{high}/CD133^+$ phenotype has the ability to self-renew.[28] Patrawala et al. performed in vivo studies in NOD/SCID mice utilizing prostate cancer cell lines that were enriched for the $CD44^+/\alpha2\beta1^{high}$ combination phenotype.[132,133] They found that the $CD44^+/\alpha2\beta1^{high}$ population had greater tumorigenicity than other

populations isolated ($CD44^{+}/\alpha2\beta1^{low}$, $CD44^{-}/\alpha2\beta1^{high}$, $CD44^{-}/\alpha2\beta1^{low}$), further supporting the evidence that the $CD44^{+}/\alpha2\beta1^{high}$ phenotype is the CSC population.[133]

Mulholland et al. later confirmed that the $Lin^{-}/Sca\text{-}1^{+}/CD49f^{high}$ subpopulation of prostate cancer cells were CSCs in a murine prostate $PTEN^{-}$ model (PTEN is a tumor suppressor gene in the protein kinase B pathway).[129] The loss of PTEN activity is strongly associated with the initiation and metastasis of prostate cancer.[134] Tissue samples were taken from murine PTEN mutant prostate tumor grafts on SCID mice after 6–8 weeks, digested into single-cell suspensions, and sorted by FACS. Through a systematic study of various potential surface markers, Sca-1 and CD49f were identified as surface markers of prostate CSCs. Sorted cells ($Lin^{-}/Sca\text{-}1^{+}/CD49f^{high}$ and $Lin^{-}/Sca\text{-}1^{+}/CD49^{flow}$) were then injected into SCID mice and only $Lin^{-}/Sca\text{-}1^{+}/CD49f^{high}$ cells induced tumor growth.[129] See **Table 1.2** for a listing of prostate CSC surface markers.

1.2.11 Ovarian cancer

The most lethal disease of the female reproductive tract is ovarian cancer.[135] High mortality rates occur due to the difficulty in diagnosing early stage ovarian cancer as well as the high prevalence of drug-refractory relapse after initial treatment, which is likely a result of CSC subpopulations that survive therapy.[136] Ovarian cancer 5-year survival rates vary depending on the stage of development of the tumor. Early stage diagnosis, when the disease has yet to metastasize, has a 5-year survival rate of 73%, while late-stage ovarian cancer diagnosis results in a 28% survival rate.[18]

Zhang et al. first identified CD44 as a potential ovarian CSC surface marker in 2008. Analysis of human ovarian specimens revealed a small population (0.14–0.2%) of

$CD44^+/CD117^+$ cells (**Table 1.2**) that were highly tumorigenic and demonstrated self-renewal by spheroid formation. Tumorigenicity was measured by engraftment of $CD44^+/CD117^+$ and $CD44^-/CD117^-$ subpopulations into nude mice. The $CD44^+/CD117^+$ subpopulation was able to repopulate the tumor following injection of only 100 cells, whereas the isolated $CD44^-/CD117^-$ phenotype required 500,000 cells for tumor development after 3 months.[135]

Ferrandina et al. identified $CD133^+$ subpopulations as ovarian CSCs in primary human samples. The $CD133^+$ subpopulation was 4.7-fold more active in a colony-forming assay, which demonstrated replicative capacity.[137] Work by Curley et al. verified the presence of a $CD133^+$ subpopulation with tumor-initiating properties and found that 0.2 – 12.5% of the tumors expressed this phenotype.[138]

$CD24^+$ has also been characterized as a potential surface marker of human ovarian CSCs. Two weeks after the plating of isolated $CD24^+$ ovarian cancer cells, analysis of the cell population revealed both $CD24^+$ and $CD24^-$ phenotypes, which suggests that $CD24^+$ cells are CSCs due to their ability to self-renew and differentiate. Conversely, the same experiment performed with $CD24^-$ cells failed to yield $CD24^+$ cells after the same amount of time in culture. Additional in vivo studies demonstrated that only 5,000 $CD24^+$ cells were needed for tumor formation after injection into nude mice, whereas $CD24^-$ cells injected at the same concentration were unable to generate tumors.[139] Therefore, $CD24^+$ cells are more tumorigenic than $CD24^-$ cells.

To add to the growing number of ovarian CSC markers, Wei et al. isolated a triple surface marker phenotype, $CD44^+/CD24^+/EpCAM^+$, which best characterized the most proliferative cell subpopulation when compared with all other marker

combinations. Cells lines OVCAR-5, SKOV-3, and IGROV-1, as well as primary human donor samples were used for experiments. Colony-formation assays were performed on $CD44^+/CD24^+/EpCAM^+$ sorted cells to measure proliferation rates and to characterize self-renewal properties. In vivo studies were performed comparing $CD44^+/CD24^+/EpCAM^+$ and $CD44^-/CD24^-/EpCAM^-$ phenotypes by injection into NOD/SCID mice. These studies demonstrated that as few as 100 $CD44^+/CD24^+/EpCAM^+$ cells injected in NOD/SCID mice were capable of tumor formation, and $CD44^+/CD24^+/EpCAM^+$ cells grew tumors faster and more aggressively than the $CD44^-/CD24^-/EpCAM^-$ population.[140] Consequently, the $CD44^+/CD24^+/EpCAM^+$ phenotype was deemed to be more tumorigenic and likely a CSC population. See **Table 1.2** for a listing of ovarian CSC surface markers.

Solid Tumor Type	Marker(s)	Reference
Breast	$CD44^+/CD24^{-/low}/Lin^-$	[66, 69]
	$CD44^+/CD24^{-/low}/EpCAM^{high}$	[66]
	$ALDH1^+/CD44^+/cytokeratin^+$	[71]
	$CD90^+/CD24^+$	[72]
	$CD133^+/CD44^+$	[73-75]
	$CD173^+/CD174^+/CD44^+$	[3, 76]
	$CD176^+/CD44^+$	[5, 77]
	$CD176^+/CD133^+$	[6, 77]
	$CD24^+/CD29^+$	[7, 8, 78]
	$CD24^+/CD49f^+$	[78]
	$CD44^+/CD201$ (PROCR)$^+$	[79]
Colorectal	$CD44^+/EpCAM^{high}$	[80]
	$CD44^+/EpCAM^{high}/CD166^+$	[80]
	$CD44^+/CD49f^+$	[80]
	$CD133^+$	[81, 82]
	$CD44^+$	[84]
	$CD133^+/CD24^+$	[13, 87]
Liver	$CD176^+/CD44^+$	[77]
	$CD133^+$	[89]
	$CD133^+/CD44^+$	[90]
	$EpCAM^+$	[91, 92]
	$CD13^+/CD133^+$	[93]
	$CD13^+/CD90^-$	[7, 93]
	$CD90^+/CD45^-$	[94]
	$OV6^+$	[96]
Pancreatic	$CD44^+/CD24^+/EpCAM^+$	[20, 98]
	$CD133^+$	[99]
	$CD133^+/CXCR4^+$	[99]
Skin	$CD133^+$	[102]
	$CD133^+/ABCG\text{-}2^+$	[25, 102]
	$Nestin^+/CD133^+$	[26, 27, 104]
	$ABCB5^+$	[28, 106]
Brain	$CD133^+$	[111]
	$CD133^+/Nestin^+$	[112]
	$CD133^+/A2B5^+$ and $CD133^-/A2B5^+$	[113]
	$A2B5^+$	[30, 114]
	$CD133^+/L1CAM^+$	[31, 116]
	$SSEA\text{-}1^+$	[118]
Lung	$CD176^+/CD44^+$	[32, 77]
	$CD176^+/CD133^+$	[77]
	$CD133^+$	[121]
Bladder	$Lin^-/CD44^+/CK5^+/CK20^-$	[124]
	$CD47^+/CD44^+$	[124]
	$CD44v6^+/EMA^-$	[125]
	$ABC\text{-}G2^+$	[36, 126]
Prostate	$CD44^+/\alpha_2\beta_1{}^{high}/CD133^+$	[28]
	$Lin^-/Sca\text{-}1^+/CD49f^{high}$	[37, 129]
	$CD44^+/\ \alpha_2\beta_1{}^{high}$	[133]
Ovarian	$CD44^+/CD117^+$	[135]
	$CD133^+$	[137, 138]
	$CD24^+$	[139]
	$CD44^+/CD24^+/EpCAM^+$	[140]

Table 1.2. Previously reported CSC markers for human solid tumors.

1.3 The chemical biology and drug targeting of cell surface markers on cancer stem cells

The repertoires of cell surface macromolecules found on CSCs are widely used as markers for characterizing CSC populations (described previously). In addition to these diagnostic applications, the unique molecules that are presented on the surfaces of CSCs are valuable targets for drug delivery. However, many of the surface markers that are presented on CSCs are known to also be expressed at varying levels on the surfaces of normal, non-cancerous cells. Some of the reported CSC surface markers, in addition, have not been rigorously queried for expression across panels of non-cancerous tissue. Therefore, cell surface markers that are selected for targeted drug delivery applications must be evaluated for cancer cell selectivity during development studies to probe for off-target effects.[8] In the following section we review, where known, several of the established chemical and structural features that are characteristic of the most common CSC surface molecules, as well as previous efforts to deliver therapeutic agents to CSCs by targeting their unique cell surface markers. We recognize that an equally exciting area of intense investigation involves the identification of small molecules that possess CSC inhibitory properties, such as the recent reports of the anti-CSC activities of the natural products parthenolide and salinomycin.[19,141] However, we have focused here on those therapeutic molecules that target CSC surface markers as part of their mechanism of inhibition.

– ***Targeting of CD133.*** CD133 is a five-transmembrane protein consisting of 865 amino acid residues. It consists of two extracellular glycosylated loops and two cytoplasmic loops, bringing the final molecular weight of CD133 to 120 kDa.[142] Under

bioenergetic stresses, such as hypoxic conditions, CD133 expression is upregulated significantly.[143] No ligands or signaling mechanisms have been defined for CD133. Although the biological functions of CD133 have not been fully elucidated, the localization of CD133 to protrusions in the plasma membrane suggests a possible role in membrane organization.[142] The rationale for this hypothesis is the observation that CD133 is commonly located on cell membrane protrusions, such as microvilli-like structures on epithelial cells, which are important for increasing the surface area and the reabsorption characteristics of those cells.[144,145] In addition to its presence on CSCs from multiple diseases (vide supra), CD133 is commonly found as a marker of somatic stem cells, ranging from hematopoietic, neural, prostate, kidney, liver, and pancreas.[146]

CD133 is one of the most prominent CSC surface markers. Although a multitude of monoclonal antibodies against CD133 have been previously described, most commercially available CD133 antibodies have limited applicability because they only recognize glycosylated $CD133^+$ epitopes.[147] Consequently, the majority of CD133 antibodies fail to identify the entire $CD133^+$ population. Nonetheless, a repertoire of CD133-recognizing antibodies is available for various uses.

Clone7 is an anti-human $CD133^+$ monoclonal antibody that recognizes glycosylated, as well as non-glycosylated, epitopes of CD133. Clone7 allows for multiple experiments with CD133 to be performed regardless of post-translational glycosylation status. Clone7 can be utilized in Western blotting, immunofluorescence, flow cytometry, and immunohistochemistry applications.[148]

Single-walled carbon nanotubes functionalized with anti-CD133 antibodies to actively target $CD133^+$ have been developed by Wang et al. Selective uptake of the

nanotubes was observed only in the $CD133^+$ population, and phototherapy eradication of the $CD133^+$ cells bearing the nanotubes was achieved by absorption of 808-nm near IR light.[149] This study has yielded a potential photothermal approach to selectively target $CD133^+$ glioblastoma cells.

Lipid nanocapsules functionalized with anti-CD133 antibodies have been shown to target $CD133^+$ CSCs, in recent work by Bourseau-Guilmain et al. Selective uptake by the $CD133^+$ population was observed by fluorescence of Nile red, which was loaded into the lipid nanocapsules. Loading of hydrophobic drugs into the lipophilic cores of the nanocapsules is now being tested for the direct therapeutic targeting of $CD133^+$ tumors with the goal of diminished side effects.[150]

– ***Targeting of EpCAM***. Epithelial cell adhesion molecules (EpCAM) are single transmembrane glycoproteins that play major roles in cell-cell adhesion, both constructively and disruptively.[151] EpCAM is specifically expressed on epithelial cancers such as breast, colorectal, pancreatic, liver and ovarian tumors and can interfere with cell-cell adhesion in various ways. One interference method is the disruption of the bonding of α-cadherin and F-actin, which translates into a loss of E-cadherin-mediated cell-cell adhesion.[152] Alternatively, EpCAM was originally observed to prevent cell scattering due to cellular adhesion characteristics.[153] Because of this dual role in adhesion of cells, EpCAM expression is both tumor promoting as well as tumor suppressive. The role EpCAM takes within a tumor is dependent on the tumor type.[151]

Catumaxomab (*Removab*®, developed by Fresenium Biotech GmbH and Trion Phama) is a rat–mouse hybrid monoclonal and tri-functional antibody against EpCAM, CD3 antigen in T cells, and antigen-presenting cells (APC; such as microphages, natural

killer cells, and dendritic cells).[154,155] Its capability of binding three different types of cells comes from its unique structure: It is a heterozygous antibody with one chain of mouse anti-EpCAM antibody and one chain of rat anti-CD3 antibody. The heavy-chain Fc region of both chains can bind to the Fc receptors on APCs. Catumaxomab is more than 1,000-fold more potent than a monospecific anti-EpCAM antibody in killing cancer cells.[154,155] Catumaxomab does not require the utilization of any additional reagent(s) to stimulate the immune response. The different specificities of the antigen binding sites of the two antibody chains enable simultaneous recognition of both tumor cells (especially CSCs) and T cells, and the functionalized heavy chain Fc domain is able to recruit and stimulate APC, resulting in the initiation of complex immune reactions. In a pivotal phase II/III clinical study, Catumaxomab treatment lead to activation of peritoneal T cells and a completion elimination of $CD133^{+}/EpCAM^{+}$ cells from the peritoneal fluid of malignant ascites patients.[156,157] Catumaxomab was approved in the European Union in 2009 and is undergoing Phase III clinical trials in the United States for the treatment of malignant ascites, ovarian cancer, and gastric cancer.[158] In addition to Catumaxomab, there are other bi-functional or trifunctional EpCAM-targeting antibodies undergoing preclinical studies or clinical trials.

MT110 (developed by Micromet GmbH) belongs to a class of single-chain antibodies called bispecific T cell engager or BiTE. MT110 was constructed by coupling the antigen binding domains of α-CD3 and α-EpCAM monoclonal antibodies, yielding a hybrid antibody with specificity for both EpCAM and CD3.[159] A BiTE antibody enables the generation of a cytolytic synapse between a cytotoxic T cell and a target cell that binds to the BiTE antibody.[160] In the case of MT110, the target cell is a tumor cell that

expresses the EpCAM cell surface marker. The formation of the cytolytic synapse induces T cells for redirected lysis of the EpCAM+ target cell at pico- to femtomolar concentrations.[159] MT110 has been shown to have high antitumor activity in various animal models[159,161] and is capable of completely eliminating colorectal CSCs in cell culture and in animal models.[162] MT110 is currently in Phase I clinical trials in the United States for lung and gastrointestinal cancers.[163]

Edrecolomab (*Mab17-1A, Panorex*®, developed by Cancer and Leukemia Group B) was one of the first monoclonal antibodies administered to humans for cancer therapy. Edrecolomab is a low-affinity murine IgG2a monoclonal antibody that targets the cell-surface glycoprotein EpCAM. Because of the extensive basal level expression of EpCAM molecules on normal epithelial cells,[164] the toxicity of EpCAM-targeting antibodies was viewed as a potential obstacle for the development of this class of therapies,[165] Since the expression level of EpCAMon the surface of CSCs is much higher than it is on the surface of normal epithelial cells, the designed low-affinity edrecolomab decreases the possibility of off-target effects while maintaining efficacy for targeting CSCs, which makes edrecolomab a well-tolerated drug with a relatively wide therapeutic window.[165] Edrecolomab, which is thought to eliminate tumor cells by antibody-dependent cell-mediated cytotoxicity (ADCC) and/or complement-dependent cytotoxicity (CDC),[166,167] underwent Phase II–III clinical trials in the United States as a potential postoperative adjuvant treatment of stage II colon cancer. However, the clinical trial was terminated in 2005 because of lack of improvement of overall or disease-free survival.[168]

Adecatumumab (*MT201*, developed by Micromet GmbH) is a fully humanized, recombinant IgG1 monoclonal antibody that specifically binds to EpCAM with low affinity. It was designed to retain the safety profile, yet improve the antitumor potency of edrecolomab. MT201 exhibited EpCAM-specific CDC with potency similar to that of edrecolomab, but the efficacy of ADCC induction of MT201 was twofold greater than that of edrecolomab.[167] It also has been reported that the combination of adecatumumab and docetaxel is safe and efficacious in heavily pretreated advanced-stage breast cancer patients.[169] MT201 is now in Phase II clinical trials in the United States for the treatment of prostate, colorectal, and metastatic breast cancers.[167]

– ***Targeting of CD44.*** The lymphocyte adhesion receptor CD44, first described in 1983,[170] is a transmembrane glycoprotein that binds hyaluronate (HA).[171] CD44 was first cloned in 1989,[172] and the binding domain was crystallized in 2004 (PDB 1POZ),[173] CD44 is involved in many important cellular processes, including cell growth, survival, differentiation, and apoptosis.[174-176] CD44 plays a crucial role in cancer migration and matrix adhesion in response to the cellular microenvironment, and high CD44 levels are associated with increasing cellular aggregation and tumor metastatic potential.[171] The importance of CD44 in cancer cells, especially in CSCs, is closely related to its unique structure and function. The extracellular domain of CD44, which is a globular structure, contains two domains: a link domain and a HA binding domain.[171,177] Binding sites for microenvironment proteins, such as laminin, collagen, and fibronectin,[178,179] receptors such as E- and L-selectin,[180] and other glycosaminoglycans have also been characterized.[181] The transmembrane region of CD44 contains a glycolipid-enriched microdomain (GEM), which is responsible for the

oligomerization of CD44s.[182] The crosslinking and GEM association of CD44s, which is often induced by the binding of HA or other ligands, leads to a conformational change of the molecule and is important in CD44-mediated signal transduction.[183] The main function of the cytoplasmic domain of CD44 is to recognize its partner molecules ankyrin, ezrin, radixin, and moesin (ERM). ERM proteins are cytoskeleton proteins that regulate cell migration, cell shape, and protein resorting in the plasma membrane.[184] The unique structure of CD44 molecules indicates that they are functionally important to CSCs. CD44 regulates cancer cell adhesion and homing,[26] cell extravasation and migration,[185] the crosstalk between stem cells and their niche,[186] epithelial mesenchymal transition,[187] and the repression of cell apoptosis.[188] Each of these functions contributes to the observation that CD44 is one of the most prevalent surface markers in CSCs.[189] CD44 is a cell surface marker extensively expressed on the surface of a large range of CSCs including AML, bladder, breast, colorectal, liver, ovarian, pancreatic, and prostate cancers (**Tables 1.1** and **1.2**).

H90 is an anti-CD44 monoclonal antibody that was first reported by John Dick and colleagues in 2006 as a therapeutic approach to treat AML.[20] Currently, the majority of leukemia chemotherapeutics are antiproliferative drugs that target rapidly cycling leukemic cells. However, disease relapse is observed in more than 70% of adult patients, indicating that quiescent AML CSCs have not been effectively removed.[190] AML CSCs are more difficult to target than highly proliferative and differentiated leukemic cells due to their quiescent nature. However, the survival and self-renewal of AML CSCs requires attachment to extracellular niche proteins.[191] Thus, targeting the interaction between niche proteins and AML CSCs, which is mediated by the cell surface marker CD44, may

provide a mechanism to eradicate AML CSCs.[192] In vivo administration of H90 to NOD/SCID mice transplanted with human AML showed a significant decrease in leukemia repopulation.[20]

P245 is another CD44-specific monoclonal antibody with a design and targeting rationale similar to H90. Administration of P245 to human breast cancer xenografts markedly decreased the growth of tumor cells and effectively prevented tumor relapse after chemotherapy-induced remission. P245 is now under preclinical study for the treatment of breast cancer.[193] Both of the above CD44-specific antibodies also have the effect of inducing differentiation in CSCs.[26]

– ***Targeting of CD33.*** CD33 is a myeloid cell surface antigen that is expressed on leukemic blasts from 85% to 90% of AML patients,[44] and the combination phenotype $CD34^{+}/CD38^{-}/CD123^{+}/CD33^{+}$ is uniquely expressed on the surface of AML CSCs.[45] CD33 is a single transmembrane protein that is activated by phosphorylation.[194] CD33 functions as a putative adhesion molecule of monocytic and myeloid lineage cells and modulates sialic acid-dependent binding and cell differentiation.[44] In immune responses, CD33 acts as an inhibitory receptor of ligand bindinginduced tyrosine phosphorylation by recruiting cellular phosphatases to its SH2 domain and blocking signal transduction through hydrolysis of the phosphates of signaling molecules.[195,196] CD33 also induces apoptosis in acute myeloid leukemia through mechanisms that are not fully characterized.[197]

Gemtuzumab ozogamicin (*Mylotarg*®, developed by Wyeth and Pfizer) is a small-molecule–anti-CD33 monoclonal antibody conjugate. The small-molecule component of this drug is N-acetyl γ-calicheamicin dimethyl hydrazide, a stable

enediyne antitumor antibiotic that was identified from a screen of potent DNA alkylators.[198] The antibody component is a humanized IgG4 anti-CD33 antibody (hP67.6) that is conjugated to calicheamicin by an acidlabile hydrazone linker. Studies have shown that the antibody–drug conjugate exhibits good potency, as well as selectivity, which is attributed to its property of only releasing the DNA alkylator in the acidic environment of cellular lysosomes (i.e., it is stable in blood).[199,200] The antibody component of gemtuzumab ozogamicin (GO) is largely non-toxic and functions to facilitate the uptake of calicheamicin into $CD33^+$ AML cells. Once released, calicheamicin undergoes rearrangement to form a diradical metabolite that is capable of binding DNA and initiating single- and double-stranded DNA breaks, which results in cell cycle arrest or apoptosis.[201] GO was marketed as an AML therapeutic from 2000 to 2010 but was voluntary withdrawn from the market in June 2010 when postclinical trials showed an increasing number of deaths and a lack of benefit compared with other conventional cancer therapies.[202] Currently, the combination of GO and other chemotherapeutics are under various stages of clinical investigations.[203]

– ***Targeting of CD34 HSC antigen***. CD34 is a single transmembrane glycoprotein and belongs to the CD34 family of proteins.[204] CD34 was first identified as a surface marker of immature lymphohematopoietic progenitor cells in 1984.[205] Four years later, Berenson et al. reported that, following the transplantation of $CD34^+$ human marrow cells, hematopoietic systems were able to reconstitute in lethally irradiated baboons.[206] CD34 has been widely used as a surface marker for the identification of non-cancerous hematopoietic stem cells for over three decades[207] and, more recently, has been identified as a CSC marker for multiple diseases (vide supra). Besides

hematopoietic and leukemic stem and progenitor cells, CD34 is also widely expressed on the surface of vascular endothelial cells and mast cells.[207] In spite of the functional importance of CD34, the crystal structure of this protein remains unsolved. As a result, the structure and function of CD34 is not as wellstudied as CD44. The extracellular domain of CD34 contains a serine-, threonine- and proline-rich domain that is extensively glycosylated and sialylated.[208,209] Moreover, a juxtamembrane stalk region, a cysteine-bonded globular domain, and a putative N-glycosylation site were also identified in the extracellular section of CD34.[204] The most well-known intercellular binding partner of CD34 is L-selectin, which is a cellular adhesion molecule expressed on the surface of leukocytes.[210] Other potential ligands of CD34 are also under exploration. In addition, each CD34 protein comprises a single transmembrane helix and a cytoplasmic domain that contains highly conserved phosphorylation sites and a C-terminal PDZ (postsynaptic density protein) binding motif.[208,211] The PDZ binding motif of CD34 recognizes Crk-like protein, which is an adaptor protein that further interacts with the N terminus of NHERF (Na(+)/H(+) exchange regulatory cofactor) scaffolding proteins. The C terminus of NHERFs contains an ERM binding domain, which facilitates the indirect interaction of actin cytoskeleton with other binding partners of NHERF proteins.[212] CD34 has been proposed to be involved in enhancing proliferation,[208] blocking differentiation,[213] promoting lymphocyte adhesion,[209] and the trafficking of hematopoietic cells.[204,214] Because of the ubiquitous expression pattern of CD44 on the surface of both cancerous and normal cells, it has not been utilized for drug delivery to CSCs.

– ***Targeting of ABCB5***. ABCB5 (ATP-binding cassette sub-family B member 5) is a member of ABC transporter proteins that contains two transmembrane domains and two nucleotide binding domains.[215] ABC transporter proteins are part of the pglycoprotein family and are responsible for the transport of a large array of substrates across cellular membranes. Due to these characteristics, ABC transporter proteins are responsible for the multidrug resistance profiles of cancer cells due to their ability to export drugs from cells. ABCB5 exists in two isoforms, α and β, and is a cell surface marker that is currently known to be expressed on skin cancer cells and is closely associated with the chemoresistance of malignantmelanoma-initiating cells (MMICs).[216]

3C2-1D12 is a monoclonal anti-ABCB5 antibody. Systematic administration of 3C2-1D12 into nude mice revealed an increase in ADCC in $ABCB5^+$ MMICs, as well as tumor-inhibitory effects.[106] This anti-ABCB5 monoclonal antibody has not yet reached preclinical testing status.

– ***Targeting of CD13***. CD13 (alanine aminopeptidase N) is a 967-amino acid single-transmembrane peptidase, consisting of a small N terminus and a large C terminus that contains the active site.[217] CD13 is found ubiquitously in various organs, such as the kidneys, small intestines, and the liver. CD13 plays an important role in antigen processing for the immune response and is expressed in T and B cells as well as macrophages.[218] CD13 has been reported as a diagnostic cell surface marker in liver CSCs.[93]

Ubenimex is a small molecule inhibitor of CD13. Ubenimex (bestatin) is a dipeptide isolated from Streptomyces olivoreticuli[219] and is known to have antitumor effects through augmentation of the host immune system.[220,221] Ubenimex is a

competitive protease inhibitor and deters the growth of lung cancer and leukemic cell lines.[222,223] A mechanism of action has been proposed by the co-crystallization of ubenimex with leukotriene A4 hydrolase (PDB 1HS6),[224] which is structurally homologous to cell surface antigen CD13.[225] Studies have shown that, in mouse xeno-graft models, the combination of CD13 inhibitor and anti-proliferation agent fluorouracil dramatically reduces tumor size, as well as tumor progression, as compared with either single agent therapy.[93] Ubenimex is not under clinical investigation at the present time.

– ***Targeting of CD123.*** CD123 is the α subunit of the interleukin-3 cell surface receptor. It has been elucidated as a CSC marker in AML[42] but also has been identified as a marker of normal hematopoietic stem cells, where it plays an important role in proliferation.[226] Structural information for CD123 is not well established.

7G3 is a monoclonal anti-CD123 antibody. Targeting of CD123 by this antibody has been shown to significantly reduce $CD34^{+}/CD38^{-}$ AML CSC cell populations and tumor engraftment in NOD/SCID mice. However, the efficacy of the antibody in established AML disease treatment models is still limited, and optimization is required before this strategy is suitable for clinical investigations. The proposed mechanism of anti-CD123 antibodies (e.g., 7G3) includes the inhibition of AML CSC homing to bone marrow and prevention of activation of human CD123 by IL-3.[227] To our knowledge, molecules of this class are not yet in clinical trials.

– ***Targeting of CD47***. The leukocyte surface antigen CD47 plays an important role in cell adhesion by acting as a platelet adhesion receptor.[228] CD47 is widely expressed at low levels in many tissues and highly expressed on AML CSCs, where increased CD47 expression is indicative of poor prognosis.[51] One functional

ligand of CD47 is signal regulatory protein-α (SIRPα), which is expressed on phagocytes. The interaction between CD47 and SIRPα activates a signal transduction cascade that results in the inhibition of phagocytosis.[229] The ecto-domain of CD47 was crystallized in 2008 (PDB 2JJS).[230]

Clone B6H12.2 is a monoclonal antibody that blocks the interaction between CD47 and SIRPα. It has been demonstrated that B6H12.2 enables phagocytosis of human AML CSCs in vitro and has therapeutic potential.[51] In NOD/SCID mice, B6H12.2 treatment depleted AML cells in peripheral blood.[231] In a preclinical in vivo mouse treatment model with high levels of engraftment, treatment with anti-CD47 antibodies resulted in the rapid clearance of AML and targeting of the CSC population.[51,231]

Antibody/Agents	Description	Cancer Indication	Reference
Clone7	Monoclonal antibody against CD133	Brain	[148]
CD133 targeted carbon nanotubes	Single walled carbon nanotubes functionalized with anti-CD133 monoclonal antibodies	Brain	[149]
CD133 targeted lipid nanocapsules	Lipid nanocapsules functionalized with anti-CD133 monoclonal antibodies	Colorectal	[150]
Catumaxomab	Monoclonal trifunctional antibody against EpCAM, CD3 and APCs	Malignant ascites, ovarian and gastric	[158]
MT110	Monoclonal single chain bispecific antibody against EpCAM and CD3	Colorectal, lung, gastric	[163]
Edrecolomab	Monoclonal antibody against EpCAM	Colorectal	[168]
Adecatumumab (MT201)	Monoclonal antibody against EpCAM	Breast, colorectal, prostate	[167]
H90	Monoclonal antibody against CD44	Acute myelogenous leukemia	[20]
P245	Monoclonal antibody against CD44	Breast	[193]
Gemtuzumab ozogamicin (GO)	Small molecule-anti-CD33 antibody conjugate	Acute myelogenous leukemia	[199, 200]
3C2-1D12	Monoclonal antibody against ABCB5	Melanoma	[106]
Ubenimex	Dipeptide small molecule inhibitor of CD13	Liver	[93]
7G3	Monoclonal antibody against CD123	Acute myelogenous leukemia	[227]
Clone B6H12.2	Monoclonal antibody against CD47	Acute myelogenous leukemia	[51]

Table 1.3: Targeting of CSC populations by antibodies and small molecules.

CSC marker	Other common names	Cancerous tissue where expressed
A2B1	α2β1 Integrin; a2b1 integrin; CD49b	Prostate
A2B5	α2β5 Integrin; a2b5 integrin	brain
ABCB5	ABCB5 P-gp; ATP-binding cassette sub-family B member 5	melanoma
ABCG2	ABC transporter G family member 2	skin, bladder
CD4	Leu-3; T4	ALL
CD7	GP40; Leu-9; TP41	ALL
CD9	BTCC-1; DRAP-27; MIC3; MRP-1; TSPAN-29; 5H9 antigen; p24	ALL
CD10	Atriopeptidase; CALLA; Enkephalinase; Neprilysin; SFE	ALL
CD13	Aminopeptidase N; Alanyl aminopeptidase; gp150; Lap1	liver
CD19	B-lymphocyte surface antigen B4; Leu-12	ALL
CD24	Small cell lung carcinoma cluster 4 antigen	breast, colorectal, ovarian, pancreatic
CD25	Interleukin-2 receptor subunit alpha; TAC antigen; p55	AML
CD29	Integrin beta-1; Fibromectin receptor subunit beta; VLA-4 subunit beta	breast
CD32	Low affinity IgG Fc receptor II-b; CDw32; Fc-gamma RIIb	AML
CD33	Siglect-3; gp67	AML, ALL
CD34	Hematopoietic progenitor cell antigen CD34	AML, ALL, CML
CD38	ADP-ribosyl cyclase 1; cADPr hydrolase 1; T10	AML, ALL, CML
CD44	CDw44; Epican; ECMR-III; GP90 receptor; HUTCH-I; Heparan sulfate proteoglycan; Hermes antigen; PGP-1; Hyaluronate receptor	AML, bladder, breast, colorectal, liver, ovarian, pancreatic, prostate
CD45	Receptor-type tyrosine-protein phosphatase C; Leukocyte common antigen; T200	AML, liver
CD47	Leukocyte surface antigen CD47; antigenic surface determinant protein OA3; integrin-associated protein; MER6	AML, bladder
CD49f	Integrin alpha-6; VLA-6	breast, colorectal, prostate
CD71	Transferrin receptor protein 1; T9; p90	AML, breast, liver
CD90	Thy-1 membrane glycoprotein	ALL, AML, breast, liver
CD96	T cell surface protein tactile; T cell-activated increased late expression protein	AML

Table 1.4. Alternative names of CSC surface markers that appear in this chapter.

CSC marker	Other common names	Cancerous tissue where expressed
CD110	Thrombopoietin receptor; Myeloproliferative leukemia protein; Proto-oncogene c-Mpl	ALL
CD117	Mast/stem cell growth factor receptor kit; Piebald trait protein; c-kit; p145; Tyrosine-protein kinase kit	AML, ovarian
CD133	Prominin-1; antigen AC133; Prominin-like protein 1	ALL, brain, breast, colorectal, liver, lung, melanoma, ovarian, pancreatic, prostate
CD166	Activated leukocyte cell adhesion molecule	colorectal
CD173	H2	breast
CD174	Lewis Y	breast
CD176	Thomsen-Friedenreich antigen (TF)	breast, liver, lung
CD201	Endothelial protein C receptor; PROCR; APC receptor	breast
CK20	Cytokeratin-20; Protein IT	bladder
CK5	Type II keratin Kb5; Cytokeratin-5; 58 kDa cytokeratin; Keratin-5; Type II cytoskeletal 5	bladder
CLL-1	C-type lectin domain family 12 member A; DCAL-2; MICL	AML
CXCR4	FB22; Fusin; HM89; LCR1; LESTR; NPYRL; SDF-1 receptor; CD184; C-X-C chemokine receptor type 4	pancreatic
Cytokeratin	Keratin	breast
EMA	Epithelial membrane antigen; MUC-1; CD227; PEM; PUM; KL-6; H23AG; Episialin; Carcinoma-associated mucin; Breast carcinoma-associated antigen DF3	bladder
EpCAM	CD326; GA733-2; KSA; KS1/4 antigen; ESA; EGP314; EGP-2; Adenocarcinoma-associated antigen; Cell surface glycoprotein Trop-1	breast, colorectal, liver, ovarian, pancreatic
HLA-DR	CD74; p33; Ia antigen-associated invariant chain	AML
L1CAM	CD171	brain
Lin	Cell lineage protein	AML, bladder, breast, prostate
OV6	-	liver
Sca-1	Stem cell antigen-1	prostate
SSEA-1	Stage-specific embryonic antigen-1; CD15	brain

Table 1.4 (continued). Alternative names of CSC surface markers that appear in this chapter.

1.4 Summary and conclusions

Numerous studies have reported the existence of tumor cell populations with abilities to self-renew, differentiate, and potently initiate tumorigenesis. These cell populations, termed cancer stem cells (CSCs), are strongly implicated in disease propagation and, if not addressed during drug therapy, can facilitate disease relapse. Consequently, there is a significant and unmet need to better characterize the unique biology of CSCs as well as develop therapies to eradicate them. CSC markers, which are macromolecules (e.g., proteins, carbohydrates, etc.) that are uniquely expressed on the surface or in the cytoplasm of CSCs, are essential for the isolation and characterization of CSC populations. Additionally, these CSC markers provide targets for the specific delivery of therapeutic molecules into CSCs. In this article, we reviewed those cell surface macromolecules that are presented on the surfaces of many tumor CSCs, described the unique chemical and structural features of the most common markers, and reported recent efforts to target CSC surface markers as part of drug delivery efforts. Clearly, the field of CSC biology is still in its infancy and even less advanced are efforts to target those cells with therapeutic molecules. However, given that the elimination of CSCs may result in significantly enhanced therapy outcomes in patients, the focus of cancer drug discovery scientists should shift, at least in part, to designing next generation drugs that target CSC populations.

Chapter 2. Elucidating the Cellular Targets of the Anticancer Natural Product Parthenolide

2.1 Introduction

Cancer is the leading cause of death worldwide, and the second leading cause of death in the United States, only after heart diseases. It accounts for 7.6 million deaths (around 13% of all deaths) in 2008 worldwide[232] as well as 565,469 deaths in the US.[233] Massive amount of research has been carried out to study the growing patterns of tumor cells, in pursuit of effective therapeutic methods against this malignant disease. Currently, there are two well-developed theories interpreting the patterns of cancer cell growth. The first one is the traditional stochastic model of cancer cell growth, which assumes that every tumor cell has the equal potential to develop into a new tumor, and their variable activities are fully or partially determined mathematically by stochastic models.[234] The other theory is hierarchical model (**Figure 2.1**), which predicts that cancer stem cells (CSCs), which are also known as tumor-propagating cells or tumor-

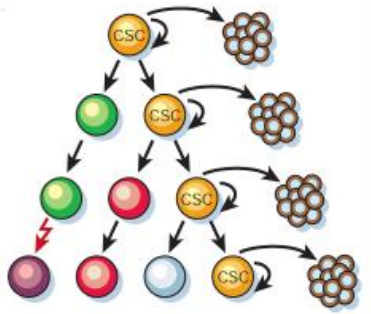

Figure 2.1: Depiction of the CSC hierarchy model of cancer growth with cells undergoing self-renewal or differentiation into discrete tumor cell types. Graphic from [1].

initiating cells, represent a biologically unique subpopulation within the total malignant cell population, although it is not necessary that CSCs are genetically or functionally homogeneous.[235] CSCs are undifferentiated, highly tumorigenic cells found within bulk tumors. CSCs have the ability to self-renew, differentiate, and generate a phenotype-identical copy of the tumor from which they were isolated. Accordingly, CSCs reside at the apex of the tumor cell hierarchy and can differentiate into all of the cell types that comprise the host tumor. Besides CSCs, all other cells in the cancer cell hierarchy have only limited proliferative capacity.[1-8] CSC theory directly challenges the traditional stochastic model of cancer cell growth; however, the rapid advances of cancer research and development of relative technologies have provided more and more evidence for the existence of CSCs. For example, with fluorescence-activated cell sorting (FACS) techniques, John Dick and colleagues provided the first seminal evidence for CSC by isolating the $CD34^{+}/CD38^{-}$ fraction of human donor acute myeloid leukemia (AML) cells and engrafting those cells into severe combined immunodeficient (SCID) mice, which resulted in the development of identical disease to that of the donor.[9,10] Isolation of the AML CSC population ($CD34^{+}/CD38^{-}$) from the recipient mouse, followed by serial transplantation into a secondary recipient mouse yielded the same disease, thereby demonstrating the self-renewal properties of the initially engrafted $CD34^{+}/CD38^{-}$ AML cell fraction. On the other hand, the engraftment of other leukemic cell population, such as $CD34^{+}/CD38^{+}$ cells or $CD34^{-}$ cells did not result in the occurrence of AML,[10] which is another critical evidence of the hierarchy model of tumor heterogeneity.

The clinical impact of the CSC hierarchy model of cancer growth is that the eradication of CSCs inevitably results in the death of tumors; on the other hand, the

failure to do so raises the possibility of disease relapse. A realized example of this concern has been documented with patients receiving the targeted BCR-ABL tyrosine kinase antagonist imatinib (Gleevec®) for chronic myelogenous leukemia (CML). Although imatinib effectively converts CML into a chronically managed disease,[22,23] withdrawing from imatinib treatment ultimately results in disease relapse in most patients because the drug does not eliminate CML CSCs.[24,25]

However, drug targeting of CSCs is extremely challenging from two aspects. First of all, under standard biological conditions, CSCs are quiescent, which means their replication rate is lower than differentiated cancer cells.[18,19] As a result, CSCs are resistant to most chemotherapeutic drugs that target the replication process of tumor cells. Other reported mechanisms of the drug resistance of CSCs include their expression of anti-apoptotic proteins,[16] and the up-regulation of ABC multidrug resistance transporter proteins.[16,17] The concern of drug resistance of CSCs is underscored by the example of cytarabine. Cytarabine is a front-line small molecule drug (nucleoside analogue) for the treatment of AML, which is designed to induce apoptosis in rapidly dividing cancer cells.[236] However, recent data have demonstrated that cytarabine actually facilitates the entry of AML CSCs into their G0/G1 phase, thereby promoting cell cycle quiescence and providing a mechanism that allows AML CSCs to evade chemotherapy.[21] Consequently, viable strategies to eradicate CSC populations are clearly needed if curative cancer therapies are to be developed.

The second barrier towards the development of cytotoxic agents of CSCs is the structural and functional similarity between CSCs and normal stem cells. Considering the critical function of normal stem cells, to maintain their population and viability is

very important during the drug targeting of CSCs. For example, AML CSCs and normal hematopoietic stem cells (HSCs), whose differentiation yields the individual cells in the blood, share the same cell surface antigen profile $CD34^{+}/CD38^{-}$.[42] Both cell types express Bmi1 and PTEN, which are involved in pathways that governs their self-renewal capability,[237,238] and both of them are highly quiescent.[239] Despite the highly biochemical similarity between AML CSCs and HSCs, some unique features of AML CSCs have recently been reported. For example, AML CSCs failed to express the known characteristic HSC cell surface antigen CD90 and CD117.[39,41] On the other hand, the expression of CD123 (IL-3 receptor alpha chain) on the surface of AML CSCs has not been found in HSCs.[42] In addition, elevated activity and over expression of transcription factor NF-κB has been observed in primitive human AML cells, including the quiescent CSC subpopulation; however, the NF-κB activity in HSCs generally remains in basal levels.[240,241] Considering the known relationship between the NF-κB activity and its involvement in trigging apoptosis and inflammation in cancerous cells,[242,243] the modulation of NF-κB signaling pathway may present a valuable and novel target for the eradication of AML CSCs.

NF-κB (nuclear factor-κB)[244] is an inducible dimeric transcription factor that consists of the combinations of p50, p52, p65, c-Rel and RelB proteins. NF-κB has been found in almost all animal cells and activates the expression of genes associated with numerous cellular processes such as differentiation, proliferation and cellular responses to stimuli, including pathogens, cytokins, stress, free radicals and so on.[245] Playing a key role in the regulation of cellular inflammatory and immune responses, the activity level of NF-κB is coordinated by complex modulation mechanisms. In the canonical NF-κB

signaling pathway (**Figure 2.2**), a dimeric NF-κB (normally a p50-p65 heterodimer) is retained in the cytoplasm via interaction with its inhibitor protein IκBα. In response to various extracellular stress signals or pathogens, the IKKα/IKKβ/NEMO complex (IKK complex) phosphorylates IκBα protein and induces its ubiquitination and subsequent degradation by the 26S proteasome.[245-247] The degradation of IκBα causes the p50/p65 heterodimer to relocate from cytoplasm to nucleus[248] and bind to NF-κB response elements to upregulate the expression of genes that involved in the enabling of cell proliferation, activation of cell invasion, secretion of anti-apoptotic proteins and so on.[245,249,250]

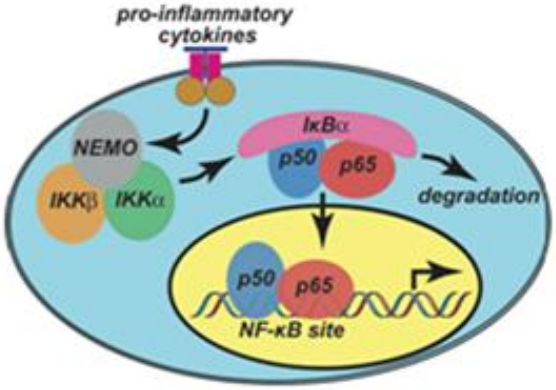

Figure 2.2: The canonical NF-κB signaling pathway.

Due to the crucial role NF-κB signaling pathway plays in the CSCs, a spectrum of known small molecule inhibitors of NF-κB signaling pathway has been screened by the Jordan laboratory (University of Rochester) as potential anti-CSC agents. Among the evaluated compounds, the natural product parthenolide (**PTL**, **1**, **Figure 2.3**) was identified as a selective cytotoxic agent against AML CSCs, while sparing normal HSCs.[19] **PTL** is sesquiterpene lactone isolated from Mexican Indian medicinal herb *Tanacetum parthenum* (feverfew plant),[251] which has been used for over a century for the treatment of various common inflammatory conditions such as arthritis, asthma,

fever, and migraine.[252,253] **PTL** has been extensively studied as an anticancer agent, showing significant efficacy towards a wide spectrum of human cancer cells, such as brain cancer,[254] prostate cancer,[255,256] breast cancer,[257,258] chronic lymphocytic leukemia,[259] and pancreatic cancer.[260] As introduced above, in 2005, the identification of **PTL** as the first stand-alone and selective cytotoxic compound against AML CSCs further heightened its therapeutic potential.[19] Besides AML, **PTL** was demonstrated to effectively inhibit the survival of CSCs in other cancer types, including breast cancer[261] and prostate cancer.[262] In addition, the modification of **PTL** to a dimethylamino derivative of parthenolide (**LC-1**, **2**, **Figure 2.3**) has yielded a water-soluble analogue, which exhibit *in vivo* (canines) therapeutic efficacy against AML CSCs and progenitor cells,[263] and is now in a phase I clinical trial for the treatment of AML in the United Kingdom.

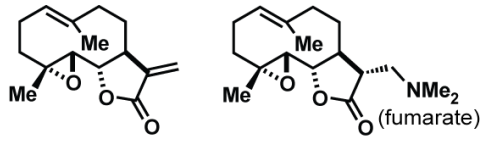

Figure 2.3: Structure of Parthenolide (**1**) and **LC-1** (**2**).

In spite of the promising anticancer activity of **PTL**, the mechanism of action by which it eliminates CSCs has not been fully understood. As introduced above, the inhibitory of NF-κB signaling is so far the most widely accepted molecular mechanism of its biological activity. In previous studies, Crews and co-workers demonstrated that **PTL** inhibited NF-κB signaling via covalent modification of IKKβ kinase;[264] Garcia-Pineres and co-workers reported that the anticancer activity of **PTL** was achieved by the covalent modification of p65 protein.[265] Both of the above studies believed that the inhibition of NF-κB signaling pathway was responsible for the biological activity of

PTL, and their theories were supported by the protein pull-down results reported by Nasim and coworkers in 2011,[266] where both IKKβ and p65 were identified as cellular targets of PTL affinity probes by western blots. However, published results from Jordan and co-workers indicated that the inactivation of NF-κB pathway in primary AML cells via the introduction of an IκB superrepressor allele, which completely blocks NF-κB signaling by the expression of a degradation-resistant IκBα protein, only partially abolishes AML CSCs viability.[241] This result questions the importance of inhibiting NF-κB pathway when targeting CSCs. In addition, experimental results from our lab, which will be shown below (**Figure 2.6**), indicated that **PTL** does not inhibit NF-κB related kinases, including IKKβ, to a significant extent, at a concentration well above its IC_{50} value *in vitro*. On the other hand, **PTL** has also been implicated to affect a wide range of other cellular processes, including the inhibition of HDAC1,[267] alkylation of p65,[268] the targeting of cell surface thiols,[269] inhibition of Hsp70,[270] activation of p53 and cellular caspases,[271] and etc. The extents to which any or all of the above cellular processes affect the toxicity of **PTL** against CSCs have not been investigated.

As a result, we proposed to utilize a "click chemistry" based protein pull-down strategy to design small molecule probes suitable for cellular target identification studies of **PTL**. As well known, the copper (I) - catalyzed Hüisgen 1,3-dipolar cycloaddition reaction, click chemistry,[272] proceeds readily and rapidly between an alkyne group and an azide group under mild condition. This kinetically favored reaction, because of its bioorthogonal characteristic, is widely utilized as a powerful tool for both *in vitro* and i*n vivo* functionalizations of biomolecules.[273,274] Protein pull-down is a technique to

selectively capture proteins of interest from solution, utilizing protein-protein or protein-immobilized ligand interactions.[275,276]

2.2 Project Design

As it has been introduced in the above section, **PTL** is a promising anticancer natural product because it selectively targets AML CSCs without inhibiting the growth of HSCs.[19] However, the detailed molecular mechanism(s) relevant to its biological activity is still widely unknown. Considering the important role CSCs play in the drug resistance and relapse of cancers, and the lack of validated targets for CSC drug discovery, we hypothesized that the elucidation of the mechanism(s) of action by which **PTL** abolishes AML CSC activity will provide invaluable information and new drug targets for diminishing the population of CSCs.

With this idea in mind, we sought to synthesize **PTL**-based affinity probes with varied biological functions and utilize them in click chemistry[272] based protein pull-down experiments to further isolate the target proteins of **PTL** from AML cells. Our design of PTL-based affinity probes is based on preliminary data from our lab (**Figure 2.4**). Previously, we synthesized a reduced exocyclic methylene analogue of **PTL**, **Red-PTL** (**3**), and an allylic oxidized analogue, **MelB** (**4**) and tested their toxicity in CCRF-CEM, a commercially available leukemic cell line. The experimental results from our lab and others[264,277,278] indicated that the removal of the exocyclic olefin completely ablated the activity of **PTL**, while the oxidative installation of a hydroxyl group to the vinyl methyl group was highly tolerated.[266] The newly introduced hydroxyl group can therefore serve as a handle for the synthesis of PTL-based affinity probes. We envisaged

installing alkyne groups as the affinity tag, which could be easily used in following click chemistry conjugation to facilitate the isolation of protein targets.

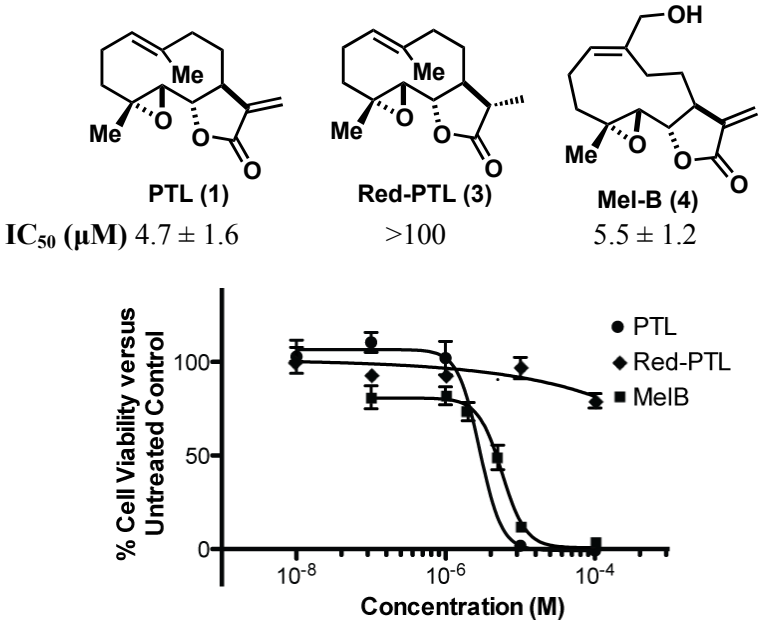

Figure 2.4: 48 hr cytotoxicity dose response curve for **PTL** and analogues in CCRF-CEM leukemic cells.

In addition, due to the innate reactivity of **PTL**, we predicted that a large amount of protein adducts would be yielded from protein pull-down experiments (which has been supported by our results shown below) and that to discriminate those PTL-protein adducts that are responsible for the AML CSC toxicity from those cellular interactions that result from off-target reactivity of **PTL** would be very challenging. As a result, besides the functional PTL-alkyne affinity probe that derived directly from **MelB** (**4**), we also designed a non-functional PTL-alkyne affinity probe, which was derived from the non-functional PTL analogue **3**. The non-functional PTL-alkyne affinity probe was envisioned to not exhibit the cytotoxicity to leukemic cells as **PTL**, but rather, retains the structure of PTL and serves as a control pull-down probe. Based on the design of the above two probes with varied biological potencies, we proposed the comparative protein

pull-down experiments (**Figure 2.5**). After the incubation of AML cells with each PTL-alkyne affinity probe, the PTL-protein adducts from cell lysates would be further modified to introduce a biotin moiety and/or a fluorescent moiety by the utilization of click chemistry. The fluorescent moiety could be used to in-gel visualize the labeled PTL-protein adducts, while taking advantage of biotin-streptavidin interaction, the biotin moiety would be used to isolate the target molecules from residual unlabeled proteins. Candidate proteins were then analyzed by mass spectrometry, and protein fragments are

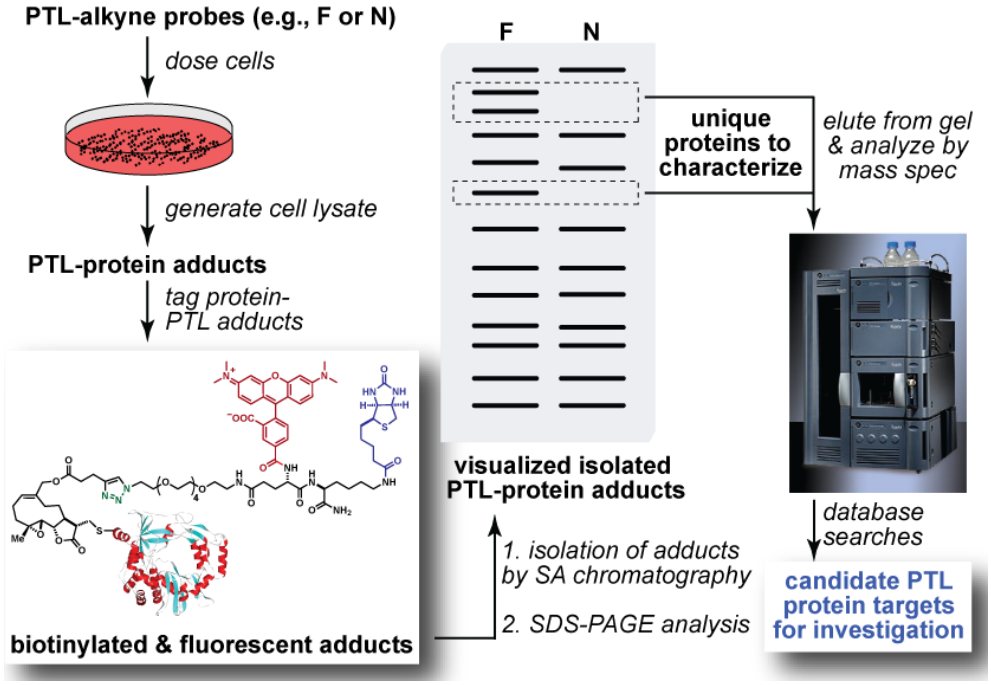

Figure 2.5: Overview of the designed comparative protein pull-down strategy to elucidate protein reactivity profile of **PTL**. "F" = functional PTL-alkyne probe; "N" = non-functional PTL-alkyne probe.

queried against known protein databases.

2.3 Results and Discussion

*2.3.1 Kinase Screening Assay of **PTL** against NF-κB Related Kinases.*

A kinase screening assay, which includes the reported NF-κB related kinases IKKα, IKKβ, PI3, IRAK1, IRAK4, TAK1 and cSRC was conducted (**Figure 2.6**) to further study **PTL**'s ability to inhibit NF-κB signaling. The kinase inhibitory activity of **PTL** was tested at two different concentrations: 2 μM and 10 μM. According to data that will be shown in the next chapter (**Table 3.1**), the 10 μM treatment is well above the IC_{50} of **PTL** in various cancer cell lines. However, even at the higher tested concentration, PTL does not show any significant inhibitory activity against NF-κB related kinases, including the reported **PTL** target IKKβ. This result suggested that the inhibition of NF-κB signaling pathway is not like to be the predominant mechanism by which **PTL** induces cancer cell death.

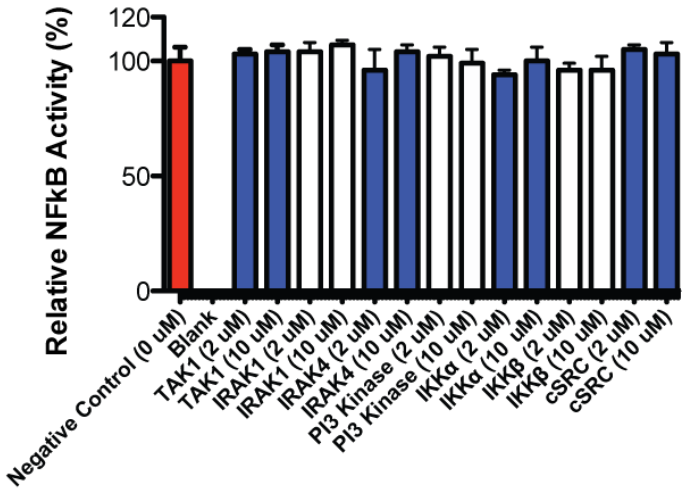

Figure 2.6: Kinase screening assay of **PTL** against NF-κB related kinases. [ATP] = 10 μM. For each data point, the concentration of tested compound (**PTL**) is indicated in the bracket; the bar indicated the relative enzymatic activity of the tested kinase and Mean ± SD values are shown. The screening was performed by Millipore KinaseProfiler Service.

2.3.2 Synthesis of Functional and Non-Functional PTL-Alkyne Probes and Testing of Their Cytotoxicity in AML Cells.

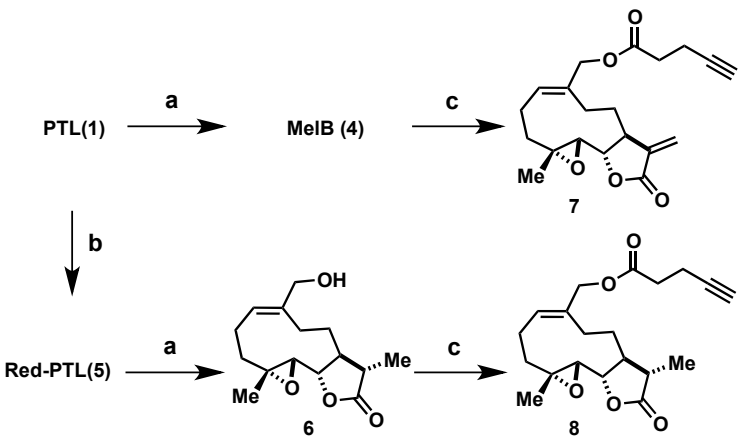

Scheme 2.1: Synthesis of PTL-alkyne affinity probes. *Reagents and Conditions:* a) SeO_2, t-BuOOH, DCM, 40 ℃, 6 hr, 47% for **4** and 68% for **6**; b) Pd/C, H_2 (1 atm), EtOH, RT, 15 min, quant.; c) DIAD, PPh_3, 4-pentynoic acid, THF, 0 ℃, 83% for **7** and 84% for **8**.

The chemical synthesis of the proposed PTL-alkyne affinity probes commenced with **PTL** (**1**), which was converted into **MelB** (**4**) in 47% yield according to published procedure[279] under standard allylic oxidation condition (SeO_2, *t*-BuOOH, **Scheme 2.1**). On the other hand, the exocyclic methylene in **PTL** was selectively reduced under carefully controlled reaction times, yielding **5** in quantitative yield.[54] The vinyl methyl group of **5** was oxidized as described above to give **6** in 68% yield. With **4** and **6** in hand, the synthesis towards alkyne substituted **PTL** probes could then proceed. Several different conditions to install the alkyne tag were examined, however, the primary allylic hydroxyl group in **4** and **6** were far less reactive than we expected, possibly due to steric hindrance. Harsh conditions such as strong bases or heating resulted in the degradation of the starting material, but milder alkylation conditions failed to accomplish the desired transformation. After the screening of several direct nucleophilic substitution reactions, we determined that substrates **4** and **6** were both reactive and stable enough under

Mitsunobu conditions,[280] and we successfully coupled them with 4-pentynoic acid to obtained PTL affinity probes **7** and **8** in 83% and 84% yields, respectively.

With compound **7** and **8** in hand, their cytotoxicity in HL-60 cells (AML cell line) was further tested (**Figure 2.7**). Consistent with our prediction, functional PTL probe **7** exhibited similar IC_{50} value (7.5 ± 1.2 μM) compared to **PTL** (9.3 ± 3.8 μM), and non-functional PTL probe **8** exhibited minimal cytotoxicity against HL-60 cells (IC_{50} > 500 μM). See section 2.5.4.2 for detailed procedure.

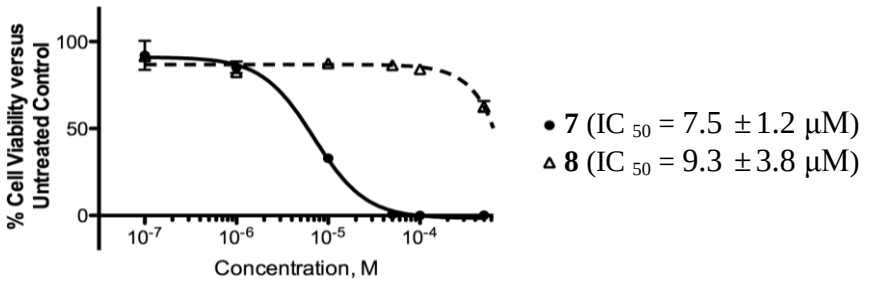

Figure 2.7: 48 hr cytotoxicity dose response curve for probe **7** and **8** in HL-60 cells. Mean ± SD values are shown.

2.3.3 Synthesis of Fluorescent Probes.

Three fluorescent probes, rhodamine azide adduct (Rh-N_3, **9**), rhodamine biotin azide adduct (Rh-Bio-N_3, **10**) and Cy5.5 biotin azide adduct (Cy-Bio-N_3, **11**) were synthesized for their use as clickable fluorescent reagents to the PTL alkyne probes. Although Rh-N_3 (**9**) and Rh-Bio-N_3 (**10**) has been previously reported,[281] these reagents were not commercially available and required synthesis. We prepared these two compounds according to reported procedures with minor modifications (**Scheme 2.2, Scheme 2.3**). Briefly, mono-Boc-protected diamine **13** was obtained in 88% yield by carefully adding Boc_2O into excess equivalents of 1,6-diaminohexane (**12**)[282]. The solvolysis of bromoacetyl bromide **14** in MeOH yielded the corresponding methyl ester,

which was converted to **15** in a S_N2 reaction. Compound **15** was saponified to yield the carboxylate acid intermediate, which was coupled to *N*-hydroxysuccinimide under standard condition to give **16**. The substitution reaction between **13** and **16** took place spontaneously to yield **17**. From compound **12** to **17**, only one column purification was performed, and the overall yield was 32% over 5 steps. Following the cleavage of Boc group in **17**, the coupling of commercially available carboxy-tetramethyl-rhodamine *N*-succinimidyl ester (**Rh-NHS**, **19**)[283] with compound **18** delivered the target molecule Rh-N_3 (**9**) in 45% yield.

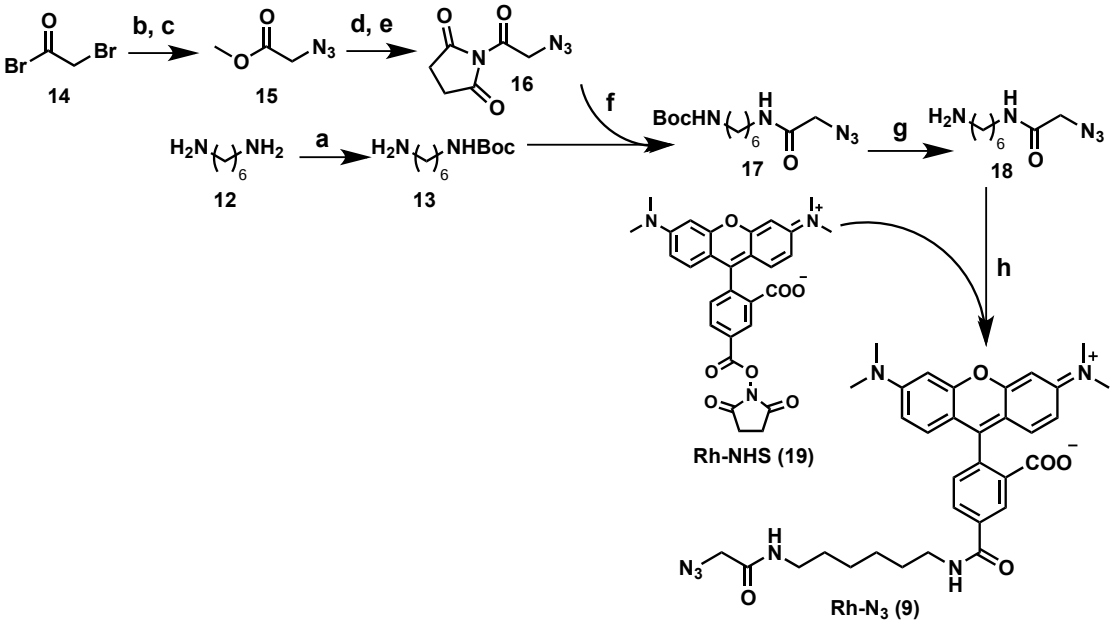

Scheme 2.2: Synthesis of Rh-N_3 fluorescent probe **9**. *Reagents and Conditions:* a) Boc_2O, dioxane/H_2O = 1:1, 88%; b) MeOH, 0 ℃; c) NaN_3, DMF, RT, overnight; d) KOH, THF/H_2O = 4:1, 40 ℃, 3 hr; e) DCC, NHS, DMF, RT, 4 hr; f) DMF, RT, overnight, 32% (over 5 steps); g) Conc. HCl, EtOAc, RT, 2 hr; h) DMF, RT, overnight, 45% (over 2 steps).

In addition to the bi-functional fluorescent probe **9**, a Rhodamine-Biotin-N_3 tri-functional probe (**10**) was also synthesized according to a reported procedure[284] with minor modifications. Compound **10** (**Scheme2.3**) was synthesized on Siever amide resin

using standard 9-fluorenylmethoxycarbonyl (Fmoc) solid phase synthesis strategy. Fmoc protected resin was deprotected with piperidine/N-methylpyrrolidinone (NMP) for multiple times and washed (with NMP, 3x; DCM, 3x; NMP, 3x) to remove the excess reagents. Then Fmoc-Lys(Biotin)-COOH was coupled to the resin under standard condition (EDCI, HOBt, DIPEA) to yield **20**. The resin was washed and deprotected to reveal the primary amine, which was subsequently coupled to Fmoc-Lys(N_3)-COOH to deliver compound **21**. After subsequent wash and deprotection as described above, rodamine was appended to the compound **22** upon reaction with Rh-NHS (**19**). The final cleavage was accomplished under mild acidic conditions (3% TFA in DCM) to yield Rh-Bio-N_3 (**10**), which was further purified by preparative HPLC. The overall yield was 27%.

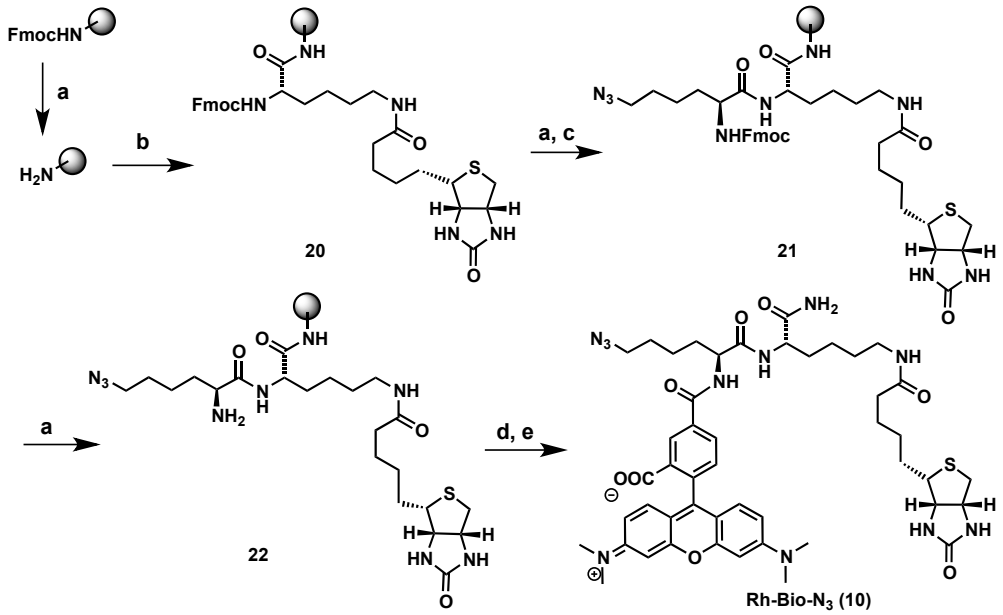

Scheme 2.3: Solid phase synthesis of tri-functional probe Rh-Bio-N_3 (**10**). *Reagents and Conditions:* a) 15% piperidine, NMP, 10 min, RT, 3x; b) Fmoc-Lys(Biotin)-COOH, EDCI, HOBt, DIPEA, NMP, RT, 2 hr; c) Fmoc-Lys(N_3)-COOH, EDCI, HOBt, DIPEA, NMP, RT, 2 hr; d) Rh-NHS, TEA, NMP, RT, overnight; e) 3% TFA, DCM, RT, 30 min, 5x, overall yield: 27%.

Rhodamine is a widely used fluorophore in protein and DNA labeling. It is bright and water soluble, with an excitation wavelength of 543 nm and an emission wavelength of 576 nm. Due to the potential drawbacks of the Rhodamine fluorophore (heat and photo-stability), a Cy5.5-Biotin-N_3 tri-functional probe (**11**, **Scheme 2.4**) was also prepared. Cy5.5 allows for more sensitive detection of covalently modified proteins, and is less light sensitive and has greater stability at elevated temperature. In addition, considering the importance of water solubility of the probe under biological conditions, a poly ethylene glycol (PEG) linker was also introduced.

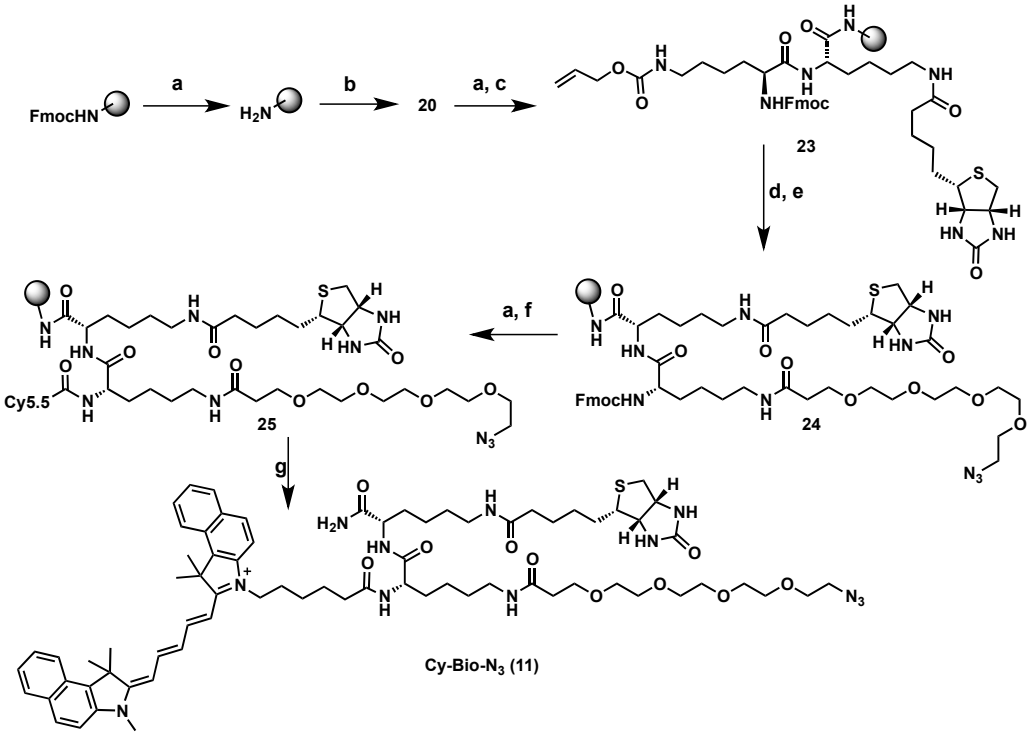

Scheme 2.4: Solid phase synthesis of tri-functional probe Cy-Bio-N_3 (**11**). *Reagents and Conditions:* a) 15% piperidine, NMP, 10 min, RT, 3x; b) Fmoc-Lys(Biotin)-COOH, HBTU, HOBt, DIPEA, NMP, RT, 2 hr; c) Fmoc-Lys(Alloc)-OH, HBTU, HOBt, DIPEA, DCM, RT, overnight; d) $Pd(PPh_3)_4$, DCM/AcOH/NMA = 37 : 2 : 1, RT, 2 hr; e) N_3-PEG-COOH, HBTU, DIPEA, NMP, RT, overnight; f) Cy5.5-NHS, TEA, NMP, RT, overnight; g) 3% TFA, DCM, 30 min, RT, 5x.

Probe **11** was synthesized on Siever amide resin using standard Fmoc solid phase strategy as well. Fmoc protected resin was deprotected with piperidine/N-methylpyrrolidinone (NMP) multiple times and washed as descripted above to remove the excess reagents. Then Fmoc-Lys(Biotin)-COOH was coupled to the resin under standard amide coupling condition to give **20**. The resin was washed and deprotected to reveal the primary amine, which was subsequently coupled to Fmoc-Lys(Alloc)-OH to yield **23**. After the cleavage of Alloc protection group under the catalyze of tetrakis(triphenylphosphine)palladium, the resulting terminal amine was coupled to N_3-PEG-COOH to install the azide moiety in **24**. After wash, the resin was deprotected and readily coupled to the NHS ester of Cy5.5 to yield resin bound **11**. After cleavage under mild acidic conditions, **11** was obtained after HPLC purification, with 29% overall yield. The structure was confirmed by HRMS.

2.3.4 Proof of Concept Experiments of Protein Pull-Down.

With both the function and non-functional PTL-alkyne affinity probes (**7** and **8**) and fluorescent probes **9-11** in hand, some proof of concept assays were conducted to (I) demonstrate the feasibility of the designed project and (II) optimize the experimental conditions in a relatively simple system with relatively less variables before the performance of any experiments in biological systems.

2.3.4.1 Click chemistry template reaction. A click chemistry proof of concept study was carried out to evaluate the ability of probes **7** and **8** to be captured by azide-based reagents under Cu-catalyzed conditions (see section 2.5.4.2 for detailed procedure). The major reason we chose *in situ* click chemistry approach to introduce the affinity tag, as opposed to dosing cells with PTL-biotin conjugates[266] is that comparing

to biotin (molecular weight of PTL-Biotin: 687; PTL: 248), the appending of small alkyne groups (molecular weight of probe **7**: 316) is less likely to perturb the recognition of the **PTL** derivatives by their target proteins.

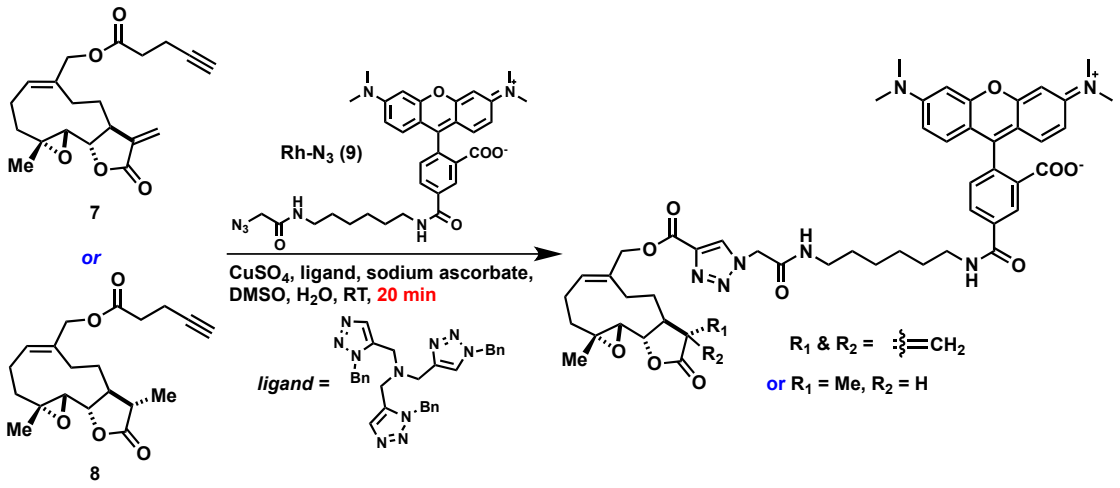

Scheme 2.5: Click chemistry template reaction.

In the template reaction (**Scheme 2.5**), DMSO solutions of Rh-N_3 (**9**) and PTL affinity probes (**7** or **8**) were added to RIPA buffer (used for cell lysis), followed by the addition of aqueous solutions of sodium ascobate, ligand (see **Scheme 2.5** for structure) and $CuSO_4$. The reaction was conducted in an aqueous condition to mimic the biological environment. The template reactions were performed in 1 mg scale and monitored by analytical HPLC at 595 nm (the characteristic UV absorption of rhodamine) and were found to finish within 20 min (**Figure 2.8**). In these reactions, excess amount of PTL probes were used, so we define the completion of the reactions as the disappearance of Rh-N_3 peak. The major products of the two template reactions were isolated and characterized by mass spectrometry. The mass data was found to be consistent with the molecular weight of our proposed click chemistry product. The above template reactions demonstrated that the coupling between the alkyne group of PTL affinity probes and the azide group of fluorescent probe is kinetically fast. Furthermore, the clear conversion

from starting materials to product makes us confident to transfer the reaction from a simple organic reaction vessel to a complicated biological system.

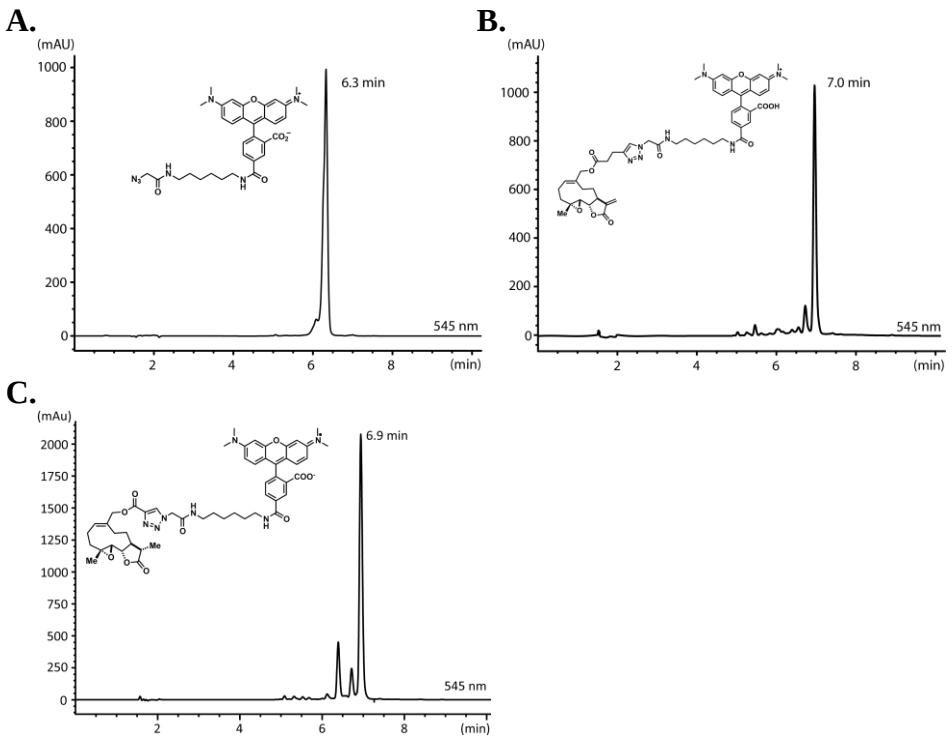

Figure 2.8: HPLC traces of template click chemistry with the reaction time of 20 min under 595 nm. A: HPLC trace of starting material **9**; B: the reaction between **7** and **9**;

2.3.4.2 In gel fluorescent labeling assay of cell lysates (see section 2.5.4.4 for detailed procedure)**.** In this project, we proposed to dose and label live cells and observe the molecular targets of **PTL**. In order to achieve this objective, the synthesized PTL affinity probes must penetrate the cell membranes and label their target proteins without killing the cells. Considering the complexity of the whole process, we decided to conduct the fluorescent labeling in cell lysates first to test the feasibility of fluorescent labeling, as well as to optimize the labeling conditions (**Figure 2.9**). First of all, HL-60 cell lysates were generated by treating HL-60 cells with RIPA lysing buffer. Then the incubation of PTL affinity probe (**7** or **8**, 0.7 mM) and HL-60 cell lysate (0.5 mg/mL)

facilitated the formation of covalent small molecule-protein adducts, which were then tagged by the fluorescent probe **9** using click chemistry method. The protein sample was then analyzed by SDS-PAGE. The resulting gel was detected for Rhodamine fluorescence (shown in **Figure 2.9**, panel B). The gel indicated clear fluorescent labeling of multiple proteins by probe **7**.

In addition, a time course assay of the in gel fluorescent labeling of HeLa cell

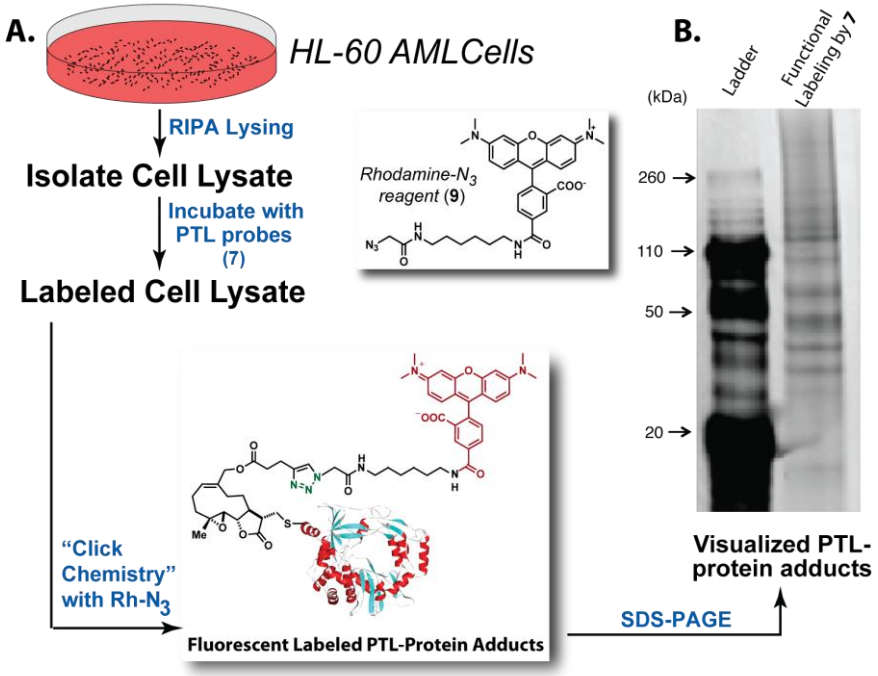

Figure 2.9: In gel fluorescent labeling of HL-60 cell lysate by PTL probe **7**. A: Overview of in gel fluorescent labeling; B: SDS-PAGE showing the functional labeling results.

lysates with functional probe **7** (**Figure 2.10**) was also conducted to determine the kinetic profile of the **PTL** labeling of its target proteins. In this assay, excess probe **7** (0.7 mM) was incubated with same concentration of HeLa cell lysates (0.5 mg/mL) for a time span from 10 min to 50 min before the performance of click chemistry step. The result of this assay reveals a fast kinetic property of the covalent modification of proteins

by **PTL**: fluorescent labeling could be observed as soon as 10 min, and the extent of labeling did not change significantly after 30 min.

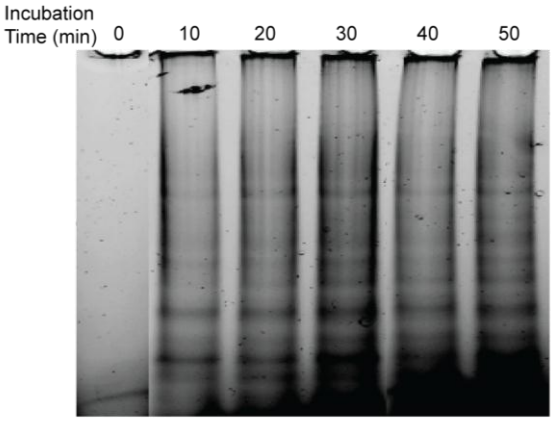

Figure 2.10: Time course assay of the in gel fluorescent labeling of HeLa cell lysates with **7**. From the first lane to the last lane, HeLa cell lysates were incubated with **7** for 0, 10, 20, 30, 40, 50 min respectively, before the performance of click chemistry. The gel was scanned for Rhodamine fluorescence.

2.3.5 Protein Pull-Down Experiments.

After getting positive results from a series of proof of concept experiments showing that the covalent binding of proteins by PTL analogues is kinetically fast and relatively robust, we then began investigating pull-down studies of PTL-bound proteins. Taking advantage of the high affinities between biotin and streptavidin, we originally proposed to use streptavidin resin to enrich proteins that were tagged with biotin from those that were not (**Figure 2.11**, see section 2.5.4.5 for detailed procedure); however, this affinity separation condition failed to yield any enrichment of proteins. Briefly, HL-60 cells were lysed by RIPA buffer to generate cell lysates, which were treated with PTL affinity probe **7** or **8** to facilitate the binding of the PTL probes with their target proteins. The tri-functional probe **10** was used in the click conjugation step, enabling the introduction of a fluorescent rhodamine tag, which could be used to visualize the bound

proteins, as well as a biotin tag, which would be associated with streptavidin resin to enable affinity separation. After the incubation of protein samples, probe **10** and click chemistry reagents, the samples were then treated with streptavidin resin. The unbound proteins were washed away and the bound proteins were eluted from the resin under standard conditions (2% SDS in PBS, 96 ℃, 20 min). The eluted protein samples were collected and analyzed by SDS-PAGE gel electrophoresis. However, no protein signals were observed either for fluorescent signals or after silver staining (a total protein stain). The affinity separation assay did not yield the desired result because one or more of the following steps likely went wrong: 1) protein labeling; 2) click chemistry; 3) enrichment and/or 4) elution (**Figure 2.11**). According to the preliminary assays, our experimental conditions for step 1 and 2 were robust. In addition, the possibility that step 3 was problematic is low, because the association of biotin and streptavidin is very tight (K_d ~ 10^{-14} mol/L) and almost the strongest non-covalent interactions known in nature.[285] As a result, we turned our attention to the elution step.

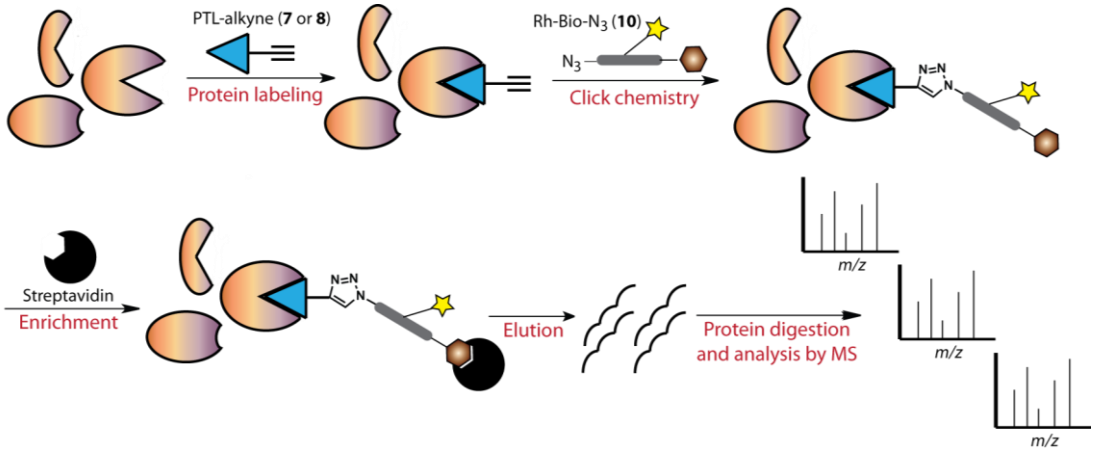

Figure 2.11: Proposed strategy to pull-down PTL target proteins from HL-60 cells (or cell lysates).

The elution of biotinylated molecules from streptavidin coated solid supports sometimes presents problems in protein pull-down studies, and as a result, various elution conditions with different recovery yields have been developed.[286] After the screening of multiple elution condition, we found that only the following harsh condition gave us a partially positive result: 2% SDS, 3 mM biotin, 2 M urea, 6 M thiourea in PBS, 96 ℃, 20 min. After the performance of this elution condition, the eluted protein samples were analyzed by SDS-PAGE gel electrophoresis (**Figure 2.12**). Although no fluorescent signals were observed, we were delighted to find that differential labeled protein showed up clearly after silver staining. We hypothesized that the absence of fluorescent signals resulted from the loss of the rhodamine moiety of the protein-PTL-Rh-Biotin complex under the harsh elution condition we used. It has also been reported that **PTL** is not stable under either basic or acidic conditions.[287]

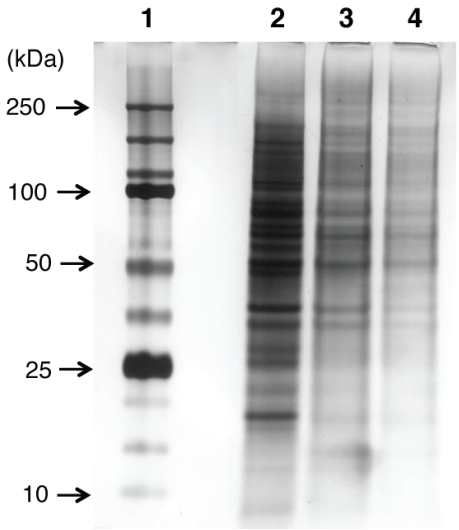

Figure 2.12: Pull-down of PTL-protein adducts from HL-60 cell lysates. The SDS-PAGE was visualized after silver staining. Lane 1: protein ladder; 2: HL-60 whole cell lysate; 3: proteins from functional pull-down (probe **7**); 4: proteins from non-functional pull-down (probe **8**).

In order to prove this hypothesis, a stability assay of Michael adducts of **PTL** was conducted (**Scheme 2.6**; **Table 2.1**, see section 2.5.4.6 for detailed procedure). In this assay, small molecule methyl thioglycolate (**26**) was used to mimic the cysteine residues of proteins. The Michael addition product **27** formed readily and instantly upon the mixture of **PTL** and **26**. After chromatography purification, the stability of **27** was tested under diverse conditions (**Table 2.1**). **27** was proved to be stable under thermodynamic condition; however, after incubated in the elution buffer at 96 ℃ for 20 min and then extracted by $CDCl_3$, compound **27** was not observed in NMR, indicating the degradation of the compound. The result echoed our hypothesis that although we were able to pull-down the target proteins of **PTL** by streptavidin resin based affinity separation, the **PTL** moiety of the PTL-protein adduct decomposed under the harsh condition of elution, and led to the loss of fluorescent signals by SDS-PAGE.

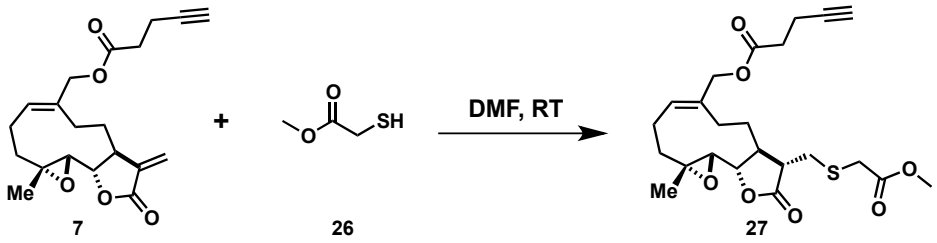

Scheme 2.6: Synthesis of PTL Michael adduct **27**.

	Conditions	Result
Thermodynamic conditions	$CDCl_3$, 55 ℃, 120 min	Stable
	d_6-DMSO, 100 ℃, 120 min	Stable
Elution condition	2% SDS, 3 mM Biotin, 2 M urea, 6 M thiourea in PBS, 96 ℃, 20 min	Decomposed

Table 2.1: Conditions and results of the stability assay of **27**.

Due to the lack of stability of PTL-protein adduct under brutal conditions, we purchased several modified (strept)avidin coated solid supports, assuming that the decreased affinities of these solid supports for biotin allow milder elution conditions.

After a screening of conditions, it turned out that the elution condition of monomeric avidin resin (Pierce®) was compatible with PTL-protein adducts (**Figure 2.13**). Streptavidin is a homo-tetramer and each subunit binds biotin with equal affinity. Multivalency is another reason of its high binding affinity to biotin.[285] On the other hand, monomeric avidin is a recombinant form of streptavidin with mutations to break the tetramer into a monomer, with a higher K_d of 10^{-7} to 10^{-8} mol/L.[288] As a result, the binding between monomeric avidin and biotin can be dissociated under neutral conditions at room temperature.[289]

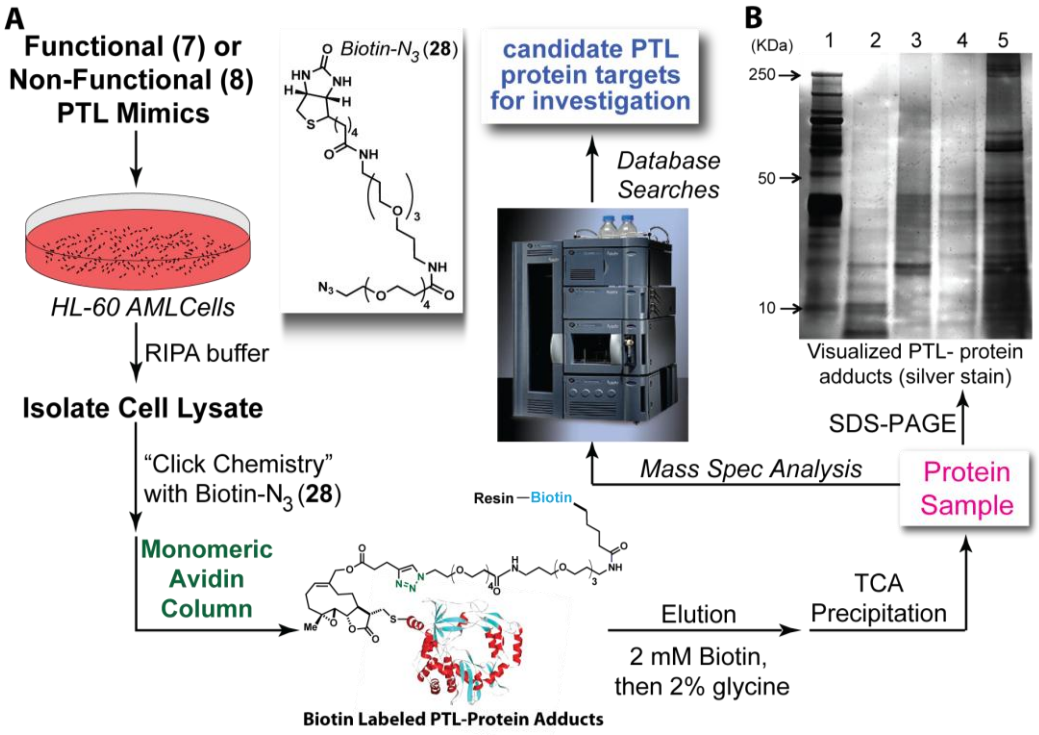

Figure 2.13: Modified strategy of comparative and competitive pull-down of PTL protein targets from HL-60 cells. A: Overview of strategy to elucidate the protein reactivity profile of PTL with chemical probes; B: SDS-PAGE (silver stain) showing the labeling results. Lane 1: protein ladder; 2: protein from functional pull-down (probe **7**); 3: protein from non-functional pull-down (probe **8**); 4: protein from competitive pull-down (**PTL** then probe **7**); 5: HL-60 whole cell lysate.

In the modified strategy of affinity separation (**Figure 2.13**, see section 2.5.4.7 for a detailed description of experimental details), HL-60 AML cells were treated with probe **7** or **8** before lysed by RIPA buffer. The incubation time (8 hr) and the concentration (40 μM) was determined in a series of cytotoxicity assay, so that highest concentration of PTL probes were used to maximize the labeling without significant cellular cytotoxicity (< 15 % cell death). After adjusted to an appropriate concentration, the cell lysates were incubated and clicked with Biotin-N_3 probe **28**. The protein samples were then loaded to a monomeric avidin resin columns to achieve the affinity separation. Briefly, the protein samples were allowed to incubate with the columns for 30 min to facilitate the binding of biotin to the resin. The non-bound proteins were removed from columns by amine free PBS buffer. The columns were then thoroughly washed by elution buffer (3 mM biotin in amine free PBS) to elute the bound proteins and regenerated by 0.1 M glycine solution (pH = 2.8). Both the elution and regeneration buffers were collected, neutralized by Tris•HCl buffer (pH = 9.5) and concentrated by 3 KDa molecular weight cut-off centrifugal filter units to yield crude samples of eluted proteins. The crude samples were precipitated by TCA to remove the extra detergents and analyzed by both SDS-PAGE and mass spectrometry. In addition to the above functional pull-down by probe **7** and non-functional pull-down by probe **8**, a competitive pull-down assay was also conducted to narrow down the target proteins of **PTL**. In the competitive assay, HL-60 cells were incubated with free **PTL** (20 μM) for 4 hours to occupy the active sites of target proteins, and then labeled with functional PTL probe **7** (20 μM). As a result, all the labeled proteins in competitive assay are the result from redundant or non-specific bindings that are actually not the target proteins of **PTL**, and

can be de-prioritized from the list of candidate **PTL** protein targets. **Figure 2.12B** shows the SDS-PAGE result of the affinity separation of functional, non-functional and competitive pull-down of HL-60 cells by PTL probes after silver staining. Analysis of the gel clearly shows the capability of probe **7** and **8** to form protein adducts, and differential labeling patterns were observed between functional, non-functional and competitive pull-down.

The above proteins samples from monometric avidin affinity separation have been analyzed by mass spectrometry (by contract to the Taplin Mass Spectrometry laboratory, Harvard University). In this proteomic study, proteins in each sample were digested by trypsin and the resulting peptide fragments were analyzed and sequenced by microcapillary LC/MS/MS techniques. In order to identify proteins from a sample, the peptides information obtained from the above experiment was then compared to IPI databases (International Protein Index). Any protein with three or more unique peptide matches compared to a known protein is considered confidently identified. Proteins with less than three matches are not considered confidently identified without further inspection of the data. In order to obtain more accurate results, multiple replicates of protein pull-down and affinity separation was performed (6 replicates for functional, 6 for non-functional and 5 for competitive) and all protein samples were analyzed by mass spectrometry in the same manner. The final data were grouped (group I: functional, group II: non-functional and group III: competitive. **Table 2.2**) and proteins that did not show enough replicates (observed for less than two times in the same group between biological replicates) were removed from the list. The candidates PTL protein targets were considered to be those identified in group I, but not appeared in either group II or

group III. The protein count data from the mass spectrometry analysis of all replicates has been included in **Table 2.2**. The identified protein targets were listed in **Table 2.3**, and their function and significances will be discussed in the next section.

Trial	Number of Proteins Oberserved		
	Group I	Group II	Group III
1	174	57	149
2	548	79	304
3	222	323	262
4	163	320	252
5	223	209	219
6	177	297	NA

Table 2.2: Number of proteins identified in each protein pull-down assay. Six biological data were performed. Group I: functional pull-down using probe **7**; Group II: non-functional pull-down using probe **8**; Group III: competitive pull-down using **PTL** then probe **7**. NA: not available.

2.3.6 Annotation of Protein Pull-Down Results.

Upon analysis of proteomic data, a total of 33 proteins have been identified as potential cellular protein targets of **PTL**. Specifically, proteins identified in non-functional pull-down assays and in competition experiments were excluded from proteins found in assays with functional probe. Those candidate proteins obtained by this method of prioritization that appeared at least two out of six times were kept for future study, yielding 33 candidate protein targets. The protein attributes, major functions and involvements in diseases of those potential targets that were observed for no less than three times will be discussed below.

Protein ID	Protein Name	Times observed	Protein ID	Protein Name	Times observed
GSN	Isoform 1 of Gelsolin	4	GSPT1	Eukaryotic peptide chain release factor GTP-binding subunit ERF3A	2
SMC3	Structural maintenance of chromosomes protein 3	4	GSTO1	Glutathione S-transferase omega-1	2
CAPZB	F-actin-capping protein subunit beta	3	HNRNPAB	Heterogeneous nuclear ribo-nucleoprotein A/B	2
GNB2	Guanine nucleotide-binding protein subunit beta-2	3	IPI-00453476.2	-	2
HDGF	Hepatoma-derived growth factor	3	NARG1	Isoform 2 of NMDA receptor-regulated protein 1	2
HNRNPH1	Heterogeneous nuclear ribonucleoprotein H	3	PCNA	Proliferating cell nuclear antigen	2
KCNAB2	Isoform 1 of Voltage-gated potassium channel subunit beta-2	3	PGAM2	Phosphoglycerate mutase 2	2
LOC-131691	Peptidyl-prolyl cis-trans isomerase-like 1	3	PRDX5	Peroxiredoxin-5, mitochondrial	2
RAB1A	Isoform 1 of Ras-related protein Rab-1A	3	PRG2	Bone marrow proteoglycan	2
RPS7P4	40S ribosomal protein S7	3	PSMA6	Proteasome subunit alpha type-6	2
ALDOC	Fructose-bisphosphate aldolase C	2	PSMA7	Proteasome subunit alpha type-7	2
ARPC1B	Actin-related protein 2/3 complex subunit 1B	2	SEPT7	Isoform 1 of Septin-7	2
CAND1	Cullin-associated NEDD8-dissociated protein 1	2	TXNL1	Thioredoxin-like protein 1	2
CLTCL1	Isoform 1 of Clathrin heavy chain 2	2	UBE2I	SUMO-conjugating enzyme UBC9	2
EIF3G	Eukaryotic translation initiation factor 3 subunit G	2	UPF1	Isoform 1 of regulator of nonsense transcripts 1	2
ERLIN1	ER lipid raft associated 1	2	WDR1	WD repeat-containing protein 1	2
ERP44	Endoplasmic reticulum resident protein ERp44	2			

Table 2.3: Identified protein targets by mass spectrometry. Protein ID: the abbreviated protein name in IPI database; Protein name: recommended name in IPI database; Times observed: the number of times the protein showed up in functional pull-down (out of 6 assays).

1. GSN (Gelsolin, also known as actin-depolymerizing factor or brevin, observed 4 times in pull-down) is a calcium-regulated, actin-modulating protein that binds to the ends of actin monomers or filaments, preventing monomer exchange (end-blocking or capping). It can promote the assembly of monomers into filaments (nucleation) as well as sever filaments already formed.[290] Defects in GSN are the cause of amyloidosis type 5[291] and were found in breast and colorectal cancers.[292] This protein has also been reported to involve in aging, regulation of cell adhesion and tissue regeneration.[293,294]

2. SMC3 (structural maintenance of chromosomes protein 3, also known as Chondroitin sulfate proteoglycan 6 or Chromosome-associated polypeptide, observed 4 times in pull-down) is a nuclear protein and the central component of cohesin, a complex required for chromosome cohesion during the cell cycle. The cohesin complex may form a large proteinaceous ring within which sister chromatids can be trapped. At anaphase, the complex is cleaved and dissociates from chromatin, allowing sister chromatids to segregate. Cohesion is coupled to DNA replication and is involved in DNA repair. The cohesin complex plays also an important role in spindle pole assembly during mitosis and in chromosomes movement.[295,296] Defects in SMC3 are the cause of Cornelia de Lange syndrome.[297] Because of the important role SMC3 plays in cell cycle and DNA repair, it presents a good target of anti-cancer of anti-CSC therapy.

3. CAPZB (F-actin-capping protein subunit beta, observed 3 times in pull-down) is a cytoskeleton protein that binds in a Ca^{2+}-independent manner to the fast growing ends of actin filaments, thereby blocking the exchange of subunits at these ends. Unlike other capping proteins (such as gelsolin and severin), these proteins do not sever actin

filaments. Plays a role in the regulation of cell morphology and cytoskeletal organization.[298] Interestingly, this protein has been reported recently to involve in the differentiation of human embryonic stem cells.[299]

4. GNB2 (Guanine nucleotide-binding protein G(I)/G(S)/G(T) subunit beta-2, observed 3 times in pull-down) is a cytoplasmic protein that locates in perinuclear region. Guanine nucleotide-binding proteins (G proteins) are involved as a modulator or transducer in various transmembrane signaling systems. The beta and gamma chains are required for the GTPase activity, for replacement of GDP by GTP, and for G protein-effector interaction.[300]

5. HDGF (Hepatoma-derived growth factor, observed 3 times in pull-down) is an acidic heparin-binding protein, with mitogenic activity for fibroblasts. It is also a transcription factor that stimulates cell proliferation when binding to DNA.[301] As a growth factor, HDGF stimulates the growth of endothelial cells, vascular smooth muscle cells and hepatoma cells. It is highly expressed in a variety of human cancers and is critical in tumorigenesis.[302]

6. HNRNPH1 (Heterogeneous nuclear ribonucleoprotein H, observed 3 times in pull-down) is a nuclear protein and a component of the heterogeneous nuclear ribo-nucleoprotein (hnRNP) complexes, which provide the substrate for the processing events that pre-mRNAs undergo before becoming functional mRNAs in the cytoplasm. Mediates pre-mRNA alternative splicing regulation.[303] Together with CUGBP1, it also inhibits insulin receptor (IR) pre-mRNA exon 11 inclusion in myoblast.[304]

7. KCNAB2 (Voltage-gated potassium channel subunit beta-2, observed 3 times in pull-down) is an accessory potassium channel protein that modulates the activity of the pore-forming alpha subunit and involved in synaptic transmission.[305]

8. LOC131691 (Peptidyl-prolyl cis-trans isomerase-like 1, also known as PPIase, observed 3 times in pull-down) accelerates the folding of proteins. It catalyzes the cis-trans isomerization of proline peptide bonds in oligopeptides. May be involved in pre-mRNA splicing. PPIase is most abundant in heart and skeletal muscle.[306]

9. RAB1A (Ras-related protein, observed 3 times in pull-down) is required for transit of protein from the endoplasmic reticulum through Golgi compartment. It binds GTP and GDP and possesses intrinsic GTPase activity.

10. RPS7P4 (40S ribosomal protein S7, observed 3 times in pull-down) is a cytoplasmic protein that is required for rRNA maturation.[307]

2.4 Conclusions and Future Direction

In conclusion, in order to identify the cellular protein targets of the anticancer natural product parthenolide and elucidate the mechanism of action of its cytotoxicity against CSCs, we designed and synthesized two PTL-alkyne affinity probes with diverse biological activity. Their capabilities of coupling with secondary probes using click chemistry and differential labeling proteins *in vitro* were demonstrated in a series of proof of concept experiments, including a click chemistry template reaction, the in-gel

fluorescent labeling assay and time course assays. When conducting the pull-down experiment, we experienced some difficulties in recovering the bound protein from affinity separation, due to the lack of stability of PTL-protein complex under elution conditions of streptavidin resin. The issue was successfully addressed by switching to monomeric avidin resin, which presents lower affinity to biotin and allows milder elution conditions than streptavidin resin. Utilizing the modified strategy, multiple replicates of comparative and competitive protein pull-down experiments were conducted. The eluted protein samples were analyzed by SDS-PAGE as well as mass spectrometry. Thirty-three potential protein targets were identified according to mass spectrometry data. Among the identified proteins, the most promising one is HDGF (Hepatoma-derived growth factor), which is a transcription factor and has been reported to be critical in tumorigenesis and highly expressed in a variety of human cancers.[302]

To further validate the protein targets of **PTL**, western blot experiments using antibodies against each identified proteins should be performed. In addition, we will utilize RNA interference (RNAi) technology to knockdown individual candidate proteins in AML cells and then test their viability. As a result, the knockdown of protein(s) that yields most reduction in AML CSC viability will likely be the cellular protein target that is responsible for the cytotoxicity of **PTL** against CSCs.

2.5 Experimentle

2.5.1 General

All reactions were performed under an anhydrous nitrogen atmostphere unless otherwise noted. Parthenolide was purchased from Enzo Life Sciences and repurified by SiO_2 chromatography prior to biological studies. Commercial grade reagents (Aldrich, Acros, Alfa Aesar) were used without further purification unless otherwise noted. Tetrahydrofuran and dichloromethane were rendered anhydrous by passing through the resin column of a solvent purification system. Benzene was purified by fractional distillation. Methanol, 1,2-dimethoxyethane, and *N*,*N*-dimethylformamide were purchased as anhydrous. All reactions were monitored by thin-layer chromatography (TLC) using silica gel 60-F_{254} TLC plates (Merck), and visualized using either iodine or charring with para-Anisaldehyde stain. Column chromatography employed Silicycle SiliaFlash® P60 (40-63 m) silica gel. SiO_2 column purification was performed using a CombiFlash® Rf 200 instrument using pre-packed silica gel column or Redisep Rf Gold High-Performance silica gel columns (Teledyne-Isco). HPLC purification was performed using an Agilent 1200 series instrument (preparative scale) equipped with a Zorbax (Agilent) preparatory column (21.2 x 250 mm, 7 μm). Analysis of compound purity was conducted on the aforementioned HPLC, using a Zorbax analytical column (4.6 x 150 mm, 5 μm). Nuclear magnetic resonance (NMR) spectroscopy employed a Bruker 400 Ultrashield 400 MHz spectrometer. Internal solvent peaks were referenced in each case. Mass spectral data was obtained from the University of Minnesota mass spectrometry lab, employing a Bruker Biotof II instrument.

2.5.2 Synthesis of Parthenolide Affinity Probes

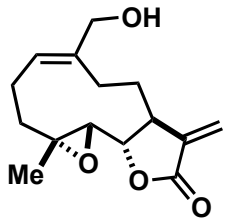

Melampomagnolide B (**4)**: MelB was prepared based on a previous literature report.[279] ^{1}H NMR ($CDCl_3$, 400 MHz): δ 6.22 (d, J = 3.5 Hz, 1H), 5.64 (t, J = 8.2 Hz, 1H), 5.54 (d, J = 3.2 Hz, 1H), 4.15 (d, J = 12.6 Hz, 1H), 4.07 (d, J = 12.6 Hz, 1H), 3.84 (t, J = 9.3 Hz, 1H), 2.83 (m, 2H), 2.41 (m, 3H), 2.21 (m, 3H), 1.66 (m, 2H), 1.54 (s, 3H), 1.08 (t, J = 12.4 Hz, 1H).

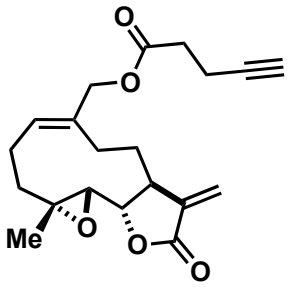

Melampomagnolide B alkyne 7: MelB (**4,** 12 mg, 0.045 mmol), pentynoic acid (8.9 mg, 0.091 mmol) and PPh_3 (26 mg, 0.10 mmol) were weighted out in a 50 mL RBF and dried over high vac for 2 hrs. To a stirred solution of the above material in dry THF (3 mL) was injected DIAD (20 μL, 0.10 mmol) dropwise at 0 °C under N_2. The reaction was slowly warmed to room temperature and allowed to stir overnight. THF was removed under reduced pressure and the residue was dissolved in CH_2Cl_2 (40 mL) and washed with brine (15 mL, 3x). The combined aqueous layer was extracted with EtOAc

(40 mL, 2x). The organic layers were collected, dried over anhydrous Na_2SO_4 and concentrated in vacuo. The crude material was subjected to SiO_2 column purification (gradient 5%-60% EtOAc in hexanes over 16 min) to yield the product (13 mg, 83%) as white solid. ^{1}H NMR ($CDCl_3$, 400 MHz): δ 6.26 (d, J = 3.5 Hz, 1H), 5.71 (t, J = 8.1 Hz, 1H), 5.55 (d, J = 3.2 Hz, 1H), 4.72 (d, J = 12.4 Hz, 1H), 4.49 (d, J = 12.4 Hz, 1H), 3.85 (t, J = 9.3 Hz, 1H), 2.86 (m, 2H), 2.54 (m, 4H), 2.30 (m, 6H), 1.98 (t, J = 2.4 Hz, 1H), 1.76 (m, 1H), 1.55 (s, 3H), 1.11 (t, J = 12.4 Hz, 1H). ^{13}C NMR ($CDCl_3$, 100 MHz): 171.5, 169.3, 138.7, 134.8, 130.9, 120.3, 82.3, 81.0, 69.2, 67.0, 63.3, 59.9, 42.7, 36.6, 33.3, 25.7, 24.4, 23.8, 18.0, 14.4. HRMS (ESI^+) *m/z* calcd for $[C_{20}H_{24}O_5+Na]^+$ 367.1521; found 367.1537.

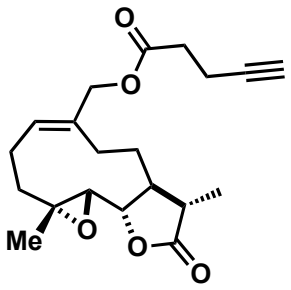

Reduced Melampomagnolide B alkyne 8: compound **6** (12.8 mg, 0.48 mmol), pentynoic acid (10 mg, 0.096 mmol) and PPh_3 (28 mg, 0.11 mmol) were weighted out in a 50 mL RBF and dried over high vac for 2 hrs. To a stirred solution of the above material in dry THF (3 mL) was injected DIAD (21 μL, 0.11 mmol) dropwise at 0 °C under N_2. The reaction was slowly warmed to room temperature and allowed to stir overnight. THF was removed under reduced pressure and the residue was dissolved in

CH_2Cl_2 (40 mL) and washed with brine (15 mL, 3x). The combined aqueous layer was extracted with EtOAc (40 mL, 2x). The organic layers were collected, dried over anhydrous Na_2SO_4 and concentrated in vacuo. The crude material was subjected to SiO_2 column purification (gradient 5%-60% EtOAc in hexanes over 16 min) to yield the product (14 mg, 84%) as white solid. ^{1}H NMR ($CDCl_3$, 400 MHz): δ 5.67 (t, J = 8.1 Hz, 1H), 4.71 (d, J = 12.5 Hz, 1H), 4.46 (d, J = 12.5 Hz, 1H), 3.83 (t, J = 9.5 Hz, 1H), 2.75 (d, J = 9.4 Hz, 1H), 2.55 (m, 5H), 2.30 (m, 6H), 1.98 (t, J = 2.5 Hz, 1H), 1.91 (m, 1H), 1.60 (m, 1H), 1.55 (s, 3H), 1.29 (d, J = 6.9 Hz, 3H), 1.08 (t, J = 12.8 Hz, 1H). ^{13}C NMR ($CDCl_3$, 100 MHz): 177.7, 171.4, 135.0, 130.1, 82.3, 81.0, 69.2, 66.4, 63.5, 59.8, 46.3, 41.5, 36.8, 33.4, 26.7, 24.3, 23.7, 17.9, 14.4, 13.1. HRMS (ESI^+) *m/z* calcd for $[C_{20}H_{26}O_5+K]^+$ 385.1417; found 385.1412.

2.5.3 Synthesis of Fluorescent Probes

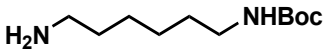

***tert*-butyl (6-aminohexyl)carbamate** (**13**):[282] to a stirred solution of 1,6-diaminohexane (2.0 g, 17.2 mmol) in 1,4-dioxane (100 mL) at 0 ℃ was added dropwise the solution of Boc_2O (0.94 g, 4.3 mmol) in deionized H_2O (100 mL) through an addition funnel. The reaction was stirred overnight and 1,4 – dioxane was removed under reduced pressure. The aqueous solution was extracted by EtOAc (100 mL, 3x), and the combined organic layers were dried over anhydrous Na_2SO_4 and concentrated in vacuo to yield compound **12** (crude, 820 mg, 88%). ^{1}H NMR ($CDCl_3$, 400 MHz): δ 4.53

(br s, 1H), 3.09 (m, 2H), 2.67 (td, *J* = 3.08 Hz, *J* = 6.8 Hz, 2H), 1.47 (m, 11H), 1.32 (m, 4H), 1.12 (br s, 4H).

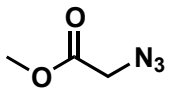

α-azidoacetic acid (15):[308] Anhydrous MeOH (15 mL) was added slowly to bromoacetyl bromide (0.74 mL, 8.5 mmol) at 0 ℃. The reaction was stirred for 2 hrs at 0 ℃ before slowly quenched by water (15 mL). MeOH was removed under reduced pressure with caution, because the product methyl 2-bromoacetate is volatile (bp: 50 ℃ at 15 mmHg). The resulting aqueous solution was neutralized by $NaHCO_3$ (saturated aq., 15 mL) and extratcted by CH_2Cl_2 (60 mL, 3x). The organic layers were collected, dried over anhydrous Na_2SO_4 and concentrated in vacuo to yield crude product of methyl 2-bromoacetate. To a stirred solution of methyl 2-bromoacetate in DMF (5 mL) was added NaN_3 (600 mg, 9.2 mmol). The reaction was allowed to stir at room temperature overnight. After the removal of DMF under reduced pressure, the residue was suspended in H_2O (40 mM) and extracted by CH_2Cl_2 (60 mM, 3x). The organic layers were collected, dried over anhydrous Na_2SO_4 and concentrated in vacuo to yield **15** (678 mg, 69%). This material was used crude in the reaction to prepare **18**.

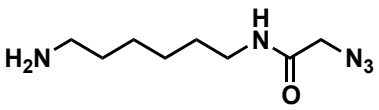

***N*-(6-aminohexyl)-2-azidoacetamide** (**18**):[281] To a stirred solution of the **15** (678 mg, 5.9 mmol) in THF (5 mL) was added dropwise KOH aqueous solution (15%, 2 mL). The reaction was stirred at 45 ℃ for 3 hr. THF was removed under reduced pressure. The remaining aqueous solution was diluted with deionized H_2O to 40 mL and washed by ether (20 mL, 2x). The aqueous layer was neutralized by conc. HCl and extracted by EtOAc (60 mL, 3x). The combined organic layers were dried over anhydrous Na_2SO_4 and concentrated in vacuo to yield azidoacetic acid (404 mg, 68%). ^{1}H NMR ($CDCl_3$, 400 MHz): δ 10.40 (s, 1H), 3.97 (s, 2H). To a stirred solution of *N*-hydroxyl-succinimide (56 mg, 0.48 mmol) and DCC (99 mg, 0.48 mmol) in DMF (2 mL) was added the solution of azidoacetic acid (40 mg, 0.39 mmol) in DMF (1 mL). After stirring at room temperature for 4 hr, the reaction was filtered and the filtrate was concentrated to give **16**. Crude **16** was added to a solution of **13** (95 mg 0.44 mmol) in DMF (2 mL). The reaction was allowed to stir overnight. DMF was then removed under reduced pressure. The residue was suspended in deionized H_2O (15 mL) and extracted by CH_2Cl_2 (40 mL, 3x). The combined organic layers were dried over anhydrous Na_2SO_4 and concentrated in vacuo. The crude compound was purified by SiO_2 chromatography (gradient 5%-80% EtOAc in hexanes over 16 min) to yield **17** (105 mg, 89%). To a stirred solution of the **17** (105 mg, 0.35 mmol) in EtOAc (10 mL) was added dropwise conc. HCl under 0 ℃ until pH = 2. The reaction was warmed to room temperature and stirred for 2 hr before quenched by deionized H_2O (10 mL), the water layer was neutralized by KOH solution (3 M in H_2O, 10 mL) and extracted by EtOAc (40 mL, 3x). The combined organic layers were dried over anhydrous Na_2SO_4 and concentrated in vacuo to yield compound **18** (54 mg, 77%). ^{1}H NMR (d_4-MeOH, 400 MHz): δ 3.86 (s,

2H), 3.37 (s, 1H), 3.22 (t, *J* = 8.0 Hz, 2H), 2.69 (t, *J* = 7.2 Hz, 1H), 1.54 (m, 4H), 1.37 (m, 4H).

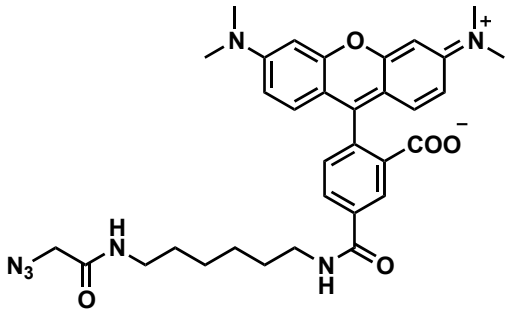

Rh-N_3 (9):[281] To a stirred solution of **18** (12 mg, 0.060 mmol) in DMF was added Rh-NHS (**19**, 19 mg, 0.030 mmol). The reaction was stirred overnight. DMF was removed under reduced pressure and the crude material was purified by preparative HPLC (gradient 10% to 100% acetonitrile in H_2O containing 0.1% TFA over 40 min, then 100% acetonitrile for 15 min) to yield **9** (10 mg, 45%). ^{1}H NMR (D_2O, 400 MHz): δ 8.76 (d, *J* = 1.6 Hz, 1H), 8.25 (dd, *J* = 1.6 Hz, *J* = 7.8 Hz, 1H), 7.51 (d, *J* = 7.9 Hz, 1H), 7.13 (m, 2H), 7.05 (dd, *J* = 2.3 Hz, *J* = 9.4Hz, 2H), 6.97 (d, *J* = 2.2 Hz, 2H), 3.86 (s, 2H), 3.46 (t, *J* = 6.9 Hz, 2H), 3.30 (s, 12H), 3.23 (t, *J* = 6.9 Hz, 2H), 1.69 (m, 2H), 1.55 (m, 2H), 1.44 (m, 4H).

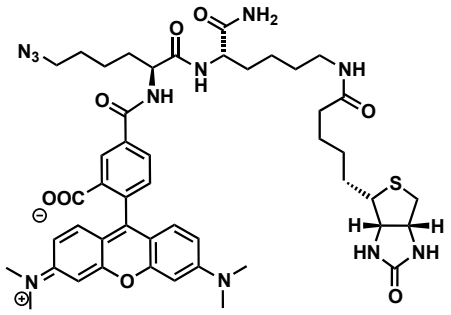

Rhodamine-Biotin-N_3 (**10**): the compound was prepared as previously described.[284]

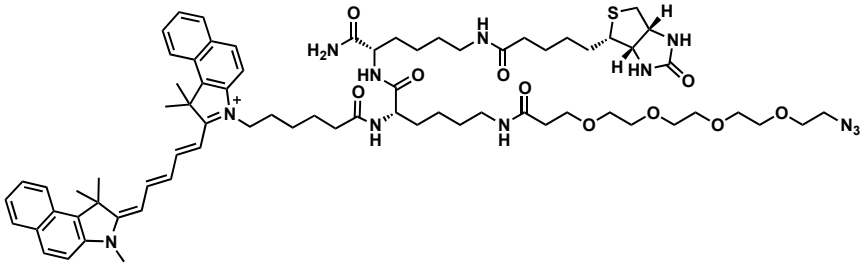

Cy5.5-Biotin-N_3 (**11**): The compound was prepared using a modification of the protocol published by Cravatt and coworkers to synthesize **10**.[284] Cy5.5-biotin-N_3 was synthesized on Sieber Amide resin (Novabiochem) using standard 9-fluorenylmethoxycarbonyl (Fmoc) solid phase synthesis. Fmoc protected resin (80 mg, 0.035 mmol) was transferred into a reaction vessel, deprotected with 15% piperidine/N-methylpyrrolidinone (NMP, 2 mL, 10 min, 3x) and washed (NMP, 2 mL, 3x; CH_2Cl_2, 2 mL, 3x; NMP, 2 mL, 3x) to remove excess reagents. Then Fmoc-Lys(Biotin)-COOH (Novabiochem, 104 mg, 0.175 mmol) was coupled to the resin (2.5 hr) using HBTU (68 mg, 0.174 mmol), HOBt (28 mg, 0.175 mmol) and DIPEA (50 μL, 0.28 mmol) in NMP (2 mL) to yield **20**. The resin was then washed and deprotected as described above.

Fmoc-Lys(Alloc)-OH was coupled to the resin using same equivalents of reagents overnight to yield **23**. After subsequent wash as described above, the alloc group was cleaved (2 hr) using $Pd(PPh_3)_4$ (8 mg, 0.07 mmol) in mixed solvent DCM/AcOH/NMA (*N*-methylaniline) = 37 : 2 : 1 (0.8 mL). After washing, N_3-PEG-COOH was coupled to the resin using the same equivalents of coupling reagents overnight to give **24**. Following the subsequent wash and cleavage of Fmoc as described above, Cy5.5 was appended to the free amine upon reaction with Cy5.5-succinimidyl ester (Lumiprobe, 15 mg, 0.021 mmol) using TEA (100 μL, 0.70 mmol) in NMP (2 mL) overnight to give **25**. The resin was then thoroughly washed (NMP, 2 mL, 3 x; CH_2Cl_2, 2 mL, 3 x; MeOH, 2 mL then 50% CH_2Cl_2/MeOH until wash was clear). Compound **11** was cleaved off resin with dilute TFA (3% in CH_2Cl_2, 3 mL, 10 min, 5x). Toluene was added to the dark red solution, and the solvent was removed under reduced pressure. The crude material was then purified by preparative HPLC (gradient 10% to 40% acetonitrile in H_2O over 10 min, gradient 40% to 100% acetonitrile in H_2O over 45 min, then 100% acetonitrile for 5 min, all solvent contains 0.1% TFA) to give compound **10** (8 mg, overall yield 29%). HRMS (ESI^+) *m/z* calcd for $[C_{79}H_{101}N_{12}O_{10}S+Na]^{++}$ 680.3689; found 680.3714. Analytical HPLC (700 nm):

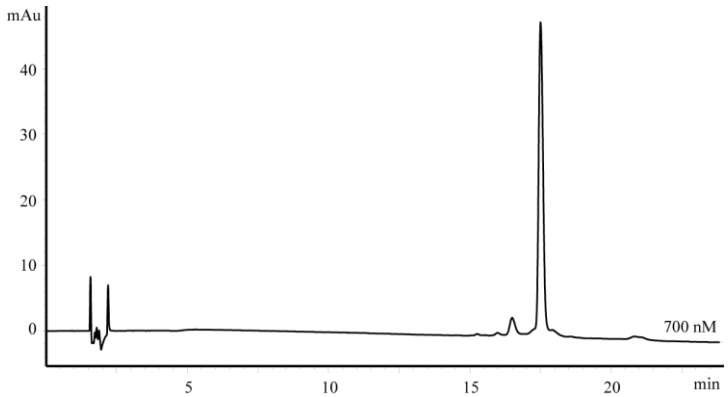

2.5.4 Procedures for Biochemical Experiments

2.5.4.1 **Kinase screening assay** (section 2.3.1). The experiments were performed by Millipore KinaseProfiler Service. For protocol, see https://www.millipore.com/techpublications/tech1/pf3036.

2.5.4.2 **Protocol for Cell Culture Cytotoxicity Assays** (section 2.3.2). A protocol for these experiments was previously published by Hexum et al.[309] HL-60 (ATCC, CCL-240) were maintained in a humidified 5% CO_2 environment at 37 ℃ in culture flasks (Corning) and cultured in IMDM media (Cellgro) supplemented with 20% FBS (Gibco), penicillin (100 I.U./mL), and streptomycin (100 μg/mL, ATCC). Cells were cultured at a density of 10,000 cells/well in cell culture media (50 μL) in standard 96-well plates (Costar) 24 h prior to treatment. Controls used were Blank (no cells) wells and control (vehicle control treated) wells and were prepared for every experiment. Tested compounds (**7** and **8**) were serially diluted in pre-warmed media and dosed to 96 well plates (final volume/well = 100 μL; final DMSO concentration = 0.5%). Approximately 1-3 h before the end of the treatment period (48 h), Alamar Blue (Invitrogen) cell viability reagent was added to the 96 well plates (10 μL). A quantitative measure of cell viability can be achieved from evaluating the ability of metabolically active cells (which are proportional to the number of living cells) to convert resazurin (non-fluorescent dye) to red-fluorescent resorufin. Fluorescence data were obtained on a Molecular Devices SpectraMax M2 plate reader. Background fluorescence (no cell controls) was subtracted from each well and cellular viability values following

compound treatment were normalized to vehicle-only treated wells (control wells only treated with aqueous DMSO, which were arbitrarily assigned 100% viability). Individual IC_{50} curves were generated by fitting data to the sigmoidal (dose response) function of varied slope in GraphPad Prism (v. 5.0) software. Only curve fits with $R^2 > 0.95$ were deemed sufficient. Each experiment was performed in biological triplicate and mean IC_{50} values were calculated from the individual IC_{50} values obtained from each replicate. Standard deviation was calculated from the individual IC_{50} values obtained for each biological replicate.

2.5.4.3 **click chemistry template reaction** (section 2.3.4.1): the following stock solutions were made beforehand: probe **7** (10 mM in DMSO), probe **8** (10 mM in DMSO), tris[(1-benyl-1*H*-1,2,3-triazol-4-yl)methyl]amine (ligand, 10 mM in DMSO), RhN_3 (**9**, 10 mM in DMSO), (+)sodium L-ascobate (50 mM in H_2O), $CuSO_4$ (50 mM in H_2O). In the template reaction, sterilized PBS buffer (150 μL), probe **7** (or probe **8**, 10 μL), RhN_3 (**9**, 8 μL), ligand (10 μL) and sodium ascobate (20 μL) were added subsequently into a 1.5 mL Eppendorf tube. The sample was gently vortexed at room temperature, and the reaction was initiated by the addition of $CuSO_4$ (20 μL). Each reaction was monitored by analytic HPLC at 595 nm every 10 min until the disappearance of RhN_3 peak.

2.5.4.4 **General protocol for RIPA lysis of HL-60 cells**: HL-60 cells (ATCC, CCL-240) were cultured in IMDM media (Cellgro, supplemented with 20% FBS (Gibco), penicillin (100 I.U./mL), and streptomycin (100 μg/mL, ATCC)) in a humidified 5% CO_2 environment at 37 ℃ in culture flasks (Corning, 75 cm^2, 20 mL media/flask). After the concentration reached 1 million/mL, HL-60 cells were

transferred to a 50 mL falcon tube and centrifuged down at 2500 x g to form a cell pellet. After the supernatant cell media was decanted, the cell pellet was suspended in cold PBS buffer (1 mL) and transferred to a 1.5 mL eppendorf tube. Again, cells were centrifuged down at 2500 x g to form a cell pellet. The supernatant was removed with a pipette. RIPA buffer (Pierce, pre-chilled, 1.1 mL) was pre-mixed with protease inhibitor (25x, generated from Roche complete® EDTA-free protease inhibitor cocktail tablets) and added to the cell pellet. The mixture was pipetted up and down to suspend the cells and then shaken gently for 15 min on ice and vortexed every 5 min. The sample was centrifuged at 14000 x g for 15 min at 4 ^{o}C to pellet the cell debris, which was removed by a p200 pipette. The protein concentration of HL-60 cell lysate was determined by 96 well-plate BCA (bicinchoninic acid) assay (Pierce BCA protein assay kit) and adjusted to 1 mg/mL by adding extra RIPA buffer. The final protein lysates were kept at -20 ℃ until use.

2.5.4.5 **In gel fluorescent labeling and time course assay** (section 2.3.4.2): HL-60 cell lysate (20 μL, 1 mg/mL) and PTL probe **7** (or **8**, 3 μL, 10 mM in DMSO) were agitated at room temperature in an 1.5 mL eppendorf tube for 60 min. Following the incubation, RhN_3 (**9**, 3 μL, 10 mM in DMSO), ligand (3 μL, 10 mM in DMSO) and sodium ascobate (6 μL, 50 mM in H_2O) were added subsequently to each sample. The samples were gently vortexed, and the reactions were initiated by the addition of $CuSO_4$ (6 μL, 50 mM in H_2O). The tubes were agitated gently at room temperature for 30 min before the proteins were denatured by LDS loading buffer (Invitrogen, NuPAGE®, 15 μL, 4x concentrated) and reducing agent DTT (Invitrogen, NuPAGE®, 6 μL, 10x concentrated) at 96 ℃ for 5 min. After the samples were cooled down to room

temperature, 20 μL of each sample were loaded to a gel (Invitrogen NuPAGE® Bis-Tris minigel, 1 mm, 10 wells, 4%-12%), together with protein ladder and denatured whole cell lysate as control. The gel electrophoresis was performed at 185 V for 35 min, and the fluorescent signals were recorded in a GE FLA7000 Typhoon biomolecular imaging system with a R710 filter, and 650 nm excitation wavelength. In the time course assay, five tubes of HeLa cell lysates (purchased, 1 mg/mL, 20 μL) were incubated with probe **7** (3 μL, 10 mM in DMSO) 50 min, 40 min, 30 min, 20 min or 10 min before the initiation of click chemistry. All the following steps were the same as described above.

2.5.4.6 **Streptavidin affinity purification** (section 2.3.5): HL-60 cell lysates (200μL, 1 mg/mL) and PTL probe **7** (or **8**, 3 μL, 10 mM in DMSO) were agitated at room temperature in an 1.5 mL eppendorf tube for 60 min. Following the incubation, Rh-Bio-N_3 (**10**, 4 μL, 10 mM in DMSO), ligand (4 μL, 10 mM in DMSO) and sodium ascobate (8 μL, 50 mM in H_2O) were added subsequently to each sample. The samples were gently vortexed, and the reactions were initiated by the addition of $CuSO_4$ (8 μL, 50 mM in H_2O). After 1 hr, the labeled protein samples were transferred to tubes with streptavidin agarose (Pierce, 100 μL) and agitated for 1 hr at room temperature. The samples were centrifuged at 1400 x g for 3 min to remove the supernatant. The residue agarose was washed by PBS (1 mL, 3x), 0.2% SDS/PBS (1 mL, 3x) and deionized H_2O (1 mL, 3x) to thoroughly remove the unbound protein. At last, 150 μL of 2% SDS/PBS (or 2% SDS, 3 mM Biotin, 2 M urea, 6 M thiourea in PBS) was added to the agarose and heated to 96 ℃ for 20 min to release the bound protein. The resin was pelleted down by centrifugation (300 x g, 1 min), and the supernatants were collected and incubated with

reducing agent DTT (Invitrogen, NuPAGE®, 10x) before the performance of SDS-PAGE.

2.5.4.7 **Stability assay** (section 2.3.5): Compound **7** (10 mg, 0.029 mmol) was added to a stirred solution of methyl thioglycolate (**26**, 10 mg, 0.094 mmol) in DMF (1 mL). The reaction was stirred at room temperature for 1 hr. DMF was removed under reduced pressure and the residue was purified by SiO_2 chromatography (gradient 5%-80% EtOAc in hexanes over 16 min) to give compound **27** (13 mg, 99%). Compound **27** (6 mg) was dissolved in $CDCl_3$ (1 mL) and heated to 55 ℃ for 2 hr. The NMR did not show any change to the ^1H spectrum. $CDCl_3$ was removed under reduced pressure, and the material was re-dissolved in DMSO-d_6. The DMSO solution was heated to 100 ℃ for 2 hr, the NMR did not show any change to the ^1H spectrum. Compound **27** (7 mg) was dissolved in DMSO (50 μL) and incubated with elution buffer of streptavidin (2% SDS, 3 mM Biotin, 2 M urea, 6 M thiourea in PBS, 0.5 mL) at 96 ℃ for 20 min. After cooling down, the above system was extracted by $CDCl_3$. Compound **27** was not observed in NMR, presumably because of the degradation of **27** under the elution conditions.

2.5.4.8 **Modified affinity separation strategy** (section 2.3.5):

a) Functional pull-down: HL-60 cells were grown in a T-75 corning flask in 20 mL media until the concentration reached 1 x 10^6 cells/mL. The cells were incubated under 37 ^oC with functional **PTL** probe (**7**, 40 μM, the probe was pre-dissolved in DMSO to form a 10 mM stock solution) for 8 hrs and then lysed by RIPA buffer. The protein concentration of the lysates was determined by BCA assay. In most cases, the

concentration is between 1.1 to 1.3 mg/mL. The concentration was adjusted to 1 mg/mL by adding extra RIPA buffer.

To functional labeled HL-60 cell lysate (1 mg/mL, 0.5 mL) was added Biotin-N_3 probe (**28**, 10 mM in DMSO, 3.3 μL), ligand (10 mM in DMSO, 3.8 μL), sodium ascorbate (50 mM in H_2O, 7 μL) and $CuSO_4$ (50 mM in H_2O, 7 μL) subsequently. The mixture was allowed to gently agitate at room temperature for 2.5 hr before loading to a monomeric avidin agrose column. The column contains 2 mL agrose and was washed with blocking buffer (10 mL, 2 mM D-biotin in PBS), regeneration buffer (12 mL, 0.1 M glycine, pH2.8) and amine free PBS buffer (12 mL, generated from pierce BupH™ Phosphate Buffered Saline pack) before using. After loaded, the protein sample was incubated the monomeric avidin column for 0.5 hr at room temperature and then, the column was washed with amine free PBS buffer (12 mL) to remove non-bound protein, blocking buffer (12 mL) to elute labeled protein and regeneration buffer (12 mL) to elute and regenerate the resin for further use. The fractions from both the blocking buffer and regeneration buffer were collected to a 15 mL centrifugal filter unit (Millipore, amicon ultra 15, PL membrane, 3 KDa) and neutralized with Tris•HCl buffer (1 mL, pH 9.5). The filter unit was centrifuged at 4000 x g for 45 min to centrifuge the sample to about 300 μL. An aliquot of the final protein sample was analyzed by SDS-PAGE (Invitrogen NuPAGE Bis-Tris minigel, 1 mm, 10 wells, 4%-12%, 185 V, 35 min), followed by silver staining. The protein sample was precipitated by 10% TCA (procedure see below) to remove salt and analyzed by mass spectrometry (at Taplin Mass Spectrometry Facility, Harvard Medical School).

b) Non-functional pull-down: HL-60 cells were grown in a T-75 corning flask in 20 mL media until the concentration reached 1 x 10^6 cells/mL. The cells were incubated under 37 ^oC with non-functional **PTL** probe (**8**, 40 μM, the probe was pre-dissolved in DMSO to form a 10 mM stock solution) for 8 hrs and lysed by RIPA buffer. The protein concentration was determined by BCA assay (Pierce BCA protein assay kit). In most cases, the concentration is between 1.4 to 1.6 mg/mL. The concentration was adjusted to 1 mg/mL by adding extra RIPA buffer.

To non-functional labeled HL-60 cell lysate (1 mg/mL, 0.5 mL) was added Biotin-N_3 probe (**15**, 10 mM in DMSO, 3.3 μL), ligand (10 mM in DMSO, 3.8 μL), sodium ascorbate (50 mM in H_2O, 7 μL) and $CuSO_4$ (50 mM in H_2O, 7 μL) subsequently. The mixture was allowed to gently agitate at room temperature for 2.5 hr before loading to a monomeric avidin agrose column. The column separation process was the same as described above. An aliquot of the protein sample was analyzed by SDS-PAGE (Invitrogen NuPAGE Bis-Tris minigel, 1 mm, 10 wells, 4%-12%, 185 V, 35 min), followed by silver staining. The protein sample was precipitated by 10% TCA to remove salt and analyzed by mass spectrometry (at Taplin Mass Spectrometry Facility, Harvard Medical School).

c) Competitive pull-down experiment: HL-60 cells were grown in a T-75 corning flask in 20 mL media until the concentration reached 1 x 10^6 cells/mL. The cells were firstly incubated under 37 ^oC with **PTL** (20 μM, the probe was pre-dissolved in DMSO to form a 10 mM stock solution) for 4 hrs and then, with functional **PTL** probe (**7**, 20 μM) for another 3 hrs. Cells were lysed by RIPA buffer and protein concentration was

determined by BCA assay (Pierce BCA protein assay kit). In most cases, the concentration is between 1.1 to 1.3 mg/mL. The concentration was adjusted to 1 mg/mL by adding extra RIPA.

To competitively labeled HL-60 cell lysate (1 mg/mL, 0.5 mL) was added Biotin-N_3 probe (**15**, 10 mM in DMSO, 3.3 μL), ligand (10 mM in DMSO, 3.8 μL), sodium ascorbate (50 mM in H_2O, 7 μL) and $CuSO_4$ (50 mM in H_2O, 7 μL) subsequentially. The mixture was allowed to gently agitate at room temperature for 2.5 hrs before loading to a monomeric avidin agrose column. The column separation process was the same as described above. An aliquot of the protein sample was analyzed by SDS-PAGE (Invitrogen NuPAGE Bis-Tris minigel, 1 mm, 10 wells, 4%-12%, 185 V, 35 min), followed by silver staining. The protein sample was precipitated by 10% TCA to remove salt and analyzed by mass spectrometry (at Taplin Mass Spectrometry Facility, Harvard Medical School).

d) TCA (Trichloroacetic acid) protein precipitation: After concentration by filter units, the protein samples were diluted to 400 μL using cold deionized H_2O. After the addition of 100 μL 100% TCA solution (prepared by dissolving 10 g TCA to a total volume of 10 mL in deionized H_2O), the protein samples were incubated on ice until a white cloudy precipitation was observed (about 20 min). The samples were centrifuged at 14000 x g at 4 °C for 20 min to yield the protein pellets. After careful removal TCA solution, 200 μL cold acetone was added to each protein pellet. The samples were votexed and centrifuged again for 10 min at 14000 x g at 4 °C and the acetone was

removed with precaution. At last, the residual acetone was dried in speed-vac over night to yield the final protein pellets that were ready for mass spectrum analysis.

e) Mass spectrometry analysis: the above mentioned protein samples were analyzed at Taplin Mass Spectrometry Facility, Harvard Medical School (https://taplin.med.harvard.edu/intro). Briefly, proteins in each sample were digested by trypsin and the resulting peptide fragments were analyzed and sequenced by microcapillary LC/MS/MS techniques. In order to identify proteins from a sample, the peptides information obtained from the above experiment was then compared to IPI databases (International Protein Index). Any protein with three or more unique peptide matches compared to a known protein is considered confidently identified. Proteins with less than three matches are not considered confidently identified without further inspection of the data.

2.6 NMR Spectrum

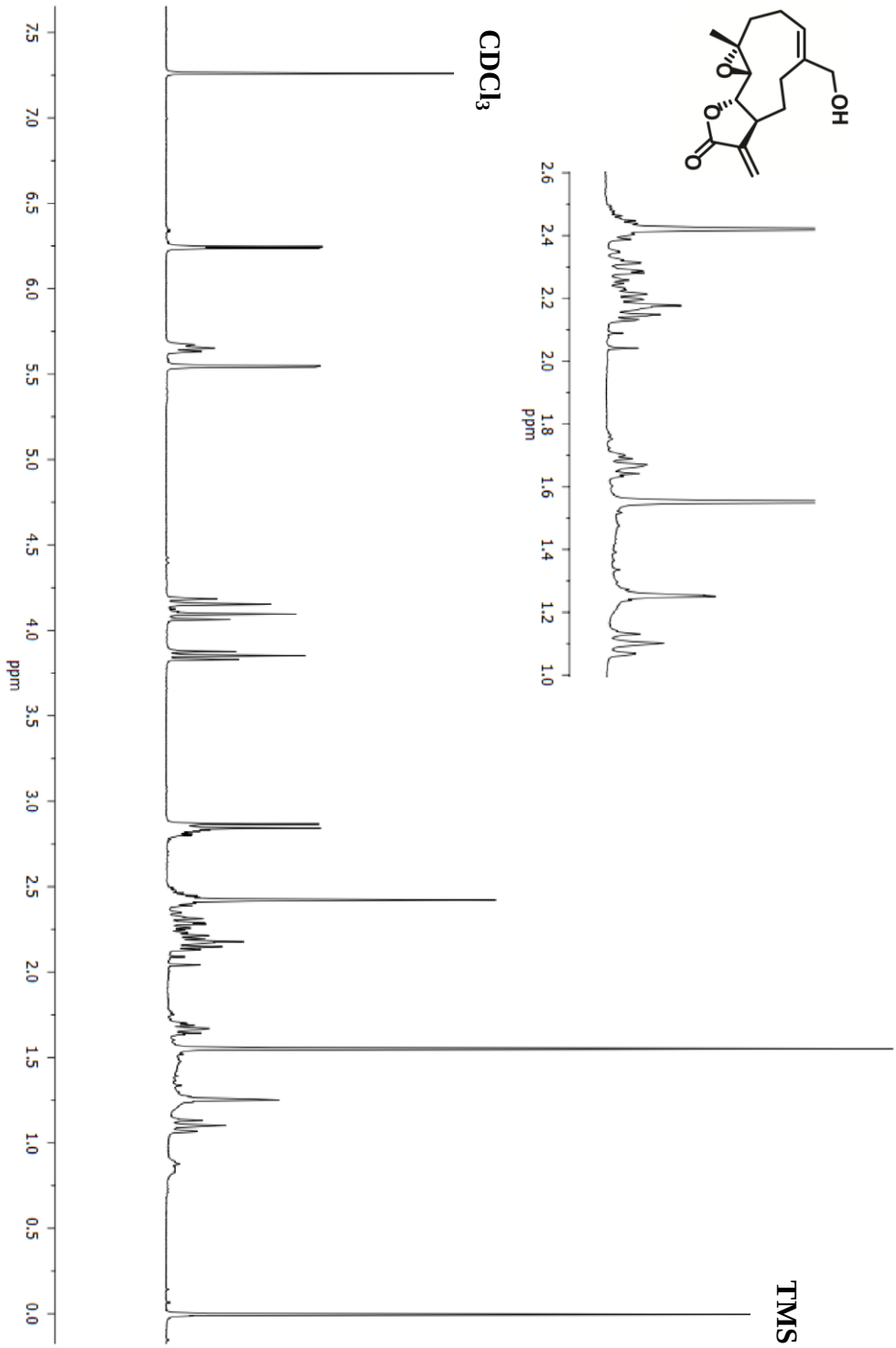

Melampomagnolide B alkyne 7
^{1}H NMR ($CDCl_3$):

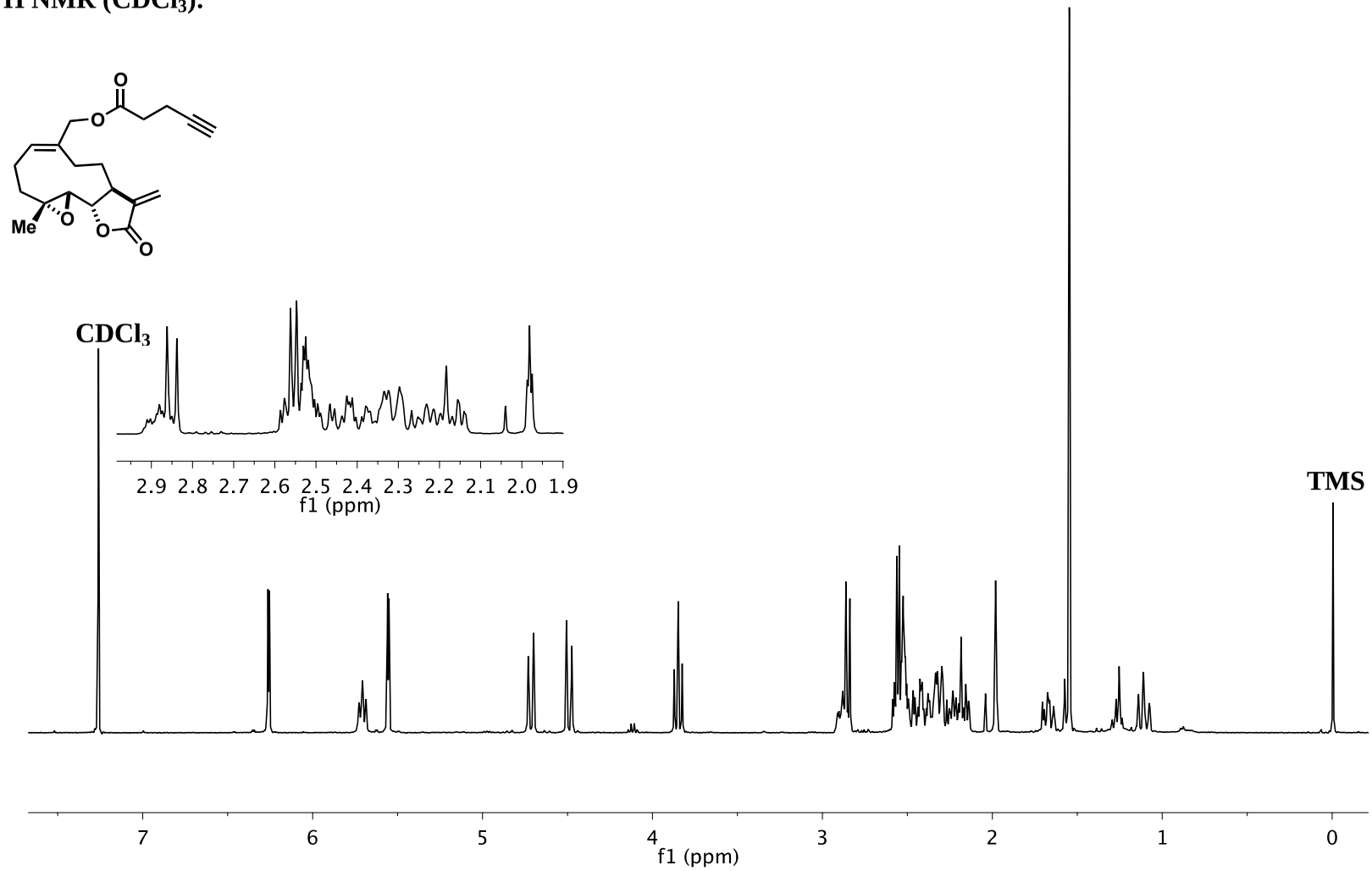

Melampomagnolide B alkyne 7
^{13}C NMR ($CDCl_3$):

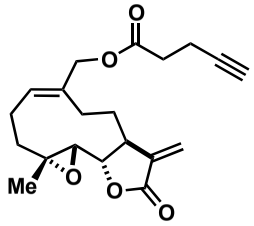

Reduced Melampomagnolide B alkyne 8
^{1}H NMR ($CDCl_3$):

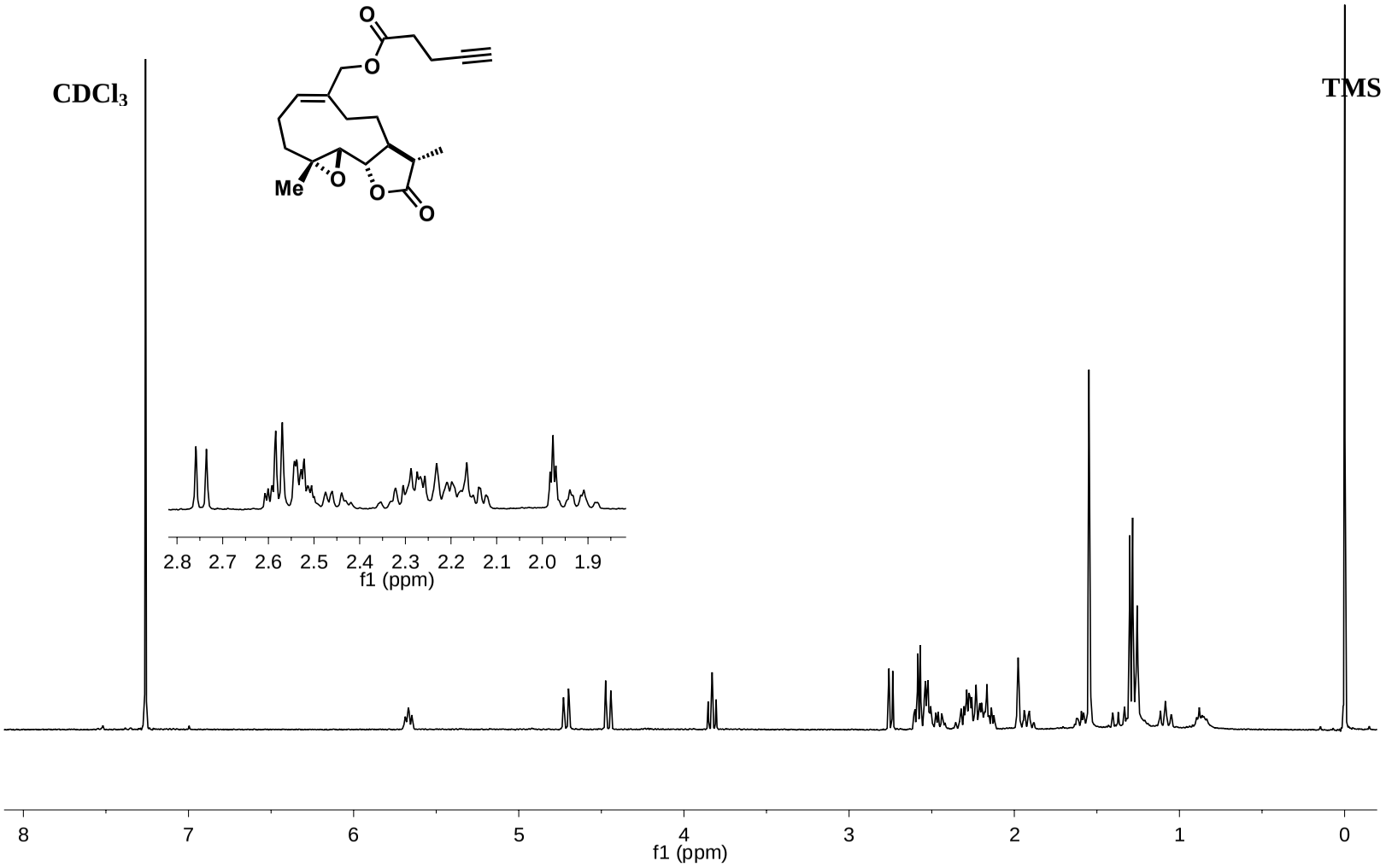

Reduced Melampomagnolide B alkyne 8

^{13}C NMR ($CDCl_3$):

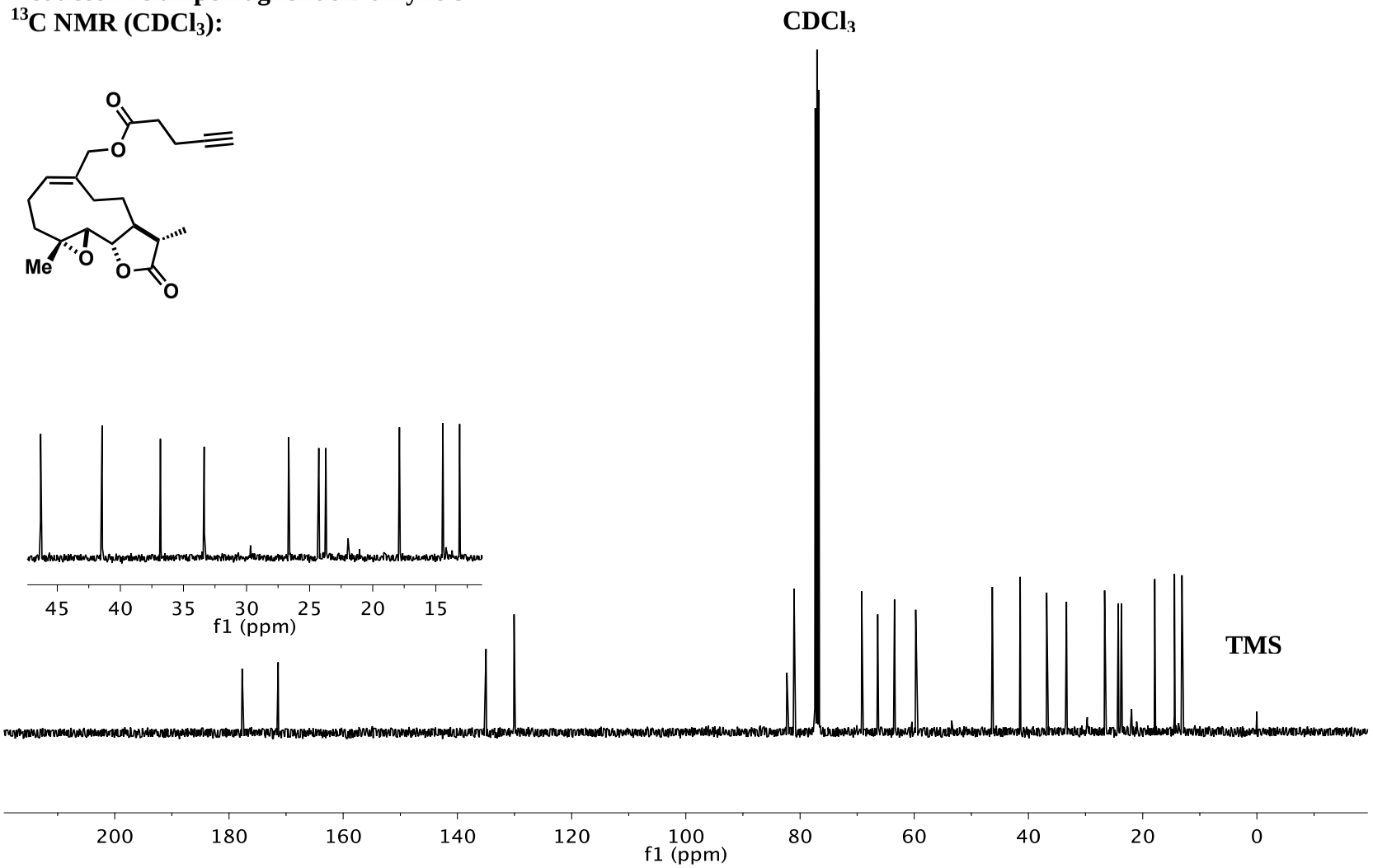

tert-butyl (6-aminohexyl)carbamate (13)
^{1}H NMR ($CDCl_3$):

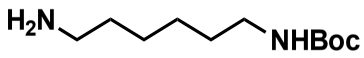

azidoacetic acid
^{1}H NMR ($CDCl_3$):

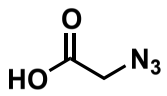

***N* - (6-aminohexyl)-2-azidoacetamide (18)**

^{1}H NMR (CD_3OD):

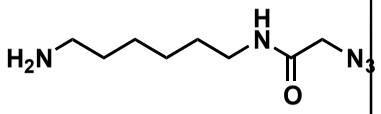

Rhodamine-N_3 9
^{1}H NMR (D_2O):

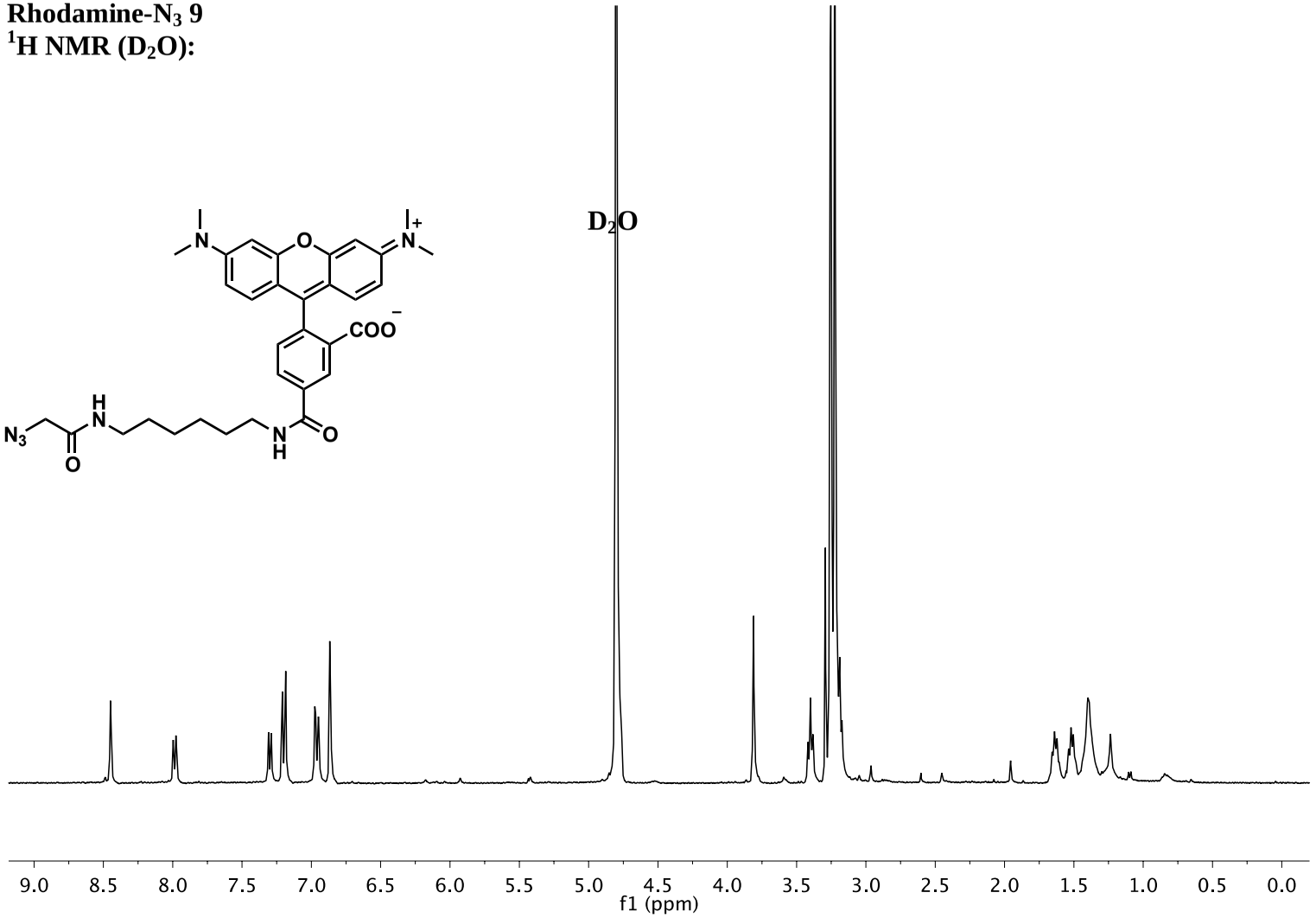

Chapter 3. Semi-Synthesis and Biological Evaluation of Parthenolide Analogues.

3.1 Introduction

The natural product Parthenolide (**PTL**, **1, figure 3.1**) is a sesquiterpene lactone isolated from the Mexican Indian medicinal herb *Tanacetum parthenum* (feverfew plant),[251] which has been used for over a century for the treatment of various common diseases such as arthritis, asthma, fever, and migraine.[252,253] **PTL** has been extensively studied as an anticancer agent, showing significant efficacy towards a wide spectrum of human cancer cells, such as brain cancer,[254] prostate cancer,[255,256] breast cancer,[257,258] chronic lymphocytic leukemia,[259] and pancreatic cancer.[260] In 2005, the identification of **PTL** as the first stand-alone cytotoxic compound against leukemia stem cells (LSCs) further heightened its therapeutic potential. In addition, **PTL** exhibits selective cytotoxicity for LSCs versus normal hematopoietic stem cells (HSCs).[19] After the discovery of **PTL**'s promising inhibitory activity against the LSCs, the study of the anti-cancer activity of **PTL** has entered a new prosperous era. Besides leukemia, **PTL** was demonstrated to inhibit the survival of cancer stem cells (CSCs) in other types of cancers, including breast cancer[261] and prostate cancer.[262]

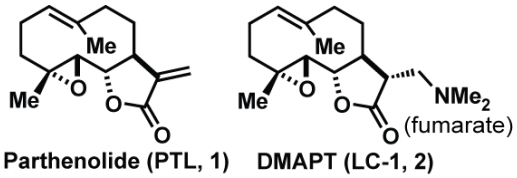

Figure 3.1: Structure of parthenolide and **LC-1**.

Despite the striking biological activity of **PTL**, two hurdles still prevent its further development. The first hurdle is the modest biological potency of **PTL**. Although

PTL is considered a covalent modifier of cancer cells, it only exhibits anti-cancer activity of low micromolar level,[19] indicating safety concerns associated with the required high dosing schedule. However, the task of boosting the anticancer activity of **PTL** is challenging. On one hand, **PTL** and PTL analogues must be reactive enough to be able to alkylate the functional target proteins to realize the anticancer activity; on the other hand, in order to diminish the off target effects to the largest extent, the reactivity of PTL analogues should be specific enough to retain the selective cytotoxicity of cancer cells over normal cells. In other words, the modification of healthy, non-cancerous cells, which may present very similar molecular targets as cancer cells or CSCs, leads to undesired toxicity and should be avoided. The second hurdle to the clinical utilization of **PTL** is its poor water solubility and thus, poor *in vivo* bioavailability. In 2004, a Phase I dose escalation trial of feverfew plant extract, which contained at least 0.2% parthenolide, was conducted to evaluate the pharmacokinetics and toxicity of feverfew plant extract as an anticancer agent. In this study, oral doses of up to 4 mg of **PTL** into healthy human volunteers did not yield any detectable concentration of the drug in the plasma, which was attributed to the poor water solubility of the compound.[310] In order to address this issue, a water-soluble PTL analogue, the fumarate salt of dimethylamino-parthenolide (**DMAPT**, **LC-1**, **2, figure 3.1**) was developed and exhibited efficacy against acute myeloid leukemia (AML) stem and progenitor cells *in vivo* (canines) [263,311]. A phase I clinical trial with **LC-1** has been initiated in the United Kingdom in 2007 for the treatment of AML; however, results have not been reported. Bearing a dimethylamino group, which can be protonated to increase water solubility, and removed in cells metabolically to recover the α-methylene-γ-butyrolactone functionality,

LC-1 is a prodrug of **PTL**, with 1000-times better water solubility and equipotent anti-proliferative activity as **PTL** *in vitro*.[263,311] The metabolism process in which **LC-1** was converted back to **PTL** likely involves the *N*-oxidation of dimethylamino group, and the subsequent Cope elimination of the *N*-oxide group.[263] However, this process has not yet been explicitly elucidated to the best of our knowledge. Due to the involvement of metabolic activation, it is possible that the cellular concentration of **PTL** may vary in different patients.

3.2 Project Design

The aim of the project is to overcome the two hurdles mentioned above, that is, to develop PTL analogues with better anticancer potency, less off-target effects, and better *in vivo* bioavailability. It has been demonstrated by our lab and others that as a covalent modifier, the "warhead" of **PTL** is the α-methylene-γ-butyrolactone moiety, and removing of that pharmocophore abolishes most of the biological activities.[263,264] However, other reactive functionalities, such as C1-C10 endocyclic olefin and electrophilic epoxide also exist in the structure of **PTL**. We hypothesized that the innate reactivity of these structural features may erode both the target specificity and contribute in part to **PTL**'s side-effects (such as the anti-proliferative effect to normal cells and contact allergic responses[312]). However, after an examination of previous literatures, we found that efforts have not been performed to the best of our knowledge to determine whether all of these reactive groups on **PTL** (e.g. endocyclic olefin, epoxide) are essential for its anticancer activity. As a result, we proposed that a systematic removal of the reactive moieties from **PTL**'s architecture would result in the identification of the

minimal **PTL** skeleton that confers its cytotoxicity against cancer cells and CSCs, which is beneficial in tuning the reactivity of this covalent drug. In addition, we also aimed at developing new types of water-soluble PTL prodrugs that does not involve metabolic activation.

3.3 Results and Discussion

3.3.1 Synthesis and Biological Evaluation of Cyclopropyl Parthenolide Analogues.

	PTL (1)	**MelB (3)**
HL-60	9.3 ± 3.8	7.5 ± 3.0
CCRF-CEM	4.7 ± 1.6	5.5 ± 1.2
GBM6	3.4 ± 1.1	3.5, 6.6
HeLa	44.1 ± 6.4	36.1 ± 3.2
DU-145	8.9 ± 4.6	14.1 ± 5.7
U-87 MG	5.8 ± 2.3	16.3 ± 6.8
MCF-7	9.7 ± 2.8	9.5 ± 1.9
NCI/Adr-Res	57.6 ± 8.9	17.8 ± 4.3
Vero	12.4 ± 0.6	15.6 ± 3.5

Table 3.1. Half maximal inhibitory concentration (IC_{50} in μM) of **PTL** (**1**) and **MelB** (**3**) in nine different cell lines. IC_{50} values are averages (n > 3) ± Standard deviation. For **MelB** in GBM6 cells, only duplicate data has been obtained.

Previously in our lab, we synthesized the allylic oxidized PTL, **Melampomagnolide B** (**MelB, 3,** see **Scheme 2.1** for preparation) according to a reported procedure[279] and demonstrated that it has anti-cancer activity in various cancer

cell lines similar to **PTL** (**Table 3.1**). Cancer cell lines investigated were HL-60 (promyelocytic leukemia), CCRF-CEM (acute lymphoblastic leukemia), GBM6 (glioblastoma multiforme), HeLa (cervical cancer), DU-145 (prostate cancer), U-87MG (glioblastoma, astrocytoma), MCF-7 (breast cancer), and NCI-ADR-RES (multidrug-resistant ovarian cancer[313]). Vero cells (African green monkey epithelial kidney cells) were utilized to gauge cytotoxicity against normal cells. This result indicated that the geometry of the endocyclic olefin and the conformation of the 10-membered ring in **PTL** were not crucial for the biological activity of the compound. Based on the above observation, we modified the C1-C10 endocyclic olefin in **PTL** by Simmons-Smith cyclopropylation reaction[314] and developed the cyclopropyl PTL analogues (**Scheme 3.1**). The hypothesis behind this modification is that cyclopropyl group is a well-known bioisostere of olefin. Due to the presence of ring strain, the sp^3 carbons in cyclopropyl group share some characteristics with sp^2 carbons, so that the molecule retains the original conformation to a large extent; however, the transformation from sp^2 carbons to sp^3 carbons abolishes the innate chemical reactivity of olefin, which may result in some of the off-target effects of the parent compound. This modification has been previously used in the synthesis of selective retinoid[315], as well as in the improvement of chemical and metabolic stability of anticancer nature product Epothilones (Epothilone A[316,317] and Epothilone B[316,318]).

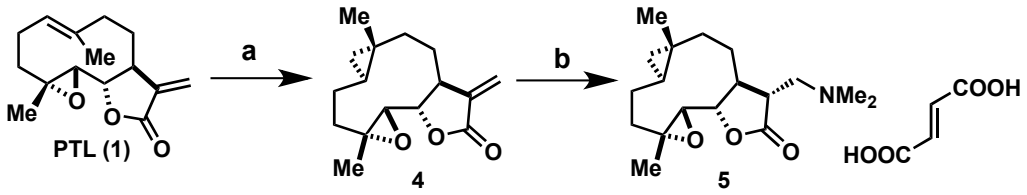

Scheme 3.1. *Reagents and Conditions:* a) $ZnEt_2$, CH_2I_2, DME, DCM, 0 ℃ to RT, 40%; b) i. dimethylamine, MeOH, overnight; ii. Fumaric acid, Et_2O, overnight, 85% over 2 steps.

Cyclopropyl PTL (**4**) was prepared by treating **PTL** (**1**) with an in situ generated reagent $Zn(CH_2I)_2$ ·DME. Compound **4** is the only detectable product of the reaction, with the recovery of 41% of **PTL** starting material. The regio- and stereo-selectivity of the reaction were confirmed by both NMR spectroscopy and X-ray crystallography (Appendix A) of compound **4**. With the similar strategy to prepare **LC-1** (**2**) from **PTL** (**1**), we synthesized the fumarate salt of dimethylamine derivative (compound **5**) to improve water solubility.

	PTL	**LC-1**	**4**	**5**
HL-60	9.3 ± 3.8	7.1 ± 0.4	4.4 ± 1.3	6.5 ± 2.7
GBM6	3.4 ± 1.1	3.5 ± 1.1	2.3 ± 0.5	2.2 ± 0.8
DU-145	8.9 ± 4.6	8.4 ± 4.5	14.8 ± 6.7	TBD
U-87 MG	5.8 ± 2.3	8.8 ± 1.9	7.4 ± 1.6	TBD
Vero	12.4 ± 0.6	15.6 ± 7.8	TBD	22.2 ± 1.3

Table 3.2. Half maximal inhibitory concentration (IC_{50} in μM) of **PTL** (**1**), **LC-1** (**2**) and cyclopropyl PTL analogues **4** and **5** in five different cell lines. IC_{50} values are averages ($n > 3$) ± Standard deviation. TBD = to be determined.

With cyclopropyl PTL analogues **4** and **5** in hand, we tested their anticancer activity in five different cell lines to probe the effect of this modification (**Table 3.2**). From the result, we can reach the conclusion that the modification of the endocyclic

olefin does not attenuate the anticancer activity of **PTL**. The synthesized **PTL** analogues possess comparable and sometimes better anti-proliferative activity than **PTL** in the tested cancer cells lines. For example, in HL-60 cell line, the IC_{50} of compound **4** (4.4 ± 1.3 μM) is lower than that of **PTL** (9.3 ± 3.8 μM) and **LC-1** (7.1 ± 0.4 μM), and in normal Vero cells, compound **5** possesses a slightly higher IC_{50} value (22.2 ± 1.3 μM) comparing with **PTL** (12.4 ± 0.6 μM) or **LC-1** (15.6 ± 7.8 μM) indicating less off-target toxicity. In other tested cancer cell lines, the cytotoxicity of the four compounds are not significantly different.

	PTL	**LC-1**	**5**
B117H	2.0 ± 0.1	2.8 ± 1.8	4.4 ± 0.7
B117P	1.1 ± 0.2	1.5 ± 0.4	1.9 ± 1.8
B140H	3.6 ± 0.9	5.7 ± 1.8	4.1 ± 1.3
B140P	2.9 ± 0.6	4.1 ± 1.2	4.2 ± 1.2

Table 3.3. Half maximal inhibitory concentration (IC_{50} in μM) of **PTL** (**1**), **LC-1** (**2**) and compound **5** in various murine AML cell lines. IC_{50} values are averages (n > 3) ± Standard deviation. Data from Sue Rathe from Dr. David Largaespada's lab, UMN.

As a result of these positive results, we further invested the cytotoxicity of the synthesized compounds in murine primary AML cell lines, B117H, B117P, B140H and B140P (**Table 3.3**). Among these four cell lines, B117P and B140P are murine AML cell lines isolated from a BXH-2 mice strain that develops AML.[319] These two cell lines are cytarabine (an FDA approved chemotherapeutic drug for AML) sensitive. Continuous low dosing of cytarabine to these two cell lines yielded B117H and B140H, respectively, which are cytarabine resistant.[319,320] Notably, in B117P cell line, cell surface molecules such as CD34 and c-kit, which are well-established markers for

cancer stem and progenitor cells in AML, are highly expressed, indicating cancer stem and progenitor characteristics of the cell line. In this experiment, all tested compounds, **PTL**, **LC-1** and compound **5** showed low micromolar level of cytotoxicity (between 2 to 6 μM) towards both cytarabine sensitive and cytarabine resistant AML cell lines. For example, the IC_{50} of compound **5** in B117H (4.4 ± 0.7 μM) is less than two fold higher than that of **PTL** (2.0 ± 0.1 μM) and **LC-1** (2.8 ± 1.8 μM), and in other three tested cell lines, the difference between the three compounds are not significant. The above result reiterated the therapeutic potency of **PTL** analogues in leukemia cells.

Due to the good *in vitro* anticancer activity of cyclopropyl PTL analogues, we further tested the *in vivo* pharmacokinetic properties of the water-soluble compounds **LC-1** and **5** in a normal mouse model. In this study, healthy CD-1 male mice were provided a single dose of tested compound by body weight via oral gavage at 100 mg/kg (the tested compounds were formulated in 0.5% methylcellulose to 10 mg/mL). Animals were sacrificed and blood and brain samples were collected 1 hour or 4 hours after the dosing to analyze the concentration of **LC-1** and **5**, as well as their parent compounds (elimination products), **PTL** and **4** in plasma (**Table 3.4**) and perfused brain (**Table 3.5**) by mass spectrometry. As a reference, 2964 ng/mL concentration equals 10.1 μM **LC-1** in plasma, and 446 ng/mL equals 1.4 μM of compound **5**. The plasma concentration of each compound includes both the prodrug (**LC-1** or **5**) and the bioactive metabolite (**PTL** or **4**). As a result, both tested compounds were detected in micromolar concentration in plasma at 1 hour, which is about or above their IC_{50} values, and dropped significantly at 4 hours. Notably, these measurements only considered the free drug and do no account for drug that has been bounded by protein. As a result, although

it appeared that compound **5** accumulated to a lower level than **LC-1** in plasma, it is possible that compound **5** has a faster kinetic properties of metabolism and target binding, yielding less free drug in plasma and larger amount of drug at its cellular targets by the time of testing.

Compound	**Time** (hour)	**Product Measured** (ng/mL)	**Elimination Product Measured** (ng/mL)
LC-1	1	2964	2142
LC-1	4	115	211
5	1	446	104
5	4	8	11

Table 3.4 Concentration of **LC-1**, **5** and their metabolites in mouse plasma. Values are averages (n = 2 or 3).

Compound	**Time** (hour)	**Product Measured** (ng/g)	**Elimination Product Measured** (ng/g)
LC-1	1	6250	2402
LC-1	4	342	113
5	1	1316	106
5	4	26	<LLOQ[a]

Table 3.5 Concentration of **LC-1**, **5** and their metabolites in mouse brain. Values are averages (n = 2 or 3). a: LLOQ: Lower limit of quantitation.

In this pharmacokinetic study, the brain penetration of **LC-1** and **5** were also tested. Strikingly, both **LC-1** and **5** were found at high concentration in perfused brain. An average of 6250 ng/g of **LC-1**, which equals 21 μM concentration, and an average of 1316 ng/g of **5**, which equals 4.3 μM concentration were detected in brain tissue after 1 hr (assuming 1 g/mL brain density). These values are well above their IC_{50} values for anti-proliferative activity in the tested brain cancer cell lines (GBM6 and U-87 MG). The permeability issue of drugs to penetrate the blood-brain barrier (BBB) is a major issue of many promising molecules towards the development of chemotherapeutic

agents for various brain cancers. The BBB consists of tight junctions all along the brain capillaries and excludes almost 100% of large molecule drugs and over 98% of small molecule drugs from the brain circulation.[321] The above pharmacokinetic results support the continued development of **PTL** analogues as next generation chemotherapeutic agents against brain tumors.

In conclusion, two cyclopropyl PTL analogues were developed. In *in vitro* assays, they exhibited comparable or even better anticancer activity than their parent compound **PTL** in various cancer cell lines, including murine drug-resistant AML cell lines. Notably, the *in vivo* pharmacokinetic study indicated not only high serum concentration, but also brain penetration of the compounds, validating the future development of this class of molecules for various cancers.

3.3.2 Synthesis and Biological Evaluation of Rearranged Parthenolide Analogues.

Taking advantage of the reactivity of the endocyclic olefin and epoxide under acidic condition, we synthesized various **PTL** analogues with 5-7-5 ring systems (**Scheme 3.2**). Rearrangements of **PTL** (**1**) using BF_3•OEt in toluene according to literature procedure yielded **Micheliolide** (**6**) as the major product, and compound **7** as the minor product. The structure and stereochemistry of **6** are confirmed by comparing to published data[322] as well as small molecule X-ray crystallography (Appendix B).

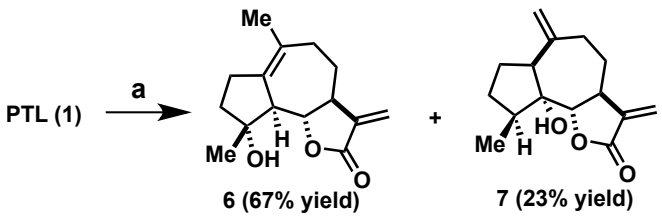

Scheme 3.2. *Reagents and Conditions:* a) BF_3•Et_2O, toluene, 1 hr.

With rearranged **PTL** analogues **6** and **7** in hand, we tested their anticancer activities in seven different cancer cell lines, as well as in Vero cells, to probe the effect of this modification (**Table 3.6**, see section 3.3.1 for the description of cell lines). The synthesized PTL analogues possess the same level of anti-proliferative activity as **PTL** in many cancer cells lines. For example, in HL-60, CCRF-CEM and HeLa cell lines, the three tested compounds exhibited very similar cytotoxicity. In GBM6 cells, **PTL** (IC_{50} = 3.4 ± 1.1 μM) is about two fold more active than rearranged PTL analogues (IC_{50} of **6** = 8.7 ± 0.6 μM, IC_{50} of **7** = 8.4 ± 1.8 μM). In DU-145 cells, **PTL** (IC_{50} = 8.9 ± 4.6 μM) is almost two fold more active than rearranged PTL analogues (IC_{50} of **6** = 14.8 ± 4.0 μM, IC_{50} of **7** = 13.9 ± 3.7 μM). In MCF-7 cells, **PTL** (IC_{50} = 9.7 ± 2.8 μM) and compound **6** (IC_{50} = 9.6 ± 1.0 μM) have similar cytotoxicity, but compound **7** is significantly less active (IC_{50} of = 25.0 ± 4.3 μM). What makes the result more meaningful is that in Vero cells, which are healthy kidney epithelial cells from the African monkey, rearranged PTL analogues **6** (IC_{50} = 36.1 ± 9.4 μM) and **7** (IC_{50} = 54.5 ± 3.0 μM) are less active than the parent compound **PTL** (IC_{50} = 12.4 ± 0.6 μM), indicating decreased toxicity against normal cells. Compared to **PTL**, compound **6** is approximately 2-fold less potent; however, it bears the structural advantage of an introduced tertiary alcohol, which is amenable to chemical manipulation, and its further modification will be introduced in section *3.3.3*. Furthermore, compound **6** and **7** do not contain the pendent epoxide group, which is an unneglectable advantage from the perspective of drug design, because epoxide groups are notoriously reactive under biological conditions. From the above results, we can reach the conclusion that the modification of the

endocyclic olefin, the removal of the electrophilic epoxide, and the alteration of ring structure do not abolish the anticancer activity of **PTL**.

	PTL	**6**	**7**
HL-60	9.3 ± 3.8	7.1 ± 1.3	11.6 ± 0.2
CCRF-CEM	4.7 ± 1.6	5.2 ± 1.8	4.8 ± 1.5
GBM6	3.4 ± 1.1	8.7 ± 0.6	8.4 ± 1.8
HELA	44.1 ± 6.4	35.6, 34.0	44.2
DU-145	8.9 ± 4.6	14.8 ± 4.0	13.9 ± 3.7
U-87 MG	5.8 ± 2.3	16.2 ± 3.6	29.3 ± 3.0
MCF-7	9.7 ± 2.8	9.6 ± 1.0	25.0 ± 4.3
Vero	12.4 ± 0.6	36.1 ± 9.4	54.5 ± 3.0

Table 3.6. Half maximal inhibitory concentration (IC_{50} in μM) of **PTL** (**1**), and rearranged PTL analogues **6** and **7** in eight different cell lines. IC_{50} values are averages (n > 3) ± Standard deviation (SD). For **6** or **7** in HeLa cells, only duplicate or single data has been obtained.

Based on the above preliminary data, we further tested the anti-proliferative potency of **PTL**, **LC-1** and compound **6** in four murine AML cell lines: B117H, B117P, B140H and B140P (**Table 3.7**, see section *3.3.1* for the description of cell lines). In this experiment, all tested compounds, **PTL**, **LC-1** and **6** exhibited low micromolar level of cytotoxicity towards both cytarabine sensitive (B117P and B140P) and cytarabine resistant (B117H and B140H) cell lines. However, in all four tested cell lines, compound **6** is about three to six fold less active the **PTL** and **LC-1**. For example, in B117 H cells, IC_{50} of **6** is 6.5 ± 1.0 μM, which is about five fold less active than **PTL** (IC_{50} = 1.1 ± 0.2 μM) or **LC-1** (IC_{50} = 1.5 ± 0.4 μM).

	PTL	LC-1	6
B117H	2.0 ± 0.1	2.8 ± 1.8	6.4 ± 1.0
B117P	1.1 ± 0.2	1.5 ± 0.4	8.8 ± 1.7
B140H	3.6 ± 0.9	5.7 ± 1.8	10.0 ± 0.4
B140P	2.9 ± 0.6	4.1 ± 1.2	9.3 ± 1.5

Table 3.7. Half maximal inhibitory concentration (IC_{50} in μM) of **PTL**, **LC-1** and compound **6** in various murine AML cell lines. IC_{50} values are averages (n > 3) ± Standard deviation. Data from Sue Rathe from Dr. David Largaespada's lab, UMN.

In conclusion, a series of rearranged **PTL** analogues with 5-7-5 ring systems were developed. In *in vitro* assays, they exhibited comparable anticancer activity with their parent compound **PTL** in various cancer cell lines, including murine drug-resistant AML cell lines.

3.3.3 Synthesis and Biological Evaluation of Parthenolide Phosphate Prodrugs.

In the above two sections, our efforts towards systematical removal of reactive functional groups of **PTL** were discussed. We synthesized two series of PTL analogues with comparable anticancer activities and less reactive groups than **PTL**, and demonstrated that they either have prominent *in vivo* pharmacokinetic properties or less extent off-target toxicity. In the meantime, we also synthesized the fumarate salts of the dimethylamino PTL analogues to increase the water solubility. However, as it has been introduced above, the limitation of the dimethylamino prodrugs is that they require metabolic activation to generate their active parent compounds. Due to the lack of knowledge of the process in which **LC-1** was converted back to **PTL**, and the enzyme(s) involved in this transformation, it is possible that the cellular concentration of the active

compounds vary in patients with different levels of drug metabolizing enzymes. In order to bypass this activation process, we designed and synthesized a new class of water-soluble PTL analogues, using another prodrug strategy.

As it has been introduced above, **MelB** (**3**) and **Micheliolide** (**6**) are two PTL analogues with micromolar anticancer activity. They have different chemical scaffolds, but the structural similarity is that both of them are bearing hydroxyl groups that can be further modified. Taking advantage of the hydroxyl groups, we synthesized the phosphate salts of **MelB** and **Micheliolide** (**Scheme 3.3**). This is hypothesized to be a better way to develop water-soluble PTL analogues, because it avoids the necessity of *in vivo* bioactivation.

Starting from **MelB** (**3**) and **Micheliolide** (**6**), phosphoramidite chemistry was carried out to realize the transformation from **3** and **6** to **9** and **11**, respectively, after a screen of phosphorylation conditions. In this step, the bis(2-cyanoethyl) diisopropylphosphoramidite (**8**), which is an unstable reagent, was synthesized according to a reported procedure[323] and used within four weeks after it is made. Compound **8** was coupled to the hydroxyl group in compound **3** or **6** to yield the phosphites, which were acid labile and used in situ without any purification. The phosphite intermediates were oxidized to phosphates by mCPBA under careful control of reaction time and temperature (otherwise the olefins in the molecule would be epoxidized) to yield phosphates **9** and **11**. The overall yield of the phosphorylation of compound **6** (57%) is lower than compound **3** (81%), presumably because of the steric hindrance of the tertiary alcohol in **6**. At last, the cyanoethyl protection groups were

removed under basic condition (DBU, ion-exchange chromatography) to yield the water-soluble phosphate salts **10** (47%) and **12** (37%).

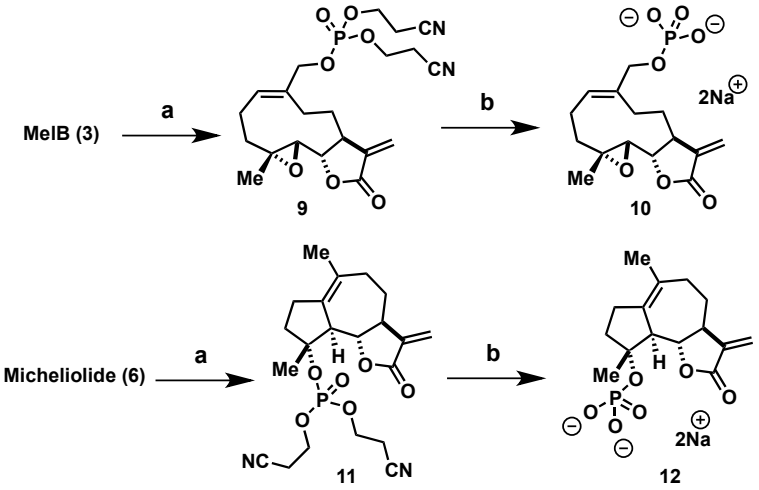

Scheme 3.3. *Reagents and Conditions:* a) i. Bis(2-cyanoethyl) diisopropyl-phosphoramidite (**8**), tetrazole, 4 Å MS, MeCN, overnight; ii. mCPBA, 1 hr, 0 ℃; yields over 2 steps: 81% for **9**, 57% for **11**; b) DBU, DCM, RT, overnight, followed by ion-exchange chromatography, 47% for **10**, 37% for **11**.

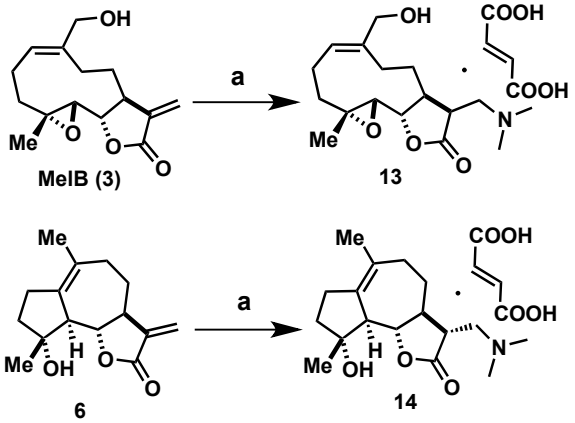

Scheme 3.4. *Reagents and Conditions:* a) i. dimethylamine, MeOH, overnight; ii. Fumaric acid, Et_2O, overnight, yield over 2 steps: 53% for **13**, 96% for **14**.

In order to compare the biological and pharmacokinetic properties of the synthesized phosphate salts **10** and **12** to the conventional dimethylamino prodrug of PTL analogues, the fumarate salts of dimethylamino MelB (**13**) and dimethylamino Micheliolide (**14**)[322] were also synthesized (**Scheme 3.4**) using procedures described above.

With compound **10**, **12 - 14** in hand, we further tested their anticancer activity in different cell lines (**Table 3.8**). The anti-proliferative testing is still underway. The current data indicated that the modification of compound **6** to its phosphate salt **12** was not tolerated (IC_{50} of **12** in HL-60 cells is > 250 μM); while the phosphate salt of **MelB** (compound **10**, IC_{50} in HL-60 = 22.5 ± 2.2 μM) is more active than the fumarate salt of the same parent compound (compound **13**, IC_{50} in HL-60 = 36.2 ± 6.1 μM). However, it is possible that the decreased *in vitro* anticancer activity of phosphate compounds resulted from the lack of phosphate diesterases in cell models, and the synthesized parthenolide phosphates would be active *in vivo*. In the presence of phosphate diesterases *in vivo*, the negatively charged phosphate prodrugs of parthenolide analogues would be converted back to parent compounds (**MelB** or rearranged PTL) before they penetrating the negatively charged cell membrane, likely leading to higher concentration of drugs in cells.

	10	**12**	**13**	**14**
HL-60	22.5 ± 2.2	> 250	36.2 ± 6.1	32.3 ± 10.4
Vero	50.0	> 250	21.1 ± 1.2	48.7 ± 5.9

Table 3.8. Half maximal inhibitory concentration (IC_{50} in μM) of compound **10**, **12**, **13** and **14** in HL-60 and Vero cell lines. IC_{50} values are averages (n > 3) ± Standard deviation (SD). For compound **10** in Vero cells, only single data has been obtained.

In addition, the theoretical distribution coefficient values (cLogD) of compound **10**, **12 - 14**, as well as **MelB** (**3**), **Micheliolide** (**6**), **LC-1** (**2**) and **PTL** (**1**) were also calculated using Marvin Sketch 5.11.5. software manufactured by ChemAxon (**Table 3.9**). Distribution coefficient represents the ratio of the sum of the concentrations of all forms of the compound (ionized and un-ionized) in hydrophobic and hydrophilic phases.

cLogD strongly affects how easily the tested compound can reach its intended target in a biological system. Under neutral condition (pH = 7.4), **PTL** (cLogD = 3.07), **MelB** (cLogD = 1.79) and **Micheliolide** (cLogD = 1.97) exhibited high LogD values, indicating their hydrophobic property. On the other hand, the fumarate prodrugs **LC-1** (cLogD = 0.50), compound **13** (cLogD = -0.78) and **14** (cLogD = -0.60) had low LogD values, indicating their moderate water solubility. The synthesized phosphate PTL analogues **10** (cLogD = -1.29) and **12** (cLogD = -1.34) exhibited even lower LogD values, indicating their good water-solubility, which is consistent with our experiment observation.

	cLogD$_{7.4}$
PTL	3.07
LC-1	0.50
MelB	1.79
Micheliolide	1.97
10	-1.29
12	-1.34
13	-0.78
14	-0.60

Table 3.9. Calculated LogD values (pH7.4) of compound **10**, **12**, **13**, **14**, **PTL**, **LC-1**, **MelB** and **Micheliolide**. Calculated by Marvin Sketch 5.11.5. software manufactured by ChemAxon

3.4 Conclusions and Future Direction

In conclusion, a library of **PTL** analogues have been synthesized and biologically evaluated to elucidate the importance of various functional groups to the cytotoxicity profile of **PTL** and to purse PTL analogues with increased anticancer potencies. The methods we employed to modify **PTL** included acidic rearrangement, cyclopropylation and phosphorylation. The modified functional groups included the endocyclic olefin, the vinyl methyl group, the epoxide, the exocyclic olefin and the 10-membered ring structure of **PTL**. In addition, phosphate prodrugs of hydroxyl containing **PTL** analogues were synthesized in pursuit of water-soluble **PTL** analogues that do not need to be bioactivated *in vivo*.

Our results revealed that minor modifications of **PTL** were well tolerated across all tested cancer cell lines, indicating large space for future modification. Among the analogues we synthesized, cyclopropyl **PTL** analogues exhibited better activity when compared to PTL in some cancer cell lines. The outstanding pharmacokinetic properties of **5** in serum and perfused brain validated the future development of this class of molecules for leukemia and brain cancers. Rearranged PTL analogues **6** and **7** also displayed interesting biological activity. Exhibiting similar level of activity as **PTL** in most cancer cell lines, they are demonstrated to be less cytotoxic against normal cell line Vero. Both compounds had up to a 5-fold loss in activity against Vero, indicating decreased off-target toxicity. In addition, both the rearranged and cyclopropyl PTL analogues were demonstrated to be effective in inhibiting the proliferation of murine drug resistant leukemia cells, iterating the important role PTL analogues will play in the future development of therapeutic agents of leukemia.

3.5 Experimentle

3.5.1 General

All reactions were performed under an anhydrous nitrogen atmostphere unless otherwise noted. Parthenolide was purchased from Enzo Life Sciences and repurified by SiO_2 chromatography prior to biological studies. Commercial grade reagents (Aldrich, Acros, Alfa Aesar) were used without further purification unless otherwise noted. Tetrahydrofuran and dichloromethane were rendered anhydrous by passing through the resin column of a solvent purification system. Benzene was purified by fractional distillation. Methanol, 1,2-dimethoxyethane, and N,N-dimethylformamide were purchased as anhydrous. All reactions were monitored by thin-layer chromatography (TLC) using silica gel 60-F_{254} TLC plates (Merck), and visualized using either iodine or charring with para-Anisaldehyde stain. Column chromatography employed Silicycle SiliaFlash® P60 (40-63 m) silica gel. SiO_2 column purification was performed using a CombiFlash® Rf 200 instrument using pre-packed silica gel columns or Redisep Rf Gold High-Performance silica gel columns (Teledyne-Isco). HPLC purification was performed using an Agilent 1200 series instrument (preparative scale) equipped with a Zorbax (Agilent) preparatory column (21.2 x 250 mm, 7 μm). Analysis of compound purity was conducted on the aforementioned HPLC, using a Zorbax analytical column (4.6 x 150 mm, 5 μm). Nuclear magnetic resonance (NMR) spectroscopy employed a Bruker 400 Ultrashield 400 MHz spectrometer. Internal solvent peaks were referenced in each case. Mass spectral data was obtained from the University of Minnesota mass spectrometry lab, employing a Bruker Biotof II instrument. X-ray diffraction was

performed by Dr. Victor G. Young, Jr., at the X-ray Crystallographic Laboratory at the University of Minnesota.

3.5.2 Synthesis of Parthenolide Analogues

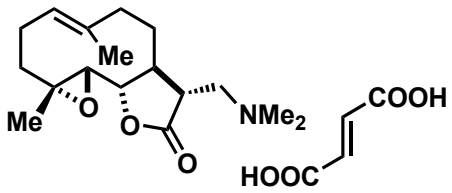

Dimethylamino Parthenolide Fumarate salt (DMAPT, LC-1, 2): This compound was prepared as previously described.[263] Briefly, to a stirred solution of parthenolide (126 mg, 50.7 mmol) in MeOH (4 mL) was added dimethylamine solution (2 M in MeOH, 1 mL). The reaction was allowed to stir at room temperature overnight, and then the solvent was removed under reduced pressure. The residue was dissolved in CH_2Cl_2 (50 mL), and washed with deionized H_2O (20 mL, 1x) and saturated aq. $NaHCO_3$ (20 mL, 1x). The combined aqueous solution was washed with CH_2Cl_2 (50 mL, 2x). The organic layers were collected, dried over anhydrous Na_2SO_4 and concentrated in vacuo. The crude material was subjected to SiO_2 chromatography (gradient 0%-50% EtOAc in hexanes over 10 min, then gradient 0%-15% MeOH in CH_2Cl_2 over 15 min) to yield the dimethylamino product (130 mg, 87%) as colorless oil. To the stirred solution of dimethylamino product (130 mg, 0.44 mmol) in ether (3 mL) was added fumaric acid (51.4 mg, 0.44 mmol). The reaction was allowed to stir at room temperature overnight until a white powder precipitated out. The solvent was removed under reduced pressure to yield **LC-1** (181 mg, quant.). Spectral data matches that previously reported.[263] ^{1}H NMR (DMSO-d_6, 400 MHz): δ 6.61 (s, 2H), 5.21 (d, J = 10.0

Hz, 1H), 3.97 (t, *J* = 9.1 Hz, 1H), 2.79 (d, *J* = 9.1 Hz, 1H), 2.62 (m, 3H), 2.35 (m, 1H), 2.19 (m, 8H), 1.98 (m, 4H), 1.66 (m, 4H), 1.20 (s, 3H), 1.12 (td, *J* = 5.8 Hz, *J* = 12.9 Hz, 1H).

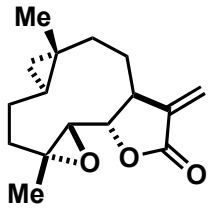

Cyclopropyl parthenolide 4: A 0.20 M solution of $Zn(CH_2I)_2$·DME complex[314] was made in the following manner: To a stirred solution of diethyl zinc (1.0 M solution in hexanes, 4.0 mL, 4 mmol) in CH_2Cl_2 (20 mL) and DME (0.50 mL) at 0 °C was added diiodomethane (0.80 mL, 9.92 mmol) under N_2. The mixture was stirred for 10 minutes. This $Zn(CH_2I)_2$·DME complex was added dropwise over 10 minutes to a solution of parthenolide (90 mg, 0.36 mmol) in CH_2Cl_2 (3 mL) at 0 °C. The reaction was stirred for 1 hour at 0 °C, and the stirring was continued overnight with gradual warming to room temperature. The crude material was quenched by pouring into NH_4Cl (saturated, aq., 20 mL) and then extracted with CH_2Cl_2 (20 mL, 4x). The combined organic layers were washed with $NaHCO_3$ (saturated aq., 20 mL), brine (saturated aq., 20 mL) and then dried over Na_2SO_4. The crude material was purified using SiO_2 chromatography (gradient 10-30% EtOAc in hexanes over 15 minutes) to yield the product (36 mg, 40%) as a colorless oil and recovered parthenolide (37 mg, 41%). ^{1}H NMR (400 MHz, $CDCl_3$) δ: 6.28 (d, *J* = 3.7 Hz, 1H), 5.57 (d, *J* = 3.3 Hz, 1H), 3.96 (t, *J* = 9.1 Hz, 1H), 2.98 (d, *J* = 9.0 Hz, 1H), 2.67 (m, 1H), 2.39 (dd, *J* = 8.0 Hz, *J* = 14.7 Hz, 1H), 2.19 (dd, *J* = 2.3 Hz, *J*

= 8.3 Hz, 1H), 1.95 (m, 2H), 1.70 (m, 1H), 1.40 (s, 3H), 1.28 (m, 2H), 1.09 (s, 3H), 0.85 (dd, *J* = 11.1 Hz, *J* = 14.7, 1H), 0.64 (td, *J* = 6.0 Hz, *J* = 9.5 Hz, 1H), 0.39 (dd, *J* = 4.3 Hz, *J* = 9.4 Hz, 1H), -0.08 (dd, *J* = 4.6 Hz, *J* = 5.6 Hz, 1H). ^{13}C NMR (100 MHz, $CDCl_3$) δ: 169.4, 139.9, 120.5,. 82.7, 65.5, 60.6, 48.0, 42.3, 38.4, 25.7, 24.5, 22.3, 20.4, 18.8, 18.5, 17.1. HRMS (ESI^+) *m/z* calcd for $[C_{16}H_{22}O_3+Na]^+$ 285.1467; found 285.1470. The structure of **4** was further confirmed by small molecule X-ray crystallography (see Appendix A).

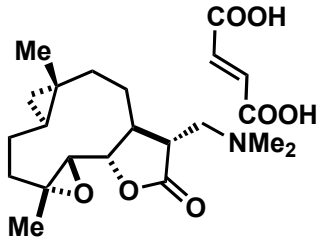

Dimethylamino cyclopropyl-Parthenolide fumarate salt 5: To a stirred solution of **4** (9 mg, 0.034 mmol) in MeOH (2 mL) was added dimethylamine solution (2M in MeOH, 1.5 mL). The reaction was stirred overnight at RT. MeOH was removed under reduced pressure and the residue was purified by Si_2O chromatography (gradient 0%-50% EtOAc in hexanes over 10 min, then gradient 0%-25% MeOH in CH_2Cl_2 over 15 min) to yield the dimethylamino product as a white solid (9 mg, 0.024 mmol, 85%). To a stirred solution of dimethylamino product in Et_2O (5 mL) was added fumaric acid (3.4 mg, 0.029 mmol). A white precipitate was observed after stirring overnight at room temperature. Et_2O was removed under reduced pressure to give the fumarate salt as white solid (12.4 mg, quant.). ^{1}H NMR (DMSO-d_6, 400 MHz): δ 6.61 (s, 2H), 4.09 (t, *J* = 9.5 Hz, 1H), 3.04 (d, *J* =9.2 Hz, 1H), 2.64 (m, 3H), 2.24 (s, 6H), 2.14 (m, 2H), 2.05

(m, 1H), 1.78 (m, 2H), 1.59 (m, 1H), 1.31 (s, 3H), 1.19 (m, 2H), 1.02 (s, 3H), 0.74 (m, 2H), 0.28 (dd, J = 3.8 Hz, J = 9.2 Hz, 1H), -0.18 (t, J = 4.8 Hz, 1H). ^{13}C NMR (DMSO-d_6, 100 MHz): 176.6, 166.1, 134.1, 81.8, 64.3, 60.3, 57.2, 47.4, 45.6, 45.3, 41.7, 38.0, 24.2, 24.0, 21.6, 20.1, 18.4, 18.3, 16.7. HRMS (ESI$^+$) *m/z* calcd for $[C_{18}H_{30}NO_3+H]^+$ 308.2226; found 308.2216.

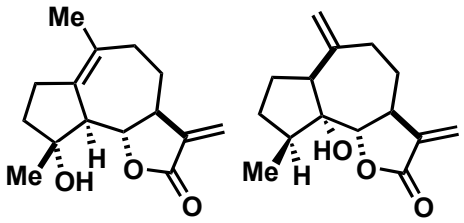

Micheliolide (6),[324] rearranged parthenolide analogue **7**[325]: These two compounds were prepared as previously described.[324, 325] Briefly, to a stirred solution of parthenolide (30 mg, 0.12 mmol) in toluene (1 mL) was added BF_3•Et_2O (7 μL, 0.072 mmol) dropwise. The reaction was allowed to stir at room temperature for 1 hr before being quenched by $NaHCO_3$ (saturated aq., 15 mL). The aqueous solution was extracted by CH_2Cl_2 (40 mL, 3x). The combined organic layers were dried over anhydrous Na_2SO_4 and concentrated in vacuo. The crude material was subjected to SiO_2 column purification (gradient 10%-50% EtOAc in hexanes over 16 min) to yield **6** (20 mg, 67%) as white solid, ^{1}H NMR ($CDCl_3$, 400 MHz): δ 6.21 (d, J = 3.3 Hz, 1H), 5.50 (d, J = 3.1 Hz, 1H), 3.81 (t, J = 10.3 Hz, 1H), 2.74 (d, J = 10.7 Hz, 1H), 2.66 (m, 2H), 2.40 (dd, J = 8.4 Hz, J = 16.3 Hz, 1H), 2.22 (m, 3H), 2.09 (ddd, J = 2.3 Hz, J = 3.9 Hz, J = 13.6 Hz, 1H), 1.81 (m, 2H), 1.68 (s, 3H), 1.34 (m, 4H); and less polar rearrangement product **7** (7

mg, 23%) as a white solid, ^{1}H NMR ($CDCl_3$, 400 MHz): δ 6.12 (d, J = 3.5 Hz, 1H), 5.48 (d, J = 3.2 Hz, 1H), 5.14 (s, 1H), 5.06 (s, 1H), 4.01 (d, J = 9.7 Hz, 1H), 2.96 (m, 1H), 2.61 (m, 1H), 2.32 (m, 5H), 2.02 (m, 1H), 1.79 (m, 2H), 1.56 (m, 2H), 1.06 (d, J = 7.1 Hz, 3H). The structure of **6** was further confirmed by small molecule X-ray crystallography (see Appendix B). The structure of **7** was confirmed by comparing to reported NMR data.[325]

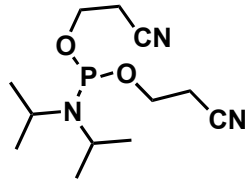

Bis(2-cyanoethyl) diisopropylphosphoramidite (**8**)**:** Reagent **8** was prepared according to reported procedure.[323] Diisopropylphosphoramidous dichloride (505 mg, 2.5 mmol) was added dropwise to a stirred solution of cyanoethenol (356 mg, 5 mmol) and DIPEA (1.3 mL, 7.5 mmol) in anhydrous THF (3 mL) at 0 ℃. The reaction mixture was warmed to room temperature and stirring was continued for 1 hr or until a white powder precipitated. The reaction mixture was filtered through celite and THF was removed from filtrate. The concentrated filtrate was redissolved in EtOAc (80 mL) and washed with H_2O (20 mL, 2x). The combined aqueous solution was washed with EtOAc (80 mL, 2x). The organic layers were collected, dried over anhydrous Na_2SO_4 and concentrated in vacuo. The crude material was subjected to SiO_2 column purification (gradient 0%-40% EtOAc in hexanes containing 1.5% Et_3N over 20 min) to yield product (307 mg, 45%) as colorless oil. The phosphoramidite product is not stable and

extremely sensitive to acid, such as silica gel. It could be stored at -20 ℃ for no more than 1 month. When NMR is taken in the solvent, $CDCl_3$ should be neutralized with Na_2CO_3 beforehand. ^1H NMR ($CDCl_3$, 400 MHz): δ 3.82 (m, 4H), 3.62 (5d, J = 6.8 Hz, J = 10.4 Hz, 2H), 2.65 (t, J = 6.3 Hz, 4H), 1.20 (d, J = 6.8 Hz, 12H). ^{31}P NMR ($CDCl_3$, 162 MHz): δ -246.6.

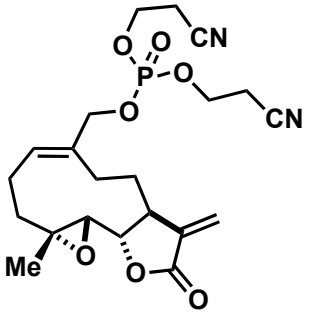

Bis(2-cyanoethyl) Melampomagnolide B phosphate 9: Compound **3** (30 mg, 0.11 mmol) and phosphoramidite (**8**, 31 mg, 0.11 mg) were weighted out in a round bottom flask and dried under high vac for 2 hr. The dried material was dissolved in anhydrous acetonitrile (5 mL) under N_2 stream. Two 4Å molecular sieves were added. After the injection of tetrazole (0.47 M in acetonitrile, 0.47 mL, 0.22 mmol), the reaction was stirred overnight at room temperature. The second day, mCPBA (61 mg, 0.27 mmol) was added to the reaction, which was quenched after 2 hrs by the addition of $NaHCO_3$ (saturated aq., 5 mL). Acetonitrile was removed under reduced pressure. The aqueous residue was diluted with deionized H_2O (15 mL) and extracted by CH_2Cl_2 (30 mL, 3x). The organic layer was combined, dried over anhydrous Na_2SO_4, and concentrated in vacuo. The crude material was purified by SiO_2 column chromatograpy (gradient 5%-100% EtOAc in hexanes over 7 min, 100% EtOAc over 8 min, then gradient 0%-15% MeOH in CH_2Cl_2 over 15 min) to yield the product (40 mg, 81%) as a

colorless oil. ^{1}H NMR ($CDCl_3$, 400 MHz): δ 6.26 (d, J = 3.4 Hz, 1H), 5.81 (t, J = 8.3 Hz, 1H), 5.62 (d, J = 3.1 Hz, 1H), 4.69 (t, J = 10.4 Hz, 1H), 4.55 (dd, J = 6.1 Hz, J = 11.5 Hz, 1H), 4.29 (m, 4H), 3.85 (t, J = 9.3 Hz, 1H), 2.80 (m, 6H), 2.32 (m, 6H), 1.71 (t, J = 9.6 Hz, 1H), 1.55 (s, 3H), 1.12 (t, J = 13.1 Hz, 1H). ^{31}P NMR ($CDCl_3$, 162 MHz): δ -2.05. HRMS (ESI$^+$) *m/z* calcd for $[C_{21}H_{27}N_2O_7P+Na]^+$ 473.1454; found 473.1466.

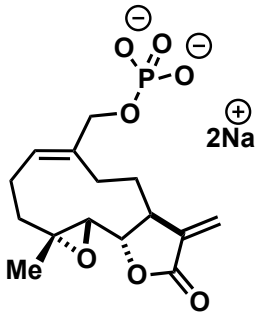

Melampomagnolide B phosphate disodium salt 10: To a stirred solution of compound **9** (25 mg, 0.056 mmol) in CH_2Cl_2 (5 mL) was injected *N,O*-Bis(trimethylsilyl) acetamide (205 μL, 0.82 mmol) and DBU (84 μL, 0.56). The reaction was stirred overnight under N_2 and quenched by the addition of MeOH. After the removal of solvent under reduced pressure, the residue was dissolved in deionized H_2O and separated by reverse phase column chromatography (Biotage isolute XL-C18 column, eluant: 100% H_2O 5 mL, 75% H_2O in MeOH 5 mL, 25% H_2O in MeOH 5 mL, then 100% MeOH 5 mL). Every fraction that stained blue under *p*-anisaldehyde in TLC was collected to yield the crude product, which contained both acid form and DBU-salt form of the product and some leftover of DBU. The crude product was acidified by Dowex 50WX8 resin (pre-acidified by HCl and washed by H_2O until eluate was neutral)

for 1 hr at room temperature in H_2O/MeOH 3:1. The resin was removed by filtration and the filtrate was concentrated and stirred with triethylammonium acetate buffer (1 M, 5 mL) overnight to give di-TEA salt of the product. The triethylammonium acetate buffer was removed under reduced pressure and loaded to an ion exchange column (Dowex50WX8-Na^+, eluant: H_2O). All fractions were collected and concentrated. The residue was further purified by reverse phase C-18 column (100% H_2O, then 75% H_2O in MeOH) to yield pure product. The product was lyophilized overnight to give white powder (10 mg, 47%). ^{1}H NMR (D_2O, 400 MHz): δ 6.25 (d, J = 3.4 Hz, 1H), 5.84 (d, J = 3.1 Hz, 1H), 5.76 (t, J = 8.1 Hz, 1H), 4.45 (dd, J = 7.0 Hz, J = 11.8 Hz, 1H), 4.26 (m, 2H), 3.23 (d, J = 9.6 Hz, 1H), 3.09 (m, 1H), 2.52 (m, 1H), 2.39 (m, 3H), 2.23 (m, 2H), 1.76 (t, J = 11.4 Hz, 1H), 1.63 (s, 3H), 1.14 (t, J = 12.3 Hz, 1H). ^{31}P NMR (D_2O, 162 MHz): δ 1.08. HR-MS (ESI) *m/z* calcd for $[C_{15}H_{20}O_7P]^-$ 343.0952; found 343.0940.

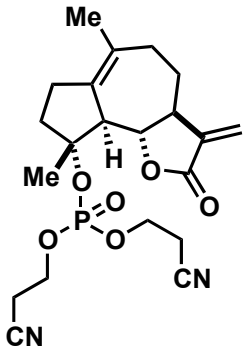

Bis(2-cyanoethyl) Micheliolide phosphate 11: Compound **6** (20 mg, 0.074 mmol) and phosphoramidite (**8**, 20 mg, 0.081 mg) were weighted out in a round bottom flask and dried under high vac for 2 hours. The dried material was dissolved in anhydrous acetonitrile (5 mL) under N_2 stream. Two 4Å molecular sieves were added.

After the injection of tetrazole (0.47 M in acetonitrile, 0.32 mL, 0.15 mmol), the reaction was stirred overnight at room temperature. The second day, mCPBA (37 mg, 0.16 mmol) was added *in situ* to the reaction at 0 ℃, which was quenched after 2 hr by the addition of $NaHCO_3$ (saturated aq., 5 mL). Acetonitrile was removed under reduced pressure. The aqueous residue was diluted with deionized H_2O (15 mL) and extracted by CH_2Cl_2 (30 mL, 3x). The organic layer was combined, dried over anhydrous Na_2SO_4, and concentrated in vacuo. The crude material was purified by SiO_2 column chromatography (gradient 5%-60% EtOAc in hexanes over 10 min, 100% EtOAc over 10 min) to yield the product (20 mg, 57%) as a colorless oil. ^{1}H NMR ($CDCl_3$, 400 MHz): δ 6.18 (d, J = 3.3 Hz, 1H), 5.49 (d, J = 3.0 Hz, 1H), 4.33 (m, 4H), 3.85 (t, J = 10.1 Hz, 1H), 3.24 (d, J = 5.1 Hz, 1H), 2.76 (m, 5H), 2.48 (m, 1H), 2.21 (m, 5H), 2.10 (dd, J = 2.2 Hz, J = 13.8 Hz, 1H), 1.70 (s, 3H), 1.57 (s, 3H), 1.35 (m, 1H). ^{31}P NMR ($CDCl_3$, 162 MHz): δ -7.50. HRMS (ESI^+) *m/z* calcd for $[C_{21}H_{27}N_2O_6P+Na]^+$ 457.1504; found 451.1522. A main byproduct, which is the mCPBA-oxidized product of the starting material, was also obtained:

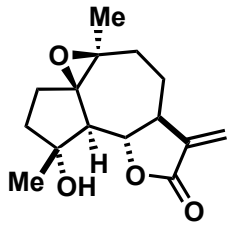

Epoxidized rearranged parthenolide:[326] ^{1}H NMR ($CDCl_3$, 400 MHz): δ 6.19 (d, J = 3.3 Hz, 1H), 5.48 (d, J = 3.1 Hz, 1H), 4.05 (t, J = 10.4 Hz, 1H), 2.80 (s, 1H), 2.30 (m, 4H), 1.92 (m, 4H), 1.65 (dt, J = 7.6 Hz, J = 15.2 Hz, 1H), 1.47 (s, 3H), 1.41 (m, 1H),

1.30 (s, 3H). ^{13}C NMR ($CDCl_3$, 100 MHz): δ 169.6, 138.1, 119.5, 81.9, 79.7, 69.9, 62.2, 55.6, 49.4, 37.3, 33.4, 29.5, 23.3, 23.3, 21.9.

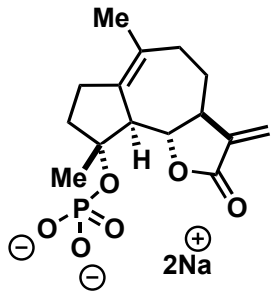

Micheliolide phosphate disodium salt 12: To a stirred solution of compound **11** (14 mg, 0.032 mmol) in CH_2Cl_2 (5 mL) was injected *N,O*-Bis(trimethylsilyl) acetamide (118 μL, 0.48 mmol) and DBU (47 μL, 0.32). The reaction was stirred overnight under N_2. The reaction was quenched by the addition of MeOH. After the removal of solvent under reduced pressure, the residue was dissolved in deionized H_2O and separated by reverse phase column chromatography (Biotage isolute XL-C18 column, eluant: 100% H_2O 5 mL, 75% H_2O in MeOH 5 mL, 25% H_2O in MeOH 5 mL, then 100% MeOH 5 mL). Every fraction that stained blue under *p*-anisaldehyde in TLC was collected to yield the crude product, which contained both acid form and DBU-salt form of the product and some leftover of DBU. The crude product was acidified by Dowex 50WX8 resin (pre-acidified by HCl and washed by H_2O until eluate was neutral) for 1 hr at room temperature in H_2O/MeOH 3:1. The resin was removed by filtration and the filtrate was concentrated and stirred with TEA (0.5 mL) in MeOH (5 mL) for 1 hr to give di-TEA salt of the product. The solvent was removed under reduced pressure and the residue was loaded to an ion exchange column (Dowex50WX8-Na^+, eluant: H_2O). All fractions were

collected and concentrated. The residue was further purified by reverse phase C-18 column (100% H_2O, then 75% H_2O in MeOH) to yield pure product. The product was lyophilized overnight to give white powder (4.5 mg, 37%). ^{1}H NMR (CD_3OD, 400 MHz): δ 6.12 (d, J = 3.4 Hz, 1H), 5.57 (d, J = 3.1 Hz, 1H), 3.87 (t, J = 10.1 Hz, 1H), 3.17 (d, J = 10.3 Hz, 1H), 2.79 (td, J = 2.5 Hz, J = 10.4 Hz 1H), 2.48 (m, 1H), 2.22 (m, 6H), 1.74 (s, 3H) 1.57 (s, 3H), 1.35 (m, 1H). ^{31}P NMR (CD_3OD, 162 MHz): δ -0.34. HRMS (ESI$^+$) *m/z* calcd for $[C_{15}H_{21}O_6P+Na]^+$ 351.0973; found 351.0990.

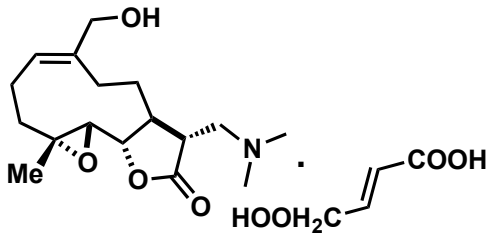

Dimethylamino Melampomagnolide B fumarate salt 13: To a stirred solution of compound **3** (12 mg, 0.045 mmol) in MeOH (2 mL) was added a solution of dimethylamine (2M in MeOH, 1.5 mL). The reaction was stirred overnight at room temperature. MeOH was removed under reduced pressure and the residue was purified by SiO_2 column chromatography (gradient 0%-50% EtOAc in hexanes over 10 min, then gradient 0%-25% MeOH in CH_2Cl_2 over 15 min) to yield the dimethylamino product as a white solid (7.4 mg, 0.024 mmol, 53%). To a stirred solution of dimethylamino product in Et_2O (5 mL) was added fumaric acid (2.8 mg, 0.024 mmol). A white precipitate was observed after the reaction was stirred overnight at room temperature. Et_2O was removed under reduced pressure to give the fumarate salt as white solid (10.2 mg, quant.). ^{1}H NMR (DMSO-d_6, 400 MHz): δ 6.61 (s, 2H), 5.48 (t, J = 7.5 Hz, 1H),

4.02 (t, J = 9.5 Hz, 1H), 3.91 (q, J =13.3 Hz, 2H), 2.68 (m, 4H), 2.27 (m, 10H), 2.07 (m, 3H), 1.57 (t, J = 9.9 Hz, 1H), 1.47 (s, 3H), 0.90 (t, J = 12.3 Hz, 1H). ^{13}C NMR (DMSO-d_6, 100 MHz): 177.0, 166.2, 141.0, 134.1, 123.4, 80.4, 63.3, 63.2, 59.8, 57.3, 45.0, 43.3, 42.6, 36.9, 25.6, 24.0, 22.9, 17.5. HR-MS (ESI) *m/z* calcd for $[C_{17}H_{28}NO_4+H]^+$ 310.2018; found 310.2004.

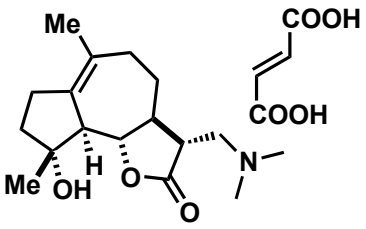

Dimethylamino Micheliolide fumarate salt 14: 14 was prepared according to the previously reported method that yielded HCl salt of the same parent compound.[322] To a stirred solution of **6** (26 mg, 0.106 mmol) in MeOH (2 mL) was added dimethylamine solution (2M in MeOH, 1.5 mL). The reaction was stirred overnight at room temperature. MeOH was removed under reduced pressure and the residue was purified by SiO_2 column chromatography (gradient 0%-50% EtOAc in hexanes over 10 min, then gradient 0%-15% MeOH in CH_2Cl_2 over 15 min) to yield the dimethylamino product as a white solid (30 mg, 0.102 mmol, 96%). To a stirred solution of dimethylamino product in Et_2O (5 mL) was added fumaric acid (11.8 mg, 0.102 mmol). A white precipitate was observed after stirring overnight at room temperature. Et_2O was removed under reduced pressure to give the fumarate salt as white solid (41 mg, quant.).

^{1}H NMR (DMSO-d_6, 400 MHz): δ 6.62 (s, 2H), 3.83 (t, J = 10.2 Hz, 1H), 2.82 (m, 3H), 2.54 (m, 1H), 2.40 (s, 6H), 2.30 (m, 2H), 2.04 (m, 5H), 1.61 (m, 5H), 1.25 (m, 1H), 1.17 (s, 3H). ^{13}C NMR (DMSO-d_6, 100 MHz): 176.9, 166.1, 134.0, 132.9, 130.6, 82.9, 79.4, 57.2, 56.1, 50.8, 44.3, 44.2, 42.5, 34.5, 29.5, 26.2, 23.5, 22.5. HRMS (ESI$^+$) *m/z* calcd for $[C_{17}H_{28}NO_3+H]^+$ 294.2069; found 294.2072.

3.5.3 Protocol for Mammalian Cell Culture

All cell lines were maintained in a humidified 5% CO_2 environment at 37 ℃ in culture flasks (Corning). Adherent cells were dissociated using 0.25% Trypsin-EDTA solution (Gibco). CCRF-CEM cells (ATCC, CCL-119) and NCI/ADR-RES (a gift from Dr. Gunda Georg's lab, UMN) were cultured in RPMI-1640 media (Cellgro) supplemented with 10% fetal bovine serum (FBS, Gibco), penicillin (100 I.U./mL), and streptomycin (100 μg/mL, ATCC) at a density of 2×10^5 - 2×10^6 cells/mL. DU-145 cells (ATCC, HTB-81), Vero cells (ATCC, CCL-81), U-87MG cells (ATCC, HTB-14**)**, and HeLa cells (ATCC, CCL-2) were cultured in MEM media (Cellgro) supplemented with 10% FBS (Gibco), penicillin (100 I.U./mL), and streptomycin (100 μg/mL, ATCC). HL-60 cells (ATCC, CCL-240) were cultured in IMDM media (Cellgro) supplemented with 20% FBS (Gibco), penicillin (100 I.U./mL), and streptomycin (100 μg/mL, ATCC). MCF-7 cells (ATCC, HTB-22) were cultured in MEM media (Cellgro) supplemented with 10% FBS (Gibco), bovine insulin (0.01 mg/mL, Sigma) penicillin (100 I.U./mL), and streptomycin (100 μg/mL, ATCC). GBM6 cells (a gift from Dr. John Ohlfest, UMN) were cultured with DMEM/F12 (1:1) with L-Glutamine, without HEPES (Thermo Scientific) supplemented with Normocin (100 μg/mL, Invivogen), 50X B-27

supplement (10 mL, Gibco), 100X N-2 supplement (5 mL, Gibco), human EGF (20 ng/μL, Peprotech), human FGF-basic (20 ng/μL, PeproTech), penicillin (50 I.U./mL), and streptomycin (50 μg/mL, ATCC).

3.5.4 Protocol for Cell Culture Cytotoxicity Assays

A protocol for these experiments was previously published by Hexum et al.[309] CCRF-CEM and HL-60 cells were cultured at a density of 10,000 cells/well in cell culture media (50 μL) in standard 96-well plates (Costar) 24 h prior to treatment. DU-145, Vero, U-87MG, GBM6, HeLa, MCF-7, and NCI/ADR-RES cells were seeded at a density of 5,000 cells/well in cell culture media (50 μL) in standard 96-well plates (Costar). Controls used were Blank (no cells) wells and control (vehicle control treated) wells and were prepared for every experiment. All PTL analogues were serially diluted in pre-warmed media and dosed to 96 well plates (final volume/well = 100 μL; final DMSO concentration = 0.5%). Approximately 1-3 h before the end of the treatment period (48 h), Alamar Blue (Invitrogen) cell viability reagent was added to the 96 well plates (10 μL). A quantitative measure of cell viability can be achieved from evaluating the ability of metabolically active cells (which are proportional to the number of living cells) to convert resazurin (non-fluorescent dye) to red-fluorescent resorufin. Fluorescence data were obtained on either a Molecular Devices SpectraMax M2 plate reader or an LJL BioSystems HT Analyst plate reader. Background fluorescence (no cell controls) was subtracted from each well and cellular viability values following compound treatment were normalized to vehicle-only treated wells (control wells only treated with aqueous DMSO, which were arbitrarily assigned 100% viability). Individual

IC_{50} curves were generated by fitting data to the sigmoidal (dose response) function of varied slope in GraphPad Prism (v. 5.0) software. Only curve fits with $R^2 > 0.95$ were deemed sufficient. Each experiment was performed in biological triplicate and mean IC_{50} values were calculated from the individual IC_{50} values obtained from each replicate. Standard deviation was calculated from the individual IC_{50} values obtained for each biological replicate.

3.6 NMR Spectrum

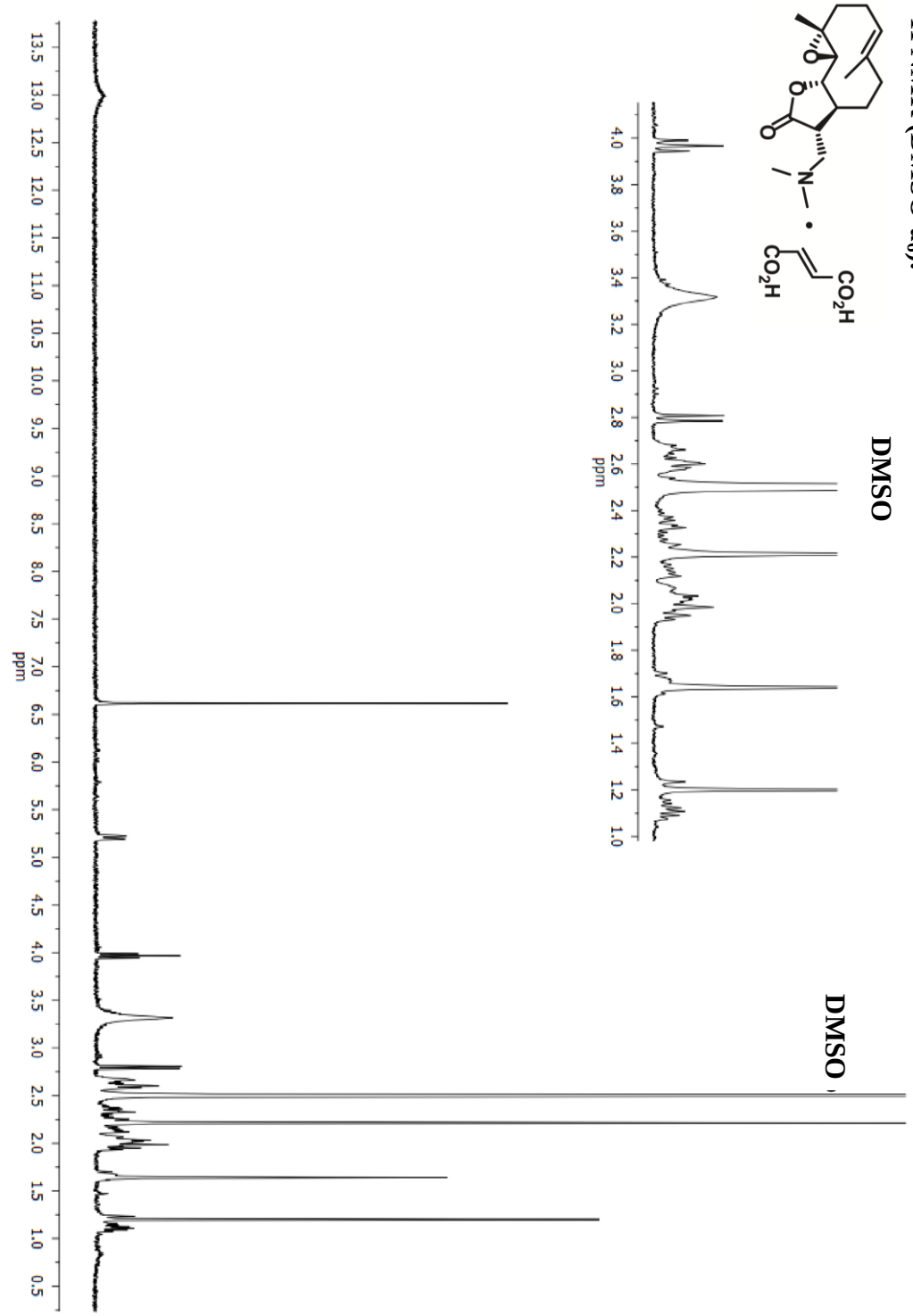

Cyclopropyl Parthenolide 4
^{1}H NMR ($CDCl_3$):

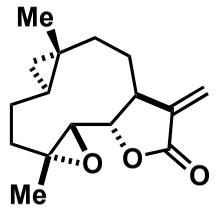

Cyclopropyl Parthenolide 4
^{13}C NMR ($CDCl_3$):

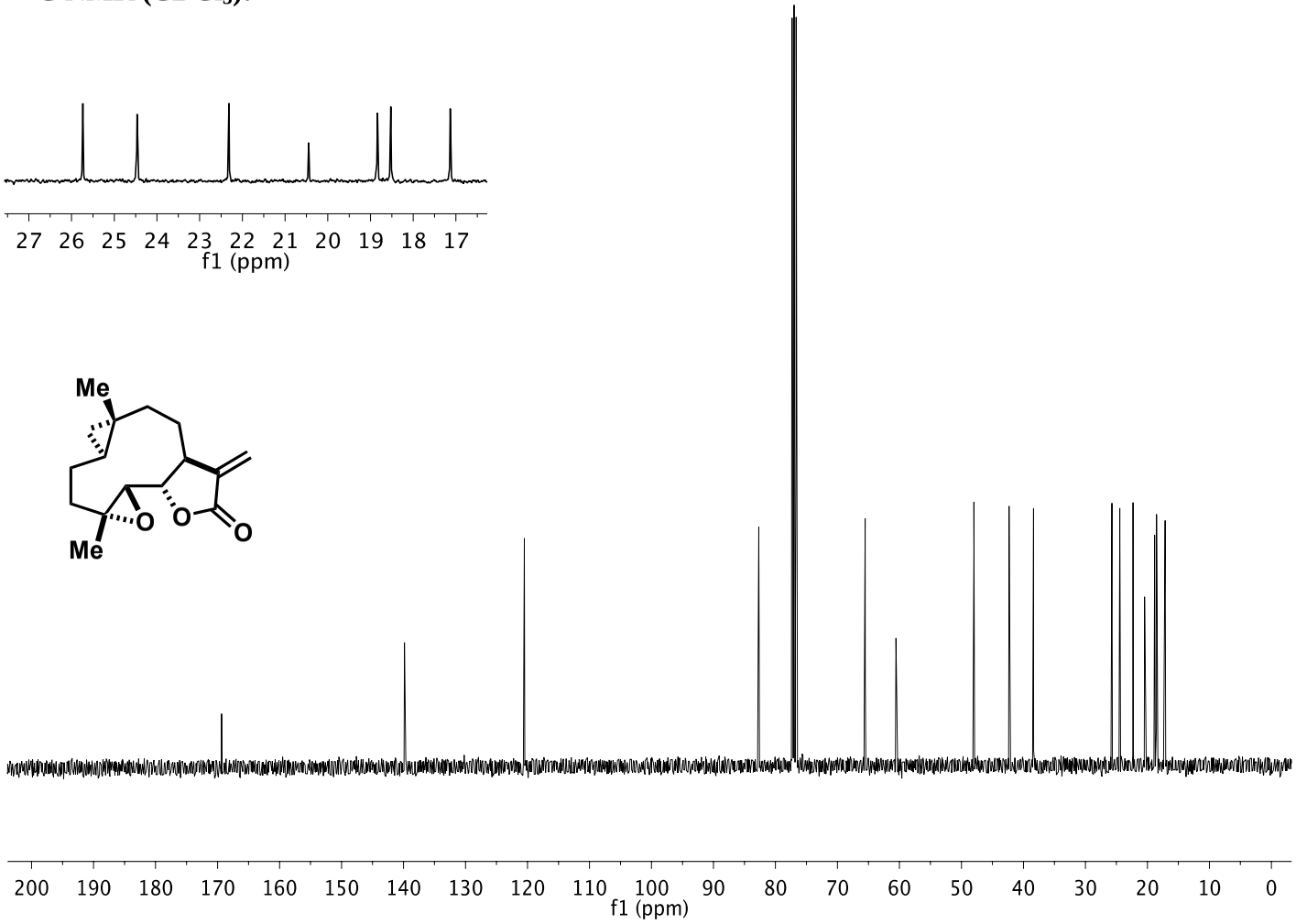

Cyclopropyl Parthenolide Dimethylamino Fumarate Salt 5
^{1}H NMR (DMSO-d_6):

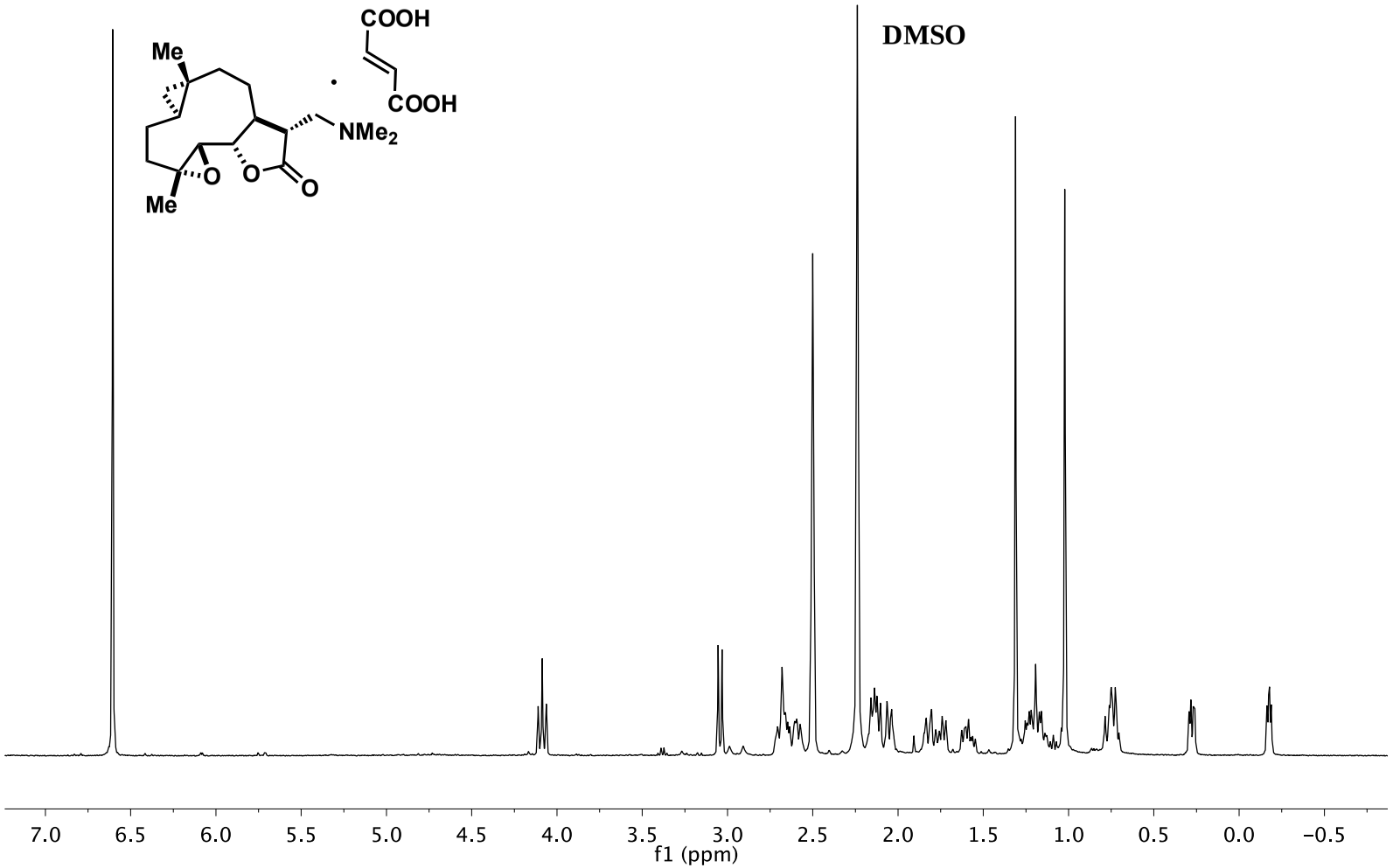

Cyclopropyl Parthenolide Dimethylamino Fumarate Salt 5
^{13}C NMR (DMSO-d_6):

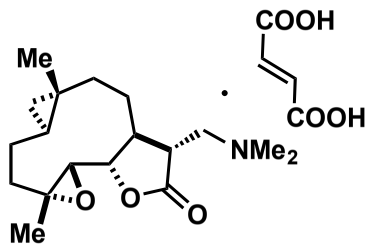

Micheliolide (6)
^{1}H NMR ($CDCl_3$):

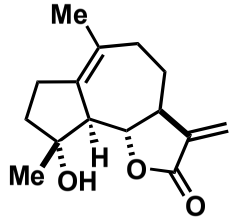

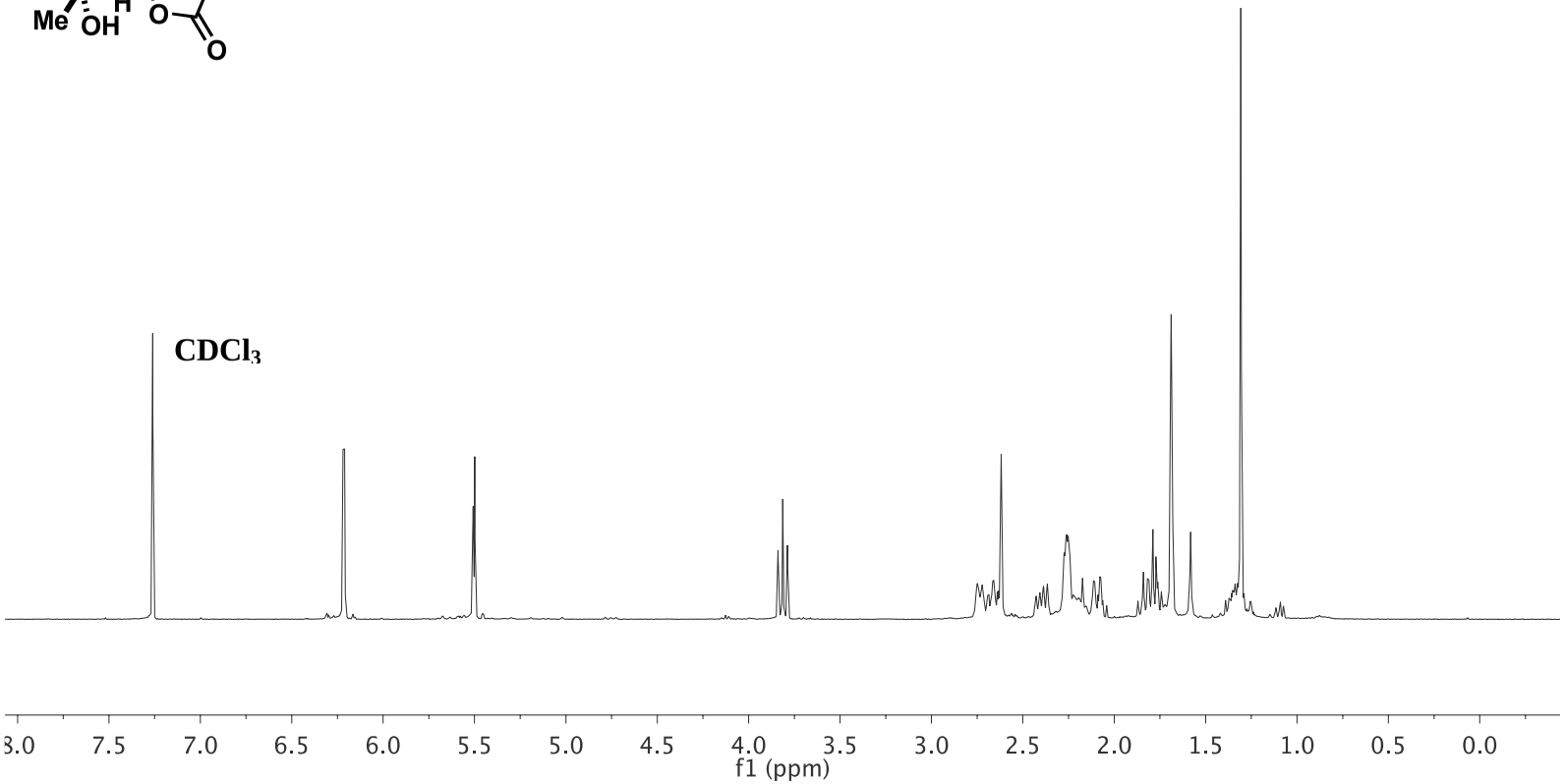

Rearranged PTL 7
^{1}H NMR ($CDCl_3$):

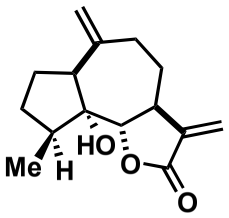

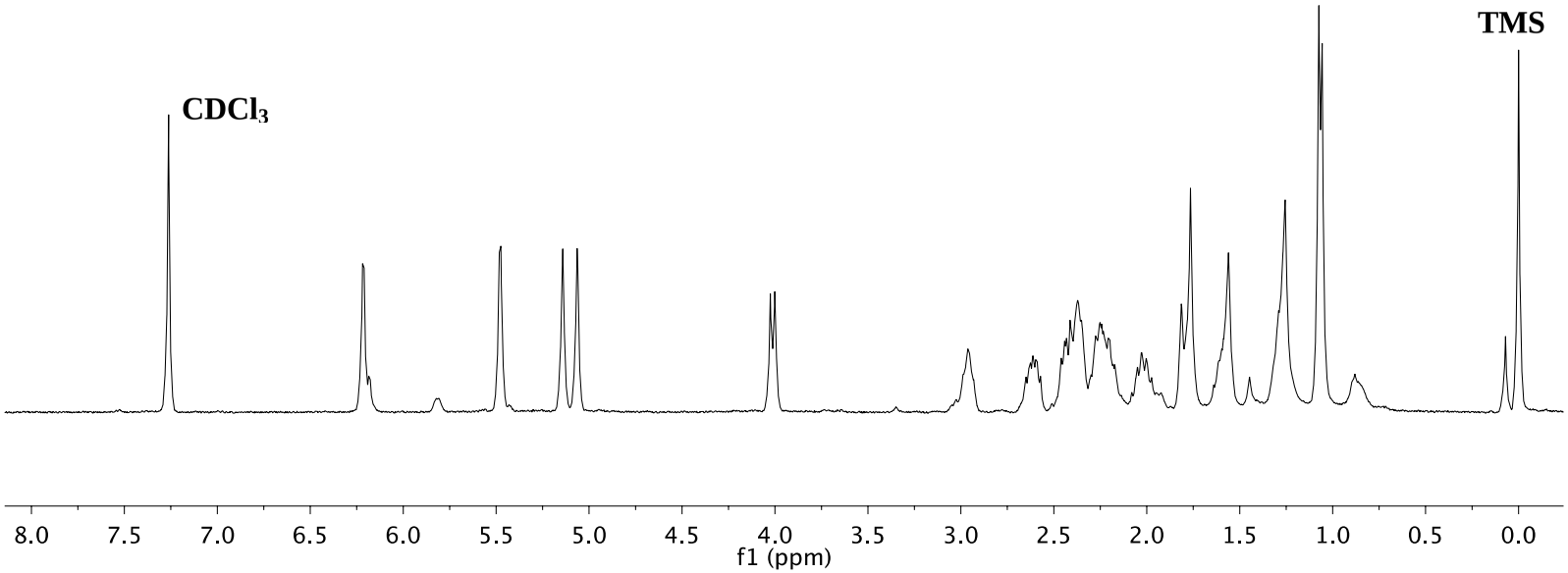

Bis(2-cyanoethyl) diisopropylphosphoramidite 8
^{1}H NMR ($CDCl_3$):

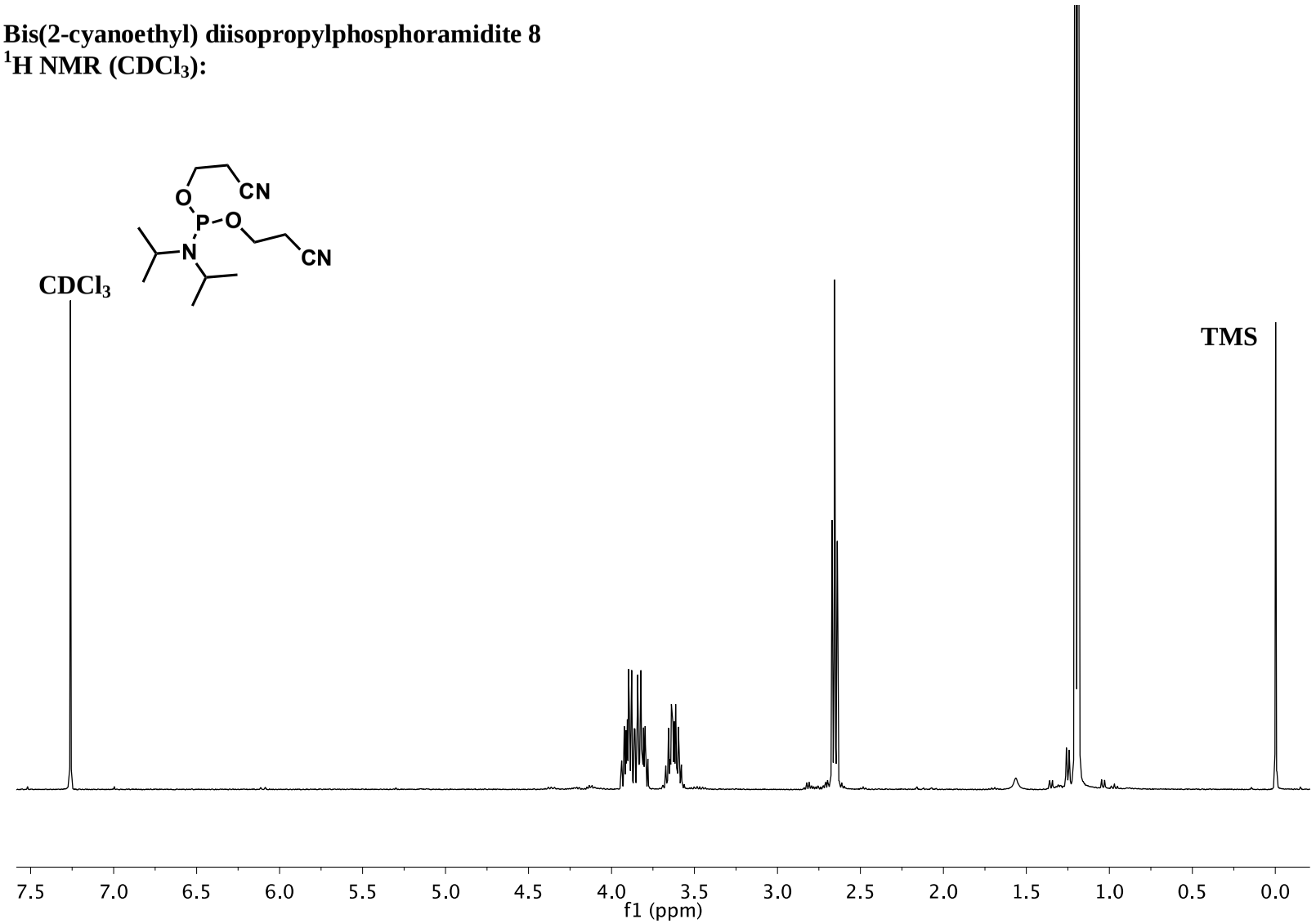

Bis(2-cyanoethyl) diisopropylphosphoramidite 8
^{31}P NMR ($CDCl_3$)

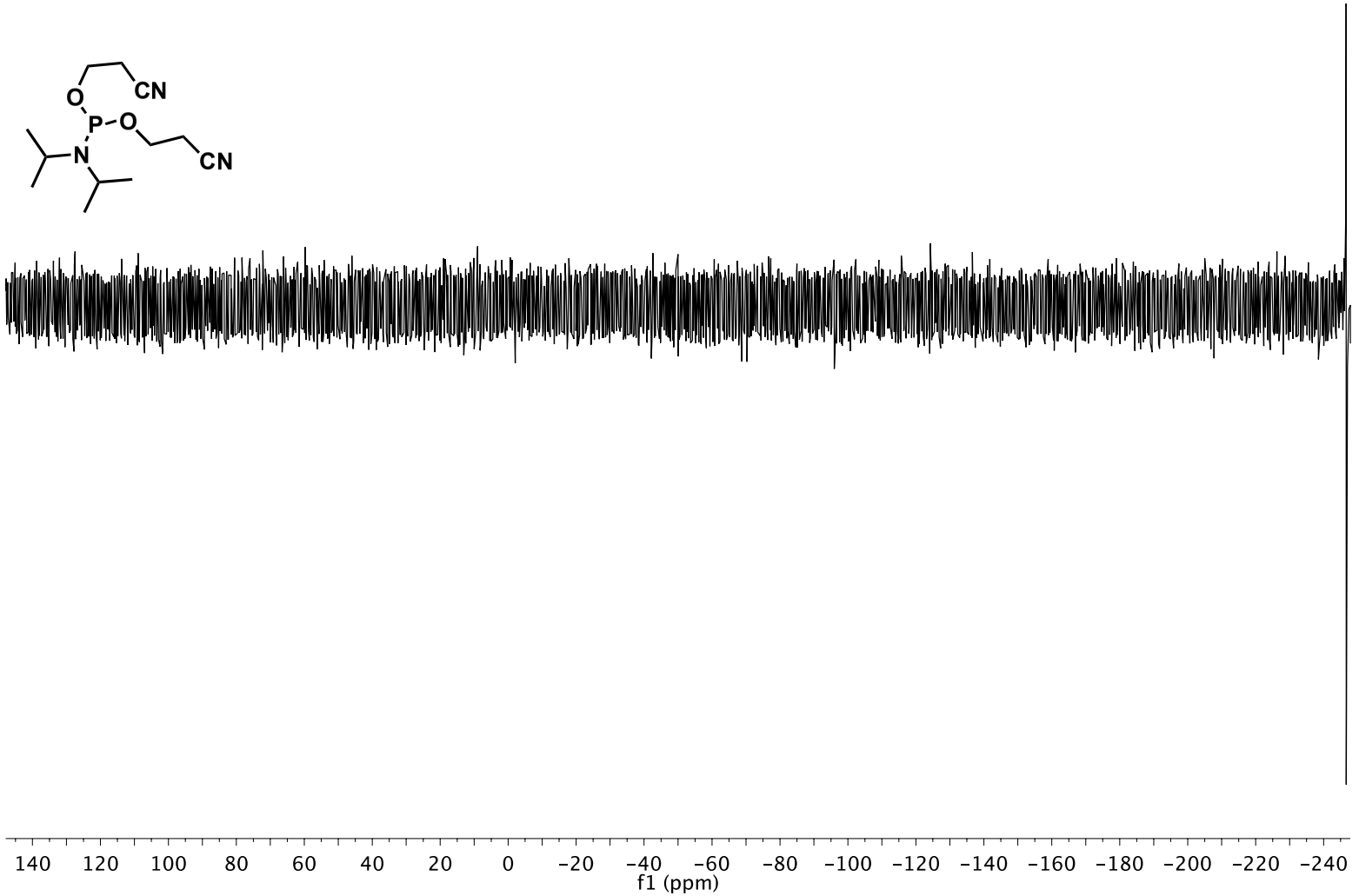

Bis(2-cyanoethyl) Melampomagnolide B phosphate 9:
^{1}H NMR ($CDCl_3$)

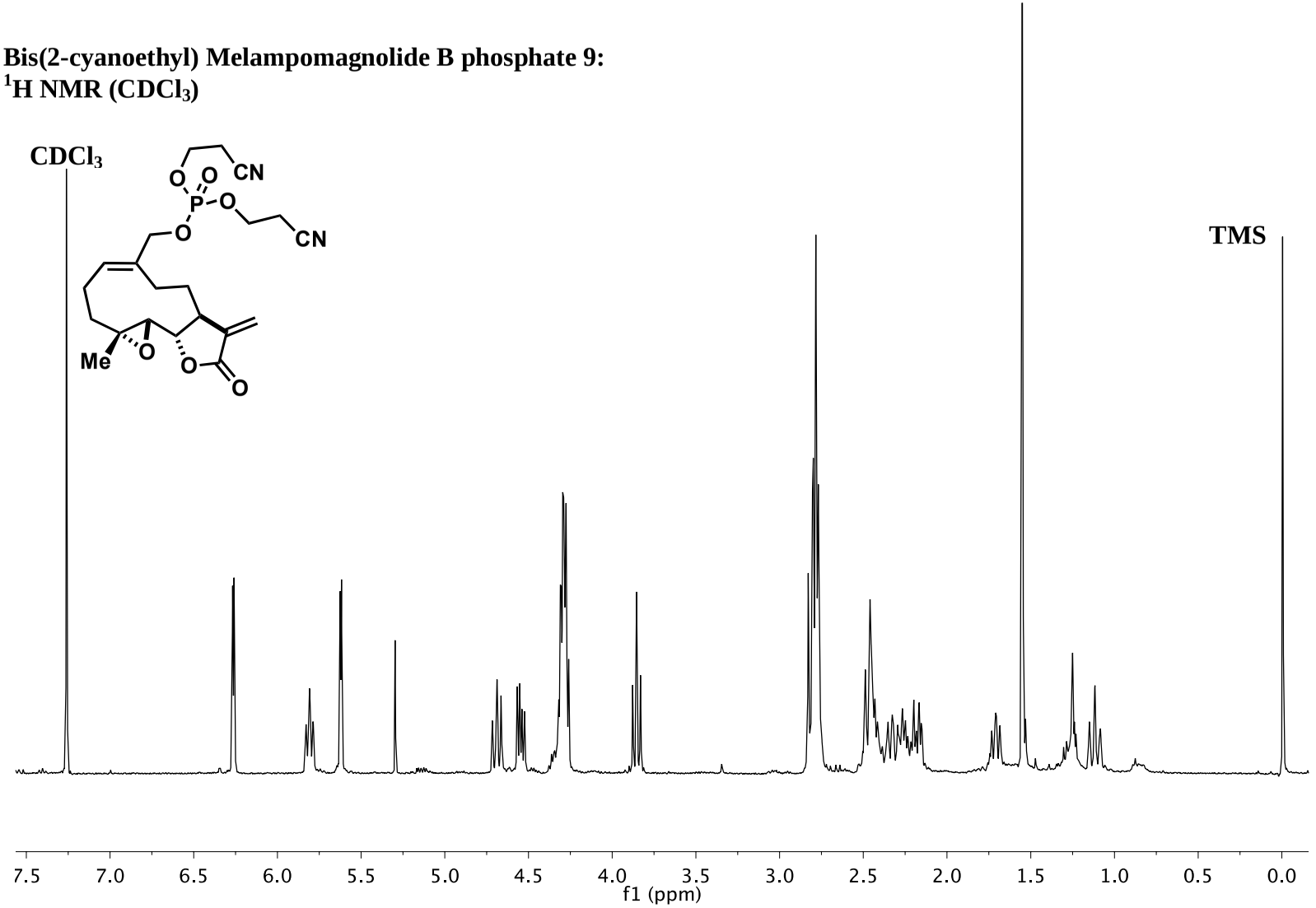

Bis(2-cyanoethyl) Melampomagnolide B phosphate 9:
^{31}P NMR ($CDCl_3$)

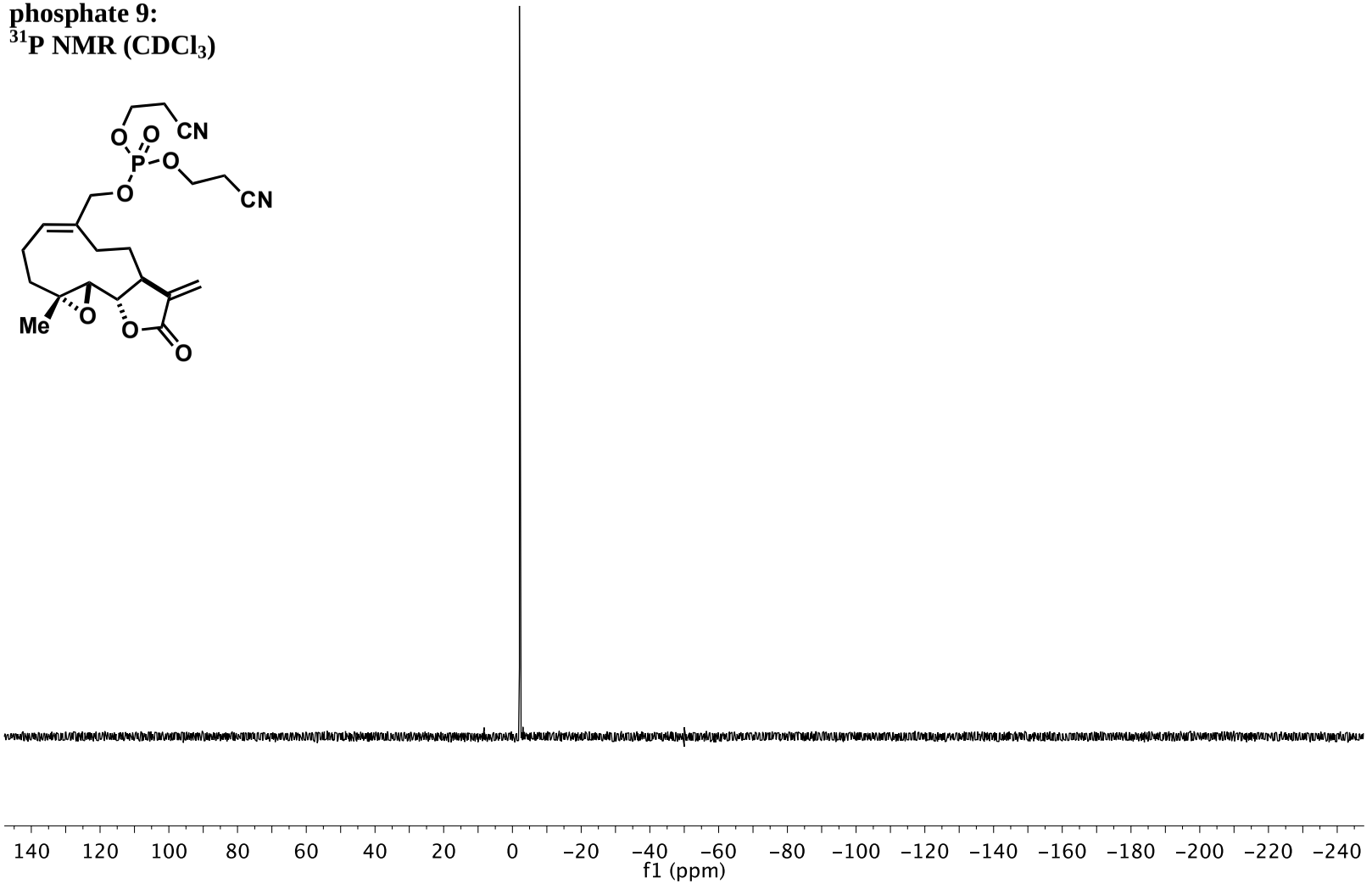

Melampomagnolide B phosphate disodium salt 10
^{1}H NMR (CD_3OD)

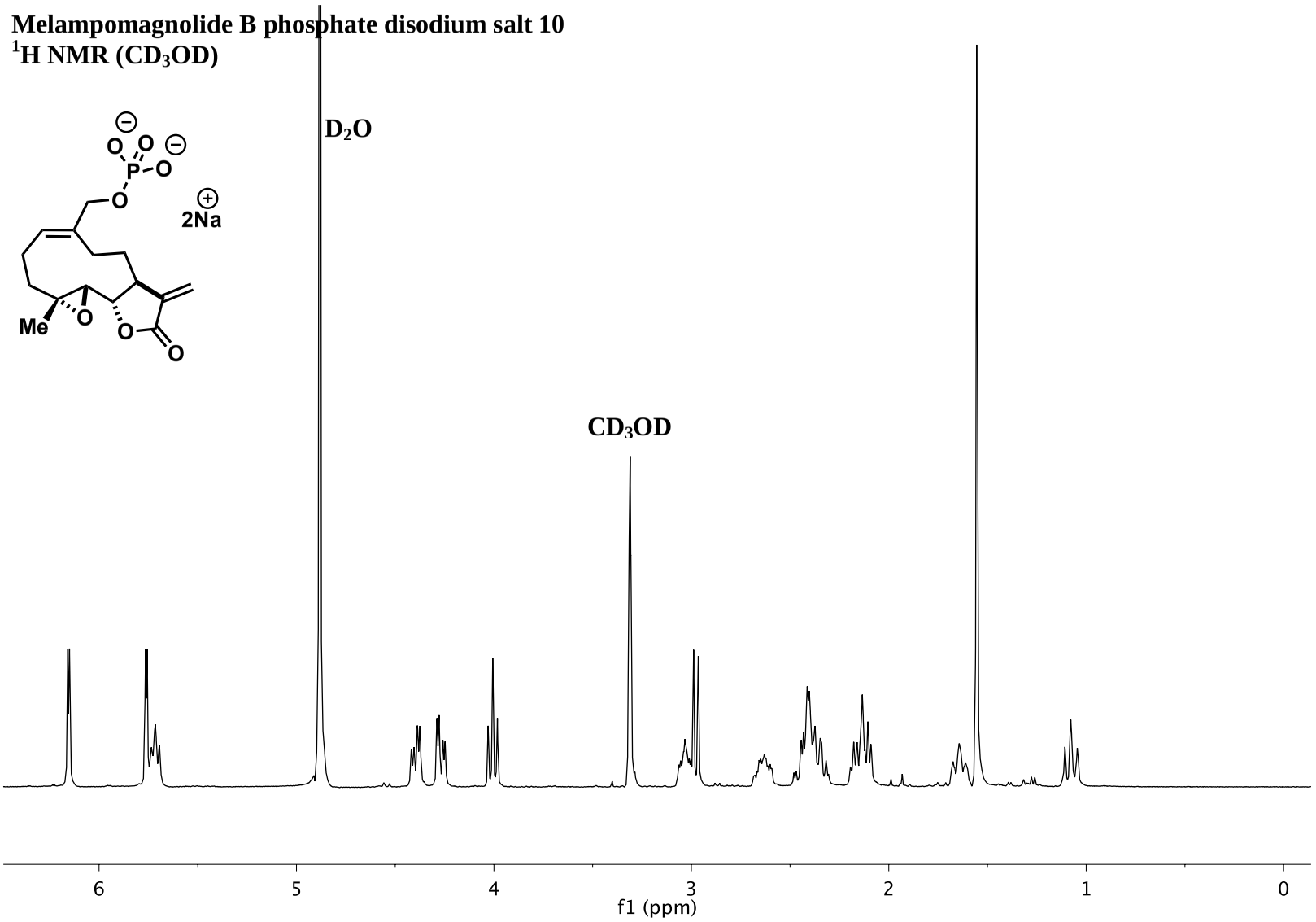

Melampomagnolide B phosphate disodium salt 10
^{31}P NMR (D_2O)

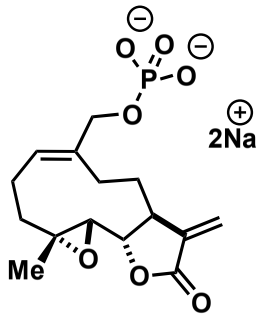

Bis(2-cyanoethyl) Micheliolide phosphate 11
^{1}H NMR ($CDCl_3$)

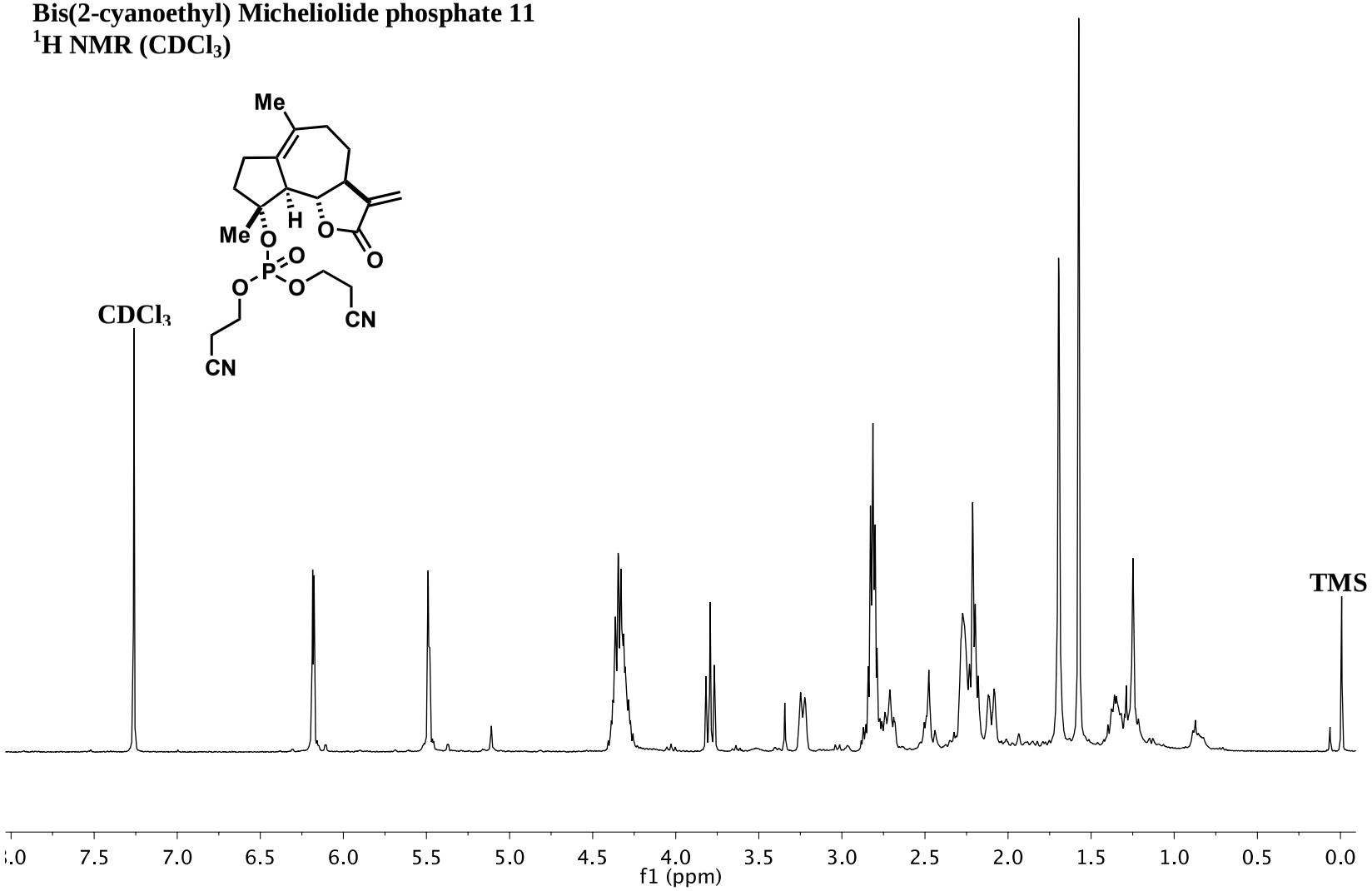

Bis(2-cyanoethyl) Micheliolide phosphate 11
^{31}P NMR ($CDCl_3$)

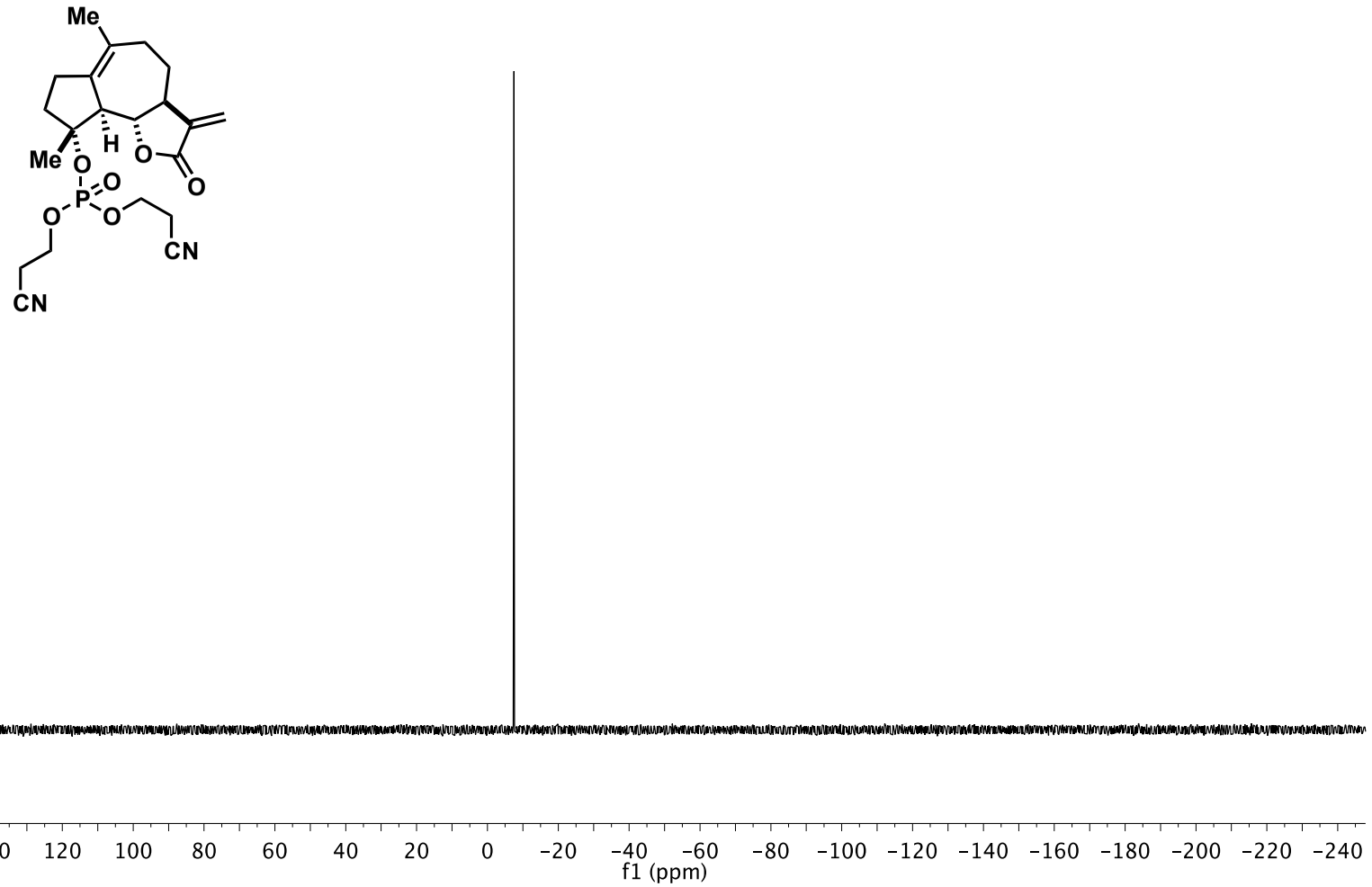

Epoxidized rearranged parthenolide
^{1}H NMR ($CDCl_3$)

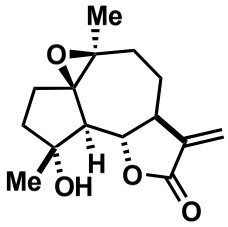

Micheliolide phosphate disodium salt 12

^{1}H NMR (CD_3OD)

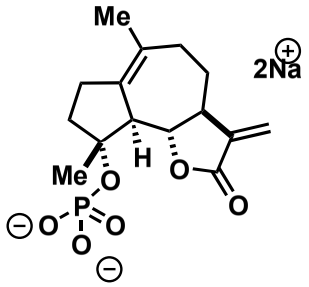

Micheliolide phosphate disodium salt 12
^{31}P NMR (CD_3OD)

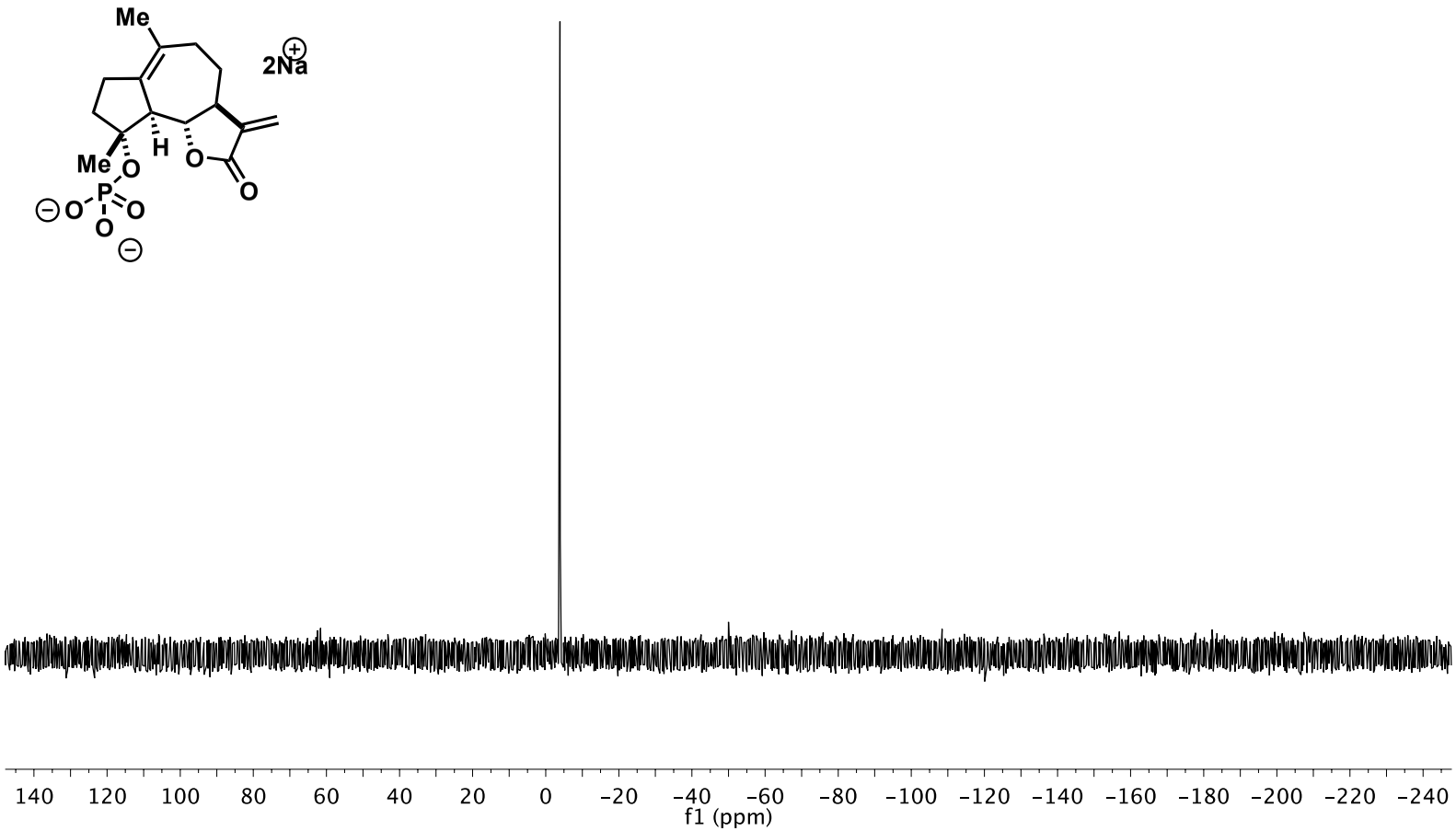

Melampomagnolide B Dimethylamino Fumarate Salt 13

^{1}H NMR (DMSO-d_6):

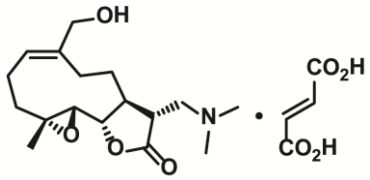

Melampomagnolide B Dimethylamino Fumarate
Salt 13
^{13}C NMR (DMSO-d_6):

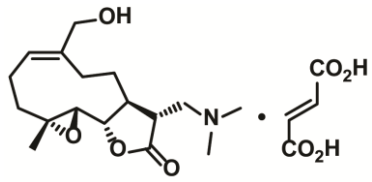

Dimethylamino Micheliolide fumarate salt 14
^{1}H NMR (DMSO-d_6):

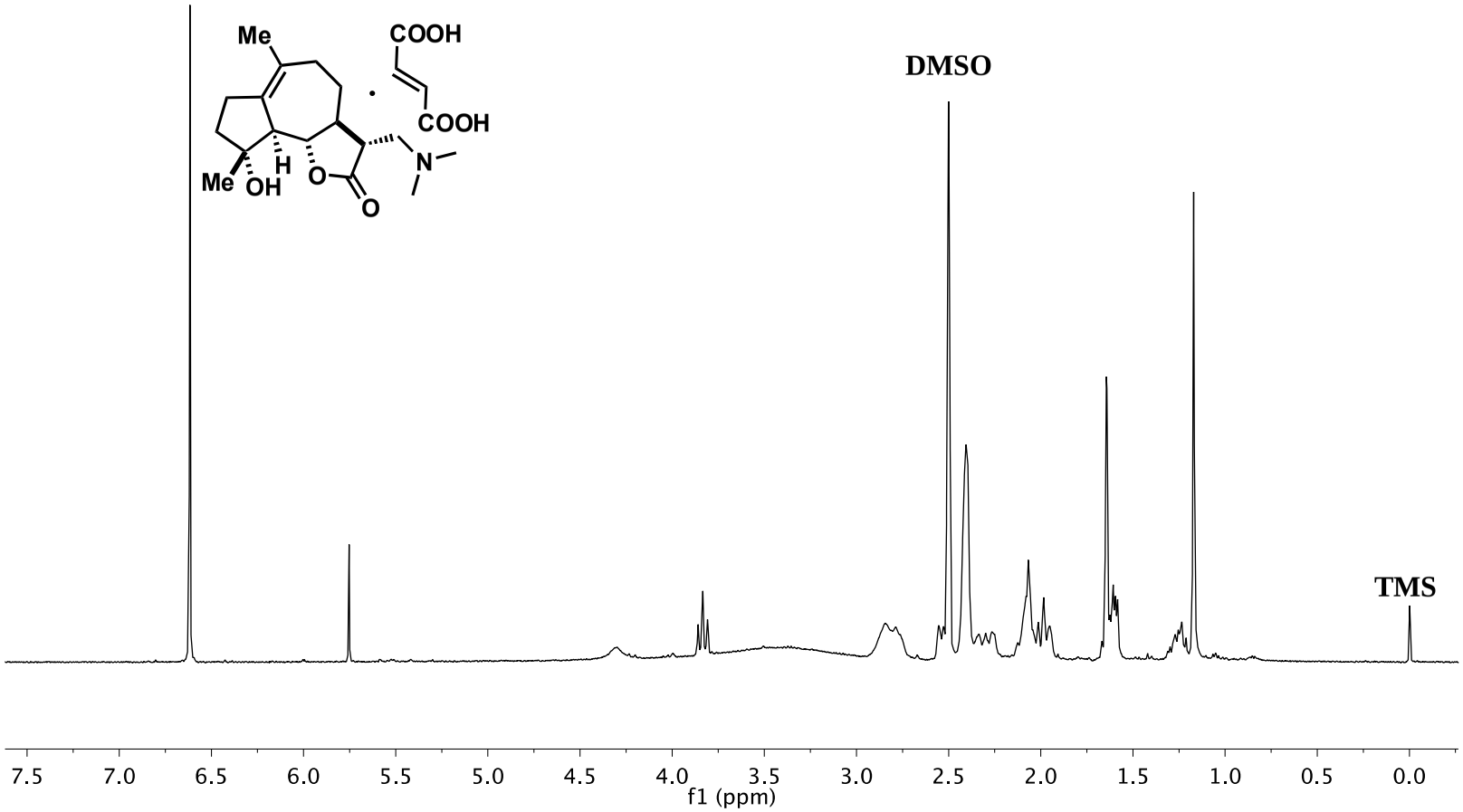

Dimethylamino Micheliolide fumarate salt 14
^{13}C NMR (DMSO-d_6):

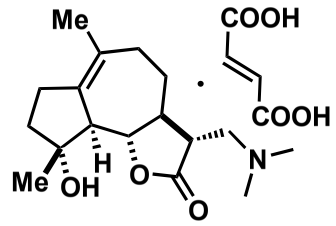

References:

(1) Reya, T.; Morrison, S. J.; Clarke, M. F.; Weissman, I. L. Stem cells, cancer, and cancer stem cells *Nature* **2001**, *414*, 105.
(2) Al-Hajj, M. Cancer stem cells and oncology therapeutics *Curr Opin Oncol* **2007**, *19*, 61.
(3) Behbod, F.; Rosen, J. M. Will cancer stem cells provide new therapeutic targets? *Carcinogenesis* **2005**, *26*, 703.
(4) Dick, J. E. Stem cell concepts renew cancer research *Blood* **2008**, *112*, 4793.
(5) Saini, V.; Shoemaker, R. H. Potential for therapeutic targeting of tumor stem cells *Cancer Sci* **2010**, *101*, 16.
(6) Wang, J. C. Y. Evaluating therapeutic efficacy against cancer stem cells: New challenges posed by a new paradigm *Cell Stem Cell* **2007**, *1*, 497.
(7) Ward, R. J.; Dirks, P. B. Cancer Stem Cells: At the Headwaters of Tumor Development *Annu Rev Pathol-Mech* **2007**, *2*, 175.
(8) Zhou, B. B. S.; Zhang, H. Y.; Damelin, M.; Geles, K. G.; Grindley, J. C.; Dirks, P. B. Tumour-initiating cells: challenges and opportunities for anticancer drug discovery *Nat Rev Drug Discov* **2009**, *8*, 806.
(9) Bonnet, D.; Dick, J. E. Human acute myeloid leukemia is organized as a hierarchy that originates from a primitive hematopoietic cell *Nat Med* **1997**, *3*, 730.
(10) Lapidot, T.; Sirard, C.; Vormoor, J.; Murdoch, B.; Hoang, T.; Caceres cortes, J.; Minden, M.; Paterson, B.; Caligiuri, M. A.; Dick, J. E. A Cell initiating human acute myeloid leukemia after transplantation into SCID mice *Nature* **1994**, *367*, 645.
(11) Fialkow, P. J.; Singer, J. W.; Raskind, W. H.; Adamson, J. W.; Jacobson, R. J.; Bernstein, I. D.; Dow, L. W.; Najfeld, V.; Veith, R. Clonal development, stem-cell differentiation, and clinical remission in acute nonlymphocytic leukemia *New Engl J Med* **1987**, *317*, 468.
(12) Griffin, J. D.; Lowenberg, B. Clonogenic cells in acute myeloblastic leukemia *Blood* **1986**, *68*, 1185.
(13) McCulloch, E. A. Stem cells in normal and leukemic hematopoiesis (Henry Stratton Lecture) *Blood* **1983**, *62*, 1.
(14) Li, L.; Bhatia, R. Stem Cell Quiescence *Clin Cancer Res* **2011**, *17*, 4936.
(15) Sehl, M.; Zhou, H.; Sinsheimer, J. S.; Lange, K. L. Extinction models for cancer stem cell therapy *Math Biosci* **2011**, *234*, 132.
(16) Dey, M.; Ulasov, I. V.; Tyler, M. A.; Sonabend, A. M.; Lesniak, M. S. Cancer Stem Cells: The Final Frontier for Glioma Virotherapy *Stem Cell Reviews and Reports* **2011**, *7*, 119.
(17) Natarajan, K.; Xie, Y.; Baer, M. R.; Ross, D. D. Role of breast cancer resistance protein (BCRP/ABCG2) in cancer drug resistance *Biochem Pharmacol* **2012**, *83*, 1084.
(18) American Cancer Society. Cancer Facts & Figures 2011 *ACS* **2011**.
(19) Guzman, M. L.; Rossi, R. M.; Karnischky, L.; Li, X. J.; Peterson, D. R.; Howard, D. S.; Jordan, C. T. The sesquiterpene lactone parthenolide induces apoptosis of

human acute myelogenous leukemia stem and progenitor cells *Blood* **2005**, *105*, 4163.
(20) Jin, L.; Hope, K. J.; Zhai, Q.; Smadja-Joffe, F.; Dick, J. E. Targeting of CD44 eradicates human acute myeloid leukemic stem cells *Nat Med* **2006**, *12*, 1167.
(21) Saito, Y.; Uchida, N.; Tanaka, S.; Suzuki, N.; Tomizawa-Murasawa, M.; Sone, A.; Najima, Y.; Takagi, S.; Aoki, Y.; Wake, A.; Taniguchi, S.; Shultz, L. D.; Ishikawa, F. Induction of cell cycle entry eliminates human leukemia stem cells in a mouse model of AML *Nat Biotechnol* **2010**, *28*, 275.
(22) Druker, B. J.; Talpaz, M.; Resta, D. J.; Peng, B.; Buchdunger, E.; Ford, J. M.; Lydon, N. B.; Kantarjian, H.; Capdeville, R.; Ohno-Jones, S.; Sawyers, C. L. Efficacy and safety of a specific inhibitor of the BCR-ABL tyrosine kinase in chronic myeloid leukemia. *New Engl J Med* **2001**, *344*, 1031.
(23) Kantarjian, H.; Talpaz, M.; O'Brien, S. S.; Garcia-Manero, G.; Verstovsek, S.; Giles, F.; Rios, M. B.; Shan, J. Q.; Letvak, L.; Thomas, D.; Faderl, S.; Ferrajoli, A.; Cortes, J. High-dose imatinib mesylate therapy in newly diagnosed Philadelphia chromosome-positive chronic phase chronic myeloid leukemia *Blood* **2004**, *103*, 2873.
(24) Nicholson, E.; Holyoake, T. The Chronic Myeloid Leukemia Stem Cell *Clinical Lymphoma, Myeloma & Leukemia* **2009**, *9*, S376.
(25) Graham, S. M.; Jorgensen, H. G.; Allan, E.; Pearson, C.; Alcorn, M. J.; Richmond, L.; Holyoake, T. L. Primitive, quiescent, Philadelphia-positive stem cells from patients with chronic myeloid leukemia are insensitive to STI571 in vitro *Blood* **2002**, *99*, 319.
(26) Zoeller, M. CD44: can a cancer-initiating cell profit from an abundantly expressed molecule? *Nat Rev Cancer* **2011**, *11*, 254.
(27) Acker, T.; Garvalov, B. K. Cancer stem cells: a new framework for the design of tumor therapies *J Mol Med-Jmm* **2011**, *89*, 95.
(28) Collins, A. T.; Berry, P. A.; Hyde, C.; Stower, M. J.; Maitland, N. J. Prospective Identification of Tumorigenic Prostate Cancer Stem Cells *Cancer Res* **2005**, *65*, 10946.
(29) Clayton, S.; Mousa, S. A. Therapeutics formulated to target cancer stem cells: Is it in our future? *Cancer Cell Int* **2011**, *11*.
(30) Klonisch, T.; Wiechec, E.; Hombach-Klonisch, S.; Ande, S. R.; Wesselborg, S.; Schulze-Osthoff, K.; Los, M. Cancer stem cell markers in common cancers – therapeutic implications *Trends Mol Med* **2008**, *14*, 450.
(31) Liu, H.-G.; Chen, C.; Yang, H.; Pan, Y.-F.; Zhang, X.-H. Cancer stem cell subsets and their relationships *J Transl Med* **2011**, *9*.
(32) Visvader, J. E.; Lindeman, G. J. Cancer stem cells in solid tumours: accumulating evidence and unresolved questions *Nat Rev Cancer* **2008**, *8*, 755.
(33) Gilbert, C. A.; Ross, A. H. Cancer Stem Cells: Cell Culture, Markers, and Targets for New Therapies *J Cell Biochem* **2009**, *108*, 1031.
(34) Alison, M. R.; Lim, S. M. L.; Nicholson, L. J. Cancer stem cells: problems for therapy? *J Pathol* **2011**, *223*, 147.
(35) Jordan, C. T. Cancer sten cell biology: from leukemia to solid tumors *Curr Opin Cell Biol* **2004**, *16*, 708.

(36) Jemal, A. Global Cancer Statistics (vol 61, pg 69, 2011) *Ca-Cancer J Clin* **2011**, *61*, 134.
(37) Siegel, R.; Ward, E.; Brawley, O.; Jemal, A. Cancer statistics, 2011: the impact of eliminating socioeconomic and racial disparities on premature cancer deaths *CA: a cancer journal for clinicians* **2011**, *61*, 212.
(38) Testa, U. Leukemia stem cells *Annals of Hematology* **2011**, *90*, 245.
(39) Blair, A.; Hogge, D. E.; Ailles, L. E.; Lansdorp, P. M.; Sutherland, H. J. Lack of expression of Thy-1 (CD90) on acute myeloid leukemia cells with long-term proliferative ability in vitro and in vivo *Blood* **1997**, *89*, 3104.
(40) Blair, A.; Hogge, D. E.; Sutherland, H. J. Most acute myeloid leukemia progenitor cells with long-term proliferative ability in vitro and in vivo have the phenotype CD34(+)/CD71(-)/HLA-DR *Blood* **1998**, *92*, 4325.
(41) Blair, A.; Sutherland, H. J. Primitive acute myeloid leukemia cells with long-term proliferative ability in vitro and in vivo lack surface expression of c-kit (CD 117) *Exp Hematol* **2000**, *28*, 660.
(42) Jordan, C. T.; Upchurch, D.; Szilvassy, S. J.; Guzman, M. L.; Howard, D. S.; Pettigrew, A. L.; Meyerrose, T.; Rossi, R.; Grimes, B.; Rizzieri, D. A.; Luger, S. M.; Phillips, G. L. The interleukin-3 receptor alpha chain is a unique marker for human acute myelogenous leukemia stem cells *Leukemia* **2000**, *14*, 1777.
(43) Florian, S.; Sonneck, K.; Hauswirth, A. W.; Krauth, M. T.; Schernthaner, G. H.; Sperr, W. R.; Valent, P. Detection of molecular targets on the surface of CD34+/CD38-stem cells in various myeloid malignancies *Leukemia Lymphoma* **2006**, *47*, 207.
(44) Dinndorf, P. A.; Andrews, R. G.; Benjamin, D.; Ridgway, D.; Wolff, L.; Bernstein, I. D. Expression of normal myeloid-associated antigens by acute leukemia cells *Blood* **1986**, *67*, 1048.
(45) Hauswirth, A. W.; Florian, S.; Printz, D.; Sotlar, K.; Krauth, M. T.; Fritsch, G.; Schernthaner, G. H.; Wacheck, V.; Selzer, E.; Sperr, W. R.; Valent, P. Expression of the target receptor CD33 in CD34(+)/CD38(-)/CD123(+) AML stem cells *Eur J Clin Invest* **2007**, *37*, 73.
(46) de Figueiredo-Pontes, L. L.; Pintao, M.-C. T.; Oliveira, L. C. O.; Dalmazzo, L. F. F.; Jacomo, R. H.; Garcia, A. B.; Falcao, R. P.; Rego, E. M. Determination of P-glycoprotein, MDR-related protein 1, breast cancer resistance protein, and lung-resistance protein expression in leukemic stem cells of acute myeloid leukemia *Cytom Part B-Clin Cy* **2008**, *74B*, 163.
(47) van Rhenen, A.; van Dongen, G. A. M. S.; Kelder, A.; Rombouts, E. J.; Feller, N.; Moshaver, B.; Stigter-van Walsum, M.; Zweegman, S.; Ossenkoppele, G. J.; Schuurhuis, G. J. The novel AML stem cell-associated antigen CLL-1 aids in discrimination between normal and leukemic stem cells *Blood* **2007**, *110*, 2659.
(48) Hosen, N.; Park, C. Y.; Tatsumi, N.; Oji, Y.; Sugiyama, H.; Gramatzki, M.; Krensky, A. M.; Weissman, I. L. CD96 is a leukemic stem cell-specific marker in human acute myeloid leukemia *P Natl Acad Sci USA* **2007**, *104*, 11008.
(49) Bendall, L. J.; Bradstock, K. F.; Gottlieb, D. J. Expression of CD44 variant exons in acute myeloid leukemia is more common and more complex than that observed in normal blood, bone marrow or CD34(+) cells *Leukemia* **2000**, *14*, 1239.

(50) Saito, Y.; Kitamura, H.; Hijikata, A.; Tomizawa-Murasawa, M.; Tanaka, S.; Takagi, S.; Uchida, N.; Suzuki, N.; Sone, A.; Najima, Y.; Ozawa, H.; Wake, A.; Taniguchi, S.; Shultz, L. D.; Ohara, O.; Ishikawa, F. Identification of Therapeutic Targets for Quiescent, Chemotherapy-Resistant Human Leukemia Stem Cells *Sci Transl Med* **2010**, *2*.
(51) Majeti, R.; Chao, M. P.; Alizadeh, A. A.; Pang, W. W.; Jaiswal, S.; Gibbs, K. D., Jr.; van Rooijen, N.; Weissman, I. L. CD47 Is an Adverse Prognostic Factor and Therapeutic Antibody Target on Human Acute Myeloid Leukemia Stem Cells *Cell* **2009**, *138*, 286.
(52) Quijano, C. A.; Moore, D.; Arthur, D.; Feusner, J.; Winter, S. S.; Pallavicini, M. G. Cytogenetically aberrant cells are present in the CD34(+)CD33(-)38(-)19(-) marrow compartment in children with acute lymphoblastic leukemia *Leukemia* **1997**, *11*, 1508.
(53) Cobaleda, C.; Gutierrez-Cianca, N.; Perez-Losada, J.; Flores, T.; Garcia-Sanz, R.; Gonzalez, M.; Sanchez-Garcia, I. A primitive hematopoietic cell is the target for the leukemic transformation in human Philadelphia-positive acute lymphoblastic leukemia *Blood* **2000**, *95*, 1007.
(54) Advani, A. S.; Pendergast, A. M. Bcr-Abl variants: biological and clinical aspects *Leukemia Res* **2002**, *26*, 713.
(55) Faderl, S.; Garcia-Manero, G.; Thomas, D. A.; Kantarjian, H. M. Philadelphia chromosome-positive acute lymphoblastic leukemia- current concepts and future perspectives *Reviews in clinical and experimental hematology* **2002**, *6*, 142.
(56) Castor, A.; Nilsson, L.; Astrand-Grundstrom, I.; Buitenhuis, M.; Ramirez, C.; Anderson, K.; Strombeck, B.; Garwicz, S.; Bekassy, A. N.; Schmiegelow, K.; Lausen, B.; Hokland, P.; Lehmann, S.; Juliusson, G.; Johansson, B.; Jacobsen, S. E. W. Distinct patterns of hematopoietic stem cell involvement in acute lymphoblastic leukemia *Nat Med* **2005**, *11*, 630.
(57) Yeoh, E. J.; Ross, M. E.; Shurtleff, S. A.; Williams, W. K.; Patel, D.; Mahfouz, R.; Behm, F. G.; Raimondi, S. C.; Relling, M. V.; Patel, A.; Cheng, C.; Campana, D.; Wilkins, D.; Zhou, X. D.; Li, J. Y.; Liu, H. Q.; Pui, C. H.; Evans, W. E.; Naeve, C.; Wong, L. S.; Downing, J. R. Classification, subtype discovery, and prediction of outcome in pediatric acute lymphoblastic leukemia by gene expression profiling *Cancer Cell* **2002**, *1*, 133.
(58) Cox, C. V.; Evely, R. S.; Oakhill, A.; Pamphilon, D. H.; Goulden, N. J.; Blair, A. Characterization of acute lymphoblastic leukemia progenitor cells *Blood* **2004**, *104*, 2919.
(59) Cox, C. V.; Martin, H. M.; Kearns, P. R.; Virgo, P.; Evely, R. S.; Blair, A. Characterization of a progenitor cell population in childhood T-cell acute lymphoblastic leukemia *Blood* **2007**, *109*, 674.
(60) Cox, C. V.; Diamanti, P.; Evely, R. S.; Kearns, P. R.; Blair, A. Expression of CD133 on leukemia-initiating cells in childhood ALL *Blood* **2009**, *113*, 3287.
(61) Nishida, H.; Yamazaki, H.; Yamada, T.; Iwata, S.; Dang, N. H.; Inukai, T.; Sugita, K.; Ikeda, Y.; Morimoto, C. CD9 correlates with cancer stem cell potentials in human B-acute lymphoblastic leukemia cells *Biochem Bioph Res Co* **2009**, *382*, 57.

(62) Yamazaki, H.; Nishida, H.; Iwata, S.; Dang, N. H.; Morimoto, C. CD90 and CD110 correlate with cancer stem cell potentials in human T-acute lymphoblastic leukemia cells *Biochem Bioph Res Co* **2009**, *383*, 172.
(63) Holyoake, T.; Jiang, X. Y.; Eaves, C.; Eaves, A. Isolation of a highly quiescent subpopulation of primitive leukemic cells in chronic myeloid leukemia *Blood* **1999**, *94*, 2056.
(64) DeSantis, C.; Siegel, R.; Bandi, P.; Jemal, A. Breast cancer statistics, 2011 *CA: a cancer journal for clinicians* **2011**, *61*, 409.
(65) Takahashi, R.-u. T., Fumitaka; Fujiwara,Tomohiro; Ono, Makiko and Ochiya, Takahiro Cancer stem cells in breast cancer *Cancers* **2011**, *3*, 1311.
(66) Al-Hajj, M.; Wicha, M. S.; Benito-Hernandez, A.; Morrison, S. J.; Clarke, M. F. Prospective identification of tumorigenic breast cancer cells *P Natl Acad Sci USA* **2003**, *100*, 3983.
(67) Phillips, T. M.; McBride, W. H.; Pajonk, F. The response of CD24(-/low)/CD44(+) breast cancer-initiating cells to radiation *J Natl Cancer I* **2006**, *98*, 1777.
(68) Buess, M.; Rajski, M.; Vogel-Durrer, B. M. L.; Herrmann, R.; Rochlitz, C. Tumor-Endothelial Interaction Links the CD44(+)/CD24(-) Phenotype with Poor Prognosis in Early-Stage Breast Cancer *Neoplasia* **2009**, *11*, 987.
(69) Sheridan, C.; Kishimoto, H.; Fuchs, R. K.; Mehrotra, S.; Bhat-Nakshatri, P.; Turner, C. H.; Goulet, R.; Badve, S.; Nakshatri, H. CD44(+)/CD24(-) breast cancer cells exhibit enhanced invasive properties: an early step necessary for metastasis *Breast Cancer Research* **2006**, *8*.
(70) Donnelly, D. S.; Zelterman, D.; Sharkis, S.; Krause, D. S. Functional activity of murine CD34(+) and CD34(-) hematopoietic stem cell populations *Exp Hematol* **1999**, *27*, 788.
(71) Neumeister, V.; Agarwal, S.; Bordeaux, J.; Camp, R. L.; Rimm, D. L. In Situ Identification of Putative Cancer Stem Cells by Multiplexing ALDH1, CD44, and Cytokeratin Identifies Breast Cancer Patients with Poor Prognosis *Am J Pathol* **2010**, *176*, 2131.
(72) Cho, R. W.; Wang, X.; Diehn, M.; Shedden, K.; Chen, G. Y.; Sherlock, G.; Gurney, A.; Lewicki, J.; Clarke, M. F. Isolation and molecular characterization of cancer stem cells in MMTV-Wnt-1 murine breast tumors *Stem Cells* **2008**, *26*, 364.
(73) Wright, M. H.; Calcagno, A. M.; Salcido, C. D.; Carlson, M. D.; Ambudkar, S. V.; Varticovski, L. Brca1 breast tumors contain distinct CD44(+)/CD24(-) and CD133(+) cells with cancer stem cell characteristics *Breast Cancer Res* **2008**, *10*.
(74) Zhao, P.; Lu, Y.; Jiang, X.; Li, X. Clinicopathological significance and prognostic value of CD133 expression in triple-negative breast carcinoma *Cancer Sci* **2011**, *102*, 1107.
(75) Liu, Q.; Li, J.-g.; Zheng, X.-y.; Jin, F.; Dong, H.-t. Expression of CD133, PAX2, ESA, and GPR30 in invasive ductal breast carcinomas *Chinese Med J-Peking* **2009**, *122*, 2763.
(76) Lin, W.-M.; Karsten, U.; Goletz, S.; Cheng, R.-C.; Cao, Y. Co-expression of CD173 (H2) and CD174 (Lewis Y) with CD44 suggests that fucosylated histo-blood group antigens are markers of breast cancer-initiating cells *Virchows Archiv* **2010**, *456*, 403.

(77) Lin, W.-M.; Karsten, U.; Goletz, S.; Cheng, R.-C.; Cao, Y. Expression of CD176 (Thomsen-Friedenreich antigen) on lung, breast and liver cancer-initiating cells *Int J Exp Pathol* **2011**, *92*, 97.
(78) Vassilopoulos, A.; Wang, R.-H.; Petrovas, C.; Ambrozak, D.; Koup, R.; Deng, C.-X. Identification and characterization of cancer initiating cells from BRCA1 related mammary tumors using markers for normal mammary stem cells *Int J Biol Sci* **2008**, *4*, 133.
(79) Shipitsin, M.; Campbell, L. L.; Argani, P.; Werernowicz, S.; Bloushtain-Qimron, N.; Yao, J.; Nikolskaya, T.; Serebryiskaya, T.; Beroukhim, R.; Hu, M.; Halushka, M. K.; Sukumar, S.; Parker, L. M.; Anderson, K. S.; Harris, L. N.; Garber, J. E.; Richardson, A. L.; Schnitt, S. J.; Nikolsky, Y.; Gelman, R. S.; Polyak, K. Molecular definition of breast tumor heterogeneity *Cancer Cell* **2007**, *11*, 259.
(80) Dalerba, P.; Dylla, S. J.; Park, I.-K.; Liu, R.; Wang, X.; Cho, R. W.; Hoey, T.; Gurney, A.; Huang, E. H.; Simeone, D. M.; Shelton, A. A.; Parmiani, G.; Castelli, C.; Clarke, M. F. Phenotypic characterization of human colorectal cancer stem cells *P Natl Acad Sci USA* **2007**, *104*, 10158.
(81) Ricci-Vitiani, L.; Lombardi, D. G.; Pilozzi, E.; Biffoni, M.; Todaro, M.; Peschle, C.; De Maria, R. Identification and expansion of human colon-cancer-initiating cells *Nature* **2007**, *445*, 111.
(82) O'Brien, C. A.; Pollett, A.; Gallinger, S.; Dick, J. E. A human colon cancer cell capable of initiating tumour growth in immunodeficient mice *Nature* **2007**, *445*, 106.
(83) Shmelkov, S. V.; Butler, J. M.; Hooper, A. T.; Hormigo, A.; Kushner, J.; Milde, T.; St Clair, R.; Baljevic, M.; White, I.; Jin, D. K.; Chadburn, A.; Murphy, A. J.; Valenzuela, D. M.; Gale, N. W.; Thurston, G.; Yancopoulos, G. D.; D'Angelica, M.; Kemeny, N.; Lyden, D.; Rafii, S. CD133 expression is not restricted to stem cells, and both CD133+ and CD133- metastatic colon cancer cells initiate tumors *J Clin Invest* **2008**, *118*, 2111.
(84) Du, L.; Wang, H.; He, L. CD44 is of functional importance for colorectal cancer stem cells. (vol 14, pg 6751, 2008) *Clin Cancer Res* **2008**, *14*, 7964.
(85) Horst, D.; Kriegl, L.; Engel, J.; Kirchner, T.; Jung, A. Prognostic Significance of the Cancer Stem Cell Markers CD133, CD44, and CD166 in Colorectal Cancer *Cancer Invest* **2009**, *27*, 844.
(86) Lugli, A.; Iezzi, G.; Hostettler, I.; Muraro, M. G.; Mele, V.; Tornillo, L.; Carafa, V.; Spagnoli, G.; Terracciano, L.; Zlobec, I. Prognostic impact of the expression of putative cancer stem cell markers CD133, CD166, CD44s, EpCAM, and ALDH1 in colorectal cancer *Brit J cancer* **2010**, *103*, 382.
(87) Vermeulen, L.; Todaro, M.; Mello, F. d. S.; Sprick, M. R.; Kemper, K.; Alea, M. P.; Richel, D. J.; Stassi, G.; Medema, J. P. Single-cell cloning of colon cancer stem cells reveals a multi-lineage differentiation capacity *P Natl Acad Sci USA* **2008**, *105*, 13427.
(88) Eguchi, S.; Kanematsu, T.; Arii, S.; Omata, M.; Kudo, M.; Sakamoto, M.; Takayasu, K.; Makuuchi, M.; Matsuyama, Y.; Monden, M.; Liver Canc Study Grp, J. Recurrence-free survival more than 10 years after liver resection for hepatocellular carcinoma *Brit J Surg* **2011**, *98*, 552.

(89) Ma, S.; Chan, K.-W.; Hu, L.; Lee, T. K.-W.; Wo, J. Y.-H.; Ng, I.-L.; Zheng, B.-J.; Guan, X.-Y. Identification and characterization of tumorigenic liver cancer stem/progenitor cells *Gastroenterology* **2007**, *132*, 2542.
(90) Zhu, Z.; Hao, X.; Yan, M.; Yao, M.; Ge, C.; Gu, J.; Li, J. Cancer stem/progenitor cells are highly enriched in CD133(+)CD44(+) population in hepatocellular carcinoma *Int J Cancer* **2010**, *126*, 2067.
(91) Kimura, O.; Takahashi, T.; Ishii, N.; Inoue, Y.; Ueno, Y.; Kogure, T.; Fukushima, K.; Shiina, M.; Yamagiwa, Y.; Kondo, Y.; Inoue, J.; Kakazu, E.; Iwasaki, T.; Kawagishi, N.; Shimosegawa, T.; Sugamura, K. Characterization of the epithelial cell adhesion molecule (EpCAM) plus cell population in hepatocellular carcinoma cell lines *Cancer Sci* **2010**, *101*, 2145.
(92) Yamashita, T.; Ji, J. F.; Budhu, A.; Forgues, M.; Yang, W.; Wang, H. Y.; Jia, H. L.; Ye, Q. H.; Qin, L. X.; Wauthier, E.; Reid, L. M.; Minato, H.; Honda, M.; Kaneko, S.; Tang, Z. Y.; Wang, X. W. EpCAM-Positive Hepatocellular Carcinoma Cells Are Tumor-Initiating Cells With Stem/Progenitor Cell Features *Gastroenterology* **2009**, *136*, 1012.
(93) Haraguchi, N.; Ishii, H.; Mimori, K.; Tanaka, F.; Ohkuma, M.; Kim, H. M.; Akita, H.; Takiuchi, D.; Hatano, H.; Nagano, H.; Barnard, G. F.; Doki, Y.; Mori, M. CD13 is a therapeutic target in human liver cancer stem cells *J Clin Invest* **2010**, *120*, 3326.
(94) Yang, Z. F.; Ho, D. W.; Ng, M. N.; Lau, C. K.; Yu, W. C.; Ngai, P.; Chu, P. W. K.; Lam, C. T.; Poon, R. T. P.; Fan, S. T. Significance of CD90(+) cancer stem cells in human liver cancer *Cancer Cell* **2008**, *13*, 153.
(95) Polakis, P. Wnt signaling and cancer *Gene Dev* **2000**, *14*, 1837.
(96) Yang, W.; Yan, H.-X.; Chen, L.; Liu, Q.; He, Y.-Q.; Yu, L.-X.; Zhang, S.-H.; Huang, D.-D.; Tang, L.; Kong, X.-N.; Chen, C.; Liu, S.-Q.; Wu, M.-C.; Wang, H.-Y. Wnt/beta-catenin signaling contributes to activation of normal and tumorigenic liver progenitor cells *Cancer Res* **2008**, *68*, 4287.
(97) Jemal, A.; Siegel, R.; Ward, E.; Hao, Y.; Xu, J.; Murray, T.; Thun, M. J. Cancer statistics, 2008 *Ca-Cancer J Clin* **2008**, *58*, 71.
(98) Li, C.; Heidt, D. G.; Dalerba, P.; Burant, C. F.; Zhang, L.; Adsay, V.; Wicha, M.; Clarke, M. F.; Simeone, D. M. Identification of pancreatic cancer stem cells *Cancer Res* **2007**, *67*, 1030.
(99) Hermann, P. C.; Huber, S. L.; Herrler, T.; Aicher, A.; Ellwart, J. W.; Guba, M.; Bruns, C. J.; Heeschen, C. Distinct populations of cancer stem cells determine tumor growth and metastatic activity in human pancreatic cancer *Cell Stem Cell* **2007**, *1*, 313.
(100) Jemal, A.; Siegel, R.; Xu, J.; Ward, E. Cancer Statistics, 2010 *Ca-Cancer J Clin* **2010**, *60*, 277.
(101) Fang, D.; Nguyen, T. K.; Leishear, K.; Finko, R.; Kulp, A. N.; Hotz, S.; Van Belle, P. A.; Xu, X. W.; Elder, D. E.; Herlyn, M. A tumorigenic subpopulation with stem cell properties in melanomas *Cancer Res* **2005**, *65*, 9328.
(102) Monzani, E.; Facchetti, F.; Galmozzi, E.; Corsini, E.; Benetti, A.; Cavazzin, C.; Gritti, A.; Piccinini, A.; Porro, D.; Santinami, M.; Invernici, G.; Parati, E.; Alessandri, G.; La Porta, C. A. M. Melanoma contains CD133 and ABCG2 positive cells with enhanced tumourigenic potential *Eur J Cancer* **2007**, *43*, 935.

(103) Grichnik, J. M.; Burch, J. A.; Schulteis, R. D.; Shan, S.; Liu, J.; Darrow, T. L.; Vervaert, C. E.; Seigler, H. F. Melanoma, a tumor based on a mutant stem cell? *J Invest Dermatol* **2006**, *126*, 142.
(104) Fusi, A.; Reichelt, U.; Busse, A.; Ochsenreither, S.; Rietz, A.; Maisel, M.; Keilholz, U. Expression of the Stem Cell Markers Nestin and CD133 on Circulating Melanoma Cells *J Invest Dermatol* **2011**, *131*, 487.
(105) Schatton, T.; Frank, N. Y.; Frank, M. H. Identification and targeting of cancer stem cells *Bioessays* **2009**, *31*, 1038.
(106) Schatton, T.; Murphy, G. F.; Frank, N. Y.; Yamaura, K.; Waaga-Gasser, A. M.; Gasser, M.; Zhan, Q.; Jordan, S.; Duncan, L. M.; Weishaupt, C.; Fuhlbrigge, R. C.; Kupper, T. S.; Sayegh, M. H.; Frank, M. H. Identification of cells initiating human melanomas *Nature* **2008**, *451*, 345.
(107) Davis, F. G.; Kupelian, V.; Freels, S.; McCarthy, B.; Surawicz, T. Prevalence estimates for primary brain tumors in the United States by behavior and major histology groups *Neuro-Oncology* **2001**, *3*, 152.
(108) Khalatbari, M. R.; Hamidi, M.; Moharamzad, Y. Glioblastoma multiforme with very rapid growth and long-term survival in children: report of two cases and review of the literature *Child Nerv Syst* **2011**, *27*, 1347.
(109) Eyler, C. E.; Rich, J. N. Survival of the fittest: Cancer stem cells in therapeutic resistance and angiogenesis *J Clin Oncol* **2008**, *26*, 2839.
(110) Binello, E.; Germano, I. M. Targeting glioma stem cells: A novel framework for brain tumors *Cancer Sci* **2011**, *102*, 1958.
(111) Singh, S. K.; Clarke, I. D.; Terasaki, M.; Bonn, V. E.; Hawkins, C.; Squire, J.; Dirks, P. B. Identification of a cancer stem cell in human brain tumors *Cancer Res* **2003**, *63*, 5821.
(112) Singh, S. K.; Hawkins, C.; Clarke, I. D.; Squire, J. A.; Bayani, J.; Hide, T.; Henkelman, R. M.; Cusimano, M. D.; Dirks, P. B. Identification of human brain tumour initiating cells *Nature* **2004**, *432*, 396.
(113) Tchoghandjian, A.; Baeza, N.; Colin, C.; Cayre, M.; Metellus, P.; Beclin, C.; Ouafik, L. H.; Figarella-Branger, D. A2B5 Cells from Human Glioblastoma have Cancer Stem Cell Properties *Brain Pathol* **2010**, *20*, 211.
(114) Ogden, A. T.; Waziri, A. E.; Lochhead, R. A.; Fusco, D.; Lopez, K.; Ellis, J. A.; Kang, J.; Assanah, M.; McKhann, G. M.; Sisti, M. B.; McCormick, P. C.; Canoll, P.; Bruce, J. N. Identification of A2B5(+)CD133-tumor-initiating cells in adult human gliomas *Neurosurgery* **2008**, *62*, 505.
(115) Wang, J.; Sakariassen, P. O.; Tsinkalovsky, O.; Immervoll, H.; Boe, S. O.; Svendsen, A.; Prestegarden, L.; Rosland, G.; Thorsen, F.; Stuhr, L.; Molven, A.; Bjerkvig, R.; Enger, P. O. CD133 negative glioma cells form tumors in nude rats and give rise to CD133 positive cells *Int J Cancer* **2008**, *122*, 761.
(116) Bao, S.; Wu, Q.; Li, Z.; Sathornsumetee, S.; Wang, H.; McLendon, R. E.; Hjehneland, A. B.; Rich, J. N. Targeting cancer stem cells through L1CAM suppresses glioma growth *Cancer Res* **2008**, *68*, 6043.
(117) Bao, S.; Wu, Q.; Sathornsumetee, S.; Hao, Y.; Li, Z.; Hjelmeland, A. B.; Shi, O.; McLendon, R. E.; Bigner, D. D.; Rich, J. N. Stem cell-like glioma cells promote tumor angiogenesis through vascular endothelial growth factor *Cancer Res* **2006**, *66*, 7843.

(118) Son, M. J.; Woolard, K.; Nam, D.-H.; Lee, J.; Fine, H. A. SSEA-1 Is an Enrichment Marker for Tumor-Initiating Cells in Human Glioblastoma *Cell Stem Cell* **2009**, *4*, 440.
(119) Read, T. A.; Fogarty, M. P.; Markant, S. L.; McLendon, R. E.; Wei, Z. Z.; Ellison, D. W.; Febbo, P. G.; Wechsler-Reya, R. J. Identification of CD15 as a Marker for Tumor-Propagating Cells in a Mouse Model of Medulloblastoma (vol 15, pg 135, 2009) *Cancer Cell* **2009**, *16*, 267.
(120) Dean, M.; Fojo, T.; Bates, S. Tumour stem cells and drug resistance *Nat Rev Cancer* **2005**, *5*, 275.
(121) Eramo, A.; Lotti, F.; Sette, G.; Pilozzi, E.; Biffoni, M.; Di Virgilio, A.; Conticello, C.; Ruco, L.; Peschle, C.; De Maria, R. Identification and expansion of the tumorigenic lung cancer stem cell population *Cell Death Differ* **2007**, *15*, 504.
(122) Dinney, C. P. N.; McConkey, D. J.; Millikan, R. E.; Wu, X. F.; Bar-Eli, M.; Adam, L.; Kamat, A. M.; Siefker-Radtke, A. O.; Tuziak, T.; Sabichi, A. L.; Grossman, H. B.; Benedict, W. F.; Czerniak, B. Focus on bladder cancer *Cancer Cell* **2004**, *6*, 111.
(123) Su, Y.; Qiu, Q.; Zhang, X.; Jiang, Z.; Leng, Q.; Liu, Z.; Stass, S. A.; Jiang, F. Aldehyde Dehydrogenase 1 A1-Positive Cell Population Is Enriched in Tumor-Initiating Cells and Associated with Progression of Bladder Cancer *Cancer Epidem Biomar* **2010**, *19*, 327.
(124) Chan, K. S.; Espinosa, I.; Chao, M.; Wong, D.; Ailles, L.; Diehn, M.; Gill, H.; Presti, J.; Chang, H. Y.; van de Rijn, M.; Shortliffe, L.; Weissman, I. L. Identification, molecular characterization, clinical prognosis, and therapeutic targeting of human bladder tumor-initiating cells *P Natl Acad Sci USA* **2009**, *106*, 14016.
(125) Yang, Y. M.; Chang, J. W. Bladder cancer initiating cells (BCICs) are among EMA(-)CD44v6(+) subset: Novel methods for isolating undetermined cancer stem (initiating) cells *Cancer Invest* **2008**, *26*, 725.
(126) Ning, Z. F.; Huang, Y. J.; Lin, T. X.; Zhou, Y. X.; Jiang, C.; Xu, K. W.; Huang, H.; Yin, X. B.; Huang, J. Subpopulations of Stem-like Cells in Side Population Cells from the Human Bladder Transitional Cell Cancer Cell Line T24 *J Int Med Res* **2009**, *37*, 621.
(127) Oates, J. E.; Grey, B. R.; Addla, S. K.; Samuel, J. D.; Hart, C. A.; Ramani, V. A. C.; Brown, M. D.; Clarke, N. W. Hoechst 33342 Side Population Identification Is a Conserved and Unified Mechanism in Urological Cancers *Stem Cells Dev* **2009**, *18*, 1515.
(128) Bostwick, D. G. E., J. N. *Urological Surgical Pathology*; 2nd ed.; Mosby, 2007.
(129) Mulholland, D. J.; Xin, L.; Morim, A.; Lawson, D.; Witte, O.; Wu, H. Lin(-)Sca-1(+)CD49f(high) Stem/Progenitors Are Tumor-Initiating Cells in the Pten-Null Prostate Cancer Model *Cancer Res* **2009**, *69*, 8555.
(130) Beltran, H.; Beer, T. M.; Carducci, M. A.; de Bono, J.; Gleave, M.; Hussain, M.; Kelly, W. K.; Saad, F.; Sternberg, C.; Tagawa, S. T.; Tannock, I. F. New Therapies for Castration-Resistant Prostate Cancer: Efficacy and Safety *European Urology* **2011**, *60*, 279.

(131) Liu, A. Y.; True, L. D.; LaTray, L.; Nelson, P. S.; Ellis, W. J.; Vessella, R. L.; Lange, P. H.; Hood, L.; vandenEngh, G. Cell-cell interaction in prostate gene regulation and cytodifferentiation *P Natl Acad Sci USA* **1997**, *94*, 10705.
(132) Patrawala, L.; Calhoun, T.; Schneider-Broussard, R.; Li, H.; Bhatia, B.; Tang, S.; Reilly, J. G.; Chandra, D.; Zhou, J.; Claypool, K.; Coghlan, L.; Tang, D. G. Highly purified CD44(+) prostate cancer cells from xenograft human tumors are enriched in tumorigenic and metastatic progenitor cells *Oncogene* **2006**, *25*, 1696.
(133) Patrawala, L.; Calhoun-Davis, T.; Schneider-Broussard, R.; Tang, D. G. Hierarchical organization of prostate cancer cells in xenograft tumors: The CD44(+)alpha 2 beta 1(+) cell population is enriched in tumor-initiating cells *Cancer Res* **2007**, *67*, 6796.
(134) Suzuki, A.; Nakano, T.; Mak, T. W.; Sasaki, T. Portrait of PTEN: Messages from mutant mice *Cancer Sci* **2008**, *99*, 209.
(135) Zhang, S.; Balch, C.; Chan, M. W.; Lai, H.-C.; Matei, D.; Schilder, J. M.; Yan, P. S.; Huang, T. H.-M.; Nephew, K. P. Identification and Characterization of Ovarian Cancer-Initiating Cells from Primary Human Tumors *Cancer Res* **2008**, *68*, 4311.
(136) Choi, Y. P.; Shim, H. S.; Gao, M.-Q.; Kang, S.; Cho, N. H. Molecular portraits of intratumoral heterogeneity in human ovarian cancer *Cancer Lett* **2011**, *307*, 62.
(137) Ferrandina, G.; Bonanno, G.; Pierelli, L.; Perillo, A.; Procoli, A.; Mariotti, A.; Corallo, M.; Martinelli, E.; Rutella, S.; Paglia, A.; Zannoni, G.; Mancuso, S.; Scambia, G. Expression of CD133-1 and CD133-2 in ovarian cancer *Int J Gynecol Cancer* **2008**, *18*, 506.
(138) Curley, M. D.; Therrien, V. A.; Cummings, C. L.; Sergent, P. A.; Koulouris, C. R.; Friel, A. M.; Roberts, D. J.; Seiden, M. V.; Scadden, D. T.; Rueda, B. R.; Foster, R. CD133 Expression Defines a Tumor Initiating Cell Population in Primary Human Ovarian Cancer *Stem Cells* **2009**, *27*, 2875.
(139) Gao, M. Q.; Choi, Y. P.; Kang, S.; Youn, J. H.; Cho, N. H. CD24+ cells from hierarchically organized ovarian cancer are enriched in cancer stem cells *Oncogene* **2010**, *29*, 2672.
(140) Wei, X.; Dombkowski, D.; Meirelles, K.; Pieretti-Vanmarcke, R.; Szotek, P. P.; Chang, H. L.; Preffer, F. I.; Mueller, P. R.; Teixeira, J.; MacLaughlin, D. T.; Donahoe, P. K. Mullerian inhibiting substance preferentially inhibits stem/progenitors in human ovarian cancer cell lines compared with chemotherapeutics *P Natl Acad Sci USA* **2010**, *107*, 18874.
(141) Gupta, P. B.; Onder, T. T.; Jiang, G. Z.; Tao, K.; Kuperwasser, C.; Weinberg, R. A.; Lander, E. S. Identification of Selective Inhibitors of Cancer Stem Cells by High-Throughput Screening *Cell* **2009**, *138*, 645.
(142) Shmelkov, S. V.; St Clair, R.; Lyden, D.; Rafii, S. Ac133/Cd133/Prominin-1 *Int J Biochem Cell B* **2005**, *37*, 715.
(143) Griguer, C. E.; Oliva, C. R.; Gobin, E.; Marcorelles, P.; Benos, D. J.; Lancaster, J. R.; Gillespie, G. Y. CD133 Is a Marker of Bioenergetic Stress in Human Glioma *Plos One* **2008**, *3*.
(144) Weigmann, A.; Corbeil, D.; Hellwig, A.; Huttner, W. B. Prominin, a novel microvilli-specific polytopic membrane protein of the apical surface of epithelial cells, is targeted to plasmalemmal protrusions of non-epithelial cells *P Natl Acad Sci USA* **1997**, *94*, 12425.

(145) Rappa, G.; Fodstad, O.; Lorico, A. The Stem Cell-Associated Antigen CD133 (Prominin-1) Is a Molecular Therapeutic Target for Metastatic Melanoma *Stem Cells* **2008**, *26*, 3008.
(146) Wu, Y.; Wu, P. Y. CD133 as a Marker for Cancer Stem Cells: Progresses and Concerns *Stem Cells Dev* **2009**, *18*, 1127.
(147) Bidlingmaier, S.; Zhu, X.; Liu, B. The utility and limitations of glycosylated human CD133 epitopes in defining cancer stem cells *J Mol Med-Jmm* **2008**, *86*, 1025.
(148) Swaminathan, S. K.; Olin, M. R.; Forster, C. L.; Cruz, K. S. S.; Panyam, J.; Ohlfest, J. R. Identification of a novel monoclonal antibody recognizing CD133 *Journal of Immunological Methods* **2010**, *361*, 110.
(149) Wang, C. H.; Chiou, S. H.; Chou, C. P.; Chen, Y. C.; Huang, Y. J.; Peng, C. A. Photothermolysis of glioblastoma stem-like cells targeted by carbon nanotubes conjugated with CD133 monoclonal antibody *Nanomed-Nanotechnol* **2011**, *7*, 69.
(150) Bourseau-Guilmain, E.; Bejaud, J.; Griveau, A.; Lautram, N.; Hindre, F.; Weyland, M.; Benoit, J. P.; Garcion, E. Development and characterization of immuno-nanocarriers targeting the cancer stem cell marker AC133 *Int J Pharm* **2012**, *423*, 93.
(151) van der Gun, B. T. F.; Melchers, L. J.; Ruiters, M. H. J.; de Leij, L. F. M. H.; McLaughlin, P. M. J.; Rots, M. G. EpCAM in carcinogenesis: the good, the bad or the ugly *Carcinogenesis* **2010**, *31*, 1913.
(152) Winter, M. J.; Nagelkerken, B.; Mertens, A. E. E.; Rees-Bakker, H. A. M.; Briaire-de Bruijn, I. H.; Litvinov, S. V. Expression of Ep-CAM shifts the state of cadherin-mediated adhesions from strong to weak *Exp Cell Res* **2003**, *285*, 50.
(153) Litvinov, S. V.; Velders, M. P.; Bakker, H. A. M.; Fleuren, G. J.; Warnaar, S. O. EP-CAM - A human epithelial antigen is a homophilic cell-cell adhesion molecule *J Cell Biol* **1994**, *125*, 437.
(154) Ruf, P.; Gires, O.; Jager, M.; Fellinger, K.; Atz, J.; Lindhofer, H. Characterisation of the new EpCAM-specific antibody HO-3: implications for trifunctional antibody immunotherapy of cancer *Brit J cancer* **2007**, *97*, 315.
(155) Chelius, D.; Ruf, P.; Gruber, P.; Ploscher, M.; Liedtke, R.; Gansberger, E.; Hess, J.; Wasiliu, M.; Lindhofer, H. Structural and functional characterization of the trifunctional antibody catumaxomab *Mabs-Austin* **2010**, *2*, 309.
(156) Lindhofer, H.; Schoberth, A.; Pelster, D.; Hess, J.; Herold, J.; Jager, M. Elimination of cancer stem cells (CD133+/EpCAM+) from malignant ascites by the trifunctional antibody catumaxomab: Results from a pivotal phase II/III study *J Clin Oncol* **2009**, *27*.
(157) Jager, M.; Schoberth, A.; Ruf, P.; Hess, J.; Hennig, M.; Schmalfeldt, B.; Wimberger, P.; Strohlein, M.; Theissen, B.; Heiss, M. M.; Lindhofer, H. Immunomonitoring Results of a Phase II/III Study of Malignant Ascites Patients Treated with the Trifunctional Antibody Catumaxomab (Anti-EpCAM x Anti-CD3) *Cancer Res* **2012**, *72*, 24.
(158) Seimetz, D.; Lindhofer, H.; Bokemeyer, C. Development and approval of the trifunctional antibody catumaxomab (anti-EpCAM x anti-CD3) as a targeted cancer immunotherapy *Cancer Treat Rev* **2010**, *36*, 458.

(159) Brischwein, K.; Schlereth, B.; Guller, B.; Steiger, C.; Wolf, A.; Lutterbuese, R.; Offner, S.; Locher, M.; Urbig, T.; Raum, T.; Kleindienst, P.; Wimberger, P.; Kimmig, R.; Fichtner, I.; Kufer, P.; Hofmeister, R.; da Silva, A. J.; Baeuerle, P. A. MT110: A novel bispecific single-chain antibody construct with high efficacy in eradicating established tumors *Mol Immunol* **2006**, *43*, 1129.

(160) Baeuerle, P. A.; Kufer, P.; Bargou, R. BiTE: Teaching antibodies to engage T-cells for cancer therapy *Curr Opin Mol Ther* **2009**, *11*, 22.

(161) Amann, M.; Brischwein, K.; Lutterbuese, P.; Parr, L.; Petersen, L.; Lorenczewski, G.; Krinner, E.; Bruckmeier, S.; Lippold, S.; Kischel, R.; Lutterbuese, R.; Kufer, P.; Baeuerle, P. A.; Schlereth, B. Therapeutic window of MuS110, a single-chain antibody construct bispecific for murine EpCAM and murine CD3 *Cancer Res* **2008**, *68*, 143.

(162) Herrmann, I.; Baeuerle, P. A.; Friedrich, M.; Murr, A.; Filusch, S.; Ruttinger, D.; Majdoub, M. W.; Sharma, S.; Kufer, P.; Raum, T.; Munz, M. Highly Efficient Elimination of Colorectal Tumor-Initiating Cells by an EpCAM/CD3-Bispecific Antibody Engaging Human T Cells *Plos One* **2010**, *5*.

(163) Haas, C.; Krinner, E.; Brischwein, K.; Hoffmann, P.; Lutterbuese, R.; Schlereth, B.; Kufer, P.; Baeuerle, P. A. Mode of cytotoxic action of T cell-engaging BiTE antibody MT110 *Immunobiology* **2009**, *214*, 441.

(164) Balzar, M.; Winter, M. J.; de Boer, C. J.; Litvinov, S. V. The biology of the 17-1A antigen (Ep-CAM) *J Mol Med-Jmm* **1999**, *77*, 699.

(165) Riethmuller, G.; Schneidergadicke, E.; Schlimok, G.; Schmiegel, W.; Raab, R.; Hoffken, K.; Gruber, R.; Pichlmaier, H.; Hirche, H.; Pichlmayr, R.; Buggisch, P.; Witte, J.; Eigler, F. W.; Facklerschwalbe, I.; Funke, I.; Schmidt, C. G.; Schreiber, H.; Schweiberer, L.; Eibleibesfeldt, B. Randomized Trial of Monoclonal-Antibody for Adjuvant Therapy of Resected Dukes-C Colorectal-Carcinoma *Lancet* **1994**, *343*, 1177.

(166) Braun, S.; Hepp, F.; Kentenich, C. R. M.; Janni, W.; Pantel, K.; Riethmuller, G.; Willgeroth, F.; Sommer, H. L. Monoclonal antibody therapy with Edrecolomab in breast cancer patients: Monitoring of elimination of disseminated cytokeratin-positive tumor cells in bone marrow *Clin Cancer Res* **1999**, *5*, 3999.

(167) Naundorf, S.; Preithner, S.; Mayer, P.; Lippold, S.; Wolf, A.; Hanakam, F.; Fichtner, I.; Kufer, P.; Raum, T.; Riethmuller, G.; Baeuerle, P. A.; Dreier, T. In vitro and in vivo activity of MT201, a fully human monoclonal antibody for pancarcinoma treatment *Int J Cancer* **2002**, *100*, 101.

(168) Hartung, G.; Hofheinz, R. D.; Dencausse, Y.; Sturm, J.; Kopp-Schneider, A.; Dietrich, G.; Fackler-Schwalbe, I.; Bornbusch, D.; Gonnermann, M.; Wojatschek, C.; Lindemann, W.; Eschenburg, H.; Jost, K.; Edler, L.; Hochhaus, A.; Queisser, W. Adjuvant therapy with edrecolomab versus observation in stage II colon cancer: A multicenter randomized phase III study *Onkologie* **2005**, *28*, 347.

(169) Schmidt, M.; Ruttinger, D.; Sebastian, M.; Hanusch, C. A.; Marschner, N.; Baeuerle, P. A.; Wolf, A.; Goppel, G.; Oruzio, D.; Schlimok, G.; Steger, G. G.; Wolf, C.; Eiermann, W.; Lang, A.; Schuler, M. Phase IB study of the EpCAM antibody adecatumumab combined with docetaxel in patients with EpCAM-positive relapsed or refractory advanced-stage breast cancer *Ann Oncol* **2012**, *23*, 2306.

(170) Gallatin, W. M.; Weissman, I. L.; Butcher, E. C. A Cell-Surface Molecule Involved in Organ-Specific Homing of Lymphocytes *Nature* **1983**, *304*, 30.
(171) Aruffo, A.; Stamenkovic, I.; Melnick, M.; Underhill, C. B.; Seed, B. CD44 is the principal cell-surface receptor for hyaluronate *Cell* **1990**, *61*, 1303.
(172) Stamenkovic, I.; Amiot, M.; Pesando, J. M.; Seed, B. A Lymphocyte Molecule Implicated in Lymph-Node Homing Is a Member of the Cartilage Link Protein Family *Cell* **1989**, *56*, 1057.
(173) Teriete, P.; Banerji, S.; Noble, M.; Blundell, C. D.; Wright, A. J.; Pickford, A. R.; Lowe, E.; Mahoney, D. J.; Tammi, M. I.; Kahmann, J. D.; Campbell, I. D.; Day, A. J.; Jackson, D. G. Structure of the regulatory hyaluronan binding domain in the inflammatory leukocyte homing receptor CD44 *Mol Cell* **2004**, *13*, 483.
(174) Nagano, O.; Saya, H. Mechanism and biological significance of CD44 cleavage *Cancer Sci* **2004**, *95*, 930.
(175) Vigetti, D.; Viola, M.; Karousou, E.; Rizzi, M.; Moretto, P.; Genasetti, A.; Clerici, M.; Hascall, V. C.; De Luca, G.; Passi, A. Hyaluronan-CD44-ERK1/2 regulate human aortic smooth muscle cell motility during aging *J Biol Chem* **2008**, *283*, 4448.
(176) Cheng, C. H.; Sharp, P. A. Regulation of CD44 alternative splicing by SRm160 and its potential role in tumor cell invasion *Mol Cell Biol* **2006**, *26*, 362.
(177) Peach, R. J.; Hollenbaugh, D.; Stamenkovic, I.; Aruffo, A. Identification of Hyaluronic-Acid Binding-Sites in the Extracellular Domain of Cd44 *J Cell Biol* **1993**, *122*, 257.
(178) Ishii, S.; Ford, R.; Thomas, P.; Nachman, A.; Steele, G.; Jessup, J. M. Cd44 Participates in the Adhesion of Human Colorectal-Carcinoma Cells to Laminin and Type-Iv Collagen *Surg Oncol* **1993**, *2*, 255.
(179) Jalkanen, S.; Jalkanen, M. Lymphocyte Cd44 Binds the Cooh-Terminal Heparin-Binding Domain of Fibronectin *J Cell Biol* **1992**, *116*, 817.
(180) Konstantopoulos, K.; Thomas, S. N. Cancer Cells in Transit: The Vascular Interactions of Tumor Cells *Annu Rev Biomed Eng* **2009**, *11*, 177.
(181) Toyamasorimachi, N.; Miyasaka, M. A Novel Ligand for Cd44 Is Sulfated Proteoglycan *Int Immunol* **1994**, *6*, 655.
(182) Liu, D. C.; Sy, M. S. Phorbol myristate acetate stimulates the dimerization of CD44 involving a cysteine in the transmembrane domain *J Immunol* **1997**, *159*, 2702.
(183) Oliferenko, S.; Paiha, K.; Harder, T.; Gerke, V.; Schwarzler, C.; Schwarz, H.; Beug, H.; Gunthert, U.; Huber, L. A. Analysis of CD44-containing lipid rafts: Recruitment of annexin II and stabilization by the actin cytoskeleton *J Cell Biol* **1999**, *146*, 843.
(184) Fehon, R. G.; McClatchey, A. I.; Bretscher, A. Organizing the cell cortex: the role of ERM proteins *Nat Rev Mol Cell Bio* **2010**, *11*, 276.
(185) Siegelman, M. H.; Stanescu, D.; Estess, P. The CD44-initiated pathway of T-cell extravasation uses VLA-4 but not LFA-1 for firm adhesion *J Clin Invest* **2000**, *105*, 683.
(186) Williams, D. A.; Cancelas, J. A. Leukaemia - Niche retreats for stem cells *Nature* **2006**, *444*, 827.

(187) Yang, J.; Weinberg, R. A. Epithelial-mesenchymal transition: At the crossroads of development and tumor metastasis *Developmental Cell* **2008**, *14*, 818.
(188) Toole, B. P. Hyaluronan: From extracellular glue to pericellular cue *Nat Rev Cancer* **2004**, *4*, 528.
(189) Lobo, N. A.; Shimono, Y.; Qian, D.; Clarke, M. F. The biology of cancer stem cells *Annu Rev Cell Dev Bi* **2007**, *23*, 675.
(190) Tallman, M. S. New strategies for the treatment of acute myeloid leukemia including antibodies and other novel agents *Hematology Am Soc Hematol Educ Program* **2005**, 143.
(191) Wilson, A.; Trumpp, A. Bone-marrow haematopoietic-stem-cell niches *Nat Rev Immunol* **2006**, *6*, 93.
(192) Lapidot, T.; Dar, A.; Kollet, O. How do stem cells find their way home? *Blood* **2005**, *106*, 1901.
(193) Marangoni, E.; Lecomte, N.; Durand, L.; de Pinieux, G.; Decaudin, D.; Chomienne, C.; Smadja-Joffe, F.; Poupon, M. F. CD44 targeting reduces tumour growth and prevents post-chemotherapy relapse of human breast cancers xenografts *Brit J cancer* **2009**, *100*, 918.
(194) Ulyanova, T.; Blasioli, J.; Woodford-Thomas, T. A.; Thomas, M. L. The sialoadhesin CD33 is a myeloid-specific inhibitory receptor *Eur J Immunol* **1999**, *29*, 3440.
(195) Taylor, V. C.; Buckley, C. D.; Douglas, M.; Cody, A. J.; Simmons, D. L.; Freeman, S. D. The myeloid-specific sialic acid-binding receptor, CD33, associates with the protein-tyrosine phosphatases, SHP-1 and SHP-2 *J Biol Chem* **1999**, *274*, 11505.
(196) Vitale, C.; Romagnani, C.; Puccetti, A.; Olive, D.; Costello, R.; Chiossone, L.; Pitto, A.; Bacigalupo, A.; Moretta, L.; Mingari, M. C. Surface expression and function of p75/AIRM-1 or CD33 in acute myeloid leukemias: Engagement of CD33 induces apoptosis of leukemic cells *P Natl Acad Sci USA* **2001**, *98*, 5764.
(197) Schwemmlein, M.; Peipp, M.; Barbin, K.; Saul, D.; Stockmeyer, B.; Repp, R.; Birkmann, J.; Oduncu, F.; Emmerich, B.; Fey, G. H. A CD33-specific single-chain immunotoxin mediates potent apoptosis of cultured human myeloid leukaemia cells *Brit J Haematol* **2006**, *133*, 141.
(198) Damle, N. K.; Frost, P. Antibody-targeted chemotherapy with immunoconjugates of calicheamicin *Current opinion in pharmacology* **2003**, *3*, 386.
(199) Hamann, P. R.; Hinman, L. M.; Hollander, I.; Beyer, C. F.; Lindh, D.; Holcomb, R.; Hallett, W.; Tsou, H. R.; Upeslacis, J.; Shochat, D.; Mountain, A.; Flowers, D. A.; Bernstein, I. Gemtuzumab ozogamicin, a potent and selective anti-CD33 antibody-calicheamicin conjugate for treatment of acute myeloid leukemia *Bioconjugate Chem* **2002**, *13*, 47.
(200) Hamann, P. R.; Hinman, L. M.; Beyer, C. F.; Lindh, D.; Upeslacis, J.; Flowers, D. A.; Bernstein, I. An anti-CD33 antibody-calicheamicin conjugate for treatment of acute myeloid leukemia. Choice of linker *Bioconjugate Chem* **2002**, *13*, 40.
(201) Linenberger, M. L. CD33-directed therapy with gemtuzumab ozogamicin in acute myeloid leukemia: progress in understanding cytotoxicity and potential mechanisms of drug resistance *Leukemia* **2005**, *19*, 176.

(202) http://www.fda.gov/Safety/MedWatch/SafetyInformation/SafetyAlertsforHumanMedicalProducts/ucm216458.htm.
(203) Walter, R. B.; Appelbaum, F. R.; Estey, E. H.; Bernstein, I. D. Acute myeloid leukemia stem cells and CD33-targeted immunotherapy *Blood* **2012**, *119*, 6198.
(204) Furness, S. G. B.; McNagny, K. Beyond mere markers - Functions for CD34 family of sialomucins in hematopoiesis *Immunol Res* **2006**, *34*, 13.
(205) Civin, C. I.; Strauss, L. C.; Brovall, C.; Fackler, M. J.; Schwartz, J. F.; Shaper, J. H. Antigenic Analysis of Hematopoiesis .3. A Hematopoietic Progenitor-Cell Surface-Antigen Defined by a Monoclonal-Antibody Raised against Kg-1a Cells *J Immunol* **1984**, *133*, 157.
(206) Berenson, R. J.; Andrews, R. G.; Bensinger, W. I.; Kalamasz, D.; Knitter, G.; Buckner, C. D.; Bernstein, I. D. Antigen Cd34+ Marrow-Cells Engraft Lethally Irradiated Baboons *J Clin Invest* **1988**, *81*, 951.
(207) Nielsen, J. S.; McNagny, K. M. Novel functions of the CD34 family *J Cell Sci* **2008**, *121*, 3683.
(208) Krause, D. S.; Fackler, M. J.; Civin, C. I.; May, W. S. CD34: Structure, biology, and clinical utility *Blood* **1996**, *87*, 1.
(209) Healy, L.; May, G.; Gale, K.; Grosveld, F.; Greaves, M.; Enver, T. The stem cell antigen CD34 functions as a regulator of hemopoietic cell adhesion *P Natl Acad Sci USA* **1995**, *92*, 12240.
(210) Baumhueter, S.; Singer, M. S.; Henzel, W.; Hemmerich, S.; Renz, M.; Rosen, S. D.; Lasky, L. A. Binding of L-Selectin to the Vascular Sialomucin Cd34 *Science* **1993**, *262*, 436.
(211) Krause, D. S.; Ito, T.; Fackler, M. J.; Smith, O. M.; Collector, M. I.; Sharkis, S. J.; May, W. S. Characterization of Murine Cd34, a Marker for Hematopoietic Progenitor and Stem-Cells *Blood* **1994**, *84*, 691.
(212) Tan, P. C.; Furness, S. G. B.; Merkens, H.; Lin, S. J.; McCoy, M. L.; Roskelley, C. D.; Kast, J.; McNagny, K. M. Na+/H+ exchanger regulatory factor-1 is a hematopoietic ligand for a subset of the CD34 family of stem cell surface proteins *Stem Cells* **2006**, *24*, 1150.
(213) Fackler, M. J.; Krause, D. S.; Smith, O. M.; Civin, C. I.; May, W. S. Full-Length but Not Truncated Cd34 Inhibits Hematopoietic-Cell Differentiation of M1 Cells *Blood* **1995**, *85*, 3040.
(214) Gangenahalli, G. U.; Singh, V. K.; Verma, Y. K.; Gupta, P.; Sharma, R. K.; Chandra, R.; Luthra, P. M. Hematopoietic stem cell antigen CD34: Role in adhesion or homing *Stem Cells Dev* **2006**, *15*, 305.
(215) Kawanobe, T.; Kogure, S.; Nakamura, S.; Sato, M.; Katayama, K.; Mitsuhashi, J.; Noguchi, K.; Sugimoto, Y. Expression of human ABCB5 confers resistance to taxanes and anthracyclines *Biochem Bioph Res Co* **2012**, *418*, 736.
(216) Frank, N. Y.; Margaryan, A.; Huang, Y.; Schatton, T.; Waaga-Gasser, A. M.; Gasser, M.; Sayegh, M. H.; Sadee, W.; Frank, M. H. ABCB5-mediated doxorubicin transport and chemoresistance in human malignant melanoma *Cancer Res* **2005**, *65*, 4320.
(217) Wickstrom, M.; Larsson, R.; Nygren, P.; Gullbo, J. Aminopeptidase N (CD13) as a target for cancer chemotherapy *Cancer Sci* **2011**, *102*, 501.

(218) Luan, Y. P.; Xu, W. F. The structure and main functions of aminopeptidase N *Curr Med Chem* **2007**, *14*, 639.
(219) Umezawa, H.; Aoyagi, T.; Suda, H.; Hamada, M.; Takeuchi, T. Bestatin, an Inhibitor of Aminopeptidase-B, Produced by Actinomycetes *J Antibiot* **1976**, *29*, 97.
(220) Talmadge, J. E.; Lenz, B. F.; Pennington, R.; Long, C.; Phillips, H.; Schneider, M.; Tribble, H. Immunomodulatory and Therapeutic Properties of Bestatin in Mice *Cancer Res* **1986**, *46*, 4505.
(221) Mathe, G. Bestatin, an Aminopeptidase Inhibitor with a Multi-Pharmacological Function *Biomed Pharmacother* **1991**, *45*, 49.
(222) Sekine, K.; Fujii, H.; Abe, F. Induction of apoptosis by bestatin (ubenimex) in human leukemic cell lines *Leukemia* **1999**, *13*, 729.
(223) Ezawa, K.; Minato, K.; Dobashi, K. Induction of apoptosis by ubenimex (Bestatin(R)) in human non-small-cell lung cancer cell lines *Biomed Pharmacother* **1996**, *50*, 283.
(224) Thunnissen, M. M. G. M.; Nordlund, P.; Haeggstrom, J. Z. Crystal structure of human leukotriene A(4) hydrolase, a bifunctional enzyme in inflammation *Nat Struct Biol* **2001**, *8*, 131.
(225) Tholander, F.; Rudberg, P.; Thunnissen, M.; Haeggstrom, J. Z. Leukotriene A4 hydrolase, the gatekeeper of chemotactic leukotriene B4 biosynthesis *Prostag Oth Lipid M* **2006**, *79*, 157.
(226) Fromm, J. R. Flow Cytometric Analysis of CD123 is Useful for Immunophenotyping Classical Hodgkin Lymphoma *Cytom Part B-Clin Cy* **2011**, *80B*, 91.
(227) Jin, L. Q.; Lee, E. M.; Ramshaw, H. S.; Busfield, S. J.; Peoppl, A. G.; Wilkinson, L.; Guthridge, M. A.; Thomas, D.; Barry, E. F.; Boyd, A.; Gearing, D. P.; Vairo, G.; Lopez, A. F.; Dick, J. E.; Lock, R. B. Monoclonal Antibody-Mediated Targeting of CD123, IL-3 Receptor alpha Chain, Eliminates Human Acute Myeloid Leukemic Stem Cells *Cell Stem Cell* **2009**, *5*, 31.
(228) Lindberg, F. P.; Gresham, H. D.; Schwarz, E.; Brown, E. J. Molecular-Cloning of Integrin-Associated Protein - an Immunoglobulin Family Member with Multiple Membrane-Spanning Domains Implicated in Alpha-Nu-Beta-3-Dependent Ligand-Binding *J Cell Biol* **1993**, *123*, 485.
(229) Brown, E. J.; Frazier, W. A. Integrin-associated protein (CD47) and its ligands *Trends Cell Biol* **2001**, *11*, 130.
(230) Hatherley, D.; Graham, S. C.; Turner, J.; Harlos, K.; Stuart, D. I.; Barclay, A. N. Paired receptor specificity explained by structures of signal regulatory proteins alone and complexed with CD47 *Mol Cell* **2008**, *31*, 266.
(231) Majeti, R. Monoclonal antibody therapy directed against human acute myeloid leukemia stem cells *Oncogene* **2011**, *30*, 1009.
(232) Ferlay, J.; Shin, H. R.; Bray, F.; Forman, D.; Mathers, C.; Parkin, D. M. Estimates of worldwide burden of cancer in 2008: GLOBOCAN 2008 *Int J Cancer* **2010**, *127*, 2893.
(233) Minino, A. M.; Murphy, S. L.; Xu, J.; Kochanek, K. D. Deaths: final data for 2008 *National vital statistics reports : from the Centers for Disease Control and*

Prevention, National Center for Health Statistics, National Vital Statistics System **2011**, *59*, 1.
(234) Gupta, P. B.; Fillmore, C. M.; Jiang, G. Z.; Shapira, S. D.; Tao, K.; Kuperwasser, C.; Lander, E. S. Stochastic State Transitions Give Rise to Phenotypic Equilibrium in Populations of Cancer Cells (vol 146, pg 633, 2011) *Cell* **2011**, *147*, 1197.
(235) Nguyen, L. V.; Vanner, R.; Dirks, P.; Eaves, C. J. Cancer stem cells: an evolving concept *Nat Rev Cancer* **2012**, *12*, 133.
(236) Keating, M. J.; Mccredie, K. B.; Bodey, G. P.; Smith, T. L.; Gehan, E.; Freireich, E. J. Improved Prospects for Long-Term Survival in Adults with Acute Myelogenous Leukemia *Jama-J Am Med Assoc* **1982**, *248*, 2481.
(237) Lessard, J.; Sauvageau, G. Bmi-1 determines the proliferative capacity of normal and leukaemic stem cells *Nature* **2003**, *423*, 255.
(238) Yilmaz, O. H.; Valdez, R.; Theisen, B. K.; Guo, W.; Ferguson, D. O.; Wu, H.; Morrison, S. J. Pten dependence distinguishes haematopoietic stem cells from leukaemia-initiating cells *Nature* **2006**, *441*, 475.
(239) Guan, Y. H.; Gerhard, B.; Hogge, D. E. Detection, isolation, and stimulation of quiescent primitive leukemic progenitor cells from patients with acute myeloid leukemia (AML) *Blood* **2003**, *101*, 3142.
(240) Guzman, M. L.; Neering, S. J.; Upchurch, D.; Grimes, B.; Howard, D. S.; Rizzieri, D. A.; Luger, S. M.; Jordan, C. T. Nuclear factor-kappa B is constitutively activated in primitive human acute myelogenous leukemia cells *Blood* **2001**, *98*, 2301.
(241) Guzman, M. L.; Swiderski, C. F.; Howard, D. S.; Grimes, B. A.; Rossi, R. M.; Szilvassy, S. J.; Jordan, C. T. Preferential induction of apoptosis for primary human leukemic stem cells *P Natl Acad Sci USA* **2002**, *99*, 16220.
(242) Wang, C. Y.; Mayo, M. W.; Baldwin, A. S. TNF- and cancer therapy-induced apoptosis: Potentiation by inhibition of NF-kappa B *Science* **1996**, *274*, 784.
(243) Wang, C. Y.; Mayo, M. W.; Korneluk, R. G.; Goeddel, D. V.; Baldwin, A. S. NF-kappa B antiapoptosis: Induction of TRAF1 and TRAF2 and c-IAP1 and c-IAP2 to suppress caspase-8 activation *Science* **1998**, *281*, 1680.
(244) Sen, R.; Baltimore, D. Multiple nuclear factors interact with the immunoglobulin enhancer sequences *Cell* **1986**, *46*, 705.
(245) Hayden, M. S.; Ghosh, S. Shared principles in NF-kappa B signaling *Cell* **2008**, *132*, 344.
(246) Naugler, W. E.; Karin, M. NF-kappa B and cancer - identifying targets and mechanisms *Current Opinion in Genetics & Development* **2008**, *18*, 19.
(247) Karin, M.; Yamamoto, Y.; Wang, Q. M. The IKKNF-kappa B system: A treasure trove for drug development *Nat Rev Drug Discov* **2004**, *3*, 17.
(248) Tergaonkar, V.; Correa, R. G.; Ikawa, M.; Verma, I. M. Distinct roles of I kappa B proteins in regulating constitutive NF-kappa B activity *Nature Cell Biology* **2005**, *7*, 921.
(249) Dey, A.; Tergaonkar, V.; Lane, D. P. Double-edged swords as cancer therapeutics: simultaneously targeting p53 and NF-kappa B pathways *Nat Rev Drug Discov* **2008**, *7*, 1031.
(250) Aggarwal, B. B. Nuclear factor-kappa-B: The enemy within *Cancer Cell* **2004**, *6*, 203.

(251) Heinrich, M.; Ankli, A.; Frei, B.; Weimann, C.; Sticher, O. Medicinal plants in Mexico: healers' consensus and cultural importance *Soc Sci Med* **1998**, *47*, 1859.
(252) Hall, I. H.; Lee, K. H.; Starnes, C. O.; Sumida, Y.; Wu, R. Y.; Waddell, T. G.; Cochran, J. W.; Gerhart, K. G. Anti-Inflammatory Activity of Sesquiterpene Lactones and Related Compounds *J Pharm Sci* **1979**, *68*, 537.
(253) Heinrich, M.; Robles, M.; West, J. E.; de Montellano, B. R. O.; Rodriguez, E. Ethnopharmacology of Mexican asteraceae (compositae) *Annu Rev Pharmacol* **1998**, *38*, 539.
(254) Anderson, K. N.; Bejcek, B. E. Parthenolide induces apoptosis in glioblastomas without affecting NF-kappa B *Journal of Pharmacological Sciences* **2008**, *106*, 318.
(255) Sweeney, C.; Li, L.; Shanmugam, R.; Bhat-Nakshatri, P.; Jayaprakasan, V.; Baldridge, L. A.; Gardner, T.; Smith, M.; Nakshatri, H.; Cheng, L. Nuclear factor-kappa B is constitutively activated in prostate cancer in vitro and is overexpressed in prostatic intraepithelial neoplasia and adenocarcinoma of the prostate *Clin Cancer Res* **2004**, *10*, 5501.
(256) Shanmugam, R.; Jayaprakasan, V.; Gokmen-Polar, Y.; Kelich, S.; Miller, K. D.; Yip-Schneider, M.; Cheng, L.; Bhat-Nakshatri, P.; Sledge, G. W.; Nakshatri, H.; Zheng, Q. H.; Miller, M. A.; DeGrado, T.; Hutchins, G. D.; Sweeney, C. J. Restoring chemotherapy and hormone therapy sensitivity by parthenolide in a xenograft hormone refractory prostate cancer model *Prostate* **2006**, *66*, 1498.
(257) Nakshatri, H.; Rice, S. E.; Bhat-Nakshatri, P. Antitumor agent parthenolide reverses resistance of breast cancer cells to tumor necrosis factor-related apoptosis-inducing ligand through sustained activation of c-Jun N-terminal kinase *Oncogene* **2004**, *23*, 7330.
(258) Sweeney, C. J.; Mehrotra, S.; Sadaria, M. R.; Kumar, S.; Shortle, N. H.; Roman, Y.; Sheridan, C.; Campbell, R. A.; Murry, D. J.; Badve, S.; Nakshatri, H. The sesquiterpene lactone parthenolide in combination with docetaxel reduces metastasis and improves survival in a xenograft model of breast cancer *Molecular Cancer Therapeutics* **2005**, *4*, 1004.
(259) Steele, A. J.; Jones, D. T.; Ganeshaguru, K.; Duke, V. M.; Yogashangary, B. C.; North, J. M.; Lowdell, M. W.; Kottaridis, P. D.; Mehta, A. B.; Prentice, A. G.; Hoffbrand, A. V.; Wickremasinghe, R. G. The sesquiterpene lactone parthenolide induces selective apoptosis of B-chronic lymphocytic leukemia cells in vitro *Leukemia* **2006**, *20*, 1073.
(260) Ramachandran, P. V.; Pratihar, D.; Nair, H. N. G.; Walters, M.; Smith, S.; Yip-Schneider, M. T.; Wu, H. B.; Schmidt, C. M. Tailored alpha-methylene-gamma-butyrolactones and their effects on growth suppression in pancreatic carcinoma cells *Bioorganic & Medicinal Chemistry Letters*, *20*, 6620.
(261) Zhou, J. B.; Zhang, H.; Gu, P. H.; Bai, J. N.; Margolick, J. B.; Zhang, Y. NF-kappa B pathway inhibitors preferentially inhibit breast cancer stem-like cells *Breast Cancer Research and Treatment* **2008**, *111*, 419.
(262) Kawasaki, B. T.; Hurt, E. M.; Kalathur, M.; Duhagon, M. A.; Milner, J. A.; Kim, Y. S.; Farrar, W. L. Effects of the Sesquiterpene Lactone Parthenolide on Prostate Tumor-Initiating Cells: An Integrated Molecular Profiling Approach *Prostate* **2009**, *69*, 827.

(263) Neelakantan, S.; Nasim, S.; Guzman, M. L.; Jordan, C. T.; Crooks, P. A. Aminoparthenolides as novel anti-leukemic agents: Discovery of the NF-kappa B inhibitor, DMAPT (LC-1) *Bioorganic & Medicinal Chemistry Letters* **2009**, *19*, 4346.
(264) Kwok, B. H. B.; Koh, B.; Ndubuisi, M. I.; Elofsson, M.; Crews, C. M. The anti-inflammatory natural product parthenolide from the medicinal herb Feverfew directly binds to and inhibits I kappa B kinase *Chem Biol* **2001**, *8*, 759.
(265) Garcia-Pineres, A. J.; Castro, V.; Mora, G.; Schmidt, T. J.; Strunck, E.; Pahl, H. L.; Merfort, I. Cysteine 38 in p65/NF-kappa B plays a crucial role in DNA binding inhibition by sesquiterpene lactones *J Biol Chem* **2001**, *276*, 39713.
(266) Nasim, S.; Pei, S. S.; Hagen, F. K.; Jordan, C. T.; Crooks, P. A. Melampomagnolide B: A new antileukemic sesquiterpene *Bioorgan Med Chem* **2011**, *19*, 1515.
(267) Gopal, Y. V.; Arora, T. S.; Van Dyke, M. W. Parthenolide specifically depletes histone deacetylase 1 protein and induces cell death through ataxia telangiectasia mutated *Chem Biol* **2007**, *14*, 813.
(268) Garcia-Pineres, A. J.; Lindenmeyer, M. T.; Merfort, I. Role of cysteine residues of p65/NF-kappa B on the inhibition by the sesquiterpene lactone parthenolide and-N-ethyl maleimide, and on its transactivating potential *Life Sciences* **2004**, *75*, 841.
(269) Skalska, J.; Brookes, P. S.; Nadtochiy, S. M.; Hilchey, S. P.; Jordan, C. T.; Guzman, M. L.; Maggirwar, S. B.; Briehl, M. M.; Bernstein, S. H. Modulation of Cell Surface Protein Free Thiols: A Potential Novel Mechanism of Action of the Sesquiterpene Lactone Parthenolide *Plos One* **2009**, *4*.
(270) Pei, S. S.; Guzman, M. L.; Nasim, S.; Shi, L.; Crooks, P. A.; Jordan, C. T. In *American Society of Hematology Conference Abstract 2734* 2009; Vol. 114.
(271) Zhang, S. Y.; Ong, C. N.; Shen, H. M. Involvement of proapoptotic Bcl-2 family members in parthenolide-induced mitochondrial dysfunction and apoptosis *Cancer Lett* **2004**, *211*, 175.
(272) Kolb, H. C.; Finn, M. G.; Sharpless, K. B. Click chemistry: Diverse chemical function from a few good reactions *Angew Chem Int Edit* **2001**, *40*, 2004.
(273) Best, M. D. Click Chemistry and Bioorthogonal Reactions: Unprecedented Selectivity in the Labeling of Biological Molecules *Biochemistry-Us* **2009**, *48*, 6571.
(274) Cravatt, B. F. Activity-based protein profiling: Chemical approaches for functional proteomics. *Abstr Pap Am Chem S* **2002**, *224*, U155.
(275) von Rechenberg, M.; Blake, B. K.; Ho, Y. S. J.; Zhen, Y. J.; Chepanoske, C. L.; Richardson, B. E.; Xu, N. F.; Kery, V. Ampicillin/penicillin-binding protein interactions as a model drug-target system to optimize affinity pull-down and mass spectrometric strategies for target and pathway identification *Proteomics* **2005**, *5*, 1764.
(276) Kool, J.; Jonker, N.; Irth, H.; Niessen, W. M. A. Studying protein-protein affinity and immobilized ligand-protein affinity interactions using MS-based methods *Anal Bioanal Chem* **2011**, *401*, 1109.
(277) Neukirch, H.; Kaneider, N. C.; Wiedermann, C. J.; Guerriero, A.; D'Ambrosio, M. Parthenolide and its photochemically synthesized 1(10)Z isomer: Chemical

reactivity and structure-activity relationship studies in human leucocyte chemotaxis *Bioorgan Med Chem* **2003**, *11*, 1503.
(278) Hwang, D. R.; Chang, C. W.; Lien, T. W.; Chen, W. C.; Tan, U. K.; Hsu, J. T. A.; Hsieh, H. P. Synthesis and anti-viral activity of a series of sesquiterpene lactones and analogues in the subgenomic HCV replicon system *Bioorgan Med Chem* **2006**, *14*, 83.
(279) El-Feraly, F. S. Melampolides from Magnolia Grandiflora *Phytochemistry* **1984**, *23*, 2372.
(280) Mitsunobu, O. The Use of Diethyl Azodicarboxylate and Triphenylphosphine in Synthesis and Transformation of Natural-Products *Synthesis-Stuttgart* **1981**, 1.
(281) Adam, G. C.; Sorensen, E. J.; Cravatt, B. F. Trifunctional chemical probes for the consolidated detection and identification of enzyme activities from complex proteomes *Mol Cell Proteomics* **2002**, *1*, 828.
(282) Takeyama, M.; Otaka, A.; Fujii, N. Enzyme-Immunoassay of Thyrotropin-Releasing-Hormone (Trh) *Chem Pharm Bull* **1992**, *40*, 2199.
(283) Yeo, D. S. Y.; Srinivasan, R.; Uttamchandani, M.; Chen, G. Y. J.; Zhu, Q.; Yao, S. Q. Cell-permeable small molecule probes for site-specific labeling of proteins *Chem Commun* **2003**, 2870.
(284) Speers, A. E.; Cravatt, B. F. Profiling enzyme activities in vivo using click chemistry methods *Chem Biol* **2004**, *11*, 535.
(285) Green, N. M. Avidin and Streptavidin *Method Enzymol* **1990**, *184*, 51.
(286) Rybak, J. N.; Scheurer, S. B.; Neri, D.; Elia, G. Purification of biotinylated proteins on streptavidin resin: A protocol for quantitative elution *Proteomics* **2004**, *4*, 2296.
(287) Jin, P.; Madieh, S.; Augsburger, L. L. The Solution and Solid State Stability and Excipient Compatibility of Parthenolide in Feverfew *Aaps Pharmscitech* **2007**, *8*.
(288) Wu, S. C.; Wong, S. L. Engineering soluble monomeric streptavidin with reversible biotin binding capability *J Biol Chem* **2005**, *280*, 23225.
(289) Lim, K. H.; Huang, H.; Pralle, A.; Park, S. Engineered Streptavidin Monomer and Dimer with Improved Stability and Function *Biochemistry-Us* **2011**, *50*, 8682.
(290) Kim, J.; Lee, J. E.; Heynen-Genel, S.; Suyama, E.; Ono, K.; Lee, K.; Ideker, T.; Aza-Blanc, P.; Gleeson, J. G. Functional genomic screen for modulators of ciliogenesis and cilium length *Nature* **2010**, *464*, 1048.
(291) Haltia, M.; Prelli, F.; Ghiso, J.; Kiuru, S.; Somer, H.; Palo, J.; Frangione, B. Amyloid Protein in Familial Amyloidosis (Finnish Type) Is Homologous to Gelsolin, an Actin-Binding Protein *Biochem Bioph Res Co* **1990**, *167*, 927.
(292) Sjoblom, T.; Jones, S.; Wood, L. D.; Parsons, D. W.; Lin, J.; Barber, T. D.; Mandelker, D.; Leary, R. J.; Ptak, J.; Silliman, N.; Szabo, S.; Buckhaults, P.; Farrell, C.; Meeh, P.; Markowitz, S. D.; Willis, J.; Dawson, D.; Willson, J. K. V.; Gazdar, A. F.; Hartigan, J.; Wu, L.; Liu, C. S.; Parmigiani, G.; Park, B. H.; Bachman, K. E.; Papadopoulos, N.; Vogelstein, B.; Kinzler, K. W.; Velculescu, V. E. The consensus coding sequences of human breast and colorectal cancers *Science* **2006**, *314*, 268.
(293) Maury, C. P. J.; Alli, K.; Baumann, M. Finnish Hereditary Amyloidosis - Amino-Acid-Sequence Homology between the Amyloid Fibril Protein and Human Plasma Gelsoline *Febs Lett* **1990**, *260*, 85.

(294) Kwiatkowski, D. J.; Stossel, T. P.; Orkin, S. H.; Mole, J. E.; Colten, H. R.; Yin, H. L. Plasma and Cytoplasmic Gelsolins Are Encoded by a Single Gene and Contain a Duplicated Actin-Binding Domain *Nature* **1986**, *323*, 455.
(295) Sumara, I.; Vorlaufer, E.; Gieffers, C.; Peters, B. H.; Peters, J. M. Characterization of vertebrate cohesin complexes and their regulation in prophase *J Cell Biol* **2000**, *151*, 749.
(296) Terret, M. E.; Sherwood, R.; Rahman, S.; Qin, J.; Jallepalli, P. V. Cohesin acetylation speeds the replication fork *Nature* **2009**, *462*, 231.
(297) Revenkova, E.; Focarelli, M. L.; Susani, L.; Paulis, M.; Bassi, M. T.; Mannini, L.; Frattini, A.; Delia, D.; Krantz, I.; Vezzoni, P.; Jessberger, R.; Musio, A. Cornelia de Lange syndrome mutations in SMC1A or SMC3 affect binding to DNA *Hum Mol Genet* **2009**, *18*, 418.
(298) Bai, S. W.; Herrera-Abreu, M. T.; Rohn, J. L.; Racine, V.; Tajadura, V.; Suryavanshi, N.; Bechtel, S.; Wiemann, S.; Baum, B.; Ridley, A. J. Identification and characterization of a set of conserved and new regulators of cytoskeletal organization, cell morphology and migration *Bmc Biol* **2011**, *9*.
(299) Rigbolt, K. T. G.; Prokhorova, T. A.; Akimov, V.; Henningsen, J.; Johansen, P. T.; Kratchmarova, I.; Kassem, M.; Mann, M.; Olsen, J. V.; Blagoev, B. System-Wide Temporal Characterization of the Proteome and Phosphoproteome of Human Embryonic Stem Cell Differentiation *Sci Signal* **2011**, *4*.
(300) Waragai, M.; Nagamitsu, S.; Xu, W. D.; Li, Y. J.; Lin, X.; Ashizawa, T. Ataxin 10 induces neuritogenesis via interaction with G-protein beta 2 subunit *J Neurosci Res* **2006**, *83*, 1170.
(301) Yang, J.; Everett, A. D. Hepatoma derived growth factor binds DNA through the N-terminal PWWP domain *Bmc Mol Biol* **2007**, *8*.
(302) Chen, S. C.; Kung, M. L.; Hu, T. H.; Chen, H. Y.; Wu, J. C.; Kuo, H. M.; Tsai, H. E.; Lin, Y. W.; Wen, Z. H.; Liu, J. K.; Yeh, M. H.; Tai, M. H. Hepatoma-derived growth factor regulates breast cancer cell invasion by modulating epithelial-mesenchymal transition *J Pathol* **2012**, *228*, 158.
(303) Markovtsov, V.; Nikolic, J. M.; Goldman, J. A.; Turck, C. W.; Chou, M. Y.; Black, D. L. Cooperative assembly of an hnRNP complex induced by a tissue-specific homolog of polypyrimidine tract binding protein *Mol Cell Biol* **2000**, *20*, 7463.
(304) Paul, S.; Dansithong, W.; Kim, D.; Rossi, J.; Webster, N. J. G.; Comai, L.; Reddy, S. Interaction of musleblind, CUG-BP1 and hnRNP H proteins in DM1-associated aberrant IR splicing *Embo J* **2006**, *25*, 4271.
(305) Mccormack, K.; Mccormack, T.; Tanouye, M.; Rudy, B.; Stuhmer, W. Alternative Splicing of the Human Shaker K+ Channel Beta-1 Gene and Functional Expression of the Beta-2 Gene-Product *Febs Lett* **1995**, *370*, 32.
(306) Jurica, M. S.; Licklider, L. J.; Gygi, S. P.; Grigorieff, N.; Moore, M. J. Purification and characterization of native spliceosomes suitable for three-dimensional structural analysis *Rna* **2002**, *8*, 426.
(307) Gazda, H. T.; Sheen, M. R.; Vlachos, A.; Choesmel, V.; O'Donohue, M. F.; Schneider, H.; Darras, N.; Hasman, C.; Sieff, C. A.; Newburger, P. E.; Ball, S. E.; Niewiadomska, E.; Matysiak, M.; Zaucha, J. M.; Glader, B.; Niemeyer, C.; Meerpohl, J. J.; Atsidaftos, E.; Lipton, J. M.; Gleizes, P. E.; Beggs, A. H.

Ribosomal Protein L5 and L11 Mutations Are Associated with Cleft Palate and Abnormal Thumbs in Diamond-Blackfan Anemia Patients *Am J Hum Genet* **2008**, *83*, 769.

(308) Glansdorp, F. G.; Spandl, R. J.; Swatton, J. E.; Loiseleur, O.; Welch, M.; Spring, D. R. Using chemical probes to investigate the sub-inhibitory effects of azithromycin *Org Biomol Chem* **2008**, *6*, 4120.

(309) Reddy, D. M.; Qazi, N. A.; Sawant, S. D.; Bandey, A. H.; Srinivas, J.; Shankar, M.; Singh, S. K.; Verma, M.; Chashoo, G.; Saxena, A.; Mondhe, D.; Saxena, A. K.; Sethi, V. K.; Taneja, S. C.; Qazi, G. N.; Sampath Kumar, H. M. Design and synthesis of spiro derivatives of parthenin as novel anti-cancer agents *Eur. J. Med. Chem.* **2011**, *46*, 3210.

(310) Curry, E. A.; Murry, D. J.; Yoder, C.; Fife, K.; Armstrong, V.; Nakshatri, H.; O'Connell, M.; Sweeney, C. J. Phase I dose escalation trial of feverfew with standardized doses of parthenolide in patients with cancer *Investigational New Drugs* **2004**, *22*, 299.

(311) Guzman, M. L.; Rossi, R. M.; Neelakantan, S.; Li, X.; Corbett, C. A.; Hassane, D. C.; Becker, M. W.; Bennett, J. M.; Sullivan, E.; Lachowicz, J. L.; Vaughan, A.; Sweeney, C. J.; Matthews, W.; Carroll, M.; Liesveld, J. L.; Crooks, P. A.; Jordan, C. T. An orally bioavailable parthenolide analog selectively eradicates acute myelogenous leukemia stem and progenitor cells *Blood* **2007**, *110*, 4427.

(312) Lundh, K.; Hindsen, M.; Gruvberger, B.; Moller, H.; Svensson, A.; Bruze, M. Contact allergy to herbal teas derived from Asteraceae plants *Contact Dermatitis* **2006**, *54*, 196.

(313) Scudiero, D. A.; Monks, A.; Sausville, E. A. Cell line designation change: Multidrug-resistant cell line in the NCI anticancer screen *J Natl Cancer I* **1998**, *90*, 862.

(314) Simmons, H. E.; Smith, R. D. A new synthesis of cyclopropanes from olefins *J Am Chem Soc* **1958**, *80*, 5323.

(315) Vuligonda, V.; Lin, Y.; Chandraratna, R. A. S. Synthesis of highly potent RXR-specific retinoids: The use of a cyclopropyl group as a double bond isostere *Bioorganic & Medicinal Chemistry Letters* **1996**, *6*, 213.

(316) Johnson, J.; Kim, S. H.; Bifano, M.; DiMarco, J.; Fairchild, C.; Gougoutas, J.; Lee, F.; Long, B.; Tokarski, J.; Vite, G. Synthesis, structure proof, and biological activity of epothilone cyclopropanes *Organic Letters* **2000**, *2*, 1537.

(317) Nicolaou, K. C.; Namoto, K.; Ritzen, A.; Ulven, T.; Shoji, M.; Li, J.; D'Amico, G.; Liotta, D.; French, C. T.; Wartmann, M.; Altmann, K. H.; Giannakakou, P. Chemical synthesis and biological evaluation of cis- and trans-12,13-cyclopropyl and 12,13-cyclobutyl epothilones and related pyridine side chain analogues *J Am Chem Soc* **2001**, *123*, 9313.

(318) Schiess, R.; Gertsch, J.; Schweizer, W. B.; Altmann, K. H. Stereoselective Synthesis of 12,13-Cyclopropyl-Epothilone B and Side-Chain-Modified Variants *Organic Letters* **2011**, *13*, 1436.

(319) Largaespada, D. A.; Shaughnessy, J. D.; Jenkins, N. A.; Copeland, N. G. Retroviral integration at the evi-2 locus in BXH-2 myeloid-leukemia cell-lines disruptes NF1 expression without changes in steady-state RAS-GTP levels *Journal of Virology* **1995**, *69*, 5095.

(320) Yin, B.; Kogan, S. C.; Dickins, R. A.; Lowe, S. W.; Largaespada, D. A. Trp53 loss during in vitro selection contributes to acquired Ara-C resistance in acute myeloid leukemia *Exp Hematol* **2006**, *34*, 631.
(321) Pardridge, W. M. The blood-brain barrier: bottleneck in brain drug development *NeuroRx : the journal of the American Society for Experimental NeuroTherapeutics* **2005**, *2*, 3.
(322) Zhang, Q.; Lu, Y.; Ding, Y.; Zhai, J.; Ji, Q.; Ma, W.; Yang, M.; Fan, H.; Long, J.; Tong, Z.; Shi, Y.; Jia, Y.; Han, B.; Zhang, W.; Qiu, C.; Ma, X.; Li, Q.; Shi, Q.; Zhang, H.; Li, D.; Zhang, J.; Lin, J.; Li, L. Y.; Gao, Y.; Chen, Y. Guaianolide sesquiterpene lactones, a source to discover agents that selectively inhibit acute myelogenous leukemia stem and progenitor cells *J Med Chem* **2012**, *55*, 8757.
(323) Imoto, S.; Patro, J. N.; Jiang, Y. L.; Oka, N.; Greenberg, M. M. Synthesis, DNA polymerase incorporation, and enzymatic phosphate hydrolysis of formamidopyrimidine nucleoside triphosphates *J Am Chem Soc* **2006**, *128*, 14606.
(324) Castanedaacosta, J.; Fischer, N. H.; Vargas, D. Biomimetic transformation of parthenolide *J Nat Prod* **1993**, *56*, 90.
(325) Neukirch, H.; Guerriero, A.; D'Ambrosio, M. Transannular cyclization in cyclodecenes: The case study of melampolides *Eur J Org Chem* **2003**, 3969.
(326) Zhai, J. D.; Li, D. M.; Long, J.; Zhang, H. L.; Lin, J. P.; Qiu, C. J.; Zhang, Q.; Chen, Y. Biomimetic Semisynthesis of Arglabin from Parthenolide *J Org Chem* **2012**, *77*, 7103.

Appendix A X-Ray Crystallography Data for Cycprypyl PTL (4)

A.1 General Experimentle

A crystal (approximate dimensions 0.45x 0.40 x 0.05mm^3) was placed onto the tip of a 0.1 mm diameter glass capillary and mounted on a CCD area detector diffractometer for a data collection at 123(2) K. A preliminary set of cell constants was calculated from reflections harvested from three sets of 20 frames. These initial sets of frames were oriented such that orthogonal wedges of reciprocal space were surveyed. This produced initial orientation matrices determined from 61 reflections. The data collection was carried out using MoK radiation (graphite monochromator) with a frame time of 60 seconds and a detector distance of 4.8 cm. A randomly oriented region of reciprocal space was surveyed to the extent of one sphere and to a resolution of 0.77 Å. Four major sections of frames were collected with 0.30º steps in at four different settings and a detector position of -28º in2 . The intensity data were corrected for absorption and decay (SADABS). Final cell constants were calculated from 2944 strong reflections from the actual data collection after integration.

The structure was solved using Bruker SHELXTL4 and refined using Bruker SHELXTL. The space group $P2_1$ was determined based on systematic absences and intensity statistics. A direct-methods solution was calculated which provided most non-hydrogen atoms from the E-map. Full-matrix least squares / difference Fourier cycles were performed which located the remaining non-hydrogen atoms. All non-hydrogen atoms were refined with anisotropic displacement parameters. All hydrogen atoms were placed in ideal positions and refined as riding atoms with relative isotropic displacement

parameters. The final full matrix least squares refinement converged to $R1 = 0.0496$ and $wR2 = 0.1335$ ($F2$, all data).

There are two identical, unique molecules per asymmetric unit with $Z'=2$. The chirality is as follows: C4-R, C5-R, C6-S, and C7-S. The CheckCIF program made no assignment at C1 due to its geometry, but this appears to be R. There is only slight pseudo-symmetry between the two unique molecules resulting in a pseudo 2_1 relationship along an irrational axis in the monoclinic setting. Data collection and structure solution were conducted at the X-Ray Crystallographic Laboratory, 192 Kolthoff Hall, Department of Chemistry, UMN. All calculations were performed using Pentium computers using the current SHELXTL suite of programs.

A.2 Thermal Ellipsoid Drawing of 4

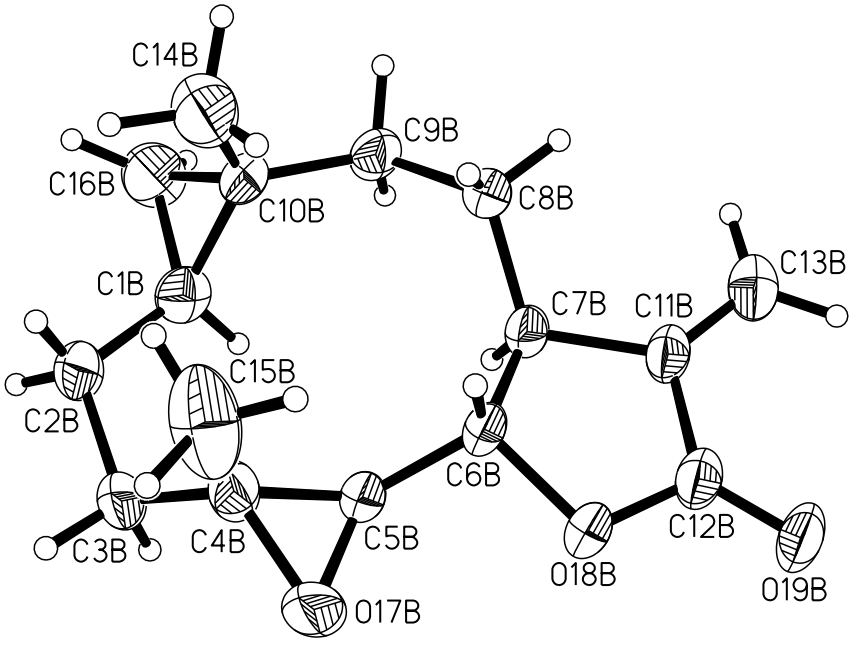

A.3 Crystallographic Information

Table 1. Crystal data and structure refinement for **4**.

Empirical formula	$C_{16}H_{22}O_3$	
Formula weight	262.34	
Temperature	123(2) K	
Wavelength	0.71073 Å	
Crystal system	Monoclinic	
Space group	$P2_1$	
Unit cell dimensions	a = 11.106(2) Å	= 90°
	b = 7.9397(16) Å	= 104.024(2)°
	c = 16.668(3) Å	= 90°
Volume	1426.0(5) $Å^3$	
Z	4	
Density (calculated)	1.222 Mg/m^3	
Absorption coefficient	0.083 mm^{-1}	
F(000)	568	
Crystal color, morphology	Colorless, Plate	
Crystal size	0.45 x 0.40 x 0.05 mm^3	
Theta range for data collection	1.26 to 27.47 °	
Index ranges	$-14 \le h \le 13, 0 \le k \le 10, 0 \le l \le 21$	
Reflections collected	12785	
Independent reflections	3465 [R(int) = 0.0291]	
Observed reflections	3001	
Completeness to theta = 27.47 °	98.9%	
Absorption correction	Mulit-scan	
Max. and min. transmission	0.9959 and 0.9637	
Refinement method	Full-matrix least-squares on F^2	
Data / restraints / parameters	3465 / 1 / 347	
Goodness-of-fit on F^2	1.046	
Final R indices [I>2sigma(I)]	$R1$ = 0.0496, $wR2$ = 0.1256	
R indices (all data)	$R1$ = 0.0599, $wR2$ = 0.1335	
Absolute structure parameter	0.1(15)	
Largest diff. peak and hole	0.621 and -0.368 e.$Å^{-3}$	

Table 2. Atomic coordinates($x\ 10^4$) and equivalent isotropic displacement parameters ($Å^2 x\ 10^3$). U_{eq} is defined as one third of the trace of the orthogonalized U_{ij} tensor.

	x	y	z	U_{eq}
C1A	8313(3)	687(4)	520(2)	31(1)
C2A	8620(3)	1643(5)	-194(2)	38(1)
C3A	7538(3)	2720(5)	-688(2)	35(1)
C4A	6994(3)	3875(4)	-157(2)	31(1)
C5A	5932(2)	3222(4)	137(2)	29(1)
C6A	5669(2)	3698(4)	947(2)	29(1)
C7A	6002(2)	2262(4)	1579(2)	29(1)
C8A	7322(3)	2326(5)	2160(2)	42(1)
C9A	8141(3)	814(5)	2062(2)	39(1)
C10A	8911(2)	1022(4)	1428(2)	32(1)
C11A	4927(3)	2308(4)	1983(2)	31(1)
C12A	3916(3)	3269(5)	1432(2)	37(1)
C13A	4790(4)	1644(5)	2679(2)	44(1)
C14A	9949(3)	2292(5)	1687(2)	48(1)
C15A	7819(3)	5283(4)	271(2)	40(1)
C16A	9237(3)	-539(5)	1021(2)	40(1)
O17A	5732(2)	4447(3)	-522(1)	39(1)
O18A	4329(2)	3954(3)	809(1)	37(1)
O19A	2862(2)	3477(4)	1489(2)	55(1)
C1B	713(3)	5269(5)	3394(2)	37(1)
C2B	395(3)	4385(5)	4116(2)	43(1)
C3B	1423(3)	3229(5)	4589(2)	45(1)
C4B	2643(3)	4147(5)	4866(2)	45(1)
C5B	3465(3)	4052(4)	4296(2)	41(1)
C6B	4357(3)	5391(4)	4187(2)	36(1)
C7B	4056(3)	6167(4)	3317(2)	34(1)
C8B	3290(3)	7798(4)	3200(2)	44(1)
C9B	1898(3)	7615(5)	2807(2)	39(1)
C10B	1037(3)	7116(4)	3346(2)	36(1)
C11B	5342(3)	6323(4)	3156(2)	34(1)
C12B	6199(3)	5248(4)	3765(2)	37(1)

C13B	5715(3)	7165(5)	2578(2)	43(1)
C14B	1028(5)	8333(6)	4018(3)	66(1)
C15B	2688(4)	5548(9)	5485(2)	73(2)
C16B	-212(3)	6446(6)	2883(3)	63(1)
O17B	3732(2)	3103(4)	5061(2)	78(1)
O18B	5573(2)	4563(3)	4291(2)	41(1)
O19B	7271(2)	4924(3)	3817(2)	48(1)

Table 3. Bond lengths [Å].

C(1A)-C(16A)	1.512(4)
C(1A)-C(2A)	1.518(4)
C(1A)-C(10A)	1.522(4)
C(1A)-H(1AA)	1.0000
C(2A)-C(3A)	1.541(4)
C(2A)-H(2AA)	0.9900
C(2A)-H(2AB)	0.9900
C(3A)-C(4A)	1.498(4)
C(3A)-H(3AA)	0.9900
C(3A)-H(3AB)	0.9900
C(4A)-O(17A)	1.459(3)
C(4A)-C(5A)	1.476(4)
C(4A)-C(15A)	1.511(4)
C(5A)-O(17A)	1.443(4)
C(5A)-C(6A)	1.497(4)
C(5A)-H(5AA)	1.0000
C(6A)-O(18A)	1.465(3)
C(6A)-C(7A)	1.536(4)
C(6A)-H(6AA)	1.0000
C(7A)-C(11A)	1.507(4)
C(7A)-C(8A)	1.549(4)
C(7A)-H(7AA)	1.0000
C(8A)-C(9A)	1.539(5)
C(8A)-H(8AA)	0.9900
C(8A)-H(8AB)	0.9900

C(9A)-C(10A)	1.521(4)
C(9A)-H(9AA)	0.9900
C(9A)-H(9AB)	0.9900
C(10A)-C(16A)	1.499(4)
C(10A)-C(14A)	1.514(5)
C(11A)-C(13A)	1.317(5)
C(11A)-C(12A)	1.479(4)
C(12A)-O(19A)	1.209(4)
C(12A)-O(18A)	1.347(4)
C(13A)-H(13A)	0.9500
C(13A)-H(13B)	0.9500
C(14A)-H(14A)	0.9800
C(14A)-H(14B)	0.9800
C(14A)-H(14C)	0.9800
C(15A)-H(15A)	0.9800
C(15A)-H(15B)	0.9800
C(15A)-H(15C)	0.9800
C(16A)-H(16A)	0.9900
C(16A)-H(16B)	0.9900
C(1B)-C(16B)	1.493(5)
C(1B)-C(2B)	1.507(5)
C(1B)-C(10B)	1.517(5)
C(1B)-H(1BA)	1.0000
C(2B)-C(3B)	1.527(5)
C(2B)-H(2BA)	0.9900
C(2B)-H(2BB)	0.9900
C(3B)-C(4B)	1.509(5)

Table 4. Bond angles [°].

c C(16A)-C(1A)-C(2A)	120.3(3)
C(16A)-C(1A)-C(10A)	59.2(2)
C(2A)-C(1A)-C(10A)	124.5(3)
C(16A)-C(1A)-H(1AA)	114.0
C(2A)-C(1A)-H(1AA)	114.0
C(10A)-C(1A)-H(1AA)	114.0
C(1A)-C(2A)-C(3A)	113.7(2)
C(1A)-C(2A)-H(2AA)	108.8
C(3A)-C(2A)-H(2AA)	108.8
C(1A)-C(2A)-H(2AB)	108.8
C(3A)-C(2A)-H(2AB)	108.8
H(2AA)-C(2A)-H(2AB)	107.7
C(4A)-C(3A)-C(2A)	113.5(2)
C(4A)-C(3A)-H(3AA)	108.9
C(2A)-C(3A)-H(3AA)	108.9
C(4A)-C(3A)-H(3AB)	108.9
C(2A)-C(3A)-H(3AB)	108.9
H(3AA)-C(3A)-H(3AB)	107.7
O(17A)-C(4A)-C(5A)	58.89(18)
O(17A)-C(4A)-C(3A)	115.4(2)
C(5A)-C(4A)-C(3A)	116.7(3)
O(17A)-C(4A)-C(15A)	112.2(3)
C(5A)-C(4A)-C(15A)	123.0(3)
C(3A)-C(4A)-C(15A)	116.5(3)
O(17A)-C(5A)-C(4A)	59.95(18)
O(17A)-C(5A)-C(6A)	119.2(3)
C(4A)-C(5A)-C(6A)	123.9(3)
O(17A)-C(5A)-H(5AA)	114.3
C(4A)-C(5A)-H(5AA)	114.3
C(6A)-C(5A)-H(5AA)	114.3
O(18A)-C(6A)-C(5A)	107.9(2)
O(18A)-C(6A)-C(7A)	106.1(2)
C(5A)-C(6A)-C(7A)	111.4(2)
O(18A)-C(6A)-H(6AA)	110.4

C(5A)-C(6A)-H(6AA)	110.4
C(7A)-C(6A)-H(6AA)	110.4
C(11A)-C(7A)-C(6A)	101.7(2)
C(11A)-C(7A)-C(8A)	116.9(2)
C(6A)-C(7A)-C(8A)	116.0(3)
C(11A)-C(7A)-H(7AA)	107.2
C(6A)-C(7A)-H(7AA)	107.2
C(8A)-C(7A)-H(7AA)	107.2
C(9A)-C(8A)-C(7A)	113.7(3)
C(9A)-C(8A)-H(8AA)	108.8
C(7A)-C(8A)-H(8AA)	108.8
C(9A)-C(8A)-H(8AB)	108.8
C(7A)-C(8A)-H(8AB)	108.8
H(8AA)-C(8A)-H(8AB)	107.7
C(10A)-C(9A)-C(8A)	115.8(3)
C(10A)-C(9A)-H(9AA)	108.3
C(8A)-C(9A)-H(9AA)	108.3
C(10A)-C(9A)-H(9AB)	108.3
C(8A)-C(9A)-H(9AB)	108.3
H(9AA)-C(9A)-H(9AB)	107.4
C(16A)-C(10A)-C(14A)	115.4(3)
C(16A)-C(10A)-C(9A)	117.5(3)
C(14A)-C(10A)-C(9A)	113.1(3)
C(16A)-C(10A)-C(1A)	60.05(19)
C(14A)-C(10A)-C(1A)	121.3(3)
C(9A)-C(10A)-C(1A)	119.2(2)
C(13A)-C(11A)-C(12A)	121.4(3)
C(13A)-C(11A)-C(7A)	131.1(3)
C(12A)-C(11A)-C(7A)	107.4(2)
O(19A)-C(12A)-O(18A)	121.5(3)
O(19A)-C(12A)-C(11A)	128.7(3)
O(18A)-C(12A)-C(11A)	109.8(2)
C(11A)-C(13A)-H(13A)	120.0
C(11A)-C(13A)-H(13B)	120.0
H(13A)-C(13A)-H(13B)	120.0
C(10A)-C(14A)-H(14A)	109.5

C(10A)-C(14A)-H(14B)109.5
H(14A)-C(14A)-H(14B)109.5
C(10A)-C(14A)-H(14C) 109.5
H(14A)-C(14A)-H(14C) 109.5
H(14B)-C(14A)-H(14C) 109.5
C(4A)-C(15A)-H(15A) 109.5
C(4A)-C(15A)-H(15B) 109.5
H(15A)-C(15A)-H(15B) 109.5
C(4A)-C(15A)-H(15C) 109.5
H(15A)-C(15A)-H(15C) 109.5
H(15B)-C(15A)-H(15C) 109.5
C(10A)-C(16A)-C(1A) 60.7(2)
C(10A)-C(16A)-H(16A) 117.7
C(1A)-C(16A)-H(16A) 117.7
C(10A)-C(16A)-H(16B) 117.7
C(1A)-C(16A)-H(16B) 117.7
H(16A)-C(16A)-H(16B) 114.8
C(5A)-O(17A)-C(4A) 61.15(17)
C(12A)-O(18A)-C(6A) 110.2(2)
C(16B)-C(1B)-C(2B) 119.0(3)
C(16B)-C(1B)-C(10B) 60.3(2)
C(2B)-C(1B)-C(10B) 126.6(3)
C(16B)-C(1B)-H(1BA) 113.5
C(2B)-C(1B)-H(1BA) 113.5
C(10B)-C(1B)-H(1BA) 113.5
C(1B)-C(2B)-C(3B) 113.7(3)
C(1B)-C(2B)-H(2BA) 108.8
C(3B)-C(2B)-H(2BA) 108.8
C(1B)-C(2B)-H(2BB) 108.8
C(3B)-C(2B)-H(2BB) 108.8
H(2BA)-C(2B)-H(2BB) 107.7
C(4B)-C(3B)-C(2B) 111.8(3)
C(4B)-C(3B)-H(3BA) 109.3
C(2B)-C(3B)-H(3BA) 109.3
C(4B)-C(3B)-H(3BB) 109.3
C(2B)-C(3B)-H(3BB) 109.3

H(3BA)-C(3B)-H(3BB)	107.9
O(17B)-C(4B)-C(5B)	59.7(2)
O(17B)-C(4B)-C(3B)	115.8(4)
C(5B)-C(4B)-C(3B)	115.5(3)
O(17B)-C(4B)-C(15B)	112.5(3)
C(5B)-C(4B)-C(15B)	123.8(3)
C(3B)-C(4B)-C(15B)	116.3(3)
O(17B)-C(5B)-C(4B)	59.0(2)
O(17B)-C(5B)-C(6B)	118.5(3)
C(4B)-C(5B)-C(6B)	125.2(3)
O(17B)-C(5B)-H(5BA)	114.3
C(4B)-C(5B)-H(5BA)	114.3
C(6B)-C(5B)-H(5BA)	114.3
O(18B)-C(6B)-C(5B)	106.5(3)
O(18B)-C(6B)-C(7B)	105.9(2)
C(5B)-C(6B)-C(7B)	113.6(3)
O(18B)-C(6B)-H(6BA)	110.2
C(5B)-C(6B)-H(6BA)	110.2
C(7B)-C(6B)-H(6BA)	110.2
C(11B)-C(7B)-C(8B)	115.1(3)
C(11B)-C(7B)-C(6B)	101.6(2)
C(8B)-C(7B)-C(6B)	116.5(3)
C(11B)-C(7B)-H(7BA)	107.7
C(8B)-C(7B)-H(7BA)	107.7
C(6B)-C(7B)-H(7BA)	107.7
C(9B)-C(8B)-C(7B)	116.4(3)
C(9B)-C(8B)-H(8BA)	108.2
C(7B)-C(8B)-H(8BA)	108.2
C(9B)-C(8B)-H(8BB)	108.2
C(7B)-C(8B)-H(8BB)	108.2
H(8BA)-C(8B)-H(8BB)	107.3
C(10B)-C(9B)-C(8B)	119.2(3)
C(10B)-C(9B)-H(9BA)	107.5
C(8B)-C(9B)-H(9BA)	107.5
C(10B)-C(9B)-H(9BB)	107.5
C(8B)-C(9B)-H(9BB)	107.5

H(9BA)-C(9B)-H(9BB)	107.0
C(14B)-C(10B)-C(16B)	116.2(3)
C(14B)-C(10B)-C(9B)	113.5(3)
C(16B)-C(10B)-C(9B)	115.0(3)
C(14B)-C(10B)-C(1B)	123.1(3)
C(16B)-C(10B)-C(1B)	59.1(2)
C(9B)-C(10B)-C(1B)	118.4(3)
C(13B)-C(11B)-C(12B)	122.0(3)
C(13B)-C(11B)-C(7B)	130.1(3)
C(12B)-C(11B)-C(7B)	107.9(3)
O(19B)-C(12B)-O(18B)	121.5(3)
O(19B)-C(12B)-C(11B)	129.3(3)
O(18B)-C(12B)-C(11B)	109.2(2)
C(11B)-C(13B)-H(13C)	120.0
C(11B)-C(13B)-H(13D)	120.0
H(13C)-C(13B)-H(13D)	120.0
C(10B)-C(14B)-H(14D)	109.5
C(10B)-C(14B)-H(14E)	109.5
H(14D)-C(14B)-H(14E)	109.5
C(10B)-C(14B)-H(14F)	109.5
H(14D)-C(14B)-H(14F)	109.5
H(14E)-C(14B)-H(14F)	109.5
C(4B)-C(15B)-H(15D)	109.5
C(4B)-C(15B)-H(15E)	109.5
H(15D)-C(15B)-H(15E)	109.5
C(4B)-C(15B)-H(15F)	109.5
H(15D)-C(15B)-H(15F)	109.5
H(15E)-C(15B)-H(15F)	109.5
C(1B)-C(16B)-C(10B)	60.6(2)
C(1B)-C(16B)-H(16C)	117.7
C(10B)-C(16B)-H(16C)	117.7
C(1B)-C(16B)-H(16D)	117.7
C(10B)-C(16B)-H(16D)	117.7
H(16C)-C(16B)-H(16D)	114.8
C(4B)-O(17B)-C(5B)	61.3(2)
C(12B)-O(18B)-C(6B)	110.1(2)

Table 5. Anisotropic displacement parameters ($Å^2 x\ 10^3$). The anisotropic displacement factor exponent takes the form: $-2\ ^2[\ h^2 a^{*2} U_{11} + ... + 2\ h\ k\ a^*\ b^*\ U_{12}\ ]$.

	U_{11}	U_{22}	U_{33}	U_{23}	U_{13}	U_{12}
C1A	23(1)	32(2)	35(2)	-4(1)	-1(1)	2(1)
C2A	32(2)	49(2)	36(2)	-1(2)	12(1)	3(2)
C3A	33(2)	44(2)	29(1)	2(1)	10(1)	1(1)
C4A	28(1)	33(2)	31(1)	7(1)	6(1)	2(1)
C5A	22(1)	35(2)	27(1)	1(1)	0(1)	-1(1)
C6A	19(1)	33(2)	32(1)	-1(1)	3(1)	-1(1)
C7A	22(1)	36(2)	26(1)	-3(1)	1(1)	3(1)
C8A	26(1)	67(2)	28(1)	-10(2)	-3(1)	9(2)
C9A	30(1)	53(2)	28(1)	9(1)	-2(1)	12(2)
C10A	21(1)	36(2)	34(1)	-2(1)	-2(1)	4(1)
C11A	29(1)	32(2)	33(1)	-6(1)	7(1)	-2(1)
C12A	27(1)	43(2)	42(2)	-5(2)	7(1)	-1(1)
C13A	55(2)	39(2)	41(2)	-1(2)	20(2)	3(2)
C14A	30(2)	55(2)	50(2)	-11(2)	-5(1)	-5(2)
C15A	36(2)	35(2)	51(2)	2(2)	14(1)	-8(1)
C16A	35(2)	40(2)	41(2)	-4(2)	1(1)	11(1)
O17A	33(1)	45(1)	37(1)	12(1)	3(1)	8(1)
O18A	23(1)	48(1)	39(1)	7(1)	7(1)	7(1)
O19A	24(1)	81(2)	63(2)	1(2)	14(1)	5(1)
C1B	27(1)	41(2)	39(2)	-2(1)	-2(1)	-3(1)
C2B	23(1)	47(2)	59(2)	10(2)	8(1)	-3(1)
C3B	29(2)	46(2)	63(2)	18(2)	15(2)	-2(2)
C4B	26(1)	60(2)	49(2)	25(2)	7(1)	2(2)
C5B	26(1)	33(2)	66(2)	11(2)	18(1)	4(1)
C6B	21(1)	33(2)	57(2)	3(2)	14(1)	3(1)
C7B	22(1)	31(2)	48(2)	0(1)	9(1)	-2(1)
C8B	29(2)	33(2)	70(2)	12(2)	16(2)	3(1)
C9B	31(2)	47(2)	40(2)	16(2)	9(1)	11(1)
C10B	27(1)	39(2)	45(2)	6(1)	11(1)	7(1)
C11B	24(1)	34(2)	46(2)	-9(1)	12(1)	-4(1)

C12B	25(1)	34(2)	52(2)	-10(2)	12(1)	-3(1)
C13B	36(2)	50(2)	48(2)	-6(2)	16(1)	-6(2)
C14B	88(3)	43(2)	87(3)	-16(2)	58(3)	-6(2)
C15B	70(3)	121(5)	31(2)	-8(2)	17(2)	-28(3)
C16B	32(2)	71(3)	79(3)	29(3)	-4(2)	2(2)
O17B	33(1)	75(2)	122(3)	65(2)	11(2)	10(1)
O18B	23(1)	41(1)	59(1)	8(1)	13(1)	5(1)
O19B	24(1)	53(2)	68(2)	-5(1)	16(1)	2(1)

Table 6. Hydrogen coordinates (x 10^4) and isotropic displacement parameters ($Å^2$x 10^3).

	x	y	z	U(eq)
H1AA	7431	301	411	38
H2AA	8865	826	-574	46
H2AB	9340	2386	25	46
H3AA	7836	3402	-1098	42
H3AB	6877	1963	-996	42
H5AA	5679	2050	-49	35
H6AA	6128	4748	1168	34
H7AA	5938	1185	1260	34
H8AA	7736	3374	2049	50
H8AB	7249	2372	2740	50
H9AA	8711	576	2606	46
H9AB	7599	-184	1907	46
H13A	4029	1777	2837	52
H13B	5452	1031	3024	52
H14A	10500	1942	2213	72
H14B	9597	3400	1754	72
H14C	10423	2357	1263	72
H15A	7367	5962	593	60
H15B	8062	5996	-143	60
H15C	8563	4805	642	60
H16A	8916	-1627	1173	48
H16B	10071	-597	907	48
H1BA	1126	4521	3058	45
H2BA	-367	3710	3910	52
H2BB	212	5242	4501	52
H3BA	1180	2769	5080	55
H3BB	1524	2271	4231	55
H5BA	3131	3359	3790	49
H6BA	4405	6291	4613	43
H7BA	3584	5310	2924	40

H8BA	3390	8337	3747	52
H8BB	3644	8573	2852	52
H9BA	1600	8704	2543	47
H9BB	1801	6770	2359	47
H13C	6555	7095	2544	52
H13D	5143	7844	2196	52
H14D	1848	8352	4406	100
H14E	402	7993	4311	100
H14F	829	9458	3782	100
H15D	3438	6223	5523	110
H15E	2701	5064	6028	110
H15F	1954	6266	5307	110
H16C	-944	6753	3092	76
H16D	-372	6351	2274	76

Appendix B X-Ray Crystallography Data for Rearranged PTL (6)

B.1 General Experimentle

A crystal (approximate dimensions 0.50 x 0.08 x 0.04 mm3) was placed onto the tip of a 0.1 mm diameter glass capillary and mounted on a Bruker APEX-II CCD diffractometer for a data collection at 173(2) K. A preliminary set of cell constants was calculated from reflections harvested from three sets of 20 frames. These initial sets of frames were oriented such that orthogonal wedges of reciprocal space were surveyed. This produced initial orientation matrices determined from 755 reflections. The data collection was carried out using MoK radiation (graphite monochromator) with a frame time of 120 seconds and a detector distance of 6.0 cm. A randomly oriented region of reciprocal space was surveyed to the extent of one sphere and to a resolution of 0.77 Å. Four major sections of frames were collected with 0.50º steps in at four different settings and a detector position of -28º in 2 . The intensity data were corrected for absorption and decay (SADABS). Final cell constants were calculated from 2972 strong reflections from the actual data collection after integration.

The data were merged as though the structure was centrosymmetric since absolute configuration could not be determined experimentally for lack of a heavy atom. In this case the Flack parameter is meaningless and the enantiomer was chosen based on known chiral centers. Data collection and structure solution were conducted at the X-Ray Crystallographic Laboratory, 192 Kolthoff Hall, Department of Chemistry, UMN. All calculations were performed using Pentium computers using the current SHELXTL suite of programs.

B.2 Thermal Ellipsoid Drawing of 6

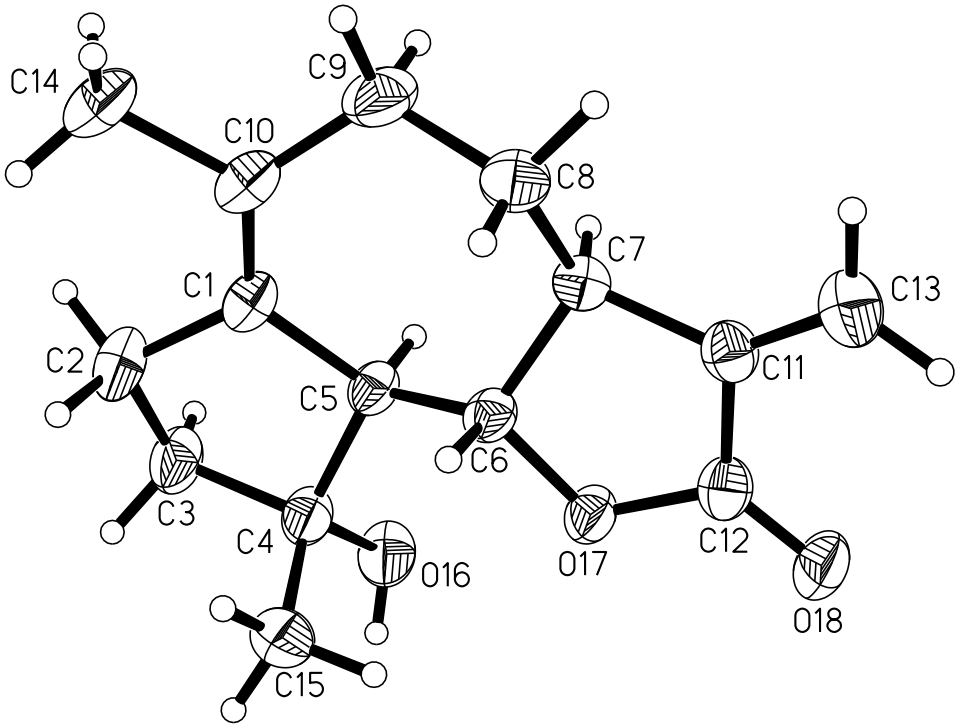

B.3 Crystallographic Information

Table 1. Crystal data and structure refinement.

Empirical formula	$C_{15}\ H_{20}\ O_3$	
Formula weight	248.31	
Temperature	173(2) K	
Wavelength	0.71073 Å	
Crystal system	Orthorhombic	
Space group	$C222_1$	
Unit cell dimensions	a = 7.4777(9) Å	= 90°
	b = 15.4839(18) Å	= 90°
	c = 22.319(3) Å	= 90°
Volume	2584.2(5) $Å^3$	
Z	8	
Density (calculated)	1.276 Mg/m^3	
Absorption coefficient	0.087 mm^{-1}	
F(000)	1072	
Crystal color, morphology	colourless, Needle	
Crystal size	0.50 x 0.08 x 0.04 mm^3	
Theta range for data collection	2.63 to 27.52 °	
Index ranges	$0 \le h \le 9$, $0 \le k \le 19$, $0 \le l \le 29$	
Reflections collected	12579	
Independent reflections	1686 [R(int) = 0.0415]	
Observed reflections	1475	
Completeness to theta = 27.52 °	99.6%	
Absorption correction	Multi-scan	
Max. and min. transmission	0.9965 and 0.9576	
Refinement method	Full-matrix least-squares on F^2	
Data / restraints / parameters	1686 / 0 / 166	
Goodness-of-fit on F^2	1.042	
Final R indices [I>2sigma(I)]	$R1$ = 0.0373, $wR2$ = 0.0958	
R indices (all data)	$R1$ = 0.0442, $wR2$ = 0.1008	
Absolute structure parameter	4.3(16)	
Largest diff. peak and hole	0.179 and -0.192 e.$Å^{-3}$	

Table 2. Atomic coordinates (x 10^4) and equivalent isotropic displacement parameters ($Å^2$x 10^3). U_{eq} is defined as one third of the trace of the orthogonalized U_{ij} tensor.

	x	y	z	U_{eq}
C1	2832(3)	1293(1)	3111(1)	30(1)
C2	2644(4)	403(2)	2828(1)	41(1)
C3	3409(4)	-224(2)	3288(1)	41(1)
C4	2964(3)	189(1)	3891(1)	33(1)
C5	3338(3)	1158(1)	3769(1)	27(1)
C6	2429(3)	1782(1)	4188(1)	27(1)
C7	3078(3)	2712(1)	4148(1)	28(1)
C8	2203(4)	3210(1)	3642(1)	36(1)
C9	2909(4)	2940(2)	3027(1)	43(1)
C10	2634(3)	2027(2)	2804(1)	34(1)
C11	2755(3)	3021(1)	4776(1)	30(1)
C12	2813(3)	2242(1)	5162(1)	32(1)
C13	2389(3)	3796(2)	4989(1)	42(1)
C14	2190(4)	1991(2)	2141(1)	43(1)
C15	1045(4)	8(2)	4072(1)	44(1)
O16	4187(3)	-112(1)	4335(1)	44(1)
O17	2776(2)	1531(1)	4813(1)	32(1)
O18	2878(3)	2192(1)	5700(1)	43(1)

Table 3. Bond angles [ ].

C(10)-C(1)-C(2)	123.20(18)
C(10)-C(1)-C(5)	129.46(19)
C(2)-C(1)-C(5)	107.29(16)
C(1)-C(2)-C(3)	105.21(17)
C(1)-C(2)-H(2A)	110.7
C(3)-C(2)-H(2A)	110.7
C(1)-C(2)-H(2B)	110.7
C(3)-C(2)-H(2B)	110.7
H(2A)-C(2)-H(2B)	108.8
C(2)-C(3)-C(4)	104.22(18)
C(2)-C(3)-H(3A)	110.9
C(4)-C(3)-H(3A)	110.9
C(2)-C(3)-H(3B)	110.9
C(4)-C(3)-H(3B)	110.9
H(3A)-C(3)-H(3B)	108.9
O(16)-C(4)-C(15)	111.19(18)
O(16)-C(4)-C(3)	109.60(18)
C(15)-C(4)-C(3)	111.4(2)
O(16)-C(4)-C(5)	108.83(18)
C(15)-C(4)-C(5)	113.33(19)
C(3)-C(4)-C(5)	102.15(17)
C(6)-C(5)-C(1)	113.37(16)
C(6)-C(5)-C(4)	115.49(17)
C(1)-C(5)-C(4)	104.84(16)
C(6)-C(5)-H(5A)	107.6
C(1)-C(5)-H(5A)	107.6
C(4)-C(5)-H(5A)	107.6
O(17)-C(6)-C(5)	109.87(16)
O(17)-C(6)-C(7)	104.50(15)
C(5)-C(6)-C(7)	115.23(17)
O(17)-C(6)-H(6A)	109.0
C(5)-C(6)-H(6A)	109.0
C(7)-C(6)-H(6A)	109.0
C(11)-C(7)-C(8)	117.62(18)

C(11)-C(7)-C(6)	101.23(16)
C(8)-C(7)-C(6)	112.87(18)
C(11)-C(7)-H(7A)	108.2
C(8)-C(7)-H(7A)	108.2
C(6)-C(7)-H(7A)	108.2
C(7)-C(8)-C(9)	112.4(2)
C(7)-C(8)-H(8A)	109.1
C(9)-C(8)-H(8A)	109.1
C(7)-C(8)-H(8B)	109.1
C(9)-C(8)-H(8B)	109.1
H(8A)-C(8)-H(8B)	107.9
C(10)-C(9)-C(8)	120.2(2)
C(10)-C(9)-H(9A)	107.3
C(8)-C(9)-H(9A)	107.3
C(10)-C(9)-H(9B)	107.3
C(8)-C(9)-H(9B)	107.3
H(9A)-C(9)-H(9B)	106.9
C(1)-C(10)-C(9)	127.72(19)
C(1)-C(10)-C(14)	119.5(2)
C(9)-C(10)-C(14)	112.7(2)
C(13)-C(11)-C(12)	122.4(2)
C(13)-C(11)-C(7)	131.3(2)
C(12)-C(11)-C(7)	106.20(16)
O(18)-C(12)-O(17)	121.6(2)
O(18)-C(12)-C(11)	129.23(19)
O(17)-C(12)-C(11)	109.13(15)
C(11)-C(13)-H(13A)	120.0
C(11)-C(13)-H(13B)	120.0
H(13A)-C(13)-H(13B)	120.0
C(10)-C(14)-H(14A)	109.5
C(10)-C(14)-H(14B)	109.5
H(14A)-C(14)-H(14B)	109.5
C(10)-C(14)-H(14C)	109.5
H(14A)-C(14)-H(14C)	109.5
H(14B)-C(14)-H(14C)	109.5
C(4)-C(15)-H(15A)	109.5

C(4)-C(15)-H(15B)	109.5
H(15A)-C(15)-H(15B)	109.5
C(4)-C(15)-H(15C)	109.5
H(15A)-C(15)-H(15C)	109.5
H(15B)-C(15)-H(15C)	109.5
C(4)-O(16)-H(16A)	109.5
C(12)-O(17)-C(6)	109.58(15)

Table 4. Hydrogen coordinates (x 10^4) and isotropic displacement parameters ($Å^2$ x 10^3).

	x	y	z	U(eq)
H2A	3322	371	2448	49
H2B	1372	270	2746	49
H3A	4718	-286	3238	49
H3B	2844	-799	3251	49
H5A	4657	1250	3805	32
H6A	1111	1767	4113	32
H7A	4397	2704	4075	33
H8A	2423	3835	3701	43
H8B	894	3114	3656	43
H9A	2367	3333	2728	51
H9B	4212	3053	3024	51
H13A	2149	3870	5404	51
H13B	2364	4280	4727	51
H14A	1645	1431	2047	65
H14B	3288	2062	1906	65
H14C	1351	2455	2042	65
H15A	795	286	4458	65
H15B	867	-617	4109	65
H15C	234	238	3766	65
H16A	3735	-532	4519	65

Table 5. Anisotropic displacement parameters ($Å^2 x\ 10^3$). The anisotropic displacement factor exponent takes the form: $-2^2[\ h^2\ a^{*2} U_{11} + ...\ + 2\ h\ k\ a^*\ b^*\ U_{12}\ ]$

	U_{11}	U_{22}	U_{33}	U_{23}	U_{13}	U_{12}
C1	28(1)	38(1)	22(1)	0(1)	-1(1)	6(1)
C2	50(2)	46(1)	26(1)	-7(1)	-6(1)	10(1)
C3	58(2)	34(1)	30(1)	-7(1)	-1(1)	7(1)
C4	47(1)	27(1)	26(1)	-1(1)	-3(1)	3(1)
C5	31(1)	28(1)	22(1)	1(1)	-1(1)	5(1)
C6	30(1)	28(1)	22(1)	3(1)	-3(1)	2(1)
C7	26(1)	26(1)	30(1)	1(1)	0(1)	2(1)
C8	44(1)	28(1)	36(1)	6(1)	-3(1)	4(1)
C9	55(1)	39(1)	34(1)	12(1)	1(1)	3(1)
C10	31(1)	45(1)	25(1)	5(1)	2(1)	6(1)
C11	28(1)	30(1)	33(1)	-3(1)	-1(1)	0(1)
C12	31(1)	33(1)	31(1)	-4(1)	-1(1)	4(1)
C13	47(1)	36(1)	44(1)	-7(1)	-2(1)	2(1)
C14	42(1)	61(2)	26(1)	11(1)	-1(1)	6(1)
C15	54(2)	35(1)	42(1)	-1(1)	4(1)	-9(1)
O16	68(1)	28(1)	35(1)	6(1)	-12(1)	6(1)
O17	45(1)	28(1)	23(1)	0(1)	-1(1)	3(1)
O18	58(1)	47(1)	24(1)	-3(1)	-1(1)	-1(1)

Table 6. Torsion angles [°] for 11143a.

C10-C1-C2-C3	166.6(2)
C5-C1-C2-C3	-11.2(2)
C1-C2-C3-C4	32.5(3)
C2-C3-C4-O16	-156.0(2)
C2-C3-C4-C15	80.6(2)
C2-C3-C4-C5	-40.7(3)
C10-C1-C5-C6	41.7(3)
C2-C1-C5-C6	-140.7(2)
C10-C1-C5-C4	168.5(2)
C2-C1-C5-C4	-13.9(2)
O16-C4-C5-C6	-85.2(2)
C15-C4-C5-C6	39.0(3)
C3-C4-C5-C6	158.93(18)
O16-C4-C5-C1	149.26(17)
C15-C4-C5-C1	-86.5(2)
C3-C4-C5-C1	33.4(2)
C1-C5-C6-O17	171.77(17)
C4-C5-C6-O17	50.8(2)
C1-C5-C6-C7	-70.5(2)
C4-C5-C6-C7	168.45(18)
O17-C6-C7-C11	-30.0(2)
C5-C6-C7-C11	-150.70(17)
O17-C6-C7-C8	-156.67(18)
C5-C6-C7-C8	82.7(2)
C11-C7-C8-C9	169.2(2)
C6-C7-C8-C9	-73.5(3)
C7-C8-C9-C10	62.9(3)
C2-C1-C10-C9	-175.6(2)
C5-C1-C10-C9	1.7(4)
C2-C1-C10-C14	0.4(3)
C5-C1-C10-C14	177.6(2)
C8-C9-C10-C1	-43.2(4)
C8-C9-C10-C14	140.6(2)
C8-C7-C11-C13	-27.5(4)

C6-C7-C11-C13	-150.9(3)
C8-C7-C11-C12	149.1(2)
C6-C7-C11-C12	25.7(2)
C13-C11-C12-O18	-14.8(4)
C7-C11-C12-O18	168.3(2)
C13-C11-C12-O17	165.0(2)
C7-C11-C12-O17	-12.0(2)
O18-C12-O17-C6	171.6(2)
C11-C12-O17-C6	-8.2(2)
C5-C6-O17-C12	148.90(19)
C7-C6-O17-C12	24.7(2)

Table 7. Bond lengths [Å].

C(1)-C(10)	1.336(3)	C(8)-C(9)	1.530(3)
C(1)-C(2)	1.522(3)	C(8)-H(8A)	0.9900
C(1)-C(5)	1.531(3)	C(8)-H(8B)	0.9900
C(2)-C(3)	1.524(3)	C(9)-C(10)	1.513(3)
C(2)-H(2A)	0.9900	C(9)-H(9A)	0.9900
C(2)-H(2B)	0.9900	C(9)-H(9B)	0.9900
C(3)-C(4)	1.527(3)	C(10)-C(14)	1.518(3)
C(3)-H(3A)	0.9900	C(11)-C(13)	1.319(3)
C(3)-H(3B)	0.9900	C(11)-C(12)	1.483(3)
C(4)-O(16)	1.427(3)	C(12)-O(18)	1.204(2)
C(4)-C(15)	1.516(4)	C(12)-O(17)	1.349(2)
C(4)-C(5)	1.550(3)	C(13)-H(13A)	0.9500
C(5)-C(6)	1.507(3)	C(13)-H(13B)	0.9500
C(5)-H(5A)	1.0000	C(14)-H(14A)	0.9800
C(6)-O(17)	1.472(2)	C(14)-H(14B)	0.9800
C(6)-C(7)	1.521(3)	C(14)-H(14C)	0.9800
C(6)-H(6A)	1.0000	C(15)-H(15A)	0.9800
C(7)-C(11)	1.502(3)	C(15)-H(15B)	0.9800
C(7)-C(8)	1.515(3)	C(15)-H(15C)	0.9800
C(7)-H(7A)	1.0000		